INFORMATION TO USERS

This manuscript has been reproduced from the microfilm master. UMI films the text directly from the original or copy submitted. Thus, some thesis and dissertation copies are in typewriter face, while others may be from any type of computer printer.

The quality of this reproduction is dependent upon the quality of the copy submitted. Broken or indistinct print, colored or poor quality illustrations and photographs, print bleedthrough, substandard margins, and improper alignment can adversely affect reproduction.

In the unlikely event that the author did not send UMI a complete manuscript and there are missing pages, these will be noted. Also, if unauthorized copyright material had to be removed, a note will indicate the deletion.

Oversize materials (e.g., maps, drawings, charts) are reproduced by sectioning the original, beginning at the upper left-hand corner and continuing from left to right in equal sections with small overlaps.

ProQuest Information and Learning
300 North Zeeb Road, Ann Arbor, MI 48106-1346 USA
800-521-0600

SINGLE- AND MULTIPHOTON STUDIES OF ATOMIC NEGATIVE IONS: ELECTRON AFFINITIES, THRESHOLD LAWS, AND NEAR-THRESHOLD STRUCTURE

By

RENÉ CLAUDE BILODEAU, B.Sc. (Hon. Phys., Hon. Math.)

A Thesis

Submitted to the School of Graduate Studies

in Partial Fulfilment of the Requirements

for the Degree

Doctor of Philosophy

McMaster University

SINGLE- AND MULTIPHOTON STUDIES OF ATOMIC NEGATIVE IONS

DOCTOR OF PHILOSOPHY (2001)
(Physics)

McMaster University
Hamilton, Ontario

TITLE: Single- and multiphoton studies of atomic negative ions:
Electron affinities, threshold laws, and near-threshold structure

AUTHOR: René Claude Bilodeau
DEC Sc. (Champlain Regional College, Lennoxville)
B.Sc. Hon. Phys. Hon. Math. (Bishop's University)

SUPERVISOR: Dr. Harold K. Haugen

NUMBER OF PAGES: xxiv, 220

Abstract

While neutral atoms and positively charged ions are bound in a Coulomb potential, the excess electron in an atomic negative ion is bound in an induced dipole potential (falling off as r^{-4}). One consequence is that only a small number of states are bound in a negative ion, typically only the fine structure of one term, in contrast to the infinite number of states bound in a neutral or positively charged atomic system. The novel structure and binding potential of negative ions have attracted much interest on a fundamental level. In addition, negative ions play an important role in such areas as accelerator mass spectroscopy (AMS), atmospheric physics, and astrophysics. Despite considerable ongoing theoretical and experimental efforts, a number of atomic negative ion states remain poorly known or even completely unknown. Recently, tunable pulsed laser techniques have led the way in high precision measurements in atomic negative ions. This thesis presents results obtained with the tunable infrared laser source at McMaster University using single-photon threshold detachment and multiphoton resonant detachment spectroscopy, as well as non-resonant multiphoton threshold studies. Experiments investigating the structure of 13 elemental negative ions are detailed: Cs^-, Cr^-, Mo^-, W^-, Ru^-, Os^-, Ir^-, Pt^-, Cu^-, Ag^-, B^-, Al^-, and Bi^-. Of particular note are the results of the first measurements on the negative ion of osmium which have provided the first and only known example of an atomic negative ion having both even and odd parity bound states. Strong continuum structures are

also observed in Cs^-, Os^-, and W^- for the first time, and appear as near-threshold Feshbach and shape resonances. Investigations of the behaviour of single- and multiphoton threshold laws are also presented. Specifically, single photon *s*-wave and *p*-wave threshold behaviours are measured to energies well above threshold and are compared to the models proposed by O'Malley and Farley. It is found that better results may be obtained if the two models are combined. Finally, two-photon experiments in Au^- have demonstrated the extreme sensitivity of the near-threshold multiphoton detachment cross sections and the multiphoton threshold law to the polarisation state of the laser. These studies have led to the first observation of a Wigner *d*-wave law, and the technique is argued to have valuable applications to studies of negative ions which have structure lying near a photodetachment threshold.

Acknowledgements

Many consider the completion of a PhD as a goal in itself; a milestone marking the end of one long road and the beginning of a new one. As I think back on events that have led me to where I am now, I recognize that this goal represents more than just the last few years but the entire journey. If I have succeeded now, it is because I have been fortunate enough to have had encouragement from mentors and peers, every step of the way. I feel indebted to the marvelous professors at Champlain, where I first recognized my attraction to the beauty and wonders of science and learning. I was first introduced to the excitement of research at Bishop's, and I owe thanks to Lorne for his confidence in me. Chris, Eric, Naomi, and Trevor you made those days, and many days since then, great times. I will always cherish your friendship. Todd, what can I say, you've always been and will always be a great friend.

When I moved on to graduate school, I considered many options and spoke to many professors, and I was fortunate to find the best supervisor any student could hope for. Harold, in addition to all the things you've taught me, your advice, support, patience, and encouragement have been greatly appreciated. Mike, I owe so much of what I know to you; it was a joy to work with you and to be your friend. Cicely, Mike, Pat, Steve, and Tim, thanks for sharing your knowledge and office space. A special thanks to Cicely for keeping care of the plants while Naomi and I were in Denmark and letting us use your apartment while we were homeless. I would also

like to thank my supervisory committee (Adam Hitchcock, Bob Brooks, and Jim Waddington) for their advice and enthusiasm. I am grateful to Bob Brooks, Dag Hanstorp, Hartmut Hotop, Joe Macek, Torkild Andersen, and Victor Petrunin, for the many stimulating conversations and communications and the valuable advice on drafts of various articles. To Lars Andersen and the rest of the gang (CP, Henrik, Marie, Igor, and the others who visited the group): thanks for the wonderful time at Aarhus and the great opportunity to work with you — I learned a lot from you. Susanna, I cannot thank you enough for pushing Naomi's visa through, for organizing all the details of the trip, and for the great time we had visiting you.

Finally, I would like to thank my family: Mom et Dad, vous m'avez souvent encouragé par votre intérêt dans mes efforts et j'ai toujours senti que vous étiez là pour m'aider quand le besoin se présentait — je vous aime très fort. My brothers (Guy, Normand, and Daniel) for forgiving my mess, for teaching me about computers and getting parts for my computer, for giving me a place to stay in Lennoxville, and for putting up with me and helping me out in so many ways; and of course their better halves (Désiré, Nicole, and Phyllis) for making those family-get-togethers all that much more fun. The Jambors for visiting me and having me up for visits while I was away from home. The Blacks for their generosity, interesting conversations, and their daughter. And lastly, but certainly not least, I would like to thank my lovely wife Naomi for her support, patience, sacrifice, love, and affection through some difficult times and some grand times.

Contents

List of Figures

List of Tables

Preface

The work presented in this Thesis has been previously published in the form of several refereed journal articles. I was the primary contributor to the experimental realisation, data analysis, and writing of the 6 works listed below.

Paper 1:

Infrared laser photodetachment of transition metal negative ions: Studies on Cr^-, Mo^-, Cu^- and Ag^-,

René C. Bilodeau, Michael Scheer, and Harold K. Haugen,

Journal of Physics B **31**, 3885–3891 (1998).

Paper 2:

Near threshold spectroscopy of iridium and platinum negative ions: Electron affinities and the threshold law,

René C. Bilodeau, Michael Scheer, Harold K. Haugen, and Robert L. Brooks,

Physical Review A **61**, 012505-1–012505-7 (2000).

Paper 3:

Theoretical and experimental binding energies for $d^7s^2\ ^4F$ in Ru^-, including calculated hyperfine structure and M1 decay rates,

Peggy L. Norquist and Donald R. Beck;

René C. Bilodeau, Michael Scheer, Raphaël A. Srawley, and Harold K. Haugen,

Physical Review A **59**, 1896–1902 (1999).

Paper 4:

Electron affinity of Bi using high resolution photodetachment threshold spectroscopy,

René C. Bilodeau and Harold K. Haugen,

Physical Review A **64**, 024501-1–024501-3 (2001).

Paper 5:

Experimental Studies of Os^-: Observation of a Bound-Bound Electric Dipole Transition in an Atomic Negative Ion,

René C. Bilodeau and Harold K. Haugen,

Physical Review Letters **85**, 534–537 (2000).

Paper 6:

Control of Near-threshold Detachment Cross Sections via Laser Polarization,

René C. Bilodeau, Michael Scheer, and Harold K. Haugen,

Physical Review Letters (Accepted July, 2001).

I have also participated in the experimental realisation and data analysis of other related research projects, which have resulted in the following 6 publications. The last three of these will not be discussed in detail in the present Thesis, but only the results will be reported.

Paper 7:

Negative Ion of Boron: An Experimental Study of the ^3P Ground State,

Michael Scheer, René C. Bilodeau, and Harold K. Haugen,

Physical Review Letters **80**, 2562–2565 (1998).

Paper 8:

Threshold photodetachment of Al^-: Electron affinity and fine structure.

Michael Scheer, René C. Bilodeau, Jan Thøgersen, and Harold K. Haugen,

Physical Review A **57**, R1493–R1496 (1998).

Paper 9:

Experimental Evidence that the $6s6p\ ^3P_J$ States of Cs^- are Shape Resonances,

M. Scheer, J. Thøgersen, R. C. Bilodeau, C. A. Brodie, and H. K. Haugen;

H. H. Andersen, P. Kristensen, and T. Andersen,

Physical Review Letters **80**, 684–687 (1998).

Paper 10:

Systematic study of the stable states of C^-, Si^-, Ge^-, and Sn^- via infrared laser spectroscopy,

Michael Scheer, René C. Bilodeau, Cicely A. Brodie, and Harold K. Haugen,

Physical Review A **58**, 2844–2856 (1998).

Paper 11:

Laser spectroscopic measurements of binding energies and fine structure splittings of Co^-, Ni^-, Rh^-, and Pd^-,

Michael Scheer, Cicely A. Brodie, René C. Bilodeau, and Harold K. Haugen,

Physical Review A **58**, 2051–2062 (1998).

Paper 12:

Observation of the magnetic-dipole fine-structure transition in the tellurium negative ion,

Michael Scheer, René C Bilodeau and Harold K Haugen,

Journal of Physics B **31**, L11–L15 (1998).

Finally, I have participated in the experimental research and data analysis of other projects conducted with Lars H. Andersen's group during a 7 month stay at the University of Aarhus, which resulted in the 3 publications listed below, but which are not directly related to the present thesis.

Paper 13:

Coulomb and centrifugal barrier bound dianion resonances of NO_2,

L. H. Andersen, R. C. Bilodeau, M. J. Jensen, S. B. Nielsen, C. P. Safvan, and K. Seiersen,

Journal of Chemical Physics **114**, 147–151 (2001).

Paper 14:

Dissociative recombination of H_3O^+, HD_2O^+, and D_3O^+,

M. J. Jensen, R. C. Bilodeau, C. P. Safvan, K. Suiersen, and L. H. Andersen,

The Astrophysical Journal **543**, 764–774 (2000).

Paper 15:

Dissociative recombination and excitation of H_2O^+ and HDO^+,

M. J. Jensen, R. C. Bilodeau, O. Heber, H. B. Pedersen, C. P. Safvan, X. Urbain, D. Zajfman, and L. H. Andersen,

Physical Review A **60**, 2970–2976 (1999).

A good portion of the work in this thesis is included in Papers 1 to 9, which are reprinted here with permission of the American Physical Society and the Institute of Physics (see Appendix D). In addition to these papers, a substantial amount of new results and analysis are included, especially in Chapter 4 and Chapter 5.

For convenience, lists of symbols, fundamental constants, and conversion factors frequently used in this thesis are produced in Appendix A.

Chapter 1

Introduction

One of the first concepts taught in elementary electrostatics is that a charged particle, such as an electron, does not experience any Coulomb force from a neutral particle. Upon initial inspection, it may then be surprising to learn that an electron is usually attracted to an isolated, neutral atom. Nonetheless, for most elements of the periodic table the attractive force between an electron and an atom is strong enough to bind this "extra" electron, and form a stable atomic negative ion.

The binding process can be understood on the basis of a simple semi-classical model. Although it is true that the electron is not attracted by a neutral particle, as the electron is brought near to the atom it can distort, or polarise, the electron cloud surrounding the atom, thus inducing an electric dipole moment. This induced electric dipole moment in turn attracts the electron. In this way, the electron finds itself trapped in an *induced electric dipole potential*, and a bound state of a negative ion can be formed. The energy released in this process is called the *binding energy* of the negative ion, or equivalently, the *electron affinity* (EA) of the neutral atom.[1]

[1]Specifically, the EA is defined as the binding energy of the lowest hyperfine state of the atomic negative ion relative to the lowest hyperfine state of the corresponding neutral atom.

Therefore, while the electrons in neutral atoms and positively charged ions are bound in the Coulomb potential, which is proportional to r^{-1} (r being the separation between the electron and the nucleus), the outer electron in the negative ion is bound in a short-range potential, proportional to r^{-4}. This short-range potential gives rise to a number of exotic qualities of negative ions that cannot be found in neutral atoms or positive ions, thereby making them interesting to investigate both in experimental and theoretical contexts. For example, the short-range potential can only support a finite number of states, often only the fine-structure (if any) of one term. In contrast, the Coulomb potential supports an infinite number of bound states, converging into a Rydberg series at the ionisation threshold. Also, the binding energy of a negative ion is always far lower than the ionisation energy of the corresponding neutral atom. The EA of H is only 0.75 eV while its ionisation energy is 13.6 eV. Yet another consequence is the strikingly different threshold behaviour resulting from photodetachment of a negative ion as compared to photoionisation of an atom or positive ion, as is discussed in Section 2.1.

Looking more closely, as the electron begins to penetrate the atom's electron cloud, quantum mechanical effects become important and the qualitative semi-classical picture described above is no longer valid. Quantum mechanical calculations involving mean static field techniques, such as a Hartree analysis, obtain reasonable quantitative results for atoms. However, such techniques fail to predict binding for even the simplest of negative ions,[2] H^-. Even the Hartree-Fock approach, which is very successful at accurately determining the structure of atomic and molecular systems including positive ions, drastically underestimates the binding energies of negative ions, and frequently fails to obtain stable atomic negative ions states. For

[2]For heavier systems, bound states may be predicted in the static field, but are excluded by the Pauli principle, see [1].

example, Hartree-Fock calculations in F^- predict less than half of the observed EA of F [2]. Therefore, very sophisticated treatments, which include the effects of correlated motion of the electrons, are required in order to fully explain the stability of atomic negative ions. The comparison of experimentally obtained binding energies to these sophisticated theoretical models thus provides a very sensitive probe into their ability to model electron correlations, and this has in part motivated a number of experiments discussed in the present thesis. Correlation models are of fundamental importance to atomic theory and the recent success of these theories represents a significant advancement which can then be applied to other areas of atomic physics. As an example, the results of negative ion studies have recently been used to evaluate the suitability of advanced electron-positron correlation models for positron-atom interactions [3–5].

In addition to the fundamental interests in negative ions outlined in the preceding paragraphs, negative ions play an important role in a wide range of processes of physical and practical interest. Many important biological processes and chemical reactions involve negative ions. Binding energies of negative ions are used as input parameters to models describing ionic crystals [6]. Negative ions are known to have a very significant impact on the properties of plasmas, in particular the conductivity. Most of the mobile negative charge in the Earth's middle atmosphere is carried by negative ions [7]. Negative ions are also of astrophysical significance, being found in the atmospheres of stars and in the intergalactic medium. Wildt realised as early as 1939 [8] that negative ions, especially H^-, are the main source of opacity in stellar atmospheres.[3] [9] Accelerator mass spectroscopy [10] depends on accurate knowledge of negative ion structure to obtain ultra-sensitive isotope detection [11,12]. Many

[3]Considering the weak binding of negative ions, it may at first seem very surprising that negative ions can even survive in a star. However, the binding energy of H^- is 0.75 eV, which corresponds to a temperature of 8700 °K, slightly higher than the temperature of the solar atmosphere.

more such examples can be found in the literature.

1.1 Background on Atomic Negative Ion Experiments

Despite the large number of practical and fundamental reasons to study negative ions, they have only recently been studied to a detail that even begins to approach that of other atomic systems. Largely this is because atomic negative ions are much more fragile systems than atoms, easily destroyed by collisions with surrounding particles. Consequently they are much more difficult to produce at high concentrations in the laboratory, especially in the gas phase, and the first experimental investigations on negative ions had to wait until the early 1960s [13] with the maturation of vacuum and ion beam technologies. To make matters worse, traditional absorption and emission spectroscopy techniques, which form the backbone of experimental studies in atomic systems, cannot be used for the study of atomic negative ions due to the scarcity of excited bound states in these systems.

Two main experimental techniques have emerged to address the need for investigations on atomic negative ion structure: laser photodetached electron spectrometry (LPES) and laser photodetachment threshold spectroscopy (LPTS). In LPES, a fixed wavelength laser with photon energies well above the binding energy is used to photodetach the excess electron of a negative ion. By measuring the energy of the detached photoelectron (ε), the binding energy (ε_o) can be deduced using $\varepsilon_o = h\nu - \varepsilon$. Although the accuracy of LPES experiments are limited to the resolution of the electron spectrometer (typically a few meV), the technique can be applied to study the bound states of nearly any negative ion. This powerful technique has been applied to a vast number of atomic negative ions and constituted the bulk of the experimental

investigations reported prior to 1985 [14], principally pioneered by Lineberger and co-workers. Although LPES has largely been superseded by LPTS (see below) for high precision studies of atomic negative ions, the general applicability of LPES ensures its place as a very valuable tool, as demonstrated by a number of recent experiments conducted by Thompson and co-workers [15–18] investigating the structure of weakly bound atomic negative ions.

LPTS experiments involve the observation of a photodetachment threshold, which necessitates the use of laser light sources which can be tuned in the vicinity of the threshold energy. While sub-μeV accuracies have been achieved with this technique [19], the small binding energy of most negative ions requires that tunable infrared laser light be used, which is challenging to produce. An optical parametric oscillator was employed by Feldmann to produce the infrared light required for LPTS measurements in Li^-, P^- [20], and C^- [21], whereas the infrared studies in H^- by Lineberger and co-workers used an F-center laser [22]. More recently, the investigations by Pegg and co-workers [23] and by Andersen *et al.* [24] on alkali and alkaline earth negative ions avoided the difficulty of producing infrared light by photodetaching to excited neutral states and using a state-selective detection scheme. With these few exceptions, previous to the experiments conducted at McMaster only atomic negative ions with binding energies $\gtrsim 1.5$ eV had been studied, where readily available visible light sources could be employed. As a result, the bound states for a large portion of the elements were only poorly determined or even completely unknown until recently [25].

A great number of research groups have conducted a variety of experiments on atomic negative ions. A full list of such efforts is beyond the scope of this thesis, and the interested reader is directed to the many recent review articles published on the subject [14,24–29]. Some works of note among the more recent investigations include,

in addition to the works already mentioned above, the very high precision (3 - 10 μeV) experiments by Hanstorp and co-workers [30,31] using the LPTS technique with a coaxial beam arrangement, and by Blondel *et al.* [32] also using LPTS but with a doubly-crossed perpendicular-beam arrangement[4] Peterson and co-workers have investigated many autodetaching negative ions states; the shape resonances observed in He^- [33,34] and Ca [35] will be of particular interest for discussions in Chapter 5. Finally, recently a new technique developed by Blondel and co-workers, named photodetachment microscopy, has led to very high precision ($\approx$2.5 μeV) measurements in the negative ions of Br [36], O [37,38], F, and Si [39]. Continued efforts will no doubt lead to similar improvements in other negative ions.

1.2 Thesis Outline

This thesis describes the results of infrared laser spectroscopy experiments using the pulsed tunable infrared laser source at McMaster University. Chapter 2 will provide theoretical background on photodetachment of atomic negative ions and in particular photodetachment threshold laws, which are central to the LPTS technique. The experimental setup and technique is described in Chapter 3. The results of LPTS measurements on 10 negative ions are then discussed in Chapter 4. A large portion of that chapter is based on previously published papers (Papers 1, 2, 3, 4, 7, and 8); however, an additional discussion on the details of the observed threshold behaviour is also included. Given the scarcity of excited bound states in negative ions, it is not obvious whether the short-range binding potential could support two states having opposite parity. This important long-standing question in atomic physics is addressed in Chapter 5 with a search for opposite parity bound states in Cs^- (Paper 9) and Os^-

[4]One of the main concerns in high-precision work with an ion beam is the introduction of a Doppler shift of the laser light frequency (see Section 3.3.2). The systematic error thus introduced can be significantly reduced with these various laser-ion beam arrangements.

(Paper 5). That chapter then proceeds with a analysis of the strong near-threshold electric-dipole continuum structure observed in Cs^-, Os^-, and W^-. The final experimental results of this thesis are presented in Chapter 6 where multiphoton detachment threshold experiments conducted on Au^- (Paper 6) are discussed. Finally, Chapter 7 summarises the results and describes future perspectives in negative ion research.

1.3 References

[1] Sir H. Massey, *Negative Ions* (Cambridge University Press, Cambridge, 1976).

[2] J. J. Novoa, F. Mota, and F. Arnau, J. Chem. Phys. **95**, 3096 (1991).

[3] V. A. Dzuba, V. V. Flambaum, G. F. Gribakin, and C. Harabati, Phys. Rev. A **60**, 3641 (1999).

[4] J. Mitroy and G. Ryzhikh, J. Phys. B **32**, 2831 (1999).

[5] J. Mitroy and G. G. Ryzhikh, J. Phys. B **32**, L411 (1999).

[6] C. Kittel, *Introduction to Solid State Physics* 6th Edition (John Wiley and Sons, New York, 1986)

[7] B. M. Smirnov, *Negative Ions* (McGraw-Hill, New York, 1982).

[8] R. Wildt, Astrophys. J. **89**, 295 (1939).

[9] H. A. Bethe and E. E. Salpeter, *Quantum Mechanics of One- and Two- Electron Atoms* (Plenum, New York, 1977).

[10] C. E. Melton, *Principles of Mass Spectrometry and Negative Ions* (Marsel Dekker, New York, 1970)

[11] A. E. Litherland, Ann. Rev. Nucl. Part. Sci. **30**, 437 (1980).

[12] W. Kutschera and M. Paul, Ann. Rev. Nucl. Part. Sci. **40**, 411 (1990).

[13] L. M. Branscomb, in *Atomic and Molecular Processes* (Edited by D. R. Bates), p. 100, Academic Press, New York (1962).

[14] H. Hotop and W. C. Lineberger, J. Phys. Chem. Ref. Data **14**, 731 (1985).

[15] A. M. Covington, D. Calabrese, J. S. Thompson, and T. J. Kvale, J. Phys. B **31**, L855 (1998).

[16] W. W. Williams, D. L. Carpenter, A. M. Covington, M. C. Koepnick, D. Calabrese, and J. S. Thompson, J. Phys. B **31**, L341 (1998).

[17] W. W. Williams, D. L. Carpenter, A. M. Covington, J. S. Thompson, T. J. Kvale, and D. G. Seely, Phys. Rev. A **58**, 3582 (1998).

[18] D. L. Carpenter, A. M. Covington, and J. S. Thompson, Phys. Rev. A **61**, 042501 (2000).

[19] D. M. Neumark, K. R. Lykke, T. Andersen, and W. C. Lineberger, Phys. Rev. A **32**, 1890 (1985).

[20] D. Feldmann, Z. Phys. A **277**, 19 (1976).

[21] D. Feldmann, Chem. Phys. Lett. **47**, 338 (1977).

[22] K. R. Lykke, K. K. Murray, and W .C. Lineberger, Phys. Rev. A **43**, 6104 (1991).

[23] J. Dellwo, Y. Liu, D. J. Pegg, G. D. Alton, Phys. Rev. A **45**, 1544 (1992).

[24] T. Andersen, H. H. Andersen, P. Balling, P. Kristensen, and V. V. Petrunin, J. Phys. B **30**, 3317 (1997).

[25] T. Andersen, H. K. Haugen, and H. Hotop, J. Phys. Chem. Ref. Data **28**, 1511 (1999).

[26] C. Blondel, Phys. Scr. **T58**, 31 (1995).

[27] S. J. Buckmann, C. W. Clark, Rev. Mod. Phys. **66**, 539 (1994).

[28] D. R. Bates, Adv. At. Mol. Opt. Phys. **27**,1 (1991)

[29] T. Andersen, Phys. Scr. **T34**, 23 (1991).

[30] D. Hanstorp and M. Gustafsson, J. Phys. B **25**, 1773 (1992).

[31] K. T. Andersson, J. Sandström, I. Yu. Kiyan, D. Hanstorp, and D. J. Pegg, Phys. Rev. A **62**, 022503 (2000).

[32] C. Blondel, P. Cacciani, C. Delsart, and R. Trainham, Phys. Rev. A **40**, 3698 (1989).

[33] J. R. Peterson, Y. K. Bae, and D. L. Huestis, Phys. Rev. Lett. **55**, 692 (1985).

[34] C. W. Walter, J. A. Seifert, and J. R. Peterson, Phys. Rev. A **50**, 2257 (1994).

[35] C. W. Walter and J. R. Peterson, Phys. Rev. Lett. **68**, 2281 (1992).

[36] C. Blondel, C. Delsart, and F. Dulieu, Phys. Rev. Lett. **77**, 3735 (1996).

[37] C. Valli, C. Blondel, and C. Delsart Phys. Rev. A **59**, 3809 (1999).

[38] C. Blondel, C. Delsart, F. Dulieu, and C. Valli, Eur. Phys. J. D **77**, 207 (1999).

[39] C. Blondel, C. Delsart, and F. Goldfarb, J. Phys. B **34** (accepted).

Chapter 2

Background Theory

In LPTS experiments, the relative photodetachment cross section is measured for a range of photon energies near the threshold energy. With knowledge of the near-threshold behaviour of the cross section it is possible to accurately determine the photodetachment threshold energy, and thus the binding energy of the negative ion under study. In this chapter we shall concentrate on describing the photodetachment of negative ions, and in particular the near-threshold behaviour of the photodetachment cross section.

Section 2.1 begins with a general description of negative ion photodetachment and contrasts this process with the ionisation of neutral atoms and positively charged ions. The Wigner threshold law for negative ion photodetachment is then derived. This Wigner law is of pivotal importance to LPTS, and will be used throughout this thesis to model acquired spectra. Section 2.2 introduces the theories by O'Malley and Farley, which describe the breakdown of the Wigner law apparent at photon energies only a few percent above the threshold energy. These theories will be particularly important in Chapter 4, where investigations of the importance, and reliability, of the Farley and O'Malley correction terms are discussed. The Wigner law can also be

significantly modified when autodetaching states (e.g. shape resonances) are present near the detachment threshold. This situation arises only in Chapter 5 and a description of how the Wigner law can be modified to fit the observed spectra will therefore be discussed there. The last section of this chapter (Section 2.3) describes the new multi-photon detachment theory by Gribakin and Kuchiev. This theory will be of relevance especially in Chapter 6, where multi-photon detachment thresholds are observed in the negative ion of gold.

2.1 Basics of Negative Ion Photodetachment

The structure of negative ions is usually studied through a photodetachment process, which is analogous to the photoionisation process in a neutral atom or positively charged ion. However, while in a neutral atom (or positive ion) the electron is ejected in the presence of a Coulomb field, the Coulomb field is effectively screened from the electron in the photodetachment process. This produces significant differences in the energy dependence of the cross section for the respective processes. In particular, the cross section for photoionisation has a finite value at the ionisation limit and decreases with increasing photon energy roughly[1] as ν^{-3}. On the other hand, the photodetachment cross section of a negative ion is zero at the threshold for detachment and increases as predicted by the Wigner threshold law (see Section 2.1.1), reaches a maximum, and then falls again at larger photon energies (see Figure 2.1). The variation of the photodetachment cross section with energy can depend sensitively on the structure of the bound negative ion state and can therefore yield information not only on the binding energy of negative ion states, but also on the character of the

[1] Actually, until recently it was believed that for photoionisation from an $n\ell_0$ atomic subshell, at energies just above an absorption edge (see Figure 2.1) the cross section varies as $(h\nu)^{-8/3}$ and at very high energies as $(h\nu)^{-\ell_0-7/2}$; see for example, Section 71 of [1]. However, it has very recently been shown [2] that the cross section for any photoionisation process obeys the form $(h\nu)^{-9/2}$ for large photon energies, regardless of ℓ_0.

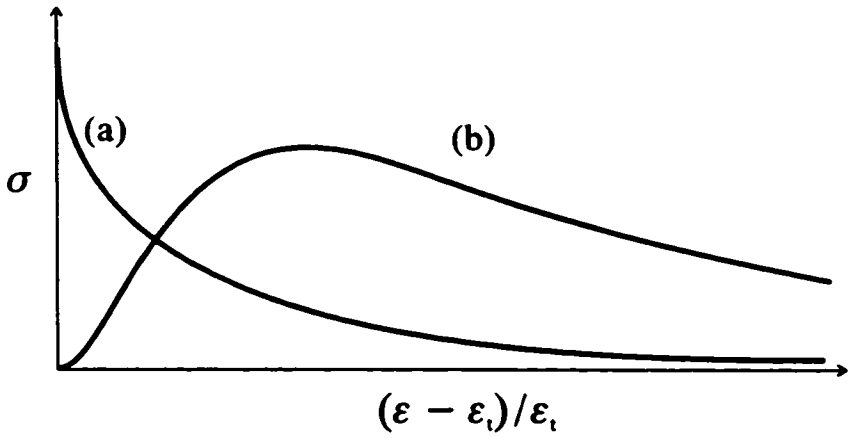

Figure 2.1: Variation of the photoabsorption cross section with energy for (a) a typical ionisation process, and (b) a typical photodetachment process. ϵ is the energy of the photoelectron ejected in the photoelectric process, and ϵ_t is the threshold for photoionisation (i.e. the ionization potential of the neutral atom or positive ion) or the threshold for photodetachment (i.e. the binding energy of the negative ion). The cross sections have been arbitrarily scaled.

bound states. The following sections discuss the variation of the photodetachment cross section with photon energies arbitrarily close to the threshold, and far above threshold.

2.1.1 Near-threshold Detachment: The Wigner threshold law

In 1948, Wigner derived general expressions for the near-threshold cross section behaviour of reactions giving rise to two products [3]. These expressions include the cases where the reaction products do not interact in the final state, or interact in an attractive or repulsive Coulomb potential. We shall be interested only in the Wigner law that applies to photodetachment, i.e. the case where the particles do not interact in the final state. This law is often called "the Wigner threshold law" or simply "the Wigner law" in the negative ion community. In fact, the final state of the photodetachment process includes one neutral particle (the atom) and one charged particle

(the electron). This is not actually covered by Wigner's original formulation, since there is an induced-dipole interaction between the electron and the neutral atom. However, it was later realized that a sufficient condition for the Wigner law to apply is for the interaction potential to be short-ranged, falling off faster than the centrifugal potential (i.e. faster than r^{-2}).

A relatively simple approach to Wigner's result follows from the application of Fermi's golden rule.[2] Given the initial (bound) negative ion state $|\psi_i\rangle$ and final (continuum) state $|\psi_f\rangle$, Fermi's golden rule states that the detachment rate is given by:

$$R_d = \frac{2\pi}{\hbar}|\langle\psi_i|\, D\,|\psi_f\rangle|^2\rho_f\,, \tag{2.1}$$

where D is the electric dipole coupling operator, corresponding to the photoabsorption process, and ρ_f is the density of final states.

The number N of free electron states available to an electron having energies less than ϵ, and confined to a box of volume V, is

$$N(\epsilon) = \frac{2V}{3\pi^2}\left(\frac{2m\,\epsilon}{\hbar^2}\right)^{\frac{3}{2}}.$$

The density of states is then $\mathrm{d}N/N = \frac{3}{2}\,\mathrm{d}\epsilon/\epsilon$. Therefore, if the wave functions are volume normalized,[3] and considering the detached electron as a free electron, the density of states is $\rho_f\,d\epsilon \propto \sqrt{\epsilon}\,d\epsilon$, with $\epsilon = h\nu - \epsilon_t$ the energy above threshold for detachment ϵ_t (or equivalently, ϵ is the excess energy carried off by the detached electron).

In contrast to photoionisation, where the core is positively charged and therefore interacts strongly with the ejected electron, we can assume that a photodetached

[2]See also the derivation by Friedrich [5] which is obtained within the framework of inelastic scattering.

[3]Volume normalization of the wave functions is required to guarantee that the factor of V remaining in ρ_f is cancelled with the factor of V^{-1} from the integral over the wave functions, $|\langle\psi_i|\, D\,|\psi_f\rangle|^2$. The final result is thus independent of V.

electron does not interact with the residual neutral atomic core. The final state can then be described in a partial wave expansion. For small ε, only the lowest order angular momentum channel ℓ will contribute significantly to the detachment cross section. Therefore the energy dependence of the final state wave function is contained in the spherical Bessel function $j_\ell(kr)$, where $k = \sqrt{2m_e\varepsilon}/\hbar$ is the wave number of the exiting electron (m_e is the mass of the electron, see Appendix A). That is to say, for small k (i.e. small ε) the energy dependence of the final state wave function is, $|\psi_f\rangle \propto j_\ell(k) \propto k^\ell \propto \varepsilon^{\ell/2}$. Finally, since the detachment cross section σ_d is proportional to the rate given by Equation 2.1 we have,

$$\sigma_d \propto \varepsilon^{\ell+\frac{1}{2}}. \tag{2.2a}$$

This is the Wigner threshold law. In terms of the momentum $p = \hbar k$ of the ejected electron the Wigner law reads,

$$\sigma_d \propto k^{2\ell+1}. \tag{2.2b}$$

A number of assumptions have been made in the above derivation. In particular we have assumed that:

1. The residual neutral core does not interact with the outgoing electron. A more careful derivation would show that it is sufficient to assume that the interaction potential between the outgoing photoelectron and the neutral core decreases faster than the centrifugal potential at large electron-atom separations r, as is always the case for the detachment of atomic negative ions.[4]

2. The energy of the photoelectron ε is small. For sufficiently small $k \propto \sqrt{\varepsilon}$, it is possible to retain only the lowest order of k in the expansion of $j_\ell(k)$.

[4]Note that this is not in general true for the photodetachment of *molecular* negative ions which can have permanent electric dipoles. In such cases the Wigner law need not apply at all, even at arbitrarily small ε. See for example Reference [6].

3. The detachment cross section is dominated by only one angular momentum channel. Only for the detachment of an s-orbital electron is this correct, where only the $\ell = 1$ (i.e. p-wave) channel is available. In general two angular momentum channels will be available: $\ell = |\ell_o \pm 1|$, where ℓ_o is the angular momentum of the bound electron to be detached. For sufficiently low photoelectron energies, however, the centrifugal barrier effectively suppresses the higher angular momentum channel. This point is therefore closely associated to assumption 2.

The following sections will address these approximations in more detail. However, it is instructive to recognize now that the Wigner law is in fact essentially the first term in an expansion of the cross section about the threshold energy. For example, this has been explicitly shown by Branscomb *et al.* for a square well binding potential [7]. If conditions 2 and/or 3 are violated, then a more general form of the threshold law would be,

$$\sigma_d = A_0 \varepsilon^{\ell+\frac{1}{2}}(1 + A_1 \varepsilon + A_2 \varepsilon^2 + \cdots). \tag{2.3}$$

Where the Wigner law appears as the first term in the expansion, with an undetermined amplitude A_0. The constants A_m ($m = 0, 1, 2, \ldots$) would have to be obtained either by some more advanced analysis, such as the ZCC approximation (see Section 2.2.2), or by fitting to the experimental data over a sufficiently large region in energy. The higher order terms in the expansion represent corrections to the Wigner law that become significant at large photon energies above threshold. Further terms are required if assumption 1 is also violated (see Section 2.2.1).

The above discussion invites the question: Over what range does the Wigner law apply? Although there is no reliable rule to answer this question, Section 2.2 will review theoretical work aimed at determining the lowest order corrections to

the Wigner law (i.e. essentially the constant A_l of Equation 2.3), while Chapter 4 (especially, Section 4.3) attempts to gain some insight on this issue with the discussion of experimental work conducted at McMaster on B^-, Al^-, Ir^-, and Pt^-.

2.1.2 Photodetachment at high photon energies

In the preceding section the energy dependence of the cross section in the limit of zero photoelectron energy was explored. Even if we continue to assume that the ejected electron can be described as a free, non-interacting electron, the cross section can vary with energy due to a decrease in the "overlap" between the initial and final states through the integral $\langle \psi_i | D | \psi_f \rangle$ of Fermi's golden rule. Before proceeding to a more quantitative description of corrections to the Wigner law, it may be helpful to explore a simple model that gives an intuitive explanation for this decrease with increasing photoelectron energy. Although the photodetachment process is assumed in the following discussion, the arguments in this section apply equally well to photoionisation. (For a qualitative account similar to the present discussion, see Section II.B.2 of Cohen-Tannoudji *et al.* [8]; a more detailed discussion can be found in Bethe and Salpeter [1, especially Section 69].) First, recall that a free electron cannot absorb a photon. The physical reason for this is simply that the electron + photon system cannot conserve both momentum and energy in the absorption process. That is, if $p_i = \hbar k_i$ and $p_f = \hbar k_f$ are respectively the initial and final momentum states of the electron, the process cannot simultaneously satisfy both of the conditions:

$$p_f = p_i + h\nu/c \tag{2.4a}$$

and,

$$E_f = E_i + h\nu\,, \tag{2.4b}$$

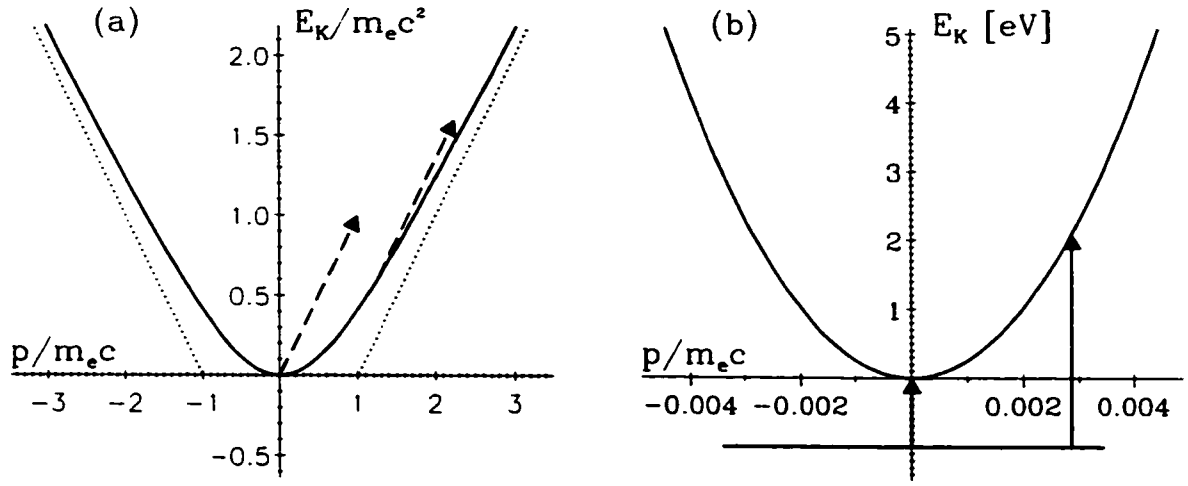

Figure 2.2: Illustration of the absorption of a photon by an electron. (a) A free electron cannot absorb a photon (dashed arrow) because the process takes it off the energy-momentum conservation curve (solid curve). (b) The momentum of a bound electron does not take on a well defined value, but rather a range of values. The absorption of a photon between the bound state and a range of continuum states is then possible. However, as the photon energy increases the overlap integral in Equation 2.1 decreases and therefore so does the photoabsorption cross section.

where E_i and E_f are the initial and final relativistic energy states, i.e. such that $E^2 = p^2c^2 + m^2c^4$. Note that the slope of the energy-momentum curve of a free electron (parabolic-like curve in Figure 2.2) never exceeds c. Therefore the line $E_{photon} = h\nu = cp_{photon}$, which has slope c, represents the absorption of a photon from an initial continuum state and always lies inside the free electron curve.[5] Therefore a photon can never connect two states of the free electron continuum, and hence a free electron cannot absorb (or emit) a photon.[6] This situation is depicted graphically in Figure 2.2a.

Now let us consider the situation where the electron is initially in a bound

[5]Note that if we had instead used the classical expression for energy $E = p^2/2m$ then $h\nu = \pm(2mc^2 - p_ic)$ would be a solution to the system of equations. However this requires that $|p_f| = |2mc - p_i| \Rightarrow v \geq c$, which is clearly not valid. The discussion in Reference [8], which uses conservation of classical energy, is misleading in this sense.

[6]A "free" electron can absorb a photon in an inverse Bremsstrahlung process, but only if it is simultaneously accelerated by an external field (for example in the field of a nearby ion).

state. The significant difference is that the momentum of a bound state is not well defined, but rather takes on a range of values. This can be easily understood on the basis of the uncertainty principle: $\Delta x \Delta p \gtrsim \hbar$. Estimating Δx for a bound state on the order the Bohr radius, we would expect significant reduction in cross section to begin at energies $\Delta p^2/2m_e$ on the order of a few eV. Simply put, the overlap of the initial and final states in momentum space is quite good for low photoelectron energies and the cross section is high. However, as the photon energy increases, the initial state appears increasingly as that of a free electron state to the photon, and the cross section rapidly decreases. This scenario is depicted in Figure 2.2(b).

Although the preceding discussion is clearly not quantitatively accurate, it gives a simple physical interpretation of a cause for the drop in cross section seen in Figure 2.1, sometimes referred to as a "breakdown" of the threshold model. More quantitative descriptions are given in the next section.

2.2 Corrections to the Wigner law in Single Photon Detachment

There are two theories which are commonly used to extend the range of the Wigner law: the short-range potential correction by O'Malley [10] and the leading-term correction by Farley [11]. There appears to be some confusion in the literature with respect to which correction should be applied in which case, and often little or no justification is given for their application. In an attempt to clarify the impact of these theories on threshold measurements, the two theories will be summarized (Sections 2.2.1 and 2.2.2) after being combined into one general expression (Equation 2.5), and finally they will be compared and contrasted (Section 2.2.3).

First, we generalize Equation 2.5 by including the short-range electron-atom

interaction in the final state. In the derivation of the Wigner threshold law, it was assumed (assumption 1 in Section 2.1.1) that the ejected electron does not interact with the residual neutral core. In fact, at small distances from the atom the photoelectron induces an electric dipole moment in the electron cloud of the atom. The electron therefore interacts weakly with the neutral atom via this induced dipole potential (which falls off as r^{-4} with electron-atom separation r). The electron can also interact with the permanent quadrupole moment of the neutral atom, assuming it is left in a non-symmetric state. O'Malley found that to correctly account for either of these short-range interactions, an additional term must appear in the threshold law expansion.[7] Including O'Malley's correction, Equation 2.3 should therefore be changed to read (using $\hbar^2 k^2 = 2m_e\,\varepsilon$):

$$\sigma_d = A'_\circ\, k^{2\ell+1} \left[1 - (B_\ell^{dp} + B_\ell^{qm})\, k^2 \ln \mathrm{a}_\circ k - (C^{sr} + C_{\ell_\circ}^{lt})\, k^2 + \mathcal{O}(k^4)\right]. \qquad (2.5)$$

Where $\mathrm{a}_\circ$ is the Bohr radius (see Appendix A), $A'_\circ = A_0\,(\hbar^2/2m)^{\ell+\frac{1}{2}}$ is the coefficient of the Wigner law, and $\mathcal{O}(k^4)$ represents further corrections on the order of k^4 or higher. The $k^2 \ln \mathrm{a}_\circ k$ term, which did not appear in Equation 2.3, is due to the short-range electron-atom final state interactions and is discussed in Section 2.2.1. The coefficient of the k^2 term is essentially A_1 of Equation 2.3 separated into two components, the first (C^{sr}) is again due to the short-range potential, while the second ($C_{\ell_\circ}^{lt}$) is due to the *leading term* correction of Farley's theory, discussed in Section 2.2.2. Although in some cases we may expect one coefficient to dominate the correction terms, usually the k dependence of $k^2 \ln \mathrm{a}_\circ k$ and k^2 cannot be distinguished for any reasonable energy range, and both terms should be included. As we shall see, the two theories explore two extreme situations, that of large or small polarisabilities,

[7] Since the quadrupole potential falls off as r^{-3} while the induced dipole polarisability potential falls off as r^{-4}, one might expect a different energy dependence for the two interactions. However, it turns out that the leading term obtained from the quadrupole interaction vanishes, and the first non-zero term is the same order as it is in the dipole interaction [10].

and are therefore in a sense incompatible. It may therefore be overly optimistic to expect Equation 2.5 to exactly describe the near-threshold behaviour. However, it is reasonable to assume that any cross terms which may arise for the intermediate situation should also be on the order of k^2 or higher and can be absorbed into C^{sr}, which is undetermined in any case (see below).

2.2.1 Effects of the Short-range Potential – O'Malley's Correction

O'Malley [10] determined an explicit expression for the magnitude of the *polarisability term*:

$$B_\ell^{dp} = \frac{4\alpha}{a_o(2\ell+3)(2\ell+1)(2\ell-1)}, \tag{2.6}$$

where α is the *static dipole polarisability*[8] of the neutral. For atoms in the ground state, α falls in the range of ≈ 1 to $500 \times a_o^3$, but can be much larger for excited states. (Values of α are tabulated for the ground states of most neutral atoms, see for example [12].) O'Malley also considered the effect of a permanent *quadrupole moment* of the neutral (not to be confused with the *quadrupole polarisability*) and found it to introduce the same energy dependence on the photodetachment cross section with a magnitude B_ℓ^{qm}. O'Malley did not give general expressions for this coefficient, but only for the s-wave detachment case:

$$B_0^{qm} = -\frac{19}{210}\left(\frac{Q_{av}}{q_e a_o}\right)^2, \tag{2.7}$$

[8]There seems to be some confusion about the use of the term "polarisablility" in the literature. In principle it should refer to the proportionality constant relating the dipole moment $\vec{d}$ to the applied electric field $\vec{E}$, i.e. $\vec{d} = \alpha_o \vec{E}$. This gives α_o the SI units of Cm^2/V (see for example [9]). However, O'Malley and Farley both (implicitly) call the polarisability $\alpha = \alpha_o/4\pi\epsilon_o$ (where ϵ_o is the permitivity of free space), giving α the SI units of m^3. Usually polarisabilities are given in cgs or atomic units (where $4\pi\epsilon_o = 1$) in which case α_o and α are admittedly equal, but one should be aware of this misleading use since the authors imply arbitrary units. For consistency with previous works, this somewhat incorrect notation will also be used here, with the understanding that $\alpha = \alpha_o/4\pi\epsilon_o$.

where the average quadrupole moment (Q_{av}) can be calculated from the value of the quadrupole moment (Q) of the $M = J$ magnetic sublevel through,

$$Q_{av}^2 = \frac{(J+1)(2J+3)}{5J(2J-1)} Q^2 . \tag{2.8}$$

However, typically the amplitude of the quadrupole correction is much smaller than B_ℓ^{dp}, and can usually be ignored [10,11,13, see also Chapter 4].

Since the polarisation correction term depends only on α, which can be determined experimentally or calculated, it would appear to be completely determined. However, the $k^2 \ln a_o k$ energy dependence is of the same order as k^2 for any typical range of energies. Furthermore, the short range potential also introduces a term which depends on k^2 with an amplitude of C^{sr}. Presumably C^{sr} also depends on α and Q, but expressions are not available for the magnitude, and it must therefore be considered as a fitting parameter.

2.2.2 Zero Core Contribution Approximation – Farley's Correction

In 1989, Farley [11] determined the coefficient A_1 of the k^2 order correction term (of Equation 2.3), under the zero core contribution (ZCC) approximation [14], which assumes that the core does not interact with the ejected electron (therefore e.g., $\alpha = 0$ and $Q_{av} = 0$). His derivation connects with the qualitative discussion of Section 2.1.2 through the parameter $\gamma = \sqrt{2m_e \varepsilon_o}/\hbar$, given that $1/\gamma$ is approximately the spatial extent of the initial wave function. For convenience his results are summarized here, albeit in a somewhat more compact form. With ℓ_o, the angular momentum of the bound electron to be detached (not to be confused with the angular momentum of the photoelectron $\ell = |\ell_o \pm 1|$), r_o the radius of the atomic core, and $x = \gamma r_o$, then

we can write his results as follows[9]:

for $\ell_o = 0$ (detachment of an s-orbital electron),

$$C_0^{lt} = \frac{x^5 + 20x^4 + 80x^3 + 240x^2 + 480x + 480}{20\gamma^2 (x^3 + 3x^2 + 6x + 6)}; \tag{2.9a}$$

for $\ell_o = 1$ (detachment of a p-orbital electron),

$$C_1^{lt} = \frac{x^4 + 5x^3 + 15x^2 + 30x + 30}{3\gamma^2 (x^2 + 3x + 3)}; \tag{2.9b}$$

and finally for $\ell_o = 2$ (detachment of a d-orbital electron),

$$C_2^{lt} = \frac{x^5 + 8x^4 + 35x^3 + 45x^2 + 210x + 210}{5\gamma^2 (x^3 + 6x^2 + 15x + 15)}. \tag{2.9c}$$

Note that since the detachment of an electron from an f-orbital ($\ell_o = 3$) has never been observed (see also Chapter 6), there was little motivation to calculate the correction terms for $\ell_o \geq 3$.

2.2.3 Remarks on Single-photon Detachment

Strictly speaking, the preceding sections apply only to single-photon detachment processes. Figure 2.3 presents these threshold laws for parameters typical of negative ions. Near the threshold we can assume $a_o k \ll 1$ (i.e. $\varepsilon \ll \hbar^2 k^2 / 2m_e \approx 27$ eV), then $\ln a_o k < 0$. Therefore the polarisation term decreases the near-threshold cross section for $\ell = 0$ (s-wave) and increases it for all other partial waves $\ell > 0$. On the other hand, the leading term correction derived by Farley always decreases the cross section, as one might expect from the discussion in Section 2.1.2. Also important is the way in which the two corrections scale with photon energy. While the O'Malley correction is independent of the threshold energy (it only depends on the photoelectron energy, ε), the Farley correction depends on the *relative* energy above threshold,

[9]The theory is in general applicable when $x < 1$. (The parameter r_o must be deduced from other experimental or theoretical knowledge of the system.)

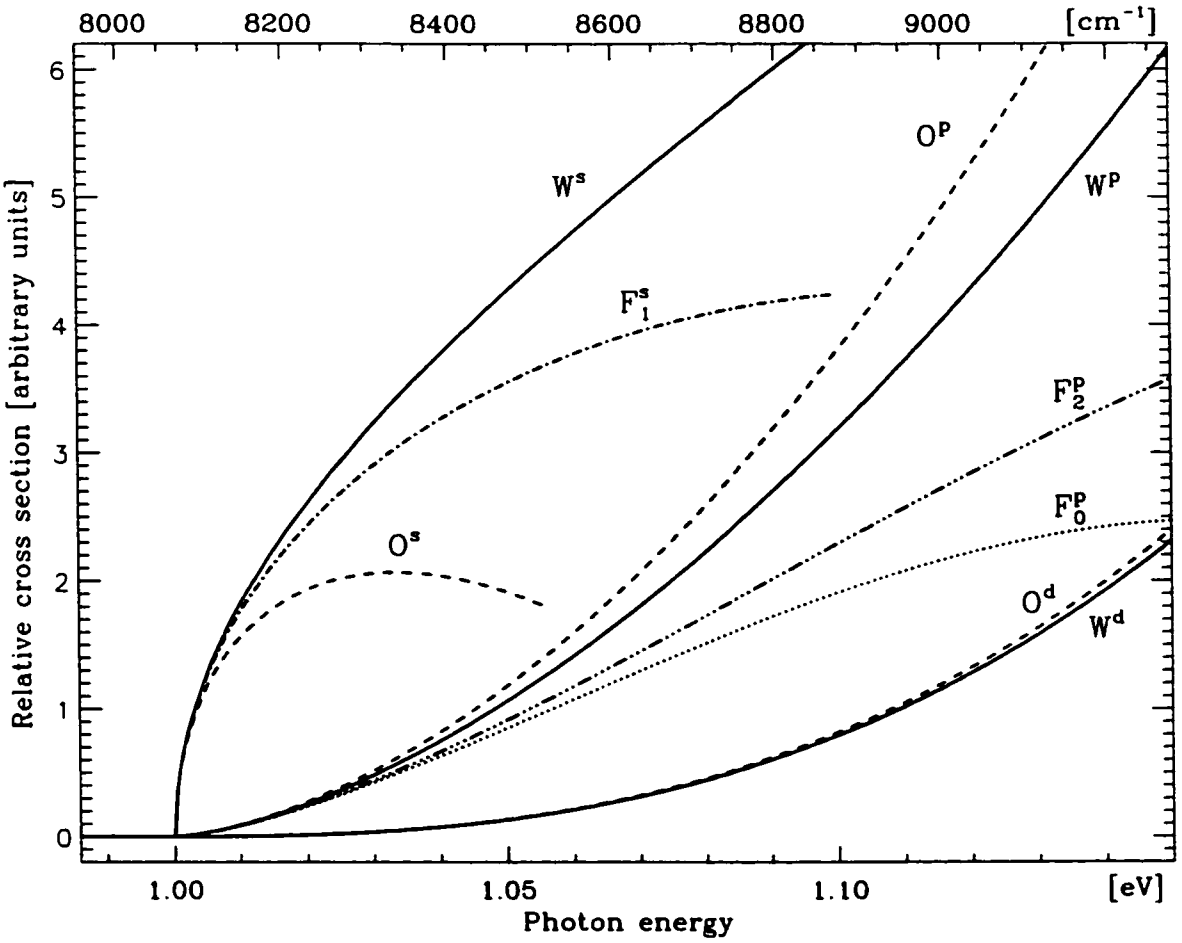

Figure 2.3: Threshold laws for detachment from a "typical" negative ion with a 1 eV threshold energy. Full curves (——) are the Wigner law (labeled W) and dashed curves (– – –) include the polarisability term by O'Malley (labeled O), assuming $\alpha = 40\,a_o^3$. Threshold laws including Farley's leading term correction (with $r_o = 3\,a_o$) are labeled with an F. The superscripts indicate the angular momentum of the photoelectron: s, p, or d for $\ell = 0$, 1, or 2 respectively; while a subscript gives the value of ℓ_o where applicable. Although partial waves with $\ell > 1$ are in principle possible, such as the *d*-wave shown here, none have been observed. The cross section scale between each set of the partial waves has been arbitrarily normalized.

since $B_{\ell_o} k^2 \propto k^2/\gamma^2 = \varepsilon/\varepsilon_o$. The polarisation term should then be more significant when the threshold energy is large, while for weakly bound species we might expect the leading correction term to be dominant.

We are now in a position to begin to answer the question of how far above

threshold the Wigner law applies. As a general "rule of thumb", based on a deviation of 10% from the Wigner law prediction with $\alpha = 40\,a_o^3$ and $r = 3\,a_o$, the polarisation term becomes important at $\varepsilon \approx 50$ or 350 cm^{-1} for s- or p-wave detachment respectively, while the leading term correction becomes important at $\varepsilon \approx 0.025 \times \varepsilon_o$. However, it is important to note that although these correction terms do have good qualitative agreement, and reasonable quantitative agreement, with observation they do not appear to be accurate enough to rely on in general for high precision experimental determination of the threshold energy. Therefore, to ensure that the Wigner law is applicable, a range only very near the threshold should be used when determining the threshold energy. These issues will be considered in more detail in Chapters 4 and 6.

2.3 Multiphoton Thresholds

Multiphoton detachment of atomic negative ions have attracted much interest in both theoretical and experimental contexts. Due to the selection rules, more continuum and bound state structures are potentially accessible using multiphoton processes instead of a single-photon process. For example, two-photon electric dipole (E1) transitions can be driven between same-parity bound states to study negative ion structure [15]. Also, excess photon detachment in negative ions (equivalent to above threshold ionization in neutral atoms) continues to be an area of active research [16 -19]. As an example with respect to theory, in addition to proposing a multiphoton scheme to observe the ^1S and ^1D resonant states in H^- [20], Crance performed extensive calculations on multiphoton detachment cross sections, excess photon detachment, and photoelectron angular distributions in H^- [21] and the halogen negative ions [22–24]. However, we are primarily interested here in the general behaviour of

multiphoton detachment, especially at energies relatively near to the threshold. In particular, we shall focus on the recent theory by Gribakin and Kuchiev.

In 1997, Gribakin and Kuchiev [25] put forward a very general theory to determine cross sections for multiphoton detachment processes. Although their theory can also predict absolute cross sections, we will be primarily concerned with relative cross sections here. The theory is made possible owing to two features of the multiphoton detachment process:

1. The electron is far from the atom when the multiphoton detachment process is said to take place.

2. The photon energy of the detaching field is much smaller than the binding energy of the negative ion: i.e., $h\nu \ll \varepsilon_o$.

Point 1 results from the fact that, in the length gauge, the interaction potential of the laser field with the electron is proportional to the electron-atom separation, and thus large distances are weighted more strongly than small ones. As a result, the asymptotic behaviour of the bound-state wave function is more important than it is near the atomic core. Also, the final state of the electron is well described by the Volkov wave function [27]. Since the details of the wave function near the atomic core are not critical, the effects of a short-range potential can largely be ignored, and the Gribakin and Kuchiev multiphoton theory neglects electron correlation effects.

Point 2 arises because an n-photon detachment process requires $nh\nu \geq \varepsilon_o$. In typical experiments, the detachment process would be observed somewhere between the n-photon channel opening and the $(n-1)$-photon channel opening. The photon energies of interest are then $h\nu \leq \varepsilon_o/(n-1)$. For large n, this leads to $h\nu \ll \varepsilon_o$. As a result, the field varies slowly compared to the electron's orbital period and the

detachment process is adiabatic. The use of adiabatic theory greatly reduces the complexity of the problem. However, this situation can hardly be considered to be true for small n, e.g. $h\nu \sim \varepsilon_o$ if $n = 2$ or 3, and the theory is indeed less accurate in this regime.

The general results of the theory predict interesting structure in multiphoton detachment. For example, oscillations in the photodetachment cross section are expected in the angular distribution. The oscillations result from interference between two classical escape trajectories for the photoelectron, which correspond to the two times of highest detachment probability within each period of the oscillating field: when the magnitude of the E-field reaches its extrema. However, we shall be concerned here with the variation of the total detachment cross section with photon energy, where this particular effect is not observed. There is nonetheless important structure in the total detachment cross section, which arises from the fact that more than one partial wave can be present. The total multiphoton cross section, integrated over all photoelectron ejection angles, is given by [26]:

$$\sigma_n = \begin{cases} 0 & (\tilde{\varepsilon} \leq 0) \\ a_n \dfrac{\tilde{\varepsilon}\, e^{2\tilde{\varepsilon}}}{(h\nu)^{2n-\frac{1}{2}}} \mathcal{F}_{n\ell_o}(\tilde{\varepsilon}) & (\tilde{\varepsilon} > 0) \end{cases} , \tag{2.10}$$

where $\tilde{\varepsilon} = (nh\nu - \varepsilon_o)/h\nu$ is the photoelectron energy in units of the photon energy and,[10]

$$\mathcal{F}_{n\ell_o}(\tilde{\varepsilon}) = \int_{-\sqrt{\tilde{\varepsilon}}}^{\sqrt{\tilde{\varepsilon}}} \frac{e^{2(z^2-\tilde{\varepsilon})}}{\sqrt{1-z^2}} \left\{ P_{\ell_o}\left(1 + \frac{2(\tilde{\varepsilon} - z^2)}{n - \tilde{\varepsilon}}\right) + (-1)^{n-\ell_o} \cos\left[(2n+1)\tan^{-1}\left(\frac{z}{\sqrt{n-z^2}}\right) + 2z\sqrt{n-z^2}\right]\right\} dz ,$$

given that P_{ℓ_o} are the Legendre polynomials: e.g., $P_0(x) = 1$, $P_1(x) = x$, and $P_2(x) = (3x^2 - 1)$. Due to contributions from larger partial waves to the to-

[10]Note that $F_{n\ell}(\tilde{\varepsilon})$ of Reference [26] equals $\sqrt{\tilde{\varepsilon}}\,\mathcal{F}_{n\ell_o}(\tilde{\varepsilon})$. The form of $\mathcal{F}_{n\ell_o}(\tilde{\varepsilon})$ has also been simplified with a change of variable $z = x\sqrt{\tilde{\varepsilon}}$. All other differences are purely cosmetic.

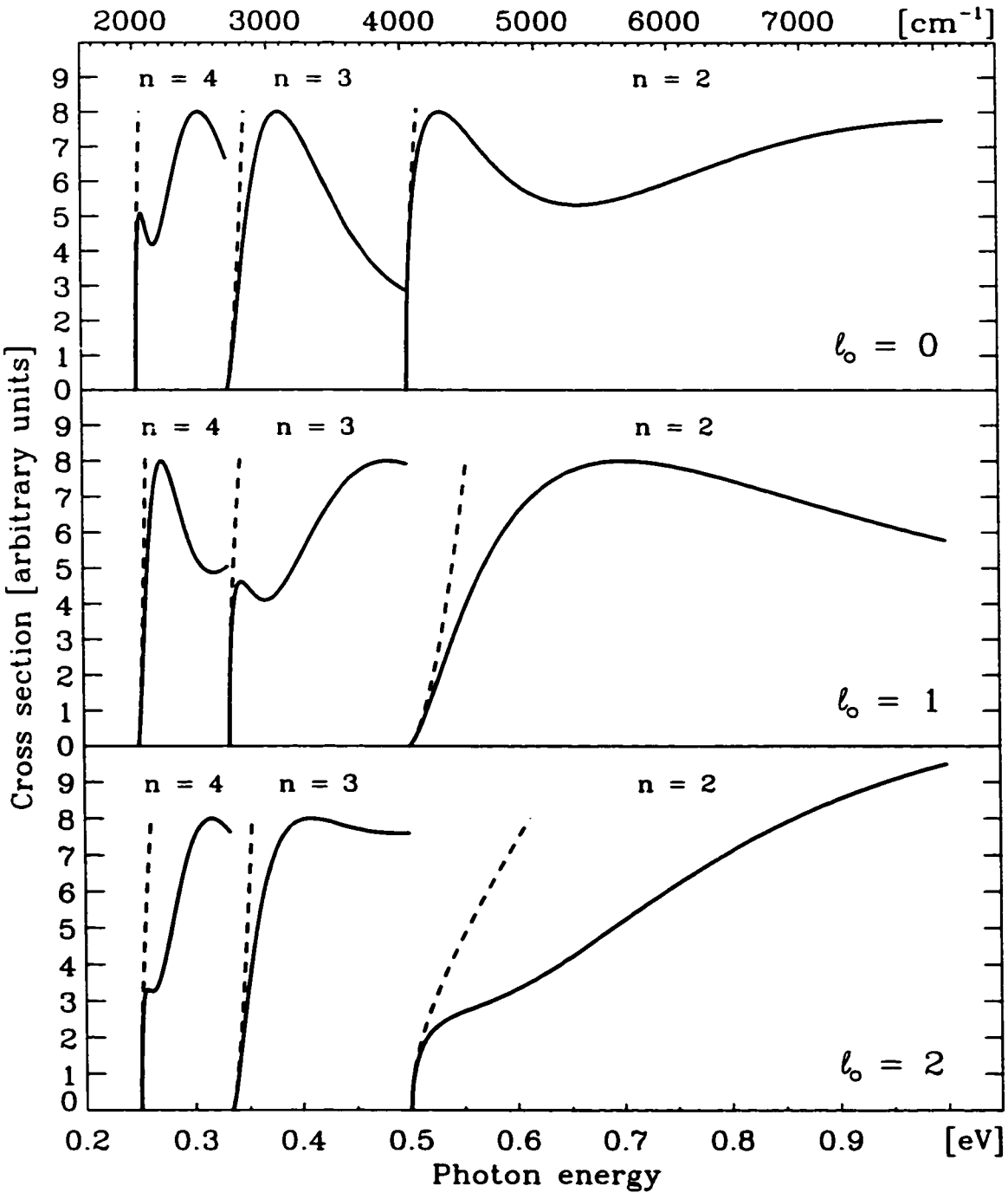

Figure 2.4: Multiphoton detachment of a negative ion with a 1 eV binding energy. Full curves (——) are based on theory by Gribakin and Kuchiev. Dashed curves (- - -) are Wigner laws. The amplitudes of the curves have been arbitrarily scaled.

tal cross section, $\mathcal{F}_{n\ell_o}(\tilde{\varepsilon})$ oscillates with increasing $\tilde{\varepsilon}$. As might be expected from semiclassical arguments, a maximum is reached whenever $pR \approx \hbar(\ell + \frac{1}{2})$, where $R = (2\hbar/\pi)\sqrt{2n/m_e h\nu}$ is the characteristic distance for the detachment process [26]. (For typical binding energies and photon energies of interest: $nh\nu \approx \varepsilon_o \approx 1$ eV, then $R \approx 4.7a_o \times n$.) Thus the maxima are reached when $\tilde{\varepsilon} \approx 0.62(\ell + \frac{1}{2})^2/n$, or equivalently when $h\nu \approx n\varepsilon_t / \left[n^2 - 0.62(\ell + \frac{1}{2})^2\right]$. The oscillations give rise in turn to oscillations in the total cross section at approximately the same energy. Since Gribakin and Kuchiev do not produce plots for the total detachment cross section, they are produced here for a few cases of general interest: detachment from *s*-, *p*-, and *d*-orbitals in 2-, 3-, and 4-photon processes (see Figure 2.4). In general, for the intensities typical for the McMaster experiments, the observed photodetachment signal decreases substantially with increasing n, and so only detachment from the lowest order process can be readily observed. The detachment cross section for a particular channel is therefore only shown up to the next lower order channel opening, e.g. 2-photon detachment is shown up to the single photon threshold. Also note that with knowledge of the asymptotic parameter of the bound-state radial wave function, a_n of Equation 2.10 can be determined, and therefore so can the absolute magnitude of the cross section.

As noted above, Equation 2.10 is less accurate for smaller n. This theory was compared with more involved perturbation theory calculations in H^-, which include the effects of the short-range interaction between the photoelectron and the atomic core [25,28]. The agreement was within a few percent for large n ($n \geq 5$), and within 20% for $n = 3$. This magnitude for the deviations is also in line with the results of two-photon detachment studies on Au^-, presented in Chapter 6. Finally, the predicted magnitudes for the absolute cross sections are also in reasonable agreement with observed two- and three-photon cross sections, although they appear to

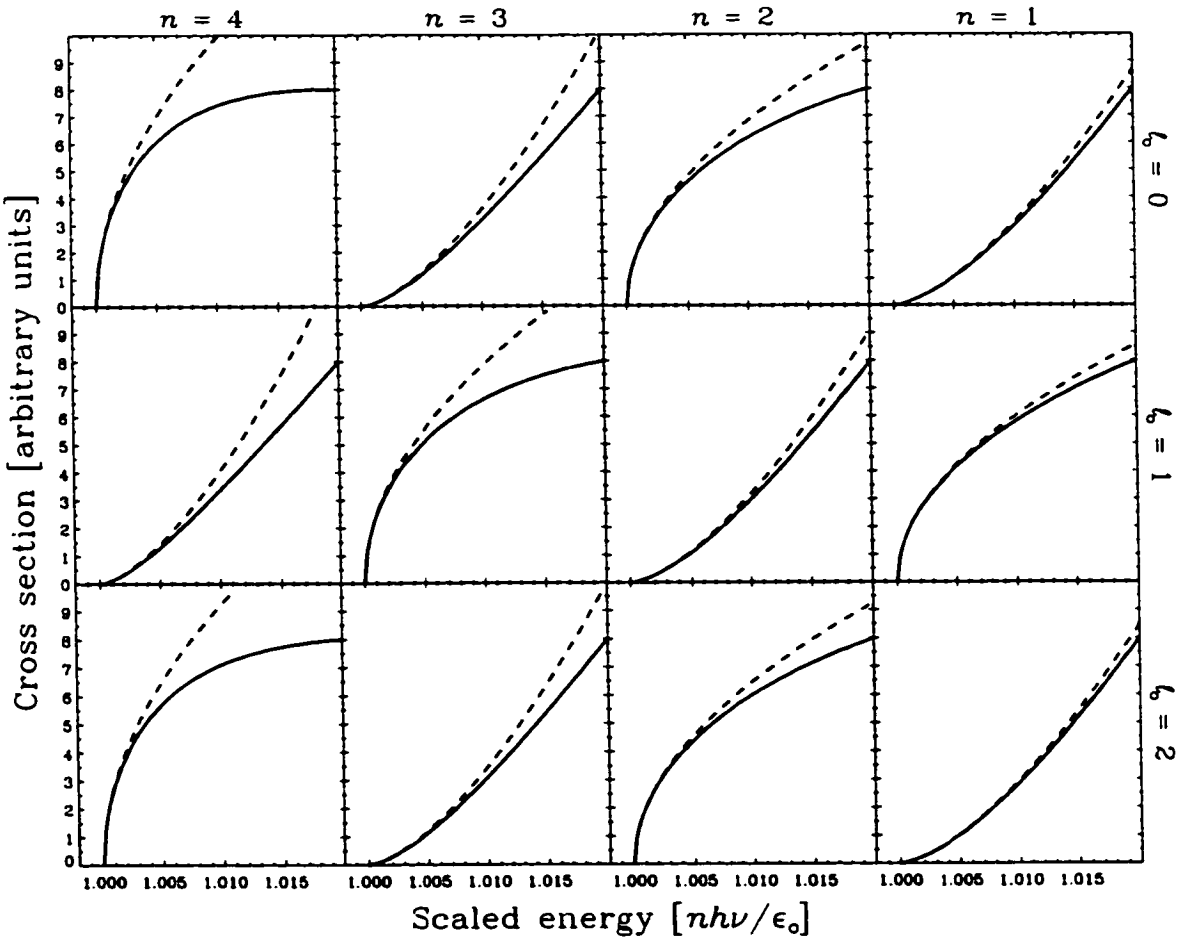

Figure 2.5: A comparison of single and multiphoton detachment thresholds. Full curves (——) with $n = 2$ to 4 are based on theory by Gribakin and Kuchiev; $n = 1$ are calculated using Farley's correction. Dashed curves (- - -) are Wigner thresholds. Note how the threshold law alternates between s-wave for even $n + \ell_o$ and p-wave for odd $n + \ell_o$. (The amplitudes of the curves have been arbitrarily scaled.)

be systematically larger than the measured values by a factor of about 2 to 6 [26].

Figure 2.5 shows the detachment cross sections near the threshold for a number of single- and multiphoton detachment processes. Equation 2.10 is used for multiphoton detachment, while for single-photon detachment Farley's leading term correction is used, since it most closely resembles the Gribakin and Kuchiev approach. The expected Wigner law behaviour, assuming the lowest partial wave is dominant, is

also plotted. In order to put the various detachment processes on an equal footing for comparison, the photon energy has been scaled to the n-photon detachment threshold, $\varepsilon_t = \varepsilon_o/n$. These plots clearly show that the threshold structure is dependent on the order of the detachment process, as well as the bound-state orbital angular momentum. However, only s- and p-wave detachment thresholds are observed for both single and multiphoton detachment. Also note that the cross sections appear to diverge from the Wigner threshold law considerably faster as the order of the process increases. These points will be discussed further in Chapter 6.

2.4 References

[1] H. A. Bethe and E. E. Salpeter, *Quantum Mechanics of One- and Two- Electron Atoms* (Plenum, New York, 1977).

[2] M. Ya. Amusia, N. B. Avdonina, E. G. Drukarev, S. T. Manson, and R. H. Pratt, Phys. Rev. Lett. **85**, 4703 (2000).

[3] E. P. Wigner, Phys. Rev. **73**, 1002 (1948).

[4] H. Hotop and W. C. Lineberger, J. Chem. Phys. **58**, 2379 (1973).

[5] H. Friedrich, *Theoretical Atomic Physics* (Springer-Verlag, New York, 1991); see especially section 4.3.

[6] J. R. Smith, J. B. Kim, and W. C. Lineberger, Phys. Rev. A **55**, 2036 (1997).

[7] L. M. Branscomb, D. S. Burch, S. J. Smith, and S. Geltman, Phys. Rev. **111**, 504 (1958).

[8] C. Cohen-Tannoudji, J. Dupont-Roc, and G. Grynberg, *Atom-Photon Interactions: Basic Processes and Applications* (Wiley, New York, 1992).

[9] D. J. Griffiths, *Introduction to Electrodynamics*, Second Edition (Prentice Hall, New Jersey, 1989).

[10] T. F. O'Malley, Phys. Rev. **137**, A1668 (1965). Note: the polarization term appears with the incorrect sign in O'Malley's paper. This error was noted by Hotop and Lineberger in Reference [4].

[11] J. W. Farley, Phys. Rev. A **40**, 6386 (1989).

[12] V. P. Shevelko, in *Atoms and Their Spectroscopic Properties*, edited by G. Ecker, P. Lambropoulos, I. I. Sobel'man, H. Walther, and H. K. V. Lotsch (Springer, New York, 1997).

[13] R. D. Mead, Keith R. Lykke, and W. C. Lineberger, in *Photodetachment Threshold Laws*, Invited papers of the XIII International Conference on the Physics of Electronic and Atomic Collisions, Berlin, 1983, edited by J. Eichler, I. V. Hertel, and N. Stolterfoht, (Elsevier Science, New York, 1984).

[14] R. M. Stehman and S. B. Woo, Phys. Rev. A **20**, 281 (1979).

[15] M. Scheer, H. K. Haugen, D. R. Beck, Phys. Rev. Lett. **79**, 4140 (1997).

[16] L. Præstegaard, T. Andersen, and P. Balling, Phys. Rev. A **59**, R3154 (1999).

[17] H. Stapelfeldt and H. K. Haugen, Phys. Rev. Lett. **69**, 2638 (1992).

[18] M. D. Davidson, H. G. Muller, and H. B. van Linden van den Heuvell, Phys. Rev. Lett. **67**, 1712 (1991).

[19] H. Stapelfeldt, P. Balling, C. Brink, and H. K. Haugen, Phys. Rev. Lett. **67**, 1731 (1991).

[20] M. Crance, J. Phys. B **21**, L557 (1988).

[21] M. Crance and M Aymar, J. Phys. B **18**, 3529 (1985).

[22] M. Crance, J. Phys. B **21**, 3559 (1988).

[23] M. Crance, J. Phys. B **20**, 6553 (1987).

[24] M. Crance, J. Phys. B **20**, L411 (1987).

[25] G. K. Gribakin and M. Yu. Kuchiev, Phys. Rev. A **55**, 3760 (1997).

[26] G. K. Gribakin and M. Yu. Kuchiev, J. Phys. B **30**, L657 (1997).

[27] D. M. Volkov, Z. Phys **90**, 250 (1935).

[28] C. Laughlin and S. I. Chu, Phys. Rev. A **48**, 4654 (1993).

Chapter 3

Experimental Method

The experimental setup and method are discussed in the papers which are reproduced in this thesis. However, often only the elements essential for the particular experiment are discussed. The purpose of this chapter is therefore to give a more complete discussion of the experimental technique. The apparatus is illustrated in Figure 3.1. A mass-analysed negative ion beam extracted from a Cs sputter source is crossed at 90° with a pulsed laser beam. The neutral atoms produced in the photodetachment process are then detected with a discrete-dynode electron multiplier detector. The ion beam apparatus, including the data acquisition system, is described in Section 3.1.1, followed by a description of the laser source in Section 3.1.2. Section 3.2 describes the data collection and analysis including the various data corrections which may be required in some experiments due to the presence of background signal or laser pulse-energy variations. The final section of this chapter (Section 3.3) discusses the various experimental uncertainties associated with the apparatus and data collection technique. Additional details can also be found in theses recently written by members of the McMaster group [1–3].

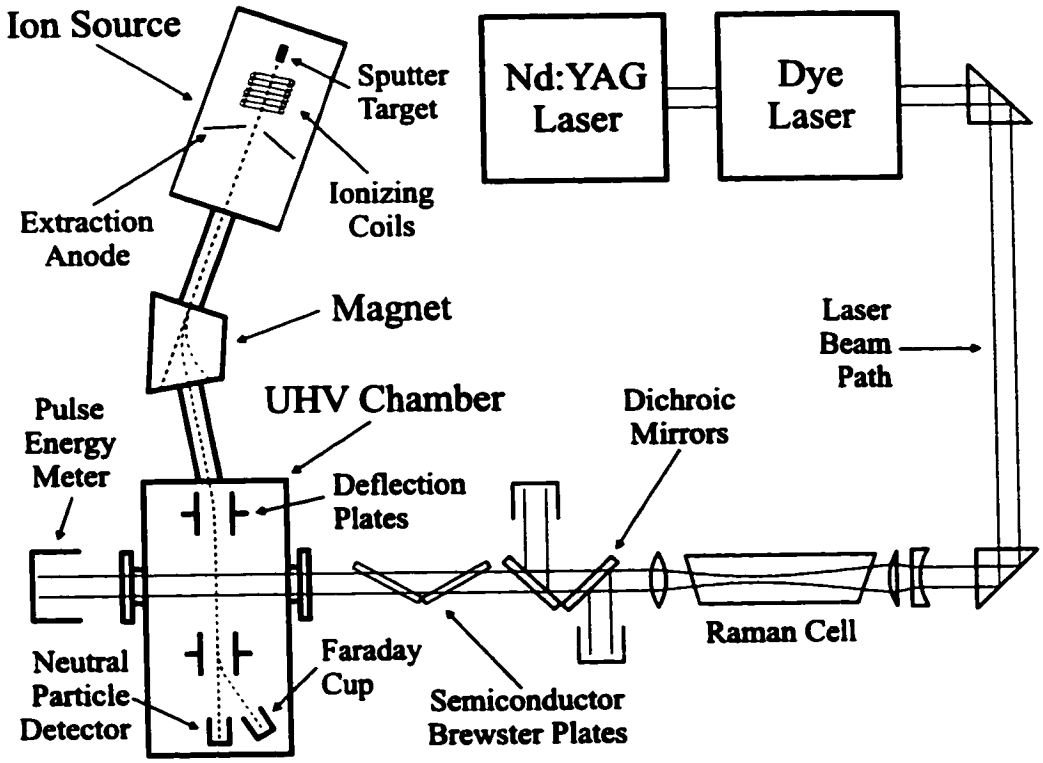

Figure 3.1: Schematic of the experimental apparatus. Details are discussed in the text.

3.1 Experimental Apparatus

3.1.1 The Negative Ion Apparatus

The ions are produced with a high-intensity Cs sputter source, based on the source developed by Middleton. Details of the Middleton Cs sputter source operation can be found in [4]. The procedure of obtaining a negative ion beam from a sputter source, followed by a description of the neutral particle detection system, with details specific to the McMaster apparatus are given in this section.

The Sputter Source

A boiler containing Cs (not shown in Figure 3.1) introduces Cs vapor into the evacuated (pressures of $\lesssim 10^{-6}$ mbar) source chamber. The purpose of the Cs vapor is

twofold. Firstly, a heated ionizing coil constructed of tantalum ionizes some of the Cs to form Cs^+ ions. A potential bias (typically 2 to 6 kV) applied between the ioniser and the target cathode accelerates (and focuses) the ions toward the cathode, thus sputtering material from its surface. Secondly, a layer of cesium condenses on the surface of the target cathode, which is kept cool by an external chilling unit. This Cs layer reduces the work function of the sputter surface, thereby greatly increasing the probability that the sputtered atoms and molecules will leave with an additional electron — i.e. as negative ions.

Negative ions of many elements of the periodic table can be produced simply by changing the material of the cathode. In most cases, the cathode is constructed of the element of interest either consisting of a pure solid metal sample, or a powder or granular sample (often mixed with silver powder) compacted into an aluminum or copper sleeve.[1] For materials with poor thermal conductivity or low melting points, a compound rich in the element of choice but having more suitable properties can be used. In many cases the work by Middleton, who systematically applied Cs sputter technology to the production of a wide range of negative ions [5], was found to be a good guide for the selection of cathode materials. Often the sputtering process will be inefficient or unstable until a sputter crater is formed on the cathode. A new cathode is therefore usually "burnt in" for a period of hours or even days before an experiment is run. It is also frequently observed that contaminant ions are greatly reduced after this burn-in period.

The population of the excited states (if any) of the negative ions typically obeys a Boltzmann distribution. The effective temperature for the distribution depends largely on the sputter area, which in turn depends sensitively on the position of

[1]See further comments on the cathode construction in Section 3.2.1, in particular page 45. See also comments in Appendix B.

the cathode. Experience with the McMaster source has indicated that temperatures ranging between 500 and 1500 K are possible while maintaining reasonable ion beam currents. A lower temperature is desirable for studies on the ground states of negative ions, as this leads to lower background signal from the excited states. On the other hand, larger excited-state populations can be obtained with higher sputter temperatures, which is favourable for studies on these states. This simple means of varying the thermal populations of the ionic states was therefore exploited in a number of experiments (e.g. Section 4.1.3).

The Ion Beam

The negative ions formed by the sputter process are accelerated back across the ioniser-cathode bias, focussed by an electrostatic Einzel lens (not shown in Figure 3.1), and accelerated by an additional extraction voltage to reach a total energy of 8 to 20 keV. In addition to the element of interest, negative ions are also formed from contaminants present in the cathode material and from the background gas. The ion beam is therefore mass-analysed by 30° deflection in a magnetic field of up to 5.2 T, which allows a mass discrimination level better than $\approx 5\%$.

Since negative ions can be easily destroyed by collisions with the background gas, the ion beam is directed through a differential pressure tube into an ultra high vacuum (UHV) chamber where a turbo-molecular pump is used to maintain pressures of $\lesssim 10^{-8}$ mbar in the UHV chamber. Electrostatic deflection plates positioned just prior to the interaction region deflect the ion beam by 10°, thus eliminating any neutral particles produced by collisions with the background gas up to that point. In the interaction region the ion beam is crossed (at 90°) with a laser beam (see Section 3.1.2) and photodetachment can take place. A second set of deflection plates are used to deflect the residual negative ion beam into a Faraday cup, where the ion

current can be monitored.[2] Any neutral particles produced by the photodetachment process which are not deflected by the plates are detected with a discrete-dynode electron multiplier.

The Detection Electronics

Electronic noise is minimized by first amplifying the signal obtained from the neutral particle detector with a fast preamplifier (EG&G). A factor of 20 or 200 is used, depending on the signal level. Since typically more than 1 photodetachment event is observed per laser pulse, analog data collection is used. The signal is then integrated over an ≈ 50 ns gate using a boxcar averager, and recorded on a personal computer. The gate size and delay ($1-2$ μs) are set to be synchronous with the laser pulse interaction events, so that collisional background events are suppressed. A narrow gate can also be used to obtain an additional mass discrimination to $\approx 2\%$, due to the time-of-flight difference associated with the different masses. This can further reduce background photodetachment events from nearly mass-coincident impurity ions.

3.1.2 The Laser Light Source

Arguably the most challenging aspect of negative ion LPTS experiments is the production of suitable tunable infrared laser light. The laser light in the McMaster setup is obtained using nanosecond technology. A neodymium doped yttrium-aluminum-garnet (Nd:YAG) laser is used to pump a dye laser that can produce high intensity, tunable, laser pulses in the visible and near-infrared. Often these pulses must be shifted further into the infrared by making use of a Raman cell, in which case the Stokes component of choice is selected using an appropriate set of filters. Details on

[2]Note that the laser light is on for only a total of 100 ns every second (see Section 3.1.2). Therefore, at most 10^{-5} percent of the ions are actually detached by the laser beam, well below the instrumental accuracy of the ion current measurement.

these steps can be found below. The laser light is then directed through a viewport to intersect with the negative ion beam. A second viewport allows the beam to exit the UHV chamber where the pulse energies can be monitored with a pyroelectric (Ophir) or volume-absorbing (Scientech) energy meter. Viewports made of AR-coated fused silica or, more typically, calcium fluoride (CaF_2) were used.

The Laser System

The output of a Q-switched (≈ 8 ns pulses) Lumonics YM-800 Nd:YAG laser operating at a 10 Hz repetition rate is frequency doubled to yield up to 400 mJ of 532 nm laser pulses. These 532 nm laser light pulses are used to pump a Lumonics HD-300 dye laser. Using an 1800 lines/mm grating in conjunction with visible and infrared laser dyes (especially the Exciton LDS series), continuous tunability up to wavelengths of 980 nm is obtained. This laser light can be used directly in experiments on some ions (see e.g. Section 4.1.2) but often even longer wavelengths are needed.

Raman Conversion

The high intensity ($\sim 10^7$ W peak powers) dye laser pulses can be focussed into a 120-cm-long high-pressure cell containing H_2 gas. Through a stimulated Raman scattering process, which involves the vibrational excitation of the H_2 molecules, some of the light is shifted to longer wavelengths. By observing well known [8] optogalvanically active lines with a hollow discharge lamp filled with argon (Hamamatsu), the resulting first Stokes field is measured to be shifted to lower photon energies by 4155.197(20) cm^{-1}, consistent with the expected shift of 4155.187(5) cm^{-1} for a H_2 pressure of 22 bar (see [6,7, and references therein]). Subsequent Raman scattering can shift the first Stokes field further into the infrared by intervals of the same energy, thereby producing second- and third-Stokes fields. However, parametric four-wave mixing of the dye laser

field with the first-Stokes field proceeds with a higher probability in the single-pass Raman cell design used here. This parametric mixing also leads to the formation of anti-Stokes fields, where the photon energy is *increased* beyond that of the dye laser light in intervals corresponding to the Raman shift. The phase-matching requirement of parametric mixing [9], and the small dispersion of H_2 gas, leads to the characteristic "doughnut" shape of the intensity profile observed in the second Stokes and the anti-Stokes beams.[3] Except for a reduction in focusing quality for the second Stokes beam, the intensity profile is largely inconsequential for the present purposes. Figure 3.2 summarizes the typical pulse energies observed for the dye laser (i.e. without a Raman cell), first Stokes (S1), and second Stokes (S2) pulses using this setup. The curves were produced based on actual pulse energies observed during various experiments. As can be seen from the figure, an uninterrupted range of wavelengths up to about 5 μm (2000 cm^{-1}) can be obtained with intensities sufficient for the present needs.

Stokes Selection

When a Raman cell is used, many laser fields are produced and the appropriate field must be selected for the experiment. This can be accomplished in two ways: by using dispersing elements (e.g. prisms or gratings) or with an optical filter system. Dispersing elements typically have excellent frequency separation capabilities and a high damage threshold. However, these systems inevitably produce variations in the beam alignment as the laser wavelength is tuned. For many experiments, it is imperative that the laser-ion crossing angle does not deviate from 90° (see Section 3.3.2), and variations are often unacceptable. A filter system is therefore preferred. Long-pass filters (Schott glass) are typically used for removing the residual dye laser light and

[3]It is important to note that stimulated Raman scattering and parametric mixing are coherent processes, and the Stokes and anti-Stokes fields otherwise largely retain the properties of the dye laser light.

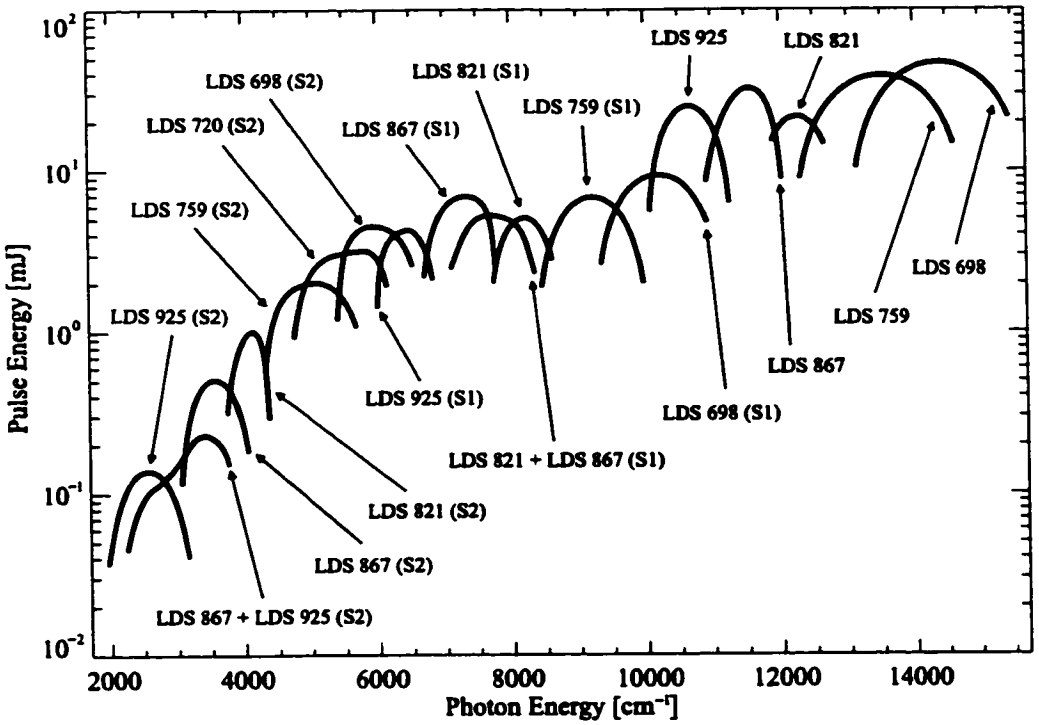

Figure 3.2: Laser pulse-energies observed with selected dyes. Included are pulse energies observed with first and second order Stokes conversion, annotated with (S1) and (S2) respectively.

anti-Stokes components in experiments where first-Stokes light is required. Removing the second Stokes beam is more difficult, requiring the use of typically inefficient short-pass filters. However, since the second Stokes beam has far lower photon-energies, this light cannot photodetach negative ions for which first Stokes radiation is required. The second-Stokes beam is therefore typically not removed.[4] For very weakly bound systems, which require the use of second Stokes radiation, dichroic mirrors are used to filter the first Stokes, anti-Stokes, and dye laser light fields with an efficiency of about 90%. Silicon or germanium semiconductor plates are then used to eliminate

[4]In cases of doubt, the spectrum is also taken with the second Stokes field removed to verify that the signal is indeed originating from the expected transition. For example, in Os^- unexpected structure was observed (see Section 5.1.2), and a verification of the effect of the second Stokes light was warranted.

the remaining light. The initial intensity reduction by the dichroic mirrors is required due to the low damage-threshold of semiconductor plates. All the optical filters are arranged at Brewster's angle in order to minimize reflection losses. The finite dispersion of optical elements can produce a small lateral displacement of the laser beam as the wavelength is tuned. To avoid this, all of the angled optical elements (e.g. the filters, UHV viewports, and Raman cell windows) are paired with a second similar element, tilted at a complementary angle, as shown in Figure 3.1.

3.2 Data Acquisition and Analysis

The laser system can be automated to scan over the region of interest. The photodetachment signal, laser pulse-energies, and ion beam current can be recorded in parallel. Typically the signal from 10 or 20 pulses is averaged per data point, with a total of about 10000 laser pulses generally accumulated for each scan. An additional dead time of a few minutes is required between the scans to verify experimental stability and to reset the laser scan. Each scan thus requires 20 to 30 minutes. The energy spacing of the data points depends largely on the required scan range for the measurement. When narrow structure is expected within a large scan range (e.g. in the case of Os^-, Section 5.1.2) then up to 5000 data points are accumulated per scan to obtain better energy resolution. The scan is generally repeated about 10 times in order to obtain an acceptable signal-to-noise ratio. Repeating the scan, rather than taking one long scan, also allows certain systematic errors to be eliminated and the stability of the system to be monitored over the course of the experiment. For example, in addition to the rare ion current fluctuation, long-term variations in the signal can also occur due to slow changes of the ion beam density distribution as material is slowly removed from the cathode during the sputter process. Thermal drift of the

magnet or laser system can cause the laser-ion overlap to change, producing long-term variations in the signal level. These effects can be monitored over the course of the experiment simply by comparing the individual scans.

3.2.1 Data Corrections

The collected data may need to be corrected for one or more effects, such as a background signal produced by collisional or photodetachment events from states other than the one under study. If a large range is scanned, the data may also need to be corrected for the observed variations in the laser pulse energy with wavelength. Finally, in a few cases very large detachment rates are observed, and it was necessary to correct for the effect of weak to moderate signal saturation. These data corrections are described in detail below.

Collisional Detachment and Electronic Noise

A source of background signal which is independent of laser tuning arises primarily from detachment events due to collisions of the ions with the background rest gas, but also from electronic noise. This background level is independent of the presence of laser light and is therefore determined by blocking the laser and collecting data over approximately 1000 to 2000 laser pulses. Numerous tests have shown that the background signal typically does not vary appreciably over the course of an experiment. Verification of the background level once immediately preceding and once immediately after the set of data scans is therefore usually sufficient. The data obtained from the separate scans are combined into a suitable number of bins and the measured background level is subtracted. This background signal is then easily removed and has no effect on the observed signal and data analysis, other than introducing a small amount of additional statistical noise.

Photodetachment Background

A second source of background signal may be observed from the detachment of a state or ion other than the one under investigation. This can be from the detachment of an excited state of the ion under investigation, or from the detachment of a mass-coincident or nearly mass-coincident impurity ion.

Signal arising from the detachment of excited states can be minimized by reducing the effective temperature of the sputter region (see Section 3.1.1), which favours the ground state population. Usually the states in question are well separated, and the excited state is detached far from its threshold energy, thus the cross section is relatively wavelength independent. The remaining weak signal therefore results in a flat or slightly sloped background signal which can be easily removed.

Although a mass resolution of up to 2% can be achieved with the present apparatus with a narrow gate set on the boxcar (see Section 3.1.1), for elements much heavier than than aluminum or silicon (28 mass units) this can still span more than one mass unit. On the other hand, even an energy resolution of 1 mass unit cannot guarantee that contaminants are absent, since in general molecular negative ions may exist whose mass is coincident with that of the element under study [13, 14]. Fortunately many molecular ions are strongly bound in comparison to atomic negative ions and the photon energy of the laser light used is too low to detach many of the potential contaminants. Nonetheless, a number of steps are taken to minimize the likelihood of molecular contaminants (see also Appendix B).

Firstly, the construction of the cathode is considered. Whenever possible, a pure sample of the element of interest is used as the target material, as this reduces the number of contaminant species which can be present in the beam. In cases where the mass resolution allows, a particular isotope of the element may be selected. For

example, in the study on boron (see Section 4.2.2) the ^{10}B isotope was selected in order to avoid possible contamination from $^{10}BH^-$ in the $^{11}B^-$ signal.[5] The target sample is mounted on a copper cylinder and the negative ions of copper clusters (Cu_n^-, with $n \geq 2$) are sometimes observed in the ion beam. When such a cluster lies near in mass to the element under study, aluminum is used instead of copper.

Secondly, the expected and observed detachment signals are compared. The vibrational and rotational structure of molecules tend to produce many closely spaced transitions, while atomic species tend to produce well isolated features. Oscillations in the cross section over relatively small wavelength ranges are also common for molecular ions (see for example [1,15]), but not for atomic negative ions. To verify that such structure is not present, a range of photon energies extending well below the detachment threshold is explored, where no detachment from the negative ion under study is observed. Since it is very unlikely that the signal from a contaminant would change significantly at precisely the position of detachment threshold under consideration, this is a good indication of the photodetachment background signal over the range of the scan.

For all the experiments presented in this thesis, the below threshold signal was very small[6] and therefore the effects of possible ionic contaminants is believed to be negligible. In all cases, a constant or slightly sloped line is found to accurately describe this background signal.

[5] In order to obtain a better $^{10}B^-$ current, an isotopically enriched sample of ^{10}B was used in the cathode.

[6] The data plots presented in this thesis (including the reproduced papers) have been scaled so that the observed below-threshold photodetachment background is equal to 1. This allows an easy evaluation of the observed signal-to-background ratio.

Pulse Energy Variations

Variations of the laser pulse energy with wavelength are inevitable. The main source of these variations is from the wavelength dependence of the gain of the laser dyes and the strong attenuation of light by air in some regions of the infrared, especially due to absorption by H_2O and CO_2. To minimize the effects of the latter, the entire optics table (including the exit of the dye laser, the Raman cell, the filters, and the pulse-energy meter) can be enclosed and continuously flushed with dry nitrogen gas. For scans spanning a large wavelength range, variation of the dye laser gain can lead to variations of pulse energy of up to 30% (see especially Section 5.1.2, Section 5.3, and Section 6.1). On the other hand, for high-precision threshold measurements only a region very near to the detachment threshold is generally scanned, and in most cases the pulse energy is reasonably constant over the scan range. Nonetheless, it is often desirable to correct for even very mild variations of pulse energies with wavelength.

Assuming the detachment probability is small (i.e., the signal is not saturated, see below), the single-photon detachment rate varies linearly with the pulse energy and the data can be corrected simply by dividing the observed signal, $N(h\nu)$, by the measured pulse energies, $E_p(h\nu)$: $N_c(h\nu) = N(h\nu)/E_p(h\nu)$. The corrected signal N_c is then proportional to the detachment cross section.

Signal Saturation

For larger detachment probabilities, saturation effects may become significant. Saturation of the detected signal can occur for two main reasons: (1) a signal which exceeds the linear dynamic range of the detector or detection electronics; or (2) a depletion of the ionic population. While the former is easily avoided by a careful selection of the preamplifier and sensitivity range, the latter is determined by the detachment probability.

To model signal saturation exactly, the velocity and density distribution of the ions as well as the intensity profile of the pulse must be taken into consideration. Detailed models of this sort have been used to determine the absolute cross section of negative ions by measuring the detachment signal with intensities large enough to saturate the detachment probability [10-12]. For the current purposes a simpler approximate model will suffice. If we assume a uniform illumination and ion density in the interaction region, then the signal observed from a single-photon detachment process with cross section σ_d is given by (see Appendix C):

$$N = N_0 \left(1 - e^{-\sigma_d P}\right). \tag{3.1}$$

If we further assume that the ions are essentially stationary over the ≈ 8 ns duration of the laser pulse, then the number of photons per unit area incident on the ions is:

$$P = \int_{pulse} \Phi \, dt = \frac{E_p}{S h\nu},$$

where Φ is the photon flux and S is the area of the laser beam cross section. The maximum signal obtainable, corresponding to the situation where all the ions are detached over the duration of the laser pulse, is given by N_0 and depends on the ion density, the ion-laser overlap, the efficiency of the detector, and the amplification of the detection electronics.

In general,[7] Equation 3.1 holds to a high accuracy over a very large range of pulse energies. By measuring the signal for a range of pulse energies, it is possible to fit the two parameters σ_d and N_0 to obtain estimates of the detachment cross section. This will be considered further in Chapter 5, especially Section 5.1.2 and Section 5.3. At the moment, we are interested in developing an expression that corrects the measured signal to obtain the signal that would have been observed if

[7] See comments in Appendix C, especially Section C.3.

no saturation and pulse-energy variations were present. This corrected signal is given by:

$$N_c = -\frac{N_\circ}{E_p} \ln\left(1 - \frac{N}{N_\circ}\right). \tag{3.2}$$

With this definition we have $N_c = \frac{N_\circ \sigma_d P}{E_p} = \frac{N_\circ}{S h\nu}\sigma_d$, which depends linearly on the detachment cross section and a few (reasonably constant) experimental parameters. The corrected signal can then be fit to the expected relative cross section behaviour, e.g. as given by the Wigner threshold law. When the detachment probability is very small ($N \ll N_\circ$) we have $\ln\left(1 - \frac{N}{N_\circ}\right) \approx -\frac{N}{N_\circ}$ and Equation 3.2 reduces to $N_c \approx N/E_p$, as argued above. Finally, notice that the actual detachment cross section σ_d is irrelevant for the correction. Therefore, assuming that the signal obtained in all regions of the scan is derived from the same initial ionic population, the saturation data needs to be obtained at only one wavelength of the scan range, usually where the largest detachment signal is observed.

It should be stressed that in general the issue of signal saturation is entirely avoided because signals only very near the threshold are measured, where the detachment probability is very small. However, when large variations of the detachment cross section are observed in the scan range, it is difficult to maintain good statistics in the regions of low cross section without saturating the signal in regions where the detachment cross section is high. In these cases, additional data can be collected with the laser wavelength set to a fixed wavelength while the laser pulse energies are varied. This data is then fit to Equation 3.1 to determine $N_\circ$ and Equation 3.2 is used to obtain a corrected signal. On the other hand, for very high detachment probabilities ($N/N_\circ \gtrsim 0.9$) the steep slope of the logarithm amplifies even small amounts of noise in the observed signal to the point of rendering the correction unreliable, and a compromise must be adopted.

3.3 Laser Calibration and Systematic Errors

The data corrections described above can lead to systematic errors. These errors are estimated by varying the correction parameters over a reasonable range to determine the possible error that the corrections could introduce. The sharp (infinite slope) onset of an s-wave threshold renders fits of s-wave thresholds quite insensitive to variations in background signal. However, due to the zero-slope onset of p-wave detachment, the fitted threshold position is very sensitive to variations in the background signal and an error in the determination of the photodetachment background signal can introduce a significant error in the determined threshold energy. Two approaches are used to estimate this error: a simultaneous fit of the background signal and above threshold signal, and a fit of the above threshold signal with various reasonable fixed (and possibly sloped) background levels. Errors introduced by uncertainties in signal saturation and pulse-energy corrections are of concern mostly in the investigations of the detachment threshold law itself (see Section 4.3 and Chapter 6), where the shape of the detachment curve is important, and in investigations covering large ranges of photon energies where pulse-energy and/or photodetachment cross sections have large variations (see Section 5.1.2 and Section 5.3).

Other experimental conditions which can produce systematic errors include laser calibration accuracy and thermal stability, Doppler shifts, and the possibility of ponderomotive shifts and *ac*-Stark shifts of the ionic and neutral states. The potential systematic errors associated with these issues are discussed below. The uncertainties associated with all final results quoted in this thesis include both the estimated systematic errors and the statistical uncertainty. All uncertainties are given to one standard deviation unless otherwise noted.

3.3.1 Laser Calibration and Thermal Stability

The dye laser is calibrated against accurately known optogalvanically active transitions in argon [8]. Although the line center of the transition can be determined to a very high precision, repeated measurements on any particular optogalvanic line indicate that the tuning mechanism can be reliably reset to an accuracy of about 0.01 cm^{-1}. In addition to this resetability of the tuning mechanism, comparisons between many lines reveal a small nonlinearity in the tuning mechanism of about 0.04 cm^{-1}. Similar local nonlinearities in the tuning mechanism were observed by measuring transmission through an etalon over small energy regions (10 to 100 cm^{-1}) at a variety of wavelengths. A conservative estimate of the laser calibration error of 0.05 cm^{-1} is therefore adopted. In addition to this, a Stokes conversion uncertainty of 0.2 or 0.4 cm^{-1} must be included whenever the first or second Stokes fields respectively are used (see Section 3.1.2).

The lasing frequency of any system is sensitive to changes in the environmental conditions, particularly the temperature. As a result, a relatively large variation ($\sim$0.1 cm^{-1}) in the laser calibration can be observed from one day to the next. The laser system is therefore recalibrated for each experiment. Also of concern is a drift in the laser calibration as the laser temperature equilibrates. To avoid this, a two hour warm-up period is provided before beginning the experiment. Repeated tests have shown that a calibration drift of < 0.01 cm^{-1} is realised after this 2 hour stabilisation period. Such a small thermal drift is insignificant for most experiments, but when a very high accuracy is desired, the thermal drift can be monitored and corrected (e.g. in Section 4.2.1).

3.3.2 Laser-ion Crossing Angle — The Doppler Shift

A particle moving in a light field with a speed v will see a shift in the frequency of the light according to the relativistic Doppler effect [16]:

$$\nu' = \nu \frac{1 - \beta \cos\theta}{\sqrt{1-\beta^2}}, \tag{3.3}$$

where ν and ν' are the frequency of the light in the lab and moving frames respectively, θ is the angle formed between the ion beam and the laser beam, and $\beta = v/c$ with c the speed of light in a vacuum. The numerator of Equation 3.3 is expected from the classical Doppler effect and is often called the *first-order* or *linear* Doppler effect. The denominator is a consequence of relativistic time dilation and gives rise to the *second-order* or *transverse* Doppler effect.

The transverse Doppler effect gives a non-zero positive frequency shift (blue shift) regardless of the crossing angle. When $\theta = \frac{\pi}{2}$ [90°] the frequency shift due to the transverse effect is:

$$\Delta\nu^{transverse} \approx \frac{1}{2}\nu\beta^2. \tag{3.4}$$

The frequency shift due to the linear Doppler effect vanishes when $\theta = \frac{\pi}{2}$. However, it is sensitive to small deviations from this ideal crossing angle. For an angle $\theta = \frac{\pi}{2} + \Delta\theta$, the error introduced by the linear Doppler shift is (assuming small $\Delta\theta$):

$$\Delta\nu^{linear} \approx \tilde{\nu}\beta\Delta\theta, \tag{3.5}$$

where $\tilde{\nu} = \nu/\sqrt{1-\beta^2} \approx \nu$. The ratio between the shift produced by the linear effect to that of the transverse effect is then:

$$\frac{\Delta\nu^{linear}}{\Delta\nu^{transverse}} \approx \frac{2\tilde{\nu}\beta\Delta\theta}{\nu\beta^2} \approx \frac{2\Delta\theta}{\beta}, \tag{3.6}$$

If the ions have a kinetic energy of $\bar{E}_k$ in units of keV per atomic mass unit (m_u), then the ion velocity is given by: $v = 4.4 \times 10^5\sqrt{\bar{E}_k}$ m/s. Given ion beam

energies ranging between 8 and 20 keV and atomic masses between 10 (boron) to 209 m_u (bismuth), velocities ranging between 86 000 and 630 000 m/s are expected. Therefore $\beta \approx 3 \times 10^{-4}$ to 2×10^{-3}. Finally, typical uncertainties in the crossing angle are $\Delta\theta = \pm 0.009$ radians [$\pm 0.5°$] (see below). By Equation 3.6 we then have, $\Delta\nu^{linear} \sim 10$ to $100 \times \Delta\nu^{transverse}$ and the transverse Doppler effect can therefore be neglected when calculating final uncertainties in measurements.

Verification of the Laser-ion Crossing Angle

On the basis of the geometry of the interaction chamber alone, an ion-laser crossing angle of 90° can be assured to an accuracy of only 2°. With this uncertainty, Equation 3.5 predicts a shift in the laser frequency of up to about 70 ppm (parts per million), for the fastest ion velocities. This is an unacceptably large error for many studies, and the crossing angle must therefore be verified by other means.

The measurement of an element with a well known electron affinity is the most convenient method of verifying that Doppler shifts are within an acceptable limit. For such a measurement, a maximum sensitivity to a Doppler shift is desired. The candidate ion should therefore be light (to maximize the beam velocity), have a large binding energy (so that ν is large), have very accurately determined structure, and be easily measured with the McMaster apparatus. O^- and S^- are ideal ions in this respect.[8] S^- was used as a calibration ion in early experiments (see [3,17,18]), and O^- was therefore selected to verify this calibration. O^- is also a more sensitive test than S^- since higher ion velocities are achieved ($v \approx 430\,000$ m/s).

A previous measurement conducted by Neumark *et al.* [19] (and later revised [20]) determined the EA of ^{16}O to be[9] 11 784.648(3) cm^{-1}. A high-resolution

[8] Si^-, F^-, and Cl^- would be other good candidates, although the binding energies of F^- and Cl^- are rather high compared to typical experiments conducted at McMaster and the beam velocities of Si^- and Cl^- are considerably lower than for O^-.

[9] The uncertainty reported in [19,20] is 0.006 at a 95% confidence level (i.e. two standard devia-

measurement of the $^2P_{3/2} \rightarrow {}^3P_2$ detachment threshold yields the electron affinity for ^{16}O of 11 784.62 cm^{-1}. To account for the blue-shift produced by the transverse Doppler effect, this value should be corrected by +0.012 cm^{-1} to give 11 784.63 cm^{-1} with an uncertainty of 0.04 cm^{-1}, including only the laser calibration uncertainty (with the possibility of a thermal drift) and the one standard deviation statistical error in the fit. This result is therefore well within one standard deviation of the previous measurement. On the basis of this measurement, θ may deviate from $\frac{\pi}{2}$ by 0.0010(23) radians [0.06(13)°]. A very recent independent measurement by Valli, Blondel, and Delsart [21] has called into question the Neumark *et al.* result, proposing that the EA of ^{16}O is instead 11 784.682(20) cm^{-1}. This value is within two standard deviations of the Neumark *et al.* result (and of our result) and may therefore simply reflect the statistics of a small sample of measurements. On the other hand, if this new result is taken to be the true electron affinity of O, then the crossing angle may be in error by 0.0030(26) radians [0.17(15)°]. This small error still includes zero to about 1.2 standard deviations.

As a second test, the $^2P_{1/2} \rightarrow {}^3P_2$ threshold in O^- was measured to obtain the energy of the $^2P_{1/2}$ fine structure level of 11 607.66 cm^{-1}, after correction for the transverse Doppler effect. An uncertainty of 0.06 cm^{-1} is assigned for the combined laser calibration error (including a possible thermal drift) and statistical error of the fit. The two thresholds were measured on the same day without any changes applied to the ion beam parameters (i.e. the acceleration voltages, the deflection plate voltages, and the magnet current). Since very similar laser frequencies were used in both experiments ($\Delta\nu/\nu \approx 0.015$), no additional Doppler error should be introduced into the $^2P_{1/2}$ measurement. Neumark *al.* [19] and Valli, Blondel, and Delsart [21] have

tions). This uncertainty has therefore been divided by two here, in order to quote uncertainties at a consistent level of one standard deviation.

measured this state to be 11 607.52(5) and 11 607.597(29) cm^{-1} respectively. From this measurement we obtain an estimate of the possible error in the angle of 0.008(5) [0.46(26)°] and 0.0036(38) radians [0.21(22)°] respectively. Again the deviation in the angle includes zero within one or two standard deviations.

An additional concern is the reproducibility of this crossing angle from one experiment to the next. Although the laser beam trajectory is easily reproduced to a high accuracy ($< 0.1°$), geometrical considerations of the interaction region indicate that the angle of the ion beam can be guaranteed to an accuracy of only 0.5° (upper limit of uncertainty). Including the possibility of $\approx 0.3°$ error from the O^- experiments and the error from the reproducibility of the ion beam trajectory, a conservative one standard deviation uncertainty for the ion-laser crossing angle is then 0.5°. This is equivalent to an uncertainty in the ion-frame laser frequency of between 2.6 and 17 ppm, depending on the ion velocity.

3.3.3 High Intensity Effects — The Ponderomotive Shift

An electron ejected into a high intensity laser field will experience an oscillatory force with a frequency given by the laser frequency. The electron will therefore undergo an oscillatory or *ponderomotive* motion [22]. The ponderomotive energy Δ associated with this motion increases the energy of the free electron state. If q_e is the magnitude of the electron charge and E is the electric field amplitude, the ponderomotive energy is given by:

$$\Delta = \frac{q_e^2 E^2}{4 m_e \omega^2}. \tag{3.7}$$

With the intensity ($I = \frac{1}{2}\epsilon_o c E^2$) in units of W/cm^2 and wavelength ($\lambda = c/\nu = 2\pi c/\omega$) in units of μm, we can obtain Δ in units of cm^{-1} using[10]:

$$\Delta = 7.53 \times 10^{-10}\, I\, \lambda^2 . \tag{3.8}$$

This additional energy must be supplied in order to photodetach a negative ion and so the detachment threshold is effectively increased in energy due to the *ponderomotive shift* by an amount equal to Δ.

Although initial experiments aimed at verifying Δ yielded shifts much smaller than expected [23–26], these observations were explained in part by the phenomenon termed "leakage detachment" in very low frequency light fields [27,28], and by unfavourable experimental conditions [29,30]. A later careful experiment by Davidson *et al.* [29] obtained results consistent with a full ponderomotive shift and Equation 3.8 is therefore expected to yield the correct value for the ponderomotive shift (see also Chapter 6).

The structure experiments presented in this thesis all use a collimated laser beam with peak intensities $\lesssim 10^7$ W/cm^2. Therefore very small ponderomotive shifts are expected, typically $\ll 0.01$ cm^{-1}, which can be neglected. As a test, the $^4S_{3/2} \rightarrow {}^3P_0$ photodetachment thresholds in C^- and Ge^- were measured with a collimated laser beam and with a laser beam focussed onto the ion beam with a 25 cm focal length cylindrical lens or a 20 cm focal length spherical lens. Identical threshold positions where observed with the collimated and cylindrical geometries, while a shift of about 1 cm^{-1} was observed with the spherical focus. Since a spherical focus is never used in a single-photon experiment, ponderomotive shifts should not be a concern. Finally, the high precision experiments on Bi^- discussed in Section 4.2.1

[10]Note that the magnitude of the ponderomotive shift appears incorrectly in Equation 17 of Reference [22]. The correct value of the coefficient is 9.3×10^{-10}, not 8.9×10^{-10}.

were repeated using a cylindrical focussing lens, and again no shift in the threshold position was observed.

In the experiments on Au^- (see Chapter 6) a very tightly focussed laser beam and high pulse-energies were required in order to observe a non-resonant two-photon detachment threshold. These large peak intensities ($\sim 10^{11}$ W/cm^2) resulted in the observation of large ponderomotive shifts ($\Delta \approx 50$ cm^{-1}), which therefore needed to be included in the detachment model.

3.3.4 Amplified Spontaneous Emission

Amplified spontaneous emission (ASE) produced in the dye laser can produce weak radiation that typically spans the frequency range of the gain medium (i.e. the laser dye). This is therefore a source of background radiation. Typically ASE is produced only when the laser is tuned near the edge of the dye gain curve, and therefore can be easily avoided by selecting dyes that have gains which peak near the wavelength of interest (see Figure 3.2). Also, any small amounts of ASE which may be present would be maintained at a constant level over the small wavelength ranges scanned in the work presented in this thesis (with the possible exception of the W^- work, see Section 5.3). At worse, a constant ASE would be manifested as an additional source of photodetachment background. Finally, stimulated Raman conversion in a single-pass cell depends exponentially on the pump (i.e. dye) laser light intensity. Since any ASE radiation that might be present is broad-band, the spectral intensity is very low, which leads to extremely low conversion efficiencies into the Stokes fields. Therefore, ASE is believed to have negligible or no effect on the observed spectra (see also discussion in Paper 2, reproduced in Section 4.1.2).

3.3.5 Other Systematic Errors — A Comparative Overview of Measurements

Although we have endeavoured to verify and minimize all sources of possible systematic error, it is difficult to guarantee that other sources have not been overlooked. It is therefore valuable to compare our results with precision measurements obtained from other research groups. In addition to the O^- measurements already discussed in Section 3.3.1, these include measurements in Te, Si, Cs, Ir, Pt, S, and Se. Table Table 3.1 summarizes these results. Some of the entries deserve additional comments, which can be found in the discussion below.

A total of 9 entries (marked with a star *) indicate differences in measurements (ΔE) which are accurate to better than 1 cm^{-1}. The weighted mean of this set is $\sum w\,\Delta E / \sum w = -0.00042$ cm^{-1} and the error in the mean is $\sqrt{\sum w} = 0.025$ cm^{-1}, where $w = 1/[\sigma(\Delta E)]^2$ are the weights. The population of differences is therefore consistent with 0 to within 0.025 cm^{-1}, and we can conclude to a high degree of certainty that no unforeseen systematic errors are present.

Measurements in the Carbon-group Elements

Recent measurements in the carbon-group elements can be found in Paper 10 listed in the Preface. In addition to fine-structure and term splittings of the ionic states,[11] the EAs of C, Si, Ge, and Sn were reported to be 10 179.67(15), 11 207.24(15), 9942.49(12), and 8969.42(12) cm^{-1} respectively. These values compare very well to the previous measurements conducted at McMaster on the negative ions of Si, Ge, and Sn where EAs of 11 207.0(5), 9942.6(4), and 8969.6(5) cm^{-1} respectively were obtained [31]. Although the two works were conducted by different lead researchers and with some modifications to the apparatus, they cannot be considered as truly independent mea-

[11] See Chapter 7 for a complete list of the states measured.

Table 3.1: High precision measurements of binding energies and fine structure splittings obtained with the McMaster setup are compared with the results of other groups having similar or better precision. All values are given in cm^{-1}.

Ion	State or Splitting	McMaster Result[a]	Comparative Result		ΔE^b
			Value	Reference	
O^-	$^2P_{3/2}$	11 784.63(4)[c]	11 784.648(3)	[19,20]	−0.018(40)[c*]
			11 784.682(20)	[21]	−0.052(45)[c*]
	$^2P_{1/2}$	11 607.66(6)[c]	11 607.52(5)	[19]	0.140(78)[c*]
			11 607.597(29)	[21]	0.063(67)[c*]
Si^-	$^4S_{3/2}$	11 207.24(15)	11 207.252(18)	[32]	−0.01(15)*
Te^-	$^2P_{3/2}$	15 896.16(18)	15 896.18(5)	[33]	−0.02(19)*
	$^2P_{1/2} - {}^2P_{3/2}$	5 005.36(10) [S2]	5 008(5)	[34]	−2.6(50)
			5 004.7(2)[d]	[35]	0.66(22)[d]
B^-	$^3P_0$	2 256.12(20) [S2]	2 160(16)[e]	[38]	96(16)[e]
			2 254(16)[e]	[39]	2(16)[e]
Cs^-	$^1S_0$	3 804.03(48) [S2]	3 802.9(24)	[40]	1.1(24)
			3 803.95(20)	[41]	0.08(52)*
Ir^-	$^3F_4$	12 617.4(12)	12 613(4)	[42]	4.4(42)
Pt^-	$^2D_{5/2}$	17 140.1(4)	17 160(16)	[43]	−20(16)
			17 125(9)	[44]	15.1(90)
			17 141(6)	[45]	−0.9(60)
S^-	$^3P_2$	16 753.1(6)	16 752.966(8)	[41,47]	−0.10(60)*
Se^-	$^3P_{3/2}$	16 297.7(4)	16 297.8(2)	[48]	−0.10(45)*

[a] Measurements marked with a superscript S2 ([S2]) were performed with second Stokes radiation; no Raman conversion was required for all other experiments.

[b] ΔE is the difference between the McMaster measurement and the comparative measurement. Entries marked with a star (*) indicate those which have been determined to better than 1 cm^{-1}.

[c] These uncertainties include only the statistical uncertainty and laser calibration error; no estimate for Doppler error has been included.

[d] This value is believed to be in error, see text.

[e] These are calculated binding energies.

surements. However, an excellent test can be offered by the very recent study of Blondel, Delsart, and Goldfarb [32], who determined the EA of Si to a very high accuracy using the newly developed electron microscopy technique. Their result of 11 207.252(18) cm^{-1} is in excellent agreement with the McMaster measurements.

Measurements in Tellurium

Paper 12 listed in the Preface describes in detail the measurements conducted at McMaster on Te^-. For brevity, we shall be content with simply quoting the results here. The excited $5p^5\ ^2P_{1/2}$ bound excited state in Te^- was determined from a threshold measurement to be 10 890.80(15) cm^{-1}. Also, the $5p^5\ ^2P_{1/2} - 5p^5\ ^2P_{3/2}$ fine structure splitting was measured to be 5005.36(10) cm^{-1}, using a two-photon resonant M1 transition.

The binding energy of the $^2P_{3/2}$ ground state of Te^- (i.e. the EA of Te) has been measured to a very high precision with the careful experiment on the ground state threshold conduced by Haeffler *et al.* [33], giving 15 896.18(5) cm^{-1}. Although this threshold was not directly observed in Paper 12, the value can be deduced simply by adding the measured $^2P_{3/2} - {}^2P_{1/2}$ fine structure splitting to the measured binding energy of the $^2P_{1/2}$ state. A binding energy of 15 896.16(18) is thereby obtained for the $^2P_{3/2}$ state, in excellent agreement with Haeffler *et al.*

Previous measurements of the $^2P_{1/2} - {}^2P_{3/2}$ fine structure interval have been conducted by Slater and Lineberger [34] and by Kristensen *et al.* [35], yielding values of 5008(5) and 5004.7(2) respectively. With respect to the last measurement, it should be noted that the authors later realized that a calibration error likely existed and which was not included in the uncertainty [36, see also Paper 12]; this likely explains the >3 standard deviation discrepancy with our measurement.

Measurements in Boron — Comparison with Theory

Section 4.2.2 presents threshold measurements on the ground state (including fine structure) of B^-. The EA of B was found to be 2256.12(20) cm^{-1}. The only previous measurement on B^- is an LPES experiment, which gives the EA of B as 2234(80) cm^{-1} [37]. However, B^- has attracted considerable theoretical interest, and extensive multiconfiguration Hartree-Fock calculations have been performed in this system. In particular Sundholm and Olsen determined an EA of 2160(16) cm^{-1} [38], and Froese Fischer *et al.* obtained 2254(16) cm^{-1} [39]. The difference between these two results is attributed to a number of differences in the approaches used by the two groups, including the choice of orbital sets, core polarisation models, and the fact that Froese Fischer *et al.* include both core-core and core-valence correlations while Sundholm and Olsen include only core-valence correlations (see Section 4.2.2 for a complete discussion).

Measurements in Cesium, Platinum, and Iridium — *p*-wave Detaching Species

Measurements on *p*-wave detaching species tend to be of considerably lower accuracy. Notable exceptions are Cu and Ag, which have been measured to an accuracy of 0.2 and 0.3 cm^{-1} respectively (see Section 4.1.1). Unfortunately there are no other measurements on these ions having similar accuracies and therefore no comparison is available. Since measurements of *p*-wave thresholds are sensitive to different sources of errors (in particular background signals), a comparison is desirable. The measurements on Cs, Pt, and Ir are therefore included.

In Section 5.1.1 the EA of Cs is found to be 3804.03(48) cm^{-1}. Slater *et al.* [40] have previously determined the EA of Cs to be 3802.9(24) cm^{-1}. A second result, which remains unpublished, was reported in the 1985 review by Hotop and

Lineberger [41], giving 3803.95(20) cm^{-1}. These values are in excellent agreement.

Values for the EA of Ir and Pt of 12617.4(12) and 17140.1(4) cm^{-1} respectively are obtained in Section 4.1.2. These values agree with the previous measurements in Ir^- [42] and Pt^- [43-45] to within one or two standard deviations (see Table 3.1 for a complete list). The somewhat surprising scatter of the previous Pt measurements is believed to be due to a combination of the significant change in the background signal observed in the experiments and the unexpectedly large deviation from the Wigner law observed in these species (see discussion in Section 4.1.2). It is believed that the present measurement is more accurate, since these issues were taken into account.

Early Measurements — Sulphur and Selenium

The EA of sulphur was measured during early experiments conducted at McMaster [45,46] to rule out any unexpected systematic errors. A value of 16753.1(6) cm^{-1} was observed, which agrees well with the accepted value of 16752.966(8) cm^{-1} [41, 47]. The EA of Se was measured to be 16297.7(4) cm^{-1} [46], which is in excellent agreement with the Mansour *et al.* measurement of 16297.8(2) cm^{-1} [48]. The $^3P_{1/2}$ fine structure level was also measured to a high precision (14019.6(4) cm^{-1}), but unfortunately no independent measurements are available for comparison.

3.4 References

[1] M. Scheer, *Single- and Multiphoton Infrared Laser Spectroscopy of Atomic Negative Ions*, Ph.D. thesis, McMaster University (1998).

[2] C. A. Brodie, *Photodetachment of Weakly Bound Atomic Negative Ions* M.Sc. thesis, McMaster University (1998).

[3] L. D. Steele, *Selected Negative Ion Experiments Using the New KeV Accelerator* M.Sc. thesis, McMaster University (1995).

[4] R. Middleton, Nuc. Instr. and Meth. **214**, 139 (1983).

[5] R. Middleton, *A Negative Ion Cookbook* (unpublished).

[6] W. K. Bischel and M. J. Dyer, Phys. Rev. A **33**, 3113 (1986).

[7] E. C. Looi, J. C. Stryland, and H. L. Welsh, Can. J. Phys. **56**, 1102 (1978).

[8] L. Minnhagen, J. Opt. Soc. Am. **63**, 1185 (1973).

[9] P. W. Milonni and J. H. Eberly, *Lasers* (Wiley and Sons, 1988).

[10] H. Hotop and W. C. Lineberger, J. Chem. Phys. **58**, 2379 (1973).

[11] C. Blondel, R.-J. Champeau, M. Crance, A. Crubellier, C. Delsart, and D. Marinescu, J. Phys. B **22**, 1335 (1989).

[12] P. Balling, C. Brink, T. Andersen, and H. K. Haugen, J. Phys. B **25**, L565 (1992).

[13] J. C. Rienstra-Kiracofe, G. S. Tschumper, H. F. Schaefer III, S. Nandi, and G. B. Ellison, Chem. Rev. (accepted, 2001).

[14] H. Hotop and W. C. Linberger, J. Phys. Chem. Ref. Data **4**, 539 (1975).

[15] H. Hotop and W. C. Lineberger, J. Chem. Phys. **58**, 2379 (1973).

[16] A discussion of the Doppler effect can be found in most books covering special relativity. See for example: A. P. French, *Special Relativity* (Chapman & Hall, 1991).

[17] J. Thøgersen, L. D. Steele, M. Scheer, C. A. Brodie, and H. K. Haugen, J. Phys. B **29**, 1323 (1996).

[18] J. Thøgersen, L. D. Steele, M. Scheer, H. K. Haugen, P. Kristensen, P. Balling, H. Stapelfeldt, and T. Andersen, Phys. Rev. A **53**, 3023 (1996).

[19] D. M. Neumark, K. R. Lykke, T. Andersen, and W. C. Lineberger, Phys. Rev. A **32**, 1890 (1985).

[20] C. Blondel, Phys. Scr. **58**, 31 (1995).

[21] C. Valli, C. Blondel, and C. Delsart, Phys. Rev. A **59**, 3809 (1999).

[22] P. Agostini and G. Petite, Contemp. Phys. **29** 57, (1988).

[23] R. Trainham, G. D. Fletcher, N. B. Mansour, and D. J. Larson, Phys. Rev. Lett. **59**, 2291 (1987).

[24] M. C. Baruch, T. F. Gallagher, and D. J. Larson, Phys. Rev. Lett. **65**, 1336 (1990).

[25] W. W. Smith, C. Y. Tang, C. R. Quick, H. C. Bryant, P. G. Harris, A. H. Mohagheghi, J. B. Donahue, R. A. Reeder, H. Sharifian, J. E. Stewart, H. Toutounchi, S. Cohen, T. C. Altman, and D. C. Risolve, J. Opt. Soc. Am. B **8**, 17 (1991).

[26] C. Y. Tang, H. C. Bryant, P. G. Harris, A. H. Mohagheghi, R. A. Reeder, H. Sharifian, H. Tootoonchi, C. R. Quick, J. B. Donahue, S. Cohen, and W. W. Smith, Phys. Rev. Lett. **66**, 3124 (1991).

[27] L. A. Bloomfield, Phys. Rev. Lett. **63**, 1578 (1989).

[28] L. A. Bloomfield, J. Opt. Soc. Am. B **7**, 472 (1990).

[29] M. D. Davidson, J. Wals, H. G. Muller, and H. B. van Linden van den Heuvell, Phys. Rev. Lett. **71**, 2192 (1993).

[30] A. R. P. Rau, Phys. Rev. A **54**, 717 (1996).

[31] J. Thøgersen, L. D. Steele, M. Scheer, C. A. Brodie, and H. K. Haugen, J. Phys. B **29**, 1323 (1996).

[32] C. Blondel, C. Delsart, and F. Goldfarb, J. Phys. B **34** (accepted).

[33] G. Haeffler, A. E. Klinkmüller, J. Rangell, U. Berzinsh, and D. Hanstorp, Z. Phys. D **38**, 211 (1996).

[34] J. Slater and W. C. Lineberger, Phys. Rev. A **15**, 2277 (1977).

[35] P. Kristensen, P. Stapelfeldt, P. Balling, T. Andersen, and H. K. Haugen, Phys. Rev. Lett. **71**, 3435 (1993).

[36] T. Andersen and V. V. Petrunin, private communication.

[37] C. S. Feigerle, R. R. Corderman, and W. C. Lineberger, J. Chem. Phys. **74**, 1513 (1981).

[38] D. Sundholm and J. Olsen, Chem. Phys. Lett. **171**, 53 (1990).

[39] C. Froese Fischer, A. Ynnerman, and G. Gaigalas, Phys. Rev. A **51**, 4611 (1995).

[40] J. Slater, F. H. Read, S. E. Novick, and W. C. Lineberger, Phys. Rev. A **17**, 201 (1978).

[41] H. Hotop and W. C. Lineberger, J. Phys. Chem. Ref. Data **14**, 731 (1985).

[42] B. J. Davies, C. W. Ingram, D. J. Larson, and U. Ljunblad, J. Chem. Phys. **106**, 5783 (1997).

[43] H. Hotop and W. C. Lineberger, J. Chem. Phys. **58**, 2379 (1973).

[44] N. D. Gibson, B. J. Davies, and D. J. Larson, J. Chem. Phys. **98**, 5104 (1993).

[45] J. Thøgersen, L. D. Steele, M. Scheer, C. A. Brodie, and H. K. Haugen, J. Phys. B **29**, 1323 (1996).

[46] J. Thøgersen, L. D. Steele, M. Scheer, H. K. Haugen, P. Kristensen, P. Balling, H. Stapelfeldt, and T. Andersen, Phys. Rev. A **53**, 3023 (1996).

[47] D. J. Larson and R. Stoneman, Phys. Rev. A **31**, 2210 (1985).

[48] N. B. Mansour, C. J. Edge, and D. J. Larson, Nucl. Instrum. Meth. Phys. Res. Sect. B **31**, 313 (1988).

Chapter 4

Threshold Detachment Experiments

This chapter is based on 6 previously published articles which describe the experimental results of photodetachment threshold measurements on 10 elements. The results are naturally divided into two sections. First, the experiments on transition metals, which are *p*-wave detaching, are presented: chromium, molybdenum, copper, and silver (Section 4.1.1), iridium and platinum (Section 4.1.2), and ruthenium (Section 4.1.3). Second, studies on elements from the main group of the periodic table (groups 13 to 17), which are *s*-wave detaching, are discussed: bismuth (Section 4.2.1), boron (Section 4.2.2) and aluminum (Section 4.2.3). The main purpose of these works was to obtain accurate binding energies of the respective species using the LPTS technique. The particular elements were chosen for a combination of reasons: because of a definite need for an accurate measurement due to conflicting previous experimental or theoretical results (e.g. B and Pt), because no previous experimental data were available on all (e.g. Ru) or most (e.g. B and Al) of the bound states, or simply because very significant improvements of the binding energies could be obtained with

the McMaster setup. Demonstrating the reliability of LPTS in a significant number of systems and acquiring experience with this technique in a wide variety of situations is also of value. This experience will aid in understanding the results of the remaining chapters of this thesis, where the technique is extended in order to study previously unobserved structure and develop new tools to study negative ions.

Finally, in addition to the important quantitative results outlined above, Sections 4.1.2, 4.2.2, and 4.2.3 present observations of deviations from the Wigner threshold law with increasing photon energies. These investigations will provide useful background and set the context for Section 4.3, which delves into a more detailed analysis of the significance of these findings in light of the Wigner law correction terms previously discussed in Chapter 2.

4.1 *p*-wave Detaching Species

4.1.1 Paper 1 — Infrared laser photodetachment of transition metal negative ions: Studies on Cr^-, Mo^-, Cu^- and Ag^-

This paper presents some of the first LPTS investigations on weakly bound transition metal negative ions. Since all the ions studied in this work have only one bound state with no fine-structure, they represent ideal elements for initial investigations of these *p*-wave detaching species. In contrast to *s*-wave thresholds (see Section 4.2), the accuracy of *p*-wave threshold measurements is primarily limited by the statistical uncertainty of the fit, due to the gradual onset of the threshold signal. The results obtained with these ions are among the highest accuracy measurements obtained for *p*-wave detaching species.

I was primarily responsible for all aspects of this work, under the supervision of H. K. Haugen. M. Scheer assisted at various stages, especially with the experiments

and editing of the article. H. K. Haugen provided input throughout the project.

J. Phys. B: At. Mol. Opt. Phys. 31 (1998) 3885–3891. Printed in the UK PII: S0953-4075(98)92940-6

Infrared laser photodetachment of transition metal negative ions: studies on Cr^-, Mo^-, Cu^- and Ag^-

René C Bilodeau, Michael Scheer and Harold K Haugen†

Department of Physics and Astronomy, McMaster University, Hamilton, Ontario, L8S 4M1, Canada

Received 1 April 1998, in final form 8 June 1998

Abstract. Photodetachment threshold spectroscopy on the negative ions of chromium, molybdenum, copper and silver has yielded values for the electron affinities of 5451.0(10), 6027(2), 9967.2(3) and 10521.3(2) cm^{-1}, respectively. The results agree well with previous measurements, with an improvement in the accuracy of up to a factor of 300.

1. Introduction

Negative ions play an important role in a number of areas of pure and applied physics. For example, negative ions form the basis for ultrasensitive detection of atoms and isotopes in accelerator mass spectrometry [1, 2]. Also, the short-range potential in which the excess electron is bound gives rise to structure fundamentally different from that found in the neutral atom or positive ions, which are bound in a Coulomb potential. Hence negative ions are also interesting from a purely fundamental viewpoint. As a result, negative ion research is currently an active area of study [3]. Although many improvements to the measured electron affinities (EAs) have been presented since the 1985 review of Hotop and Lineberger [4], the EAs of many species remain relatively poorly known or, in some cases, totally unknown. This is particularly true for the transition metal elements, which generally form weakly bound ions. Presented in this paper are the results of photodetachment threshold spectroscopy measurements on the negative ions of chromium, molybdenum, copper and silver, using tunable infrared laser light. The EAs were measured with improvements in accuracy over the previous values ranging from a factor of about 10 (for Mo) to 300 (for Ag). To our knowledge, this is the first time that atomic negative ions of transition metals have been studied with infrared laser threshold spectroscopy.

2. Methodology

The experimental set-up is illustrated in figure 1. The dye laser is pumped by the second harmonic of a 10 Hz pulsed Nd:YAG laser. Near-infrared laser dyes are utilized to produce ≈8 ns laser pulses, tunable over the region of 680–980 nm with a bandwidth of 0.1–0.06 cm^{-1}. The dye-laser beam is focused into a 120 cm long high-pressure Raman cell

† Also with: the Department of Engineering Physics, the Brockhouse Institute for Materials Research and the Center for Electrophotonic Materials and Devices, McMaster University, Hamilton, Ontario, L8S 4M1, Canada.

0953-4075/98/173885+07$19.50

3886 *R C Bilodeau et al*

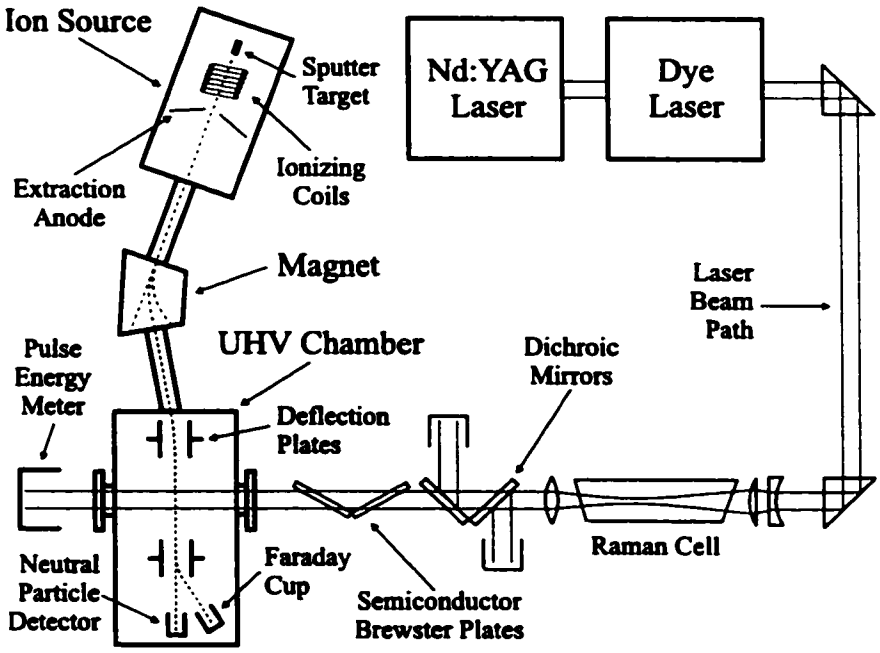

Figure 1. Schematic of the experimental apparatus, see text for details.

filled with H_2, where the dye-laser light is Raman shifted into the first and second Stokes laser beams. The first Stokes Raman shift has been directly measured against optogalvanic lines of Ar to be 4155.197(20) cm^{-1}, which agrees well with the literature value of 4155.187(5) cm^{-1} [5] for a cell pressure of 22(1) bar. After the Raman cell, the beam is recollimated and then passed through dichroic mirrors to remove the undesired anti-Stokes wavelengths as well as the residual pump wavelength with an efficiency of $\approx 90\%$. The light is then further filtered with silicon or germanium semiconductor plates arranged at Brewster's angle, and paired in order to eliminate beam walking as the laser is tuned. This system allows for the production of tunable infrared laser light over the region of 1–5 μm (see figure 2). The laser light is finally passed through a CaF_2 viewport into the ultra-high vacuum interaction chamber where it crosses the ion beam at 90°. A pulse-energy meter located after the exit port of the chamber serves to monitor the laser light. The optics table, including the pulse-energy meter assembly, can be sealed and flushed with dry nitrogen to effectively eliminate absorption of the infrared light in air.

Negative ion beams are produced with a caesium sputter source and accelerated to an energy of 16–19 keV. The ions are mass selected by bending the beam through an angle of 30° with a magnetic field of $\leqslant 5.2$ kG. The ion beam is then passed through a differential pumping section and into the ultra-high vacuum (UHV) chamber with background pressures of $\sim 10^{-8}$ mbar. The beam is further charge-state-analysed with a pair of electrostatic deflection plates, which produces a deflection of $\approx 10°$. The ions then interact with the collimated, pulsed laser. The residual negative ions are deflected into a Faraday cup by a second pair of electrostatic deflection plates, while the photodetached neutral atoms are detected with a discrete-dynode electron multiplier operating in the analogue regime. The voltage on the detector is adjusted so as to ensure that the output signal is linear with respect to the number of incident neutrals over the dynamic range of interest. Finally, the

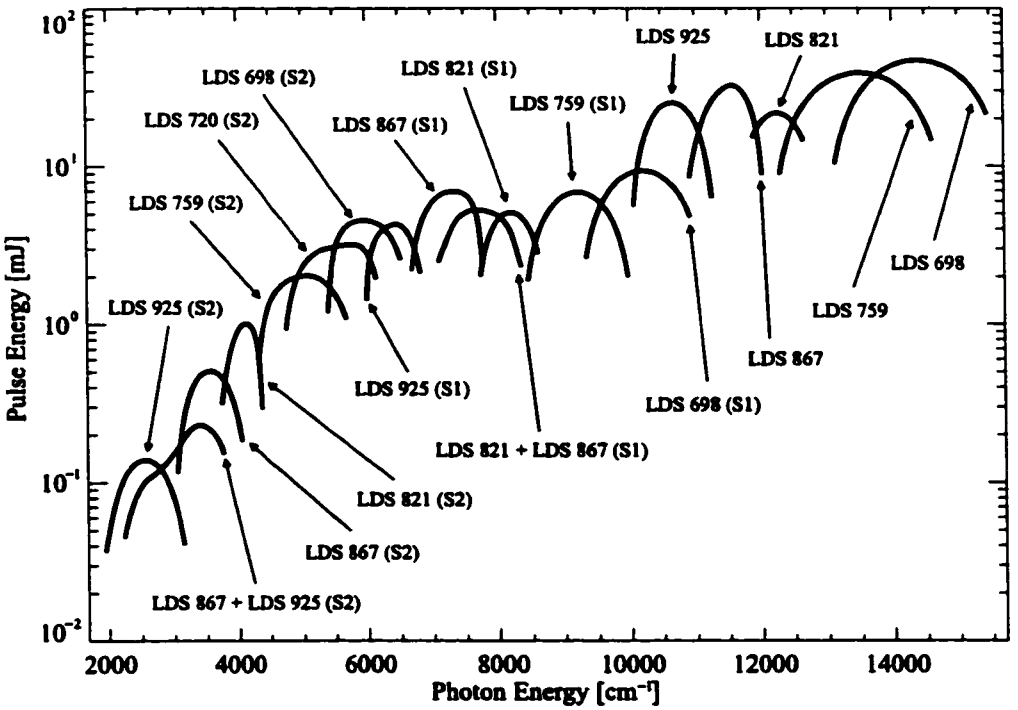

Figure 2. Approximate pulse energies realizable in the 1–5 μm tuning range with our experimental set-up. For clarity of presentation, only a selected set of laser dyes are presented. The laser dyes themselves operate up to ≈ 1 μm. For longer wavelengths, the first Stokes or second Stokes are utilized (indicated by (S1) or (S2), respectively, in the figure labels). See the text for a more detailed discussion.

output signal of the neutral particle detector is preamplified to minimize line noise, and is integrated with a boxcar averager. The boxcar gate is triggered by the laser pulse with a time delay adjusted to compensate for the time of flight of the neutral particles from the interaction region to the detector, typically ≈ 2 μs. The width of the boxcar acquisition window is adjusted so as to collect all the neutral particles produced during the pulse. In this way, an effective discrimination between the collisional background detachment events and the photodetachment signal can be achieved, allowing for an excellent signal-to-noise ratio. The integrated signal for each pulse (or the average of a number of pulses) is then collected and recorded by a personal computer.

The binding energy of a negative ion state is extracted by fitting a Wigner threshold law behaviour to the data. The Wigner threshold law states that for a photon energy ε and binding energy ε_0, the cross section for photodetachment is 0 for $\varepsilon < \varepsilon_0$, and is proportional to $(\varepsilon - \varepsilon_0)^{\ell+1/2}$ for $\varepsilon > \varepsilon_0$, where ℓ is the angular momentum of the detached electron. Therefore, if the detached electron carries no angular momentum (i.e. an s-wave electron) a square root behaviour is expected, while if the detached electron carries one unit of angular momentum (a p-wave electron) a $\frac{3}{2}$ power law is expected. The cross section for a p-wave threshold thus increases much more slowly than that for an s-wave threshold. It is comparatively much more difficult to extract the binding energy of the negative ion in the case of a p-wave threshold behaviour, especially if a baseline signal is present (see the discussion in section 4).

The negative ions of Cr, Mo, Cu and Ag are not expected to have any bound excited states or terms. Therefore only two energy levels are relevant in these systems: the negative ion ground state and the neutral atom ground state. For Cr and Mo, the negative ion state is the $^6S_{5/2}$ level of the $(n-1)d^5ns^2$ configuration and the neutral atom state is the $^7S_3$ level of the $(n-1)d^5ns$ configuration. On the other hand, for Cu and Ag the negative ion ground state is $(n-1)d^{10}ns^2\ ^1S_0$ and the neutral ground state is $(n-1)d^{10}ns\ ^2S_{1/2}$. (Note that $n = 4$ for Cr and Cu, while $n = 5$ for Mo and Ag.) As a result, in all four cases an s-electron is removed in the detachment process and the detached electron carries one unit of angular momentum, stemming from the absorbed photon. Hence, a p-wave threshold behaviour is expected for all the negative ions reported in the present paper.

3. Results

3.1. Cu^- and Ag^-

Copper is a very prolific negative ion from the caesium sputter source. The $\approx$450 nA currents obtained in the interaction region of the UHV section allowed for excellent statistics. Although a factor of 4 less ion current was obtained for silver, much more laser light could be produced at wavelengths near the threshold region (21 mJ as opposed to 8.5 mJ for the wavelengths needed for Cu, see figure 2) and so, low statistical noise could be achieved for Ag as well. Figure 3 is a plot of the neutral particle yield in the Ag^- photodetachment experiment over a range of 11 cm^{-1}, where each point represents the sum of the detachment yields from 2000 laser pulses. As can be seen by the full curve, the data agree very well with the expected p-wave behaviour discussed above. The fit to the data gives an electron affinity for Ag of 10521.3(2) cm^{-1} (1.304 47(2) eV, using 8065.5410(24) cm^{-1} eV^{-1} [6]),

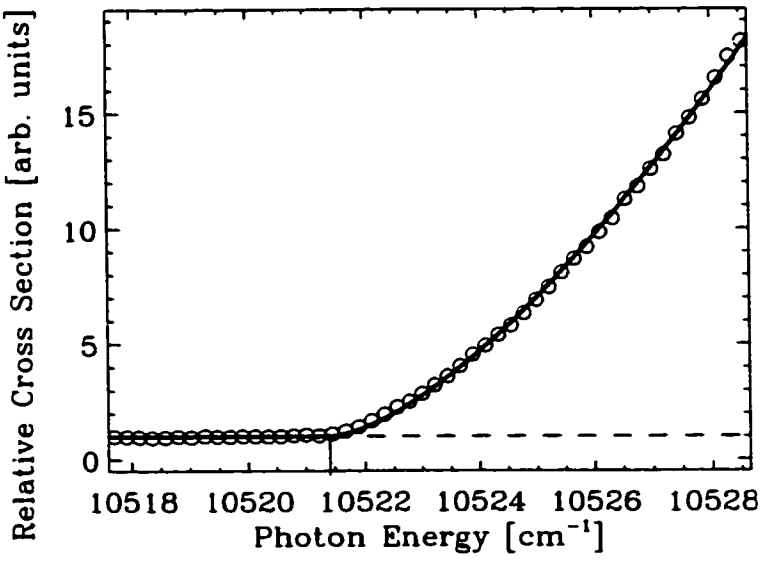

Figure 3. Relative cross section for the $^1S_0 \rightarrow {}^2S_{1/2}$ detachment threshold of Ag^-. The fitted Wigner p-wave is represented by the full curve. The vertical line indicates the best-fit location of the threshold.

where the uncertainty represents one standard deviation and includes possible systematic errors (see section 4 below). This value represents a significant improvement over the previously measured value by Hotop *et al* of 1.302(7) eV [7] (after recalibration [4]). A similar experiment on Cu^- gives an EA of 9967.3(3) cm^{-1} (1.235 79(4) eV) for copper, which agrees well with the Leopold *et al* value of 1.235(5) eV [8]. These experimental values also compare well with the theoretical EAs of Cu and Ag of 1.236 and 1.254 eV, respectively, recently calculated by Neogrády *et al* using quasi-relativistic one-component approximations to the Dirac–Coulomb Hamiltonian [9].

3.2. Cr^- and Mo^-

Unlike copper and silver, the negative ions of chromium and molybdenum are not very prolific from a Cs sputter source. Currents of only about 2.5 nA of Cr^- and 0.5 nA of Mo^- are obtained in the interaction region. A low beam current naturally gives rise to a poorer signal-to-noise ratio. It also often results in a poorer signal-to-background ratio as the background count does not necessarily scale with the beam current (see section 4 below). This effect can be compensated to some extent by increasing the scan range, but a larger uncertainty in the fit to the data is inevitable. The detachment yield for Cr^- versus photon energy is shown in figure 4 over a region of $\approx$100 cm^{-1}. A Wigner p-wave threshold fit yields a value of 5451.0(10) cm^{-1} (0.675 84(12) eV) for the electron affinity of Cr. This agrees well with, and is a substantial improvement over, the value of Feigerle *et al* of 0.666(12) eV [4, 10]. Likewise, from a scan over $\approx$200 cm^{-1} around the threshold of Mo^- we obtain an electron affinity of 6027(2) cm^{-1} (0.7472(2) eV), in good agreement with the previous result of 0.748(2) eV [11].

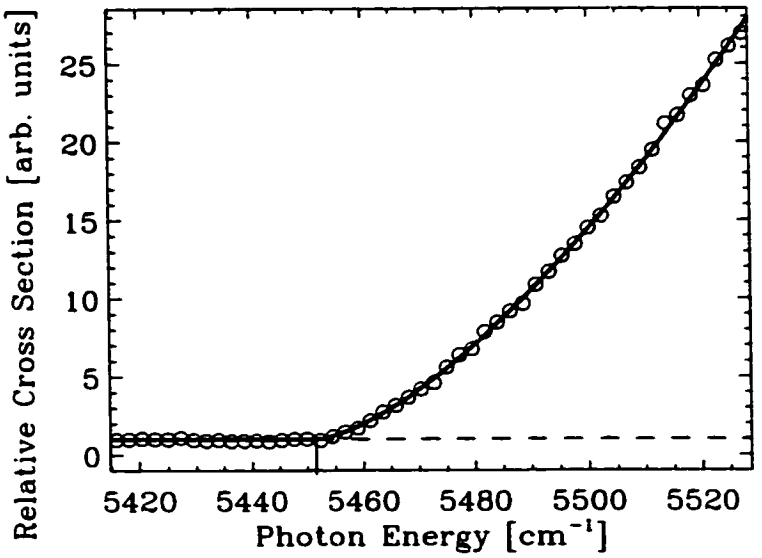

Figure 4. Plot of the relative detachment yields in the $^6S_{5/2} \rightarrow {}^7S_3$ photodetachment experiment on Cr^-. The full curve represents a fitted p-wave threshold law. The best-fit value of the threshold is indicated by a vertical line.

4. Discussion

The results of this work are summarized in table 1 (errors are given to one standard deviation); included for comparison are the results of previous works [4, 7, 8, 10, 11]. The excellent agreement of all the EAs with previous works, suggests that the previous values were likely to be more accurate than indicated by the error bars. All of the previous experiments were based on photodetachment electron spectrometry. In this technique, fixed energy photons are used to detach the electron, and the binding energy is deduced from the measured energy of the detached electrons. As a result, the accuracy of these measurements is limited by that of the electron spectrometer. In contrast, the main contribution to the final error in our experiments is typically the uncertainty in the fit. Aside from pure counting statistics, the accuracy of the fit can also be limited due to a large, and possibly sloped, photodetachment background. Populated bound excited states of the negative ion can produce such photodetachment backgrounds. If the fractional population in the excited state is sufficiently large, the binding energy of the excited state can be determined from its photodetachment threshold, analogous to the determination of the ground state binding energy. This approach works well for s-wave threshold features [12], but can be very challenging for p-wave thresholds, which is the subject of a parallel study on the transition metal ions Co^-, Rh^-, Ni^- and Pd^- [13]. If the population in the excited state is not sufficient, then more sophisticated techniques can be used to study the bound excited states, such as resonant multiphoton detachment [14]. However, the negative ions of Cr, Mo, Cu and Ag are not expected to possess bound excited states. The small photodetachment background seen in figures 3 and 4 is likely due to very small amounts of mass-coincident or nearly mass-coincident impurity molecules, such as hydrides. Finally, the laser bandwidth also limits the accuracy to which the threshold can be fitted. The bandwidth produces a broadening that can be more easily seen in s-wave thresholds [15]. The error introduced by this broadening is only a small fraction of the actual bandwidth and is typically insignificant relative to the statistical uncertainties involved.

Table 1. Summary of measured electron affinities.

Element	This work	Previous works	Reference
Cr	0.675 84(12) eV	0.666(12) eV	[10]
Mo	0.747 2(2) eV	0.748(2) eV	[11]
Cu	1.235 81(4) eV	1.235(5) eV	[8]
Ag	1.304 47(2) eV	1.302(7) eV	[7]

In addition to statistical noise and the laser bandwidth, there are possible systematic errors which limit the accuracy of the experiment. The dye laser is frequently calibrated against known optogalvanic resonance lines of low-pressure Ar gas [16]. Lines that lie near the scan wavelength ranges are selected and yield a calibration error of no more than $\pm 0.05\ cm^{-1}$. Comparing values obtained from a number of such lines reveals that the laser tuning deviates from linearity by less than 1 part in 1000, which is negligible over the scan ranges presented here. Peak pulse intensities of less than $10^8\ W\ cm^{-2}$ were produced in the experiments; therefore threshold shifts due to intense laser fields are expected to be insignificant [17]. In a separate experiment, we have verified that this effect is indeed negligible by measuring photodetachment thresholds at various laser intensities. As noted previously, uncertainties of ± 0.02 and $\pm 0.04\ cm^{-1}$ are assigned to the first and second Stokes shifts, respectively. Finally, the largest contribution to possible systematic errors

comes from possible Doppler shifts caused by any deviation of the laser–ion crossing angle from 90°. Careful measurements ensure that this angle can be realized with an accuracy of $\approx 0.5°$, which translates into a possible Doppler shift of $\leqslant 0.07$ cm^{-1} for the ions studied here. Therefore, the total of the systematic contributions to the error is less than ± 0.1 cm^{-1}, assuming that the error sources are independent. Previous measurements with this system have indicated that no other significant systematic errors are present [15].

5. Conclusions

The results of the infrared threshold photodetachment experiments on the negative ions of the transition metals yield substantial improvements for the electron affinities of Cr, Mo, Cu and Ag. The work demonstrates that highly accurate values for electron affinities can be obtained using this method, even if the negative ions are only weakly bound and detach with a p-wave threshold behaviour, as is the case for nearly all the transition metals.

Acknowledgments

We are grateful to the Natural Sciences and Engineering Research Council of Canada (NSERC) for their support of this work. We would also like to thank J D Garrett for manufacturing the cathodes used in the experiments.

References

[1] Litherland A E 1980 *Ann. Rev. Nucl. Part. Sci.* **30** 437
[2] Kutschera W and Paul M 1990 *Ann. Rev. Nucl. Part. Sci.* **40** 411
[3] Bates D R 1991 *Adv. At. Mol. Opt. Phys.* **27** 1
Andersen T 1991 *Phys. Scr.* T **34** 23
Buckmann S J and Clark C W 1994 *Rev. Mod. Phys.* **66** 539
Blondel C 1995 *Phys. Scr.* T **58** 31
[4] Hotop H and Lineberger W C 1985 *J. Phys. Chem. Ref. Data* **14** 731
[5] Bischel W K and Dyer M J 1986 *Phys. Rev.* A **33** 3113
Looi E C, Stryland J C and Welsh H L 1978 *Can. J. Phys.* **56** 1102 and references therein
[6] Cohen E R and Taylor B N 1987 *Rev. Mod. Phys.* **59** 1121
[7] Hotop H, Bennett R A and Lineberger W C 1973 *J. Chem. Phys.* **58** 2373
[8] Leopold D G, Ho J and Lineberger W C 1987 *J. Chem. Phys.* **86** 1715
[9] Neogrády P, Kellö V, Urban M and Sadlej A J 1997 *Int. J. Quantum Chem.* **63** 557
[10] Feigerle C S, Corderman R R, Bobashev and Lineberger W C 1981 *J. Chem. Phys.* **74** 1580
[11] Gunion R F, Dixon-Warren St J and Linberger W C 1996 *J. Chem. Phys.* **104** 1765
[12] Scheer M, Bilodeau R C, Thøgersen J and Haugen H K 1998 *Phys. Rev.* A **57** R1493
Scheer M, Bilodeau R C and Haugen H K 1998 *Phys. Rev. Lett.* **80** 2562
[13] Scheer M, Brodie C A, Bilodeau R C and Haugen H K *Phys. Rev.* A at press
[14] Scheer M, Haugen H K and Beck D R 1997 *Phys. Rev. Lett.* **79** 4104
Thøgersen J, Scheer M, Steele L D and Haugen H K 1996 *Phys. Rev. Lett.* **76** 2870
Kristensen P, Stapelfeldt H, Balling P, Andersen T and Haugen H K 1993 *Phys. Rev. Lett.* **71** 3435
[15] Thøgersen J, Steele L D, Scheer M, Brodie C A and Haugen H K 1996 *J. Phys. B: At. Mol. Opt. Phys.* **29** 1323
[16] Minnhagen L 1973 *J. Opt. Soc. Am.* **63** 1185
[17] Trainham R, Fletcher G D, Mansour N B and Larson D J 1987 *Phys. Rev. Lett.* **20** 2291

4.1.2 Paper 2 — Near threshold spectroscopy of iridium and platinum negative ions: Electron affinities and the threshold law

Previous measurements on Pt^- indicated poor agreement in the value of the electron affinity of Pt. This paper re-investigates Pt^- in order to obtain a very accurate and reliable binding energy. The paper stresses that because of the very slow onset of p-wave thresholds, the extraction of an accurate threshold energy is sensitive to statistical noise and variations in the background signal. Also, due to the unexpectedly large deviations from the Wigner law observed in these studies, large differences in the fitted threshold position are observed depending on whether all the data are included in the fit or if the fit is restricted to the data very near to the threshold. This demonstrates that care must be taken to ensure that a sufficiently high signal-to-noise ratio is acquired so that unexpectedly large deviations from the Wigner law can be identified and possible problems with fitting an unsuitably large region are avoided. These concerns will be discussed further in Section 4.3.

I performed the experiments with the aid of M. Scheer (for Ir) and R. L. Brooks (for Pt), and was responsible for the data analysis and composition of the manuscript. M. Scheer also performed preliminary data analysis of the Ir^- spectrum and provided feedback and editorial comments on the manuscript. R. L. Brooks assisted in the data analysis of the Pt^- spectrum and editing of the manuscript. He provided particularly useful guidance and comments on the error analysis. H. K. Haugen supervised all aspects of the study and supplied valuable input at all stages.

PHYSICAL REVIEW A, VOLUME 61, 012505

Near-threshold laser spectroscopy of iridium and platinum negative ions: Electron affinities and the threshold law

René C. Bilodeau, Michael Scheer,* and Harold K. Haugen†
Department of Physics and Astronomy, McMaster University, Hamilton, Ontario, Canada L8S 4M1

Robert L. Brooks
Department of Physics, University of Guelph, Guelph, Ontario, Canada N1G 2W1
(Received 14 July 1999; published 10 December 1999)

The electron affinity of Ir is measured to be 12617.4(12) cm^{-1} [1.56436(15) eV], from photodetachment studies on Ir^-. Previous measurements of the electron affinity of platinum reported results which were inconsistent within quoted error bars. A photodetachment study with a very improved energy resolution, signal-to-noise ratio, and signal-to-background ratio, was conducted on Pt^-, and yields a much more accurate electron affinity for Pt of 17140.1(4) cm^{-1} [2.12510(5) eV], in good agreement with the most recent measurement. Possible explanations for the poor agreement between the earlier results are discussed. In both the Ir^- and Pt^- spectra, the data indicate that the detachment cross section deviates from the expected Wigner threshold law, even near the detachment threshold. This behavior cannot be explained by the correction terms to the Wigner law proposed by the currently available threshold detachment models.

PACS number(s): 32.10.Hq, 32.80.Gc

I. INTRODUCTION

Over the past decades, many efforts have led to continually improved measurements of the bound states of atomic negative ions (for recent reviews on negative ions, see Refs. [1,2]). In addition to uses in a number of areas of pure and applied physics (such as ultrasensitive detection of atoms and isotopes in accelerator mass spectrometry [3]), negative ions have proven to be practical test subjects for subtle electron correlation and other quantum-mechanical effects. For example, negative ions have recently provided the means to enable the first direct observation of the radial component of an electronic wave function [4].

Two techniques are typically employed to study the bound states of atomic negative ions. In laser-photodetached electron spectrometry (LPES), fixed-wavelength laser light is used to photodetach the excess electron. The binding energy of the ion can then be deduced from the measured energy of the photoelectron. Although generally applicable to any atomic negative-ion system, LPES is limited by the resolution of the electron spectrometer. On the other hand, laser photodetachment threshold (LPT) spectroscopy uses a tunable light source to measure the threshold detachment energy. In this way LPT spectroscopy can achieve resolutions on the order of the bandwidth of the light source used and so very accurate measurements are possible, particularly when the excess electron is ejected into an *s*-wave continuum [5]. When an electron is ejected into a *p*-wave continuum, the very gradual onset of the photodetachment cross section near the threshold hampers the accurate determination of the threshold position. However, this technique has recently been successfully employed to obtain high accuracy measurements on the bound states of many *p*-wave detaching negative ions [6–8].

The present paper reports high resolution LPT measurements of Pt^- and Ir^-, from which high accuracy electron affinities (EA's) are deduced. The high-energy resolution and very low statistical noise obtained in these measurements have enabled the detection of a small, but clearly observable, deviation from the detachment cross-section behavior proposed by current threshold models. Similar deviations have previously been reported in negative ions for photon energies relatively far above the detachment threshold [9], but not for photon energies very near the threshold, as observed here.

II. EXPERIMENTAL METHOD

The apparatus is described in detail elsewhere [5], although for the present experiments no Raman conversion is required and hence none of the associated optical components are needed. Laser light of the required wavelength is produced using a dye laser pumped with the second harmonic of a Nd:YAG (yttrium aluminum garnet) laser, operating at a 10-Hz repetition rate. The laser beam is passed through a viewport into an UHV chamber to intersect with the negative ion beam at a 90° angle. The laser light is monitored with a pulse-energy meter located after the exit viewport to the vacuum chamber. Negative ions of the desired element are produced with a cesium sputter source. The ions are then accelerated, mass selected by 30° deflection in a magnetic field, charge state selected by electrostatic deflection plates, and sent into the UHV chamber. After crossing the laser beam, the residual ions are deflected by a second set of electrostatic plates and monitored in a Faraday cup, while the photodetached neutrals are detected with a discrete-dynode electron multiplier operating in an analog regime. The preamplified output signal is gated and integrated with a boxcar averager, and finally recorded with a personal computer for analysis.

*Present address: JILA, University of Colorado, Boulder, CO 80309-0440.

†Also with the Department of Engineering Physics, the Brockhouse Institute for Materials Research, and the Center for Electrophotonic Materials and Devices, McMaster University, Hamilton, Ontario, Canada.

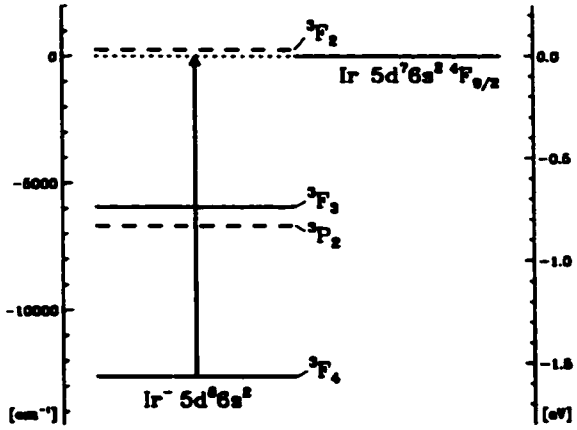

FIG. 1. Energy-level diagram for Ir^- and the ground state of Ir. Two of the negative-ion states have not yet been observed, and are located according to the predicted positions by long dashed lines in the figure. The vertical arrow indicates the detachment channel studied here.

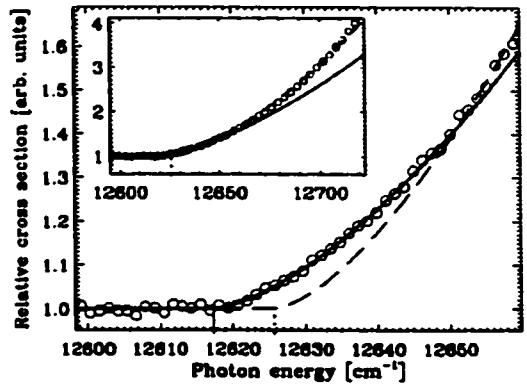

FIG. 2. Observed photodetachment spectrum of Ir^- near the ground-state detachment threshold, $^3F_4 \rightarrow {}^4F_{9/2}$. The solid curve is the Wigner threshold law determined by the best fit to the data, including points below 12 650 cm^{-1} only. This is extrapolated to include the entire range of the inset. A solid vertical line marks the fitted threshold position. The dashed curve is a Wigner law fit to the entire scan range shown in the inset. On this scale the dashed line seems to agree quite well with the data, suggesting that this deviation could be easily overlooked in a lower-resolution scan. However, a poor fit is apparent near the threshold and a fitted threshold position (dashed vertical bar) significantly higher than the solid curve is obtained. See Sec. IV for further discussion on the observed deviation from the Wigner law.

The lasing wavelength is tuned so that the relative detachment cross section can be measured over a range of photon energies. The Wigner threshold law [10] predicts that the cross section is equal to 0 for photon energies smaller than the photodetachment threshold, and is proportional to $(\epsilon - \epsilon_0)^{l+1/2}$ for photon energies ϵ that are larger than the detachment threshold energy ϵ_0. The angular momentum l of the detached electron is 1 for the Ir^- and Pt^- ions studied here, resulting in a p-wave threshold. In practice, a small photodetachment background signal stemming from the detachment of excited negative ions and/or from ionic contaminants present in the ion beam is unavoidable, and must be fit to the observed spectrum (a more detailed discussion of the p-wave fitting procedure can be found in Ref. [6]). The cross section σ is then given by

$$\sigma = \begin{cases} a, & \text{for } \epsilon \leq \epsilon_0 \\ a + c(\epsilon - \epsilon_0)^{3/2}, & \text{for } \epsilon > \epsilon_0 \end{cases} \quad (1)$$

Here the constant a has been added to the Wigner law to account for a possible photodetachment background signal, and c is the proportionality constant implicit in the Wigner law. Additionally, a linear term may be included to account for a small slope in the background signal.

III. RESULTS

A. Ir^-

An energy-level diagram for the lowest-lying states of the Ir negative ion with respect to the ground state of neutral Ir is given in Fig. 1. The ionic states presented all have a $5d^8 6s^2$ configuration, the ground state being the $^3F_4$ level. On the basis of multiconfiguration Dirac-Fock calculations, the $^3F_3$ and $^3P_2$ states are predicted to be bound, while the $^3F_2$ state is expected to be slightly unbound [11]. Thøgersen *et al.* observed a 1 + 1 photon detachment via a resonant magnetic dipole ($M1$) transition in Ir^-, locating the $^3F_3$ state at 7087.3(4) cm^{-1} above the ionic ground state [11]. The other two excited states have not yet been observed. There are two previous measurements of the binding energy of the $^3F_4$ level, and thus the EA of Ir. Using LPES, Feigerle *et al.* measured the EA of Ir to be 12630(65) cm^{-1} [12], and Davies *et al.* obtained an EA of 12613(4) cm^{-1} [13] using LPT spectroscopy.

A beam current of 100 nA of 8.5-keV Ir^- ions was obtained in the interaction chamber. A 120-cm^{-1} region including the $^3F_4 \rightarrow {}^4F_{9/2}$ threshold was selected, and scanned five times in succession. No significant variation of the signal amplitude, threshold position, or threshold shape was observed in successive scans. The sum of the scans, normalized to the magnitude of the background signal, is presented in Fig. 2. From the fitted threshold one obtains the EA of Ir to be 12617.4(12) cm^{-1} [1.56436(15) eV, using 1 eV = 8065.5410 cm^{-1} [14]] (all uncertainties, the sources of which are discussed in Sec. IV, are quoted to one standard deviation). This result is in good agreement with the previous measurements.

B. Pt^-

The accepted energy-level scheme for Pt^- is presented in Fig. 3. In addition to the $5d^9 6s^2\,{}^2D_{5/2}$ ground state, two bound states are expected in Pt^-. The $^2D_{3/2}$ level has been measured via a bound-bound resonant $M1$ transition to lie 9740.9(5) cm^{-1} above the ionic ground state, while the $5d^{10}6s\,{}^2S_{1/2}$ state is predicted to lie about 11300 cm^{-1} above

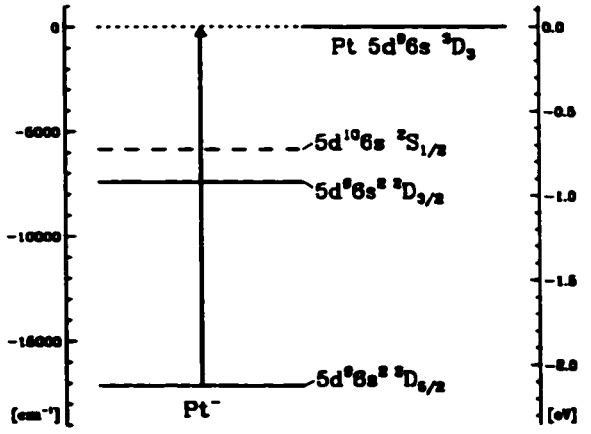

FIG. 3. Energy-level diagram for Pt^- and the ground state of Pt. The $^2S_{1/2}$ state has not been observed experimentally, and its expected position is indicated by a dashed line in the figure. The threshold studied in the present experiment is indicated by the vertical arrow.

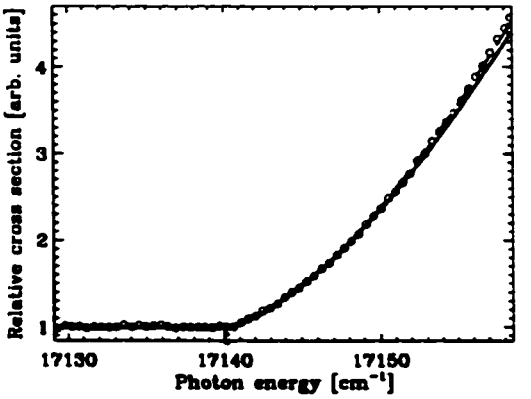

FIG. 4. The $^2D_{3/2} \rightarrow {}^3D_3$ detachment threshold in Pt^-. When only data points below 17150 cm^{-1} are included in the Wigner law fit, the solid curve is obtained. The dashed curve represents the Wigner law fit obtained when all the data points are included. As in Fig. 2, a small but conspicuous deviation from the Wigner threshold law is observed. The discrepancy is discussed in detail in Sec. IV.

the ground state on the basis of multiconfiguration Dirac-Fock calculations [11]. Three previous measurements of the EA of Pt have been performed. The photodetachment spectrum of a region including the $^2D_{3/2} \rightarrow {}^3D_3$ threshold was first measured by Hotop and Lineberger in 1973 [15], from which an EA of 17160(16) cm^{-1} was obtained. In 1992, Gibson *et al.* determined the EA of Pt to be 17125(9) cm^{-1} [16], which did not agree with the Hotop-Lineberger result within two standard deviations. Finally, a third measurement was reported in the 1996 paper by Thøgersen *et al.*, giving the EA of Pt as 17141(6) cm^{-1} [17], roughly equally spaced between the two previous results (see Sec. V for a summary of these results). Since all three experiments used the same ion production mechanism and experimental technique, the poor agreement between the three results is somewhat unexpected, and warrants further investigation. Therefore, we have measured the photodetachment spectrum of Pt^- near the ground-state detachment threshold with a set of very high-resolution scans.

A high-purity (99.98%) Pt metal pellet, set into an aluminum cathode mount, was used in the sputter source to produce 450 nA of 8.5-keV Pt^- ions in the interaction chamber. A much stronger detachment signal was observed for Pt^- than for Ir^-, mainly because an *s*-orbital electron is removed during photodetachment of Pt^-, while in Ir^- a *d* electron is removed, which is known to have a cross section typically about an order of magnitude smaller [12,18]. The larger ion current and laser-pulse energies available (30 mJ as opposed to 15 mJ for Ir^-) also increased the observed photodetachment signal. Because of the much stronger detachment signal, photon energies closer to the threshold could be scanned with the preservation of good statistics. The much smaller range (<30 cm^{-1}) scanned also reduces the uncertainty due to a possibly varying background signal, as was present in the Hotop-Lineberger experiment [15]. As with Ir, this range was repeatedly scanned, and only statistical variations in the spectrum were observed from one scan to the next. The sum of the scans, normalized to the below-threshold signal, is shown in Fig. 4. A threshold position of 17140.1(4) cm^{-1} [2.12510(5) eV] is obtained from the fit, a factor of 15 improvement in accuracy over the most recent result of 17141(6) cm^{-1} obtained by Thøgersen *et al.* [17]; the two results are in excellent agreement.

IV. DISCUSSION

The very slow onset of a *p*-wave threshold structure typically limits the accuracy with which the threshold position can be measured. However, the very good statistics obtained in the present experiments, especially for Pt^-, allow for an excellent fit to the data, and a careful consideration of potential systematic uncertainties is in order. These include uncertainties in the laser calibration, potential Doppler shifts, possible ponderomotive shifts, and uncertainties due to the Wigner approximation. A detailed discussion of the potential sources of errors associated with this apparatus can also be found elsewhere [5,6].

The dye laser tuning mechanism is calibrated against known optogalvanic lines obtained from a low-pressure Ar gas cell. A set of lines lying near the region of interest is measured immediately following each experiment, allowing for a calibration uncertainty of less than 0.2 cm^{-1} at the wavelengths used here. Small deviations from the nominally 90° angle between the laser beam and the ion beam in the interaction region can produce significant Doppler shifts. Therefore, care was taken to ensure that the angle could be realized to better than 1°, resulting in an uncertainty of less than 0.1 cm^{-1} for the photon energies and ion velocities in the present experiments. Very high-intensity light fields can also influence the apparent threshold position due to the ponderomotive potential [19]. However, for the relatively low intensities obtained in the interaction region a shift of ≤ 0.01 cm^{-1} is expected, and is negligible in the present context.

Finally, the functional form of the fitting model itself must be considered. Due to the very gradual onset (zero slope) of the p-wave threshold, a sloped background signal can produce significant apparent shifts in the fitted threshold position. A small slope can be easily accounted for by including a linear term for the background in Eq. (1), fitted to a sufficiently large region below the detachment threshold and extrapolated above the threshold [6]. However, more insidious complications can come about due to nonlinear dependencies or fluctuations in the background signal, as are typically observed from the detachment of molecular ion impurities [20]. This can render the extraction of an accurate threshold value very difficult. Furthermore, such nonlinear fluctuations may be very difficult to detect if the photon-energy spacing and/or the statistical fluctuations of the data points are large. Therefore the Ir^- and Pt^- detachment thresholds of the present work were scanned with a very high-energy resolution (i.e., small spacing between data points), and with the very small statistical scatter that is seen in Figs. 2 and 4. The very small and flat signal observed below the threshold indicates that it is very unlikely that any energy-dependent structure due to impurities is present.

There is nonetheless a clear deviation from the expected Wigner threshold law in both the Ir^- and Pt^- detachment spectra presented here; in both cases the spectra above threshold appear to have a larger curvature than the 3/2 power law predicts. The dashed lines in Figs. 2 and 4 represent the fit to all the points in the data set. Only a very slight systematic deviation of the data from the dashed curve can be detected, demonstrating that such a subtle deviation could very easily be missed by a lower-energy-resolution scan. However, when only data very near the threshold are fit to the Wigner law, the deviation becomes very obvious (the solid curve in the figures). Furthermore, differences of 5 cm^{-1} (for Ir^-) and 0.2 cm^{-1} (for Pt^-) are observed in the threshold positions depending on whether the fit is made to all the data points or only to the data points near the threshold. Such a variation of the threshold position is not negligible. A second analysis of the Ag^- detachment spectrum previously measured by the authors [7] reveals the same effect is present in Ag (although it is far less conspicuous there, presumably because of the smaller energy range scanned in that experiment). Five main effects may be imagined to explain these observations: (1) a slowly (nonlinearly) varying background signal due to the detachment of some ionic impurity; (2) the onset of a second threshold or the presence of some broad continuum resonance structure located at slightly higher energies than the primary threshold; (3) the influence of some nonlinearity of the detection system; (4) the modification of the detachment cross section due to stray electric or magnetic fields; and (5) true deviations from the approximating threshold laws. These points are discussed in turn, listed (1)–(5) below:

(1) Mass-coincident, or nearly mass-coincident, weakly bound impurity negative ions present in the ion beam can produce a strong detachment signal. Furthermore, if the impurity is a molecular negative ion, as is commonly the case, then the presence of many closely spaced vibrational and rotational states can produce both sharp and slowly varying energy-dependent signals which can lead to a misinterpretation of the detachment spectrum. However, one would expect that the effects of such impurities would differ in different parts of the spectrum. Since the same increased curvature is observed in all three independent cases, with different masses and thresholds at differing photon energies, it would be an extremely unlikely coincidence for impurities to be responsible for the observed behavior.

(2) An increase in the detachment cross section associated with the onset of a second detachment channel can produce a structure similar to that observed here, as has been observed in a number of p-wave detaching species [6,8,15]. Fortunately the energy-level structure is relatively well known in all three cases [21], and no (observable) threshold is expected within many hundreds of wave numbers. Furthermore, assuming an effective ion source temperature of 1300 K, the excited-state populations in these ions would be $\sim 10^{-3}$ that of the ground state, and would thus produce a proportionally smaller detachment signal. It is therefore not possible to explain the observed threshold deviation on the basis of the onset of a second detachment channel.

(3) A nonlinear response of the detection system can be caused by changes in the amount of amplified spontaneous emission (ASE) present in the dye laser light, variations in the ion current, and nonlinear responses of the detector and/or amplification system. ASE of the laser is avoided by measuring the relative cross section in a very small region of the dye tuning range, over which the ASE component, if present, should not vary. Also, laser dyes are selected such that the scan range is near the maximum laser output, so as to minimize possible ASE components in the dye laser light. Furthermore, in the case of Pt and Ir experiments, the laser tuning curve was such that ASE would have been preferentially produced at photon energies below the detachment thresholds as the laser was tuned to larger photon energies. Therefore, a smaller detachment signal would be detected, contrary to what is observed here. The ion current was continuously monitored and no significant variations were observed. Performing multiple scans also helps to average random fluctuations in the ion-beam current. Saturation due to a signal level that exceeds the linear range of the detector or amplification system can also produce a nonlinear response of the detection system. Although only signals well within the design specifications of the electronics are measured, the linearity of the detection system was verified by monitoring the detachment signal obtained at a fixed wavelength, while varying the laser-pulse energy. Also, signal saturation results in a smaller detected signal, rather than the larger signal amplification that would be required to explain the deviations observed here. Finally, if a nonlinear response of any component of the detection system was present, one would also expect to have seen a similar effect in the high-resolution s-wave detachment spectra measured with this apparatus [5,22–26], but no such nonlinear response was noted.

(4) Static electric fields are known to have an observable effect on the photodetachment cross section of negative ions and have been thoroughly investigated in both s- and p-wave detaching species [27]. We have also observed this effect in C^- [5], Bi^- [25], and O^- [26] due to stray static electric

fields of 10–15 V/cm present in our system. In a p-wave detachment spectrum, such a stray electric field would produce an oscillation of the cross section with a period $\ll 10$ cm^{-1} and an amplitude of $\sim 10\%$, near the photodetachment threshold. Therefore, stray electric fields cannot explain the deviation observed here. Although similar periodic oscillations in the detachment cross section can be observed in a strong static magnetic field [28], the small field strengths expected in the interaction region (on the order of the Earth's magnetic field) would cause small oscillations with a period $\ll 0.001$ cm^{-1}, which does not produce any observable net effect. Finally, the oscillating electric and magnetic fields of the detaching laser light itself could change the structure of the detachment cross section. However, this effect would be limited to a range similar in magnitude to the ponderomotive potential ($\ll 0.01$ cm^{-1}, as discussed above) [19], and hence cannot account for the experimental observations.

(5) The Wigner threshold law describes the asymptotic behavior of the photodetachment cross section "near" the threshold [10]. The range of validity of the Wigner law is not predicted by the original work; however, two theoretical models have been developed to determine the magnitude and form of the leading corrections to the threshold law. The model developed by O'Malley [29] considered the effect of the polarizability α of the neutral atom [30] on the detachment cross section of negative ions, and predicted an increase in the cross section for p-wave detachment. Under this model the threshold law given in Eq. (1) should be modified to read, for $\varepsilon > \varepsilon_0$ (note that terms of order k^4 and higher in the square brackets [ ] have been dropped here),

$$\sigma = a + c(\varepsilon - \varepsilon_0)^{3/2}[1 - C_1 k^2 \ln(a_0 k) + D k^2], \qquad (2)$$

where a_0 is the Bohr radius, $C_1 = 4\alpha/15a_0$, D is a constant, and $k = \sqrt{2m_e(\varepsilon - \varepsilon_0)}/\hbar$ is the momentum of the detached electron, with m_e being the electron mass and $\hbar$ the Planck constant. The reader should note that the second term (the "polarization term") and the third term (the "leading correction term") in the square brackets [ ] have approximately the same dependence on k. Unfortunately, the theory does not predict the amplitude D of the leading correction term, and it is left as a fitting parameter. [O'Malley also considered the effects of a permanent electric quadrupole moment of the neutral. This correction was found to contribute with the same k dependence as the static polarizability but with a typically much smaller amplitude [29,31], and is not included in Eq. (2).] When Eq. (2) is fit to the Ir^- and Pt^- detachment data, the polarization term is found to account for less than 10% of the observed deviation from the Wigner law. One must therefore conclude that the polarization correction is insignificant compared to the leading correction term. This situation corresponds to the model developed by Farley [32], which has successfully described some photodetachment spectra (see, for example, Ref. [23]). Assuming that the polarizability of the atom is negligible ($\alpha = 0$), Farley used the zero-core-contribution approximation to obtain the constant D. However, the model predicts a reduction in the detachment cross section, contrary to what is observed here. Therefore, neither of the detachment models can fully characterize the spectra of the present work.

TABLE I. Comparison between current and previous electron affinity measurements.

Element	Measured EA[a] (cm^{-1})	$R = c/a$ (10^{-3} $cm^{3/2}$)[b]	Reference
Ir	12630(65)	N/A[c]	[12]
	12613(4)	5.5	[13]
	12617.4(12)	3.1	present work
Pt	17160(16)	0.12	[15]
	17125(9)	0.13	[16]
	17141(6)	1.1	[17]
	17140.1(4)	45	present work

[a]Uncertainties (appearing in parentheses) are quoted to one standard deviation.

[b]The constants c and a, respectively, are, the amplitude of the Wigner threshold law and the background level, as defined in Eq. (1). In these units, the numbers tabulated also correspond to the signal-to-background ratio 100 cm^{-1} above the detachment threshold (i.e., $[S_{100} - A]/A$, where S_{100} is the total signal observed 100 cm^{-1} above threshold, and A is the observed background signal).

[c]The Wigner threshold law is not applicable to the LPES measurement technique used in the experiment.

The source of the observed deviation from the Wigner threshold law is therefore not obvious. A number of other works have also found disagreements between observations and the available theoretical models, although at larger photon energies above threshold [9]. It therefore seems likely that an additional effect, beyond those considered in the current detachment models, is required in order to account for the observed deviation from the Wigner law. On the other hand, essentially identical threshold values are returned if any portion of the data is fit up to 35 cm^{-1} above threshold for Ir^- (or up to 10 cm^{-1} for Pt^-), suggesting that the Wigner law is valid up to that point, at least within the resolution of the data. The threshold values obtained from a fit to the Wigner law in these restricted regions are therefore used to obtain the quoted EA's. To accommodate the uncertainties in the fit (including the effect of a possibly sloped background) uncertainties of 1.2 and 0.3 cm^{-1}, for Ir and Pt, respectively, are assigned in addition to the possible systematic errors described above.

V. SUMMARY

A summary of the previous and present results is given in Table I. For ease of comparison, a graphical representation of the results is also provided in Fig. 5. The three Ir^- measurements are in good agreement. On the other hand, the Pt EA measurements agree less well. Although the large number of variables inherent in such experiments renders speculation difficult, some insight can be gained by comparing the spectra obtained in the four works.

As pointed out by Gibson *et al.* [16], the Hotop-Lineberger work [15] was primarily aimed at determining the range in which the Wigner law held, and therefore they

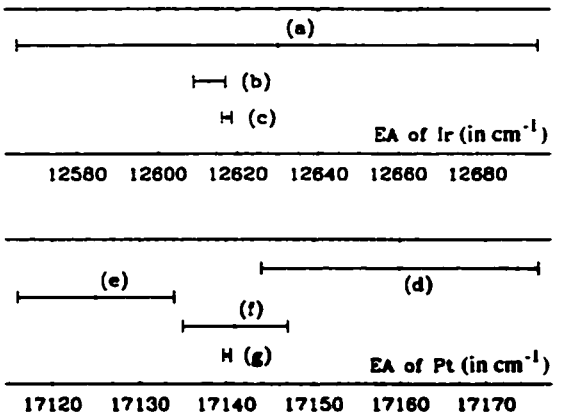

FIG. 5. Graphical representation of the previous (*a*, *b*, *d*, *e*, and *f*) and current (*c* and *g*) measurements of the electron affinities of Ir (top) and Pt (bottom). Note that the scales are different on the two sets. The results are, for Ir, (*a*) Feigerle *et al.* [12], (*b*) Davies *et al.* [13], and (*c*) present work. For Pt, (*d*) Hotop and Lineberger [15], (*e*) Gibson *et al.* [16], (*f*) Thøgersen *et al.* [17], and (*g*) present work.

acquired a spectrum over a large range of photon energies (≈2000 cm^{-1}). A gradual change in the background signal was observed over this range, and had to be accounted for in the fit. To overcome this problem, Gibson *et al.* scanned only a 200-cm^{-1} range around the detachment threshold, and assumed a zero slope background, expecting that the background signal would be constant over this much smaller energy range. Finally, Thøgersen *et al.* scanned approximately the same range and obtained a third result that (marginally) agreed with the Hotop-Lineberger result, but did not agree with the value of Gibson *et al.* within error bars. In the present experiment, we scanned only a 30-cm^{-1} range, and obtained a value which agrees well with the result of Thøgersen *et al.*, but not with the previous two results. Although some of the discrepancy might be explained by an unnoticed deviation from the Wigner law, this is unlikely to explain the difference in the second and third results which cover essentially the same energy ranges. However, comparing the data plots of the four experiments suggests that the divergent results may also be due to the drastically different background levels observed in each experiment, perhaps stemming from molecular ion impurities. As previously noted, energy-dependent variations in the background signal can have a significant effect on the fitted threshold position [6,15,16].

The ratio $R = c/a$, with c the amplitude of the Wigner law fitting function and a the background level, as defined in Eq. (1), can be used as a measure of the signal-to-background ratio. The ratio R for each experiment is included in Table I for comparison (the values for the previous experiments can be easily deduced from the plots of the relative cross section found in the respective works). It can be noted from Table I that the (relative) background signal level changed by more than two orders of magnitude between the four experiments on Pt$^-$. Since all four experiments used the same type of ion production method (a sputter ion source), and since the fine-structure splitting of Pt$^-$ is so large (nearly 10000 cm^{-1}), it is difficult to explain such a large difference in the observed background signals on the basis of varying amounts of excited-state populations in the ion beam. It is more likely that varying amounts of weakly bound ionic contaminants were present in the four experiments [20]. The much better signal-to-background ratio obtained in the current experiment (as indicated by the significantly larger ratio R) suggests that few or no impurities were present.

VI. CONCLUSIONS AND OUTLOOK

This paper has described high-precision measurements of the electron affinities of Pt and Ir, with significant improvements over previous results. Apparent disagreements in the previous EA measurements of Pt have been discussed, and are likely attributable to the much larger background signal observed in those measurements. A significant systematic deviation from the Wigner threshold law was observed in both detachment spectra, and remains unexplained under the currently available threshold models. This result strongly suggests that improvements in the threshold models may be necessary to obtain satisfactory fits to the increasingly higher-quality measurements now achievable with modern measurement techniques, even for photodetachment ranges restricted very near to the threshold. More advanced models would be particularly important for *p*-wave detaching elements because of the zero-slope onset of the threshold, which makes them especially sensitive to deviations from the threshold behavior. Further experimental work is also required to better understand the deviations observed here. Since the original work by Hotop and Lineberger [15], very few experiments have been aimed at explicitly establishing the range of validity of the threshold laws [31,33]. Considering the significant improvements to threshold measurement techniques in the past decades, a new comprehensive experimental study of this sort may now be appropriate. Good candidates for such studies on *p*-wave detaching species may be the precious metal and nickel group negative ions. In addition to the high sputter-ion currents easily obtainable for these elements, the threshold energies of these elements lie in easily accessible laser light regions, and therefore high-resolution data should be achievable. Furthermore, the relatively large energy spacings between the ionic states and between the low-lying neutral states in these elements reduce complications in the photodetachment spectrum over large energy regions. Exploring many ions with a similar electronic structure (such as all ions of a particular group) may also aid in identifying trends in the photodetachment behavior.

ACKNOWLEDGMENTS

Support for this work from the Natural Science and Engineering Research Council of Canada (NSERC) is gratefully acknowledged. We would also like to thank Victor Petrunin and Torkild Andersen for many interesting and helpful discussions.

[1] C. Blondel, Phys. Scr. **58**, 31 (1995); D. R. Bates, Adv. At. Mol. Opt. Phys. **27**, 1 (1991); T. Andersen, Phys. Scr. **34**, 23 (1991).

[2] T. Andersen, H. K. Haugen, and H. Hotop, J. Phys. Chem. Ref. Data (to be published).

[3] A. E. Litherland, Annu. Rev. Nucl. Part. Sci. **30**, 437 (1980); W. Kutschera and M. Paul, *ibid.* **40**, 411 (1990).

[4] C. Blondel, C. Delsart, and F. Dulieu, Phys. Rev. Lett. **77**, 3755 (1996).

[5] M. Scheer, R. C. Bilodeau, C. A. Brodie, and H. K. Haugen, Phys. Rev. A **58**, 2844 (1998).

[6] M. Scheer, C. A. Brodie, R. C. Bilodeau, and H. K. Haugen, Phys. Rev. A **58**, 2051 (1998).

[7] R. C. Bilodeau, M. Scheer and H. K. Haugen, J. Phys. B **31**, 3885 (1998).

[8] P. L. Norquist, D. R. Beck, R. C. Bilodeau, M. Scheer, R. A. Srawley, and H. K. Haugen, Phys. Rev. A **59**, 1896 (1999).

[9] Since models of the photodetachment threshold behavior are held to be true only "near" the detachment threshold, deviations from these predictions farther above the photodetachment threshold are not unexpected, and were observed in early photodetachment experiments (see Ref. [15] for example). However, it has proven very difficult to predict what photon energies are "close enough" to the threshold for the models to apply. For example, although the correction derived by Farley accurately described the photodetachment spectrum of B^- over a very large range [23], it was found to be inappropriate for the detachment spectrum of the very similar system Al^- [24,33].

[10] E. P. Wigner, Phys. Rev. **73**, 1002 (1948).

[11] J. Thøgersen, L. D. Steele, M. Scheer, H. K. Haugen, P. Kristensen, P. Balling, H. Stapelfelt, and T. Andersen, Phys. Rev. A **53**, 3023 (1996).

[12] C. S. Feigerle, R. R. Corderman, S. V. Bobashev, and W. C. Lineberger, J. Chem. Phys. **74**, 1580 (1981).

[13] B. J. Davies, C. W. Ingram, D. J. Larson, and U. Ljunblad, J. Chem. Phys. **106**, 5783 (1997).

[14] E. R. Cohen and B. N. Taylor, Rev. Mod. Phys. **59**, 1121 (1987).

[15] H. Hotop and W. C. Lineberger, J. Chem. Phys. **58**, 2379 (1973).

[16] N. D. Gibson, B. J. Davies, and D. J. Larson, J. Chem. Phys. **98**, 5104 (1993).

[17] J. Thøgersen, L. D. Steele, M. Scheer, C. A. Brodie, and H. K. Haugen, J. Phys. B **29**, 1323 (1996).

[18] P. C. Engelking and W. C. Lineberger, Phys. Rev. A **19**, 149 (1979); R. R. Corderman, P. C. Engelking, and W. C. Lineberger, J. Chem. Phys. **70**, 4474 (1979).

[19] R. Trainham, G. D. Fletcher, N. B. Mansour, and D. J. Larson, Phys. Rev. Lett. **59**, 2291 (1987); M. D. Davidson, J. Wals, H. G. Muller, and H. B. van Linden van den Heuvell, *ibid.* **71**, 2192 (1993).

[20] A number of molecular anions, with masses near that of Ir and Pt, are known to have photodetachment structure in the energy ranges of interest here. For example, signals from molecular impurities (attributed to the detachment of PtN^-) were studied by Hotop and Linberger [15]. An energy-dependent impurity signal was also observed during Davies *et al.* is photodetachment experiment on Ir^- (attributed to IrH^- at that time) [13]. We have observed similar detachment signals from an impurity molecule in this energy range (believed to be Cu_3^-). For more information on molecular negative ions, see for example, H. Hotop and W. C. Linberger, J. Phys. Chem. Ref. Data **4**, 539 (1975).

[21] *Atomic Energy Levels*, edited by C. E. Moore, Natl. Stand. Ref. Data Ser.–Natl. Bur. Stand. (U.S.) (U.S. GPO, Washington, DC, 1971), Vol. III.

[22] M. Scheer, R. C. Bilodeau, and H. K. Haugen, J. Phys. B **31**, L11 (1998); M. Scheer, H. K. Haugen, and D. R. Beck, Phys. Rev. Lett. **79**, 4104 (1997).

[23] M. Scheer, R. C. Bilodeau, and H. K. Haugen, Phys. Rev. Lett. **80**, 2562 (1998).

[24] M. Scheer, R. C. Bilodeau, J. Thøgersen, and H. K. Haugen, Phys. Rev. A **57**, R1493 (1998).

[25] R. C. Bilodeau, M. Scheer, and H. K. Haugen (unpublished).

[26] M. Scheer, Ph.D. thesis, McMaster University, 1998.

[27] N. D. Gibson, B. J. Davies, and D. J. Larson, Phys. Rev. A **47**, 1946 (1993); **48**, 310 (1993) (and references therein).

[28] O. H. Crawford, Phys. Rev. A **37**, 2432 (1988); D. J. Larson and R. Stoneman, *ibid.* **31**, 2210 (1985); W. A. M. Blumberg, W. M. Itano, and D. J. Larson, Phys. Rev. A **19**, 139 (1979).

[29] T. F. O'Malley, Phys. Rev. A **137**, A1668 (1965). Note: the polarization term appeared with the incorrect sign here (see, for example, Ref. [15]). The correct sign is used in Eq. (2).

[30] Approximate (calculated) ground-state static polarizabilities of 50, 51, and 44 atomic units for Ag, Ir, and Pt, respectively, can be found in complied tables. See, for example, V. P. Shevelko, in *Atoms and Their Spectroscopic Properties*, edited by G. Ecker, P. Lambropoulos, I. I. Sobel'man, H. Walther, and H. K. V. Lotsch (Springer, New York, 1997).

[31] R. D. Mead, Keith R. Lykke, and W. C. Lineberger, in *Photodetachment Threshold Laws*, Invited Papers of the XIII International Conference on the Physics of Electronic and Atomic Collisions, Berlin, 1983, edited by J. Eichler, I. V. Hertel, and N. Stolterfoht (Elsevier, New York, 1984).

[32] J. W. Farley, Phys. Rev. A **40**, 6286 (1989).

[33] D. Calabrese, A. M. Covington, J. S. Thompson, R. W. Marawar, and J. W. Farley, Phys. Rev. A **54**, 2797 (1996).

4.1.3 Paper 3 — Theoretical and experimental binding energies for $d^7s^2\ ^4F$ in Ru^-, including calculated hyperfine structure and M1 decay rates

This paper was a joint experimental-theoretical study of the negative ion of ruthenium. No previous measurement or calculations had been performed on this ion, and the study therefore marks an important step towards obtaining a complete knowledge of the elemental negative ions. It also demonstrates that measurements of nested *p*-wave thresholds can provide accurate fine structure measurements, although they are clearly much more challenging than their *s*-wave counterparts (see for example Section 4.2.2 and Section 4.2.3).

I was the primary investigator for all aspects of the *experimental* part of this work, which includes the experimental realization, data analysis, and writing of the experimental sections of the manuscript, as well as coordinating the effort with the Michigan group. M. Scheer aided in the preliminary experiments on the ground state, and provided valuable feedback in the manuscript preparation. R. Srawley assisted in the final experiments on the ion. H. K. Haugen provided supervisory support and input on the manuscript preparation. The members of the Michigan group were responsible for the *theoretical* portion of the work. It is important to note that although there was clearly interaction between the theoretical and experimental groups throughout the project, the theoretical and experimental portions of the work were completed separately. In particular, *I claim no credit for the theoretical sections.*

PHYSICAL REVIEW A VOLUME 59, NUMBER 3 MARCH 1999

Theoretical and experimental binding energies for the $d^7s^2\,^4F$ levels in Ru^-, including calculated hyperfine structure and $M1$ decay rates

Peggy L. Norquist and Donald R. Beck
Physics Department, Michigan Technological University, Houghton, Michigan 49931

René C. Bilodeau, Michael Scheer, Raphaël A. Srawley, and Harold K. Haugen*
Department of Physics and Astronomy, McMaster University, Hamilton, Ontario, Canada L8S 4M1

(Received 5 August 1998)

Relativistic configuration interaction (RCI) calculations predict that the $4d^75s^22J=9$, 7, 5 and 3 ^4F levels of Ru^- are all bound with binding energies 1.076, 0.905, 0.795, and 0.725 eV, respectively. Using laser photodetachment threshold spectroscopy, the binding energies of the $2J=9$ and $2J=7$ levels are measured to be 1.04638(25) and 0.8653(10) eV, respectively, in good agreement with the calculated values. Hyperfine structure constants for all levels and magnetic dipole decay rates have also been calculated, and a systematic study of the important role of quadruple excitations is presented. [S1050-2947(99)04503-5]

PACS number(s): 32.10.Hq, 32.10.Fn, 32.70.Cs, 32.80.Gc

I. INTRODUCTION

For different reasons, negative ions pose substantial challenges to the experimental and theoretical communities. For the theorist, electron correlation effects can be the dominant contribution to the electron affinity (EA, of the neutral atom), and for the medium to high Z species, of interest here, relativistic effects need to be included from the outset in any calculation. Experimentally, negative ions are often difficult to form in high concentrations, and they can be quite fragile, easily detaching electrons [1]. As for transition-metal negative ions, aside from Tc^- and Re^-, the least studied [2] species are Ru^- and Os^-. Previously, only semiempirical (by extrapolation) results existed [3], which predict a bound ground state $d^7s^2\,^4F$ with binding energies ~ 1.1 eV. In this work, we report relativistic configuration interaction (RCI) results for Ru^-. We are currently obtaining theoretical and experimental results for Os^-.

In addition, the results of laser photodetachment threshold (LPT) spectroscopy experiments on the $^4F_{9/2}$ and $^4F_{7/2}$ levels of Ru^- are reported. As with most transition-metal negative ions, Ru^- detaches into a p-wave continuum. A p-wave threshold can be very challenging to measure with high-precision infrared LPT spectroscopy, because of the very gradual onset of the threshold. The current work is based on the method recently demonstrated by the authors on bound states of a number of other transition-metal negative ions [4,5].

Recent relativistic correlated fully *ab initio* treatments of medium to high Z negative ions include at least four different, though related, approaches, which are (references given are only illustrative and not comprehensive) multiconfigurational Dirac-Fock [6], RCI, relativistic many-body perturbation theory [7], and relativistic coupled cluster theory [8]. Currently, a strength of the first two methods lies in their general applicability, whereas a strength of the last two lies in their achieved accuracy for "simple" systems. One may also note the closely related work of the "Russian group" [9] which is competitive, though not always fully *ab initio*.

II. THEORETICAL METHODOLOGY

We begin by solving the Dirac-Fock equations for the dominant configuration using Desclaux's program [10] and a Dirac-Coulomb Hamiltonian. This provides a reference function (DF), which is then improved systematically, by using perturbation theory to provide a form for the correlated part of the wave function. Initially, we make single and double excitations from the DF function's outermost subshells (e.g., $4d$ and $5s$ for Ru). Subshells not present in the DF function are called "virtual," and their radial functions are represented by relativistic screened hydrogenic functions, with effective charge Z^*. The unknowns, Z^*, and the correlation functions' coefficients are determined by application of the variational principle, which leads to the relativistic configuration interaction (RCI) matrix [11]. In practice, electronlike solutions are assured by constraining the virtual's radial functions to have an $\langle r\rangle$ similar to the DF radial function they are replacing; we also find requiring $n=l+1$ to yield the best convergence.

During computation, several decisions must be made. (i) At what symmetry (l) are the virtuals cut off? In practice, $l=4$ is usually sufficient. (ii) How many radial functions are needed per l? Usually 2 for each l, per originating shell, is sufficient. (iii) How much of the core is excited (opened)? For the most accurate results presented here (atom and $2J=9$ ion), it appears opening the outermost closed p shell is adequate. (iv) Do we need to go beyond a first-order (singles and doubles) "form," and if so what must be included? Briefly, the answer is yes, as can be determined by monitoring the largest valence energy contributions (e.g., $5s^2\rightarrow p^2$) as the core is opened. These decline as the core is opened. We interpret this as partly being due to the pulling away of e.g., $5s^2$ from $5p^2$, due to the greater amount of correlation

*Also with the Department of Engineering Physics, the Brockhouse Institute for Materials Research, and the Center for Electrophotonic Materials and Devices.

introduced in $5s^2$ as the core is opened. We partly correct this [12] by introducing the equivalent correlation into $5p^2$; such configurations are frequently triple or quadruple excitations with respect to DF, so that we are beginning to construct a second-order wave function. The remainder of the correction arises from other quadruple excitations formed from products of the largest pair excitations. These partially cancel the pair-pair interactions which decrease the correlation energy.

Due to the presence of open-shell d electrons, most correlation configurations can have many parents (a few thousand), which are constructed from many determinants ($\lesssim$14 000 here). Left in this form, one could be dealing with an RCI matrix of one hundred thousand parents, involving matrix elements which are constructed from (double) sums of tens of thousands of determinants. However, within the first order (in form) correlated wave function, one can reduce the number of correlation parents greatly, by realizing that their interaction with the DF (zeroth-order) function can be expressed in terms of a small number of radial integrals. To use this, we rotate the original set of parents, for each nonrelativistic manifold (group of relativistic configurations reducing to the same configuration in the nonrelativistic limit), to maximize the number of zeros. Rotated parents having zero interaction with the DF reference function are discarded. This process is called REDUCE and has been automated [13]. Calculations for Zr I [14] using REDUCE introduced errors in the total energy of 10–20 meV as compared to a calculation when REDUCE was not used.

In carrying out this work, and especially that for the homologous Os-Os$^-$ case [15], it was found that rather large errors in the EA existed (above 100 meV for Os-Os$^-$), when obtained in the conventional way. Results presented here will demonstrate that this is mainly due to the absence of a few important quadruple excitations in the negative ions, and that which excitations these are can be predicted *a priori*, based on energy analysis tables such as Table I of this work. Such excitations are needed to help correct the well known size inconsistency in the CI process.

Basically, these important quadruple effects arise from products of the most important pair contributions, viz. products of $5s^2 \rightarrow p^2, 4d5s \rightarrow p^2 + sd + pf$. But, treatment of these excitations requires substantial revision of our existing algorithm [13], for two reasons: (i) the number of determinants in the final rotated functions greatly exceeds the existing limit of 5000 (at least 25 000 will be needed); (ii) each quadruple excitation will have multiple references (pair excitations), and some of these will be REDUCE vectors themselves. This is a "new" type of reference function, as well as being more complicated, and new programming must be done to accommodate them. It is of course desirable to keep the number of reference functions to a minimum, because the number of final (rotated) quadruple vectors kept is directly proportional to this number. As an illustration, the $4d^5vp^2vf^2 2J=9$ rotated manifold has 33 vectors formed from 13 935 determinants. Prior to rotation, there were 4598 vectors, so we have achieved a reduction of a factor of 139. It is important to understand that the more complicated the atomic state (greater number of open d/f subshell electrons), the *larger* the reduction.

After diagonalization, the size of the RCI matrix may be further reduced (allowing for additional configurations) by removing "small" parents ("scrubbing"). For single and double excitations, this may be done on an energy basis [16]. For triple and quadruple excitations, we use a coefficient test. Currently energy and coefficient thresholds are 0.04 meV and 0.0004, and they result in removal of about 50% of the parents, with only a few meV loss in total energy. For Ru$^-$ $2J=9$, the fully scrubbed REDUCE'd matrix is of order 5619.

A final computational advantage lies in the fact that all states (atom and ion) involve the d^7 electrons "pretty much" coupled to a ^4F. We would expect that, to a considerable degree, correlation associated with just these electrons will be much the same for all states, and so can be ignored. This strategy should be most effective for the ion states, as we have seen for Sn$^-$ [12] where the terms, but not the configurations, do change. We make use of this by doing less extensive calculations (p shell remaining closed; limited triple and quadruple excitations) for $2J=7$, 5, and 3 and computing their energy differences with the "cruder" (p shell remaining closed, etc.) $2J=9$ state. In this process, it is essential that all states be treated at the same correlation level (equivalent basis sets).

Once the RCI wave functions are generated, both hyperfine structure (HFS) constants (dipole and quadrupole) and magnetic dipole ($M1$) decay rates are obtained. Expressions for HFS matrix elements have been given elsewhere [14] and are based on earlier work of Lindgren and Rosen [17]. Expressions for $M1$ transition rates have been given in Ref. [12]; they are based on the work of Grant [18]. It should be noted that since the RCI wave functions are obtained independently of one another, their basis sets are not orthonormal. In calculating the $M1$ decay rates, nonorthonormality effects are fully accounted for [19] following the work of King *et al.* [20].

The Breit contribution has been treated only at the average [10] energy DF level. Nonaverage magnetic effects are below 0.05 meV. Breit contributions to EAs are small, $\sim$1 meV, so that a more thorough treatment is unnecessary.

III. EXPERIMENTAL METHOD

A schematic diagram of the experimental apparatus is shown in Fig. 1. A more detailed description of the experimental apparatus can be found elsewhere [5]. A 13 keV beam of negative ions is produced with a cesium sputter source and mass analyzed with a 30° bending magnet, set to produce a 4.4 kG magnetic field. The beam then passes through a differential pumping tube and enters an ultrahigh-vacuum (UHV) chamber where pressures of $\sim 10^{-8}$ mbar are maintained. A pair of electrostatic deflection plates serves to charge-state analyze and direct the beam to cross a pulsed laser beam at 90°. The photodetached neutral atoms are detected with a discrete-dynode electron multiplier while the residual negative ions are deflected by a second set of electrostatic plates into a Faraday cup, where currents of $\sim$2.5 nA of Ru$^-$ are observed. A boxcar averager with an $\sim$125 ns gate, triggered via the laser pulse, integrates the signal from the detector. The integrated signal is collected by a personal computer and recorded for subsequent analyses.

The 1000–1375 nm tunable infrared laser light required in

TABLE I. Energy contributions in eV to $Ru^- 4d^7 5s^2 2J=9$ and Ru $4d^7 5s 2J=10$. (Assigned according to "first-order" analysis [16]. Triple and quadruple excitations given as "0.")

Excitation	$Ru^- 2J=9$ No quads	$Ru^- 2J=9$ With quads	Ru $2J=10$
DF	0.3167	0.3167	0
$5s^2 \rightarrow s^2$	−0.0522	−0.0476	N/A[a]
$5s^2 \rightarrow p^2$	−0.4595	−0.5773	N/A[a]
$5s^2 \rightarrow d^2$ (incl. $4d$)	−0.0317	−0.0248	N/A[a]
$5s^2 \rightarrow f^2$	−0.0140	−0.0118	N/A[a]
$5s^2 \rightarrow g^2$	−0.0028	−0.0026	N/A[a]
$5s^2 \rightarrow pf+sd$	"0"	"0"	N/A[a]
$5s \rightarrow s$	−0.0342	−0.0314	0
$5s \rightarrow d$ (incl. $4d$)	−0.0143	−0.0142	−0.0100
$5s \rightarrow g$	−0.0172	−0.0172	−0.0028
$4d5s \rightarrow p^2$	−0.3446	−0.3461	−0.1354
$4d5s \rightarrow d^2$	−0.0085	−0.0085	−0.0049
$4d5s \rightarrow f^2$	−0.0165	−0.0165	−0.0098
$4d5s \rightarrow g^2$	−0.0052	−0.0051	−0.0018
$4d5s \rightarrow sd$	−0.2809	−0.2841	−0.1541
$4d5s \rightarrow pf$	−0.7799	−0.7755	−0.5420
$4d5s \rightarrow dg$	−0.0673	−0.0675	−0.0408
$4d5s \rightarrow fh$	−0.0205	−0.0207	−0.0137
$4d \rightarrow s$ (incl. $5s$)	−0.0173	−0.0172	−0.0131
$4d \rightarrow d$	−0.0682	−0.0682	−0.0469
$4d \rightarrow g$	−0.0922	−0.0922	−0.0990
$4p5s \rightarrow sp$	−0.0462	−0.0454	−0.0290
$4p5s \rightarrow pd$ (incl. $4d$)	−0.1706	−0.1678	−0.1446
$4p5s \rightarrow df$ (incl. $4d$)	−0.0493	−0.0493	−0.0319
$4p5s \rightarrow fg$	−0.0074	−0.0074	−0.0068
$4s5s \rightarrow s^2$	NC[b]	NC[b]	−0.0004
$4s5s \rightarrow p^2$	NC[b]	NC[b]	−0.0015
$4s5s \rightarrow d^2$ (incl. $4d$)	NC[b]	NC[b]	−0.0045
$4d5s^2 \rightarrow p^2d+pdf+pfg+sp^2+spf+s^2d+p^2g$	"0"	"0"	N/A[a]
$4p5s^2 \rightarrow pd^2+p^3+pf^2+spd+pdg$	"0"	"0"	N/A[a]
$4d^25s^2 \rightarrow p^2f^2+p^4+p^3f+p^2sd$	NC[b]	"0"	N/A[a]
$4p \rightarrow p+f$[c]	−1.7616		−1.7807
Breit	+0.0007		0

[a]N/A = not applicable to this state.
[b]NC = not calculated.
[c]Obtained via separate calculation (DF+$4p \rightarrow p+f$).

the experiments is obtained by using the first Stokes beam of Raman converted 8 ns laser light pulses from a Nd:YAG pumped dye-laser, operating at a 10 Hz repetition rate. The Raman conversion is obtained by focusing the dye laser light into a 120 cm long Raman cell filled with H_2 gas at 22(1) bar, producing a Stokes shift of 4155.197(20) cm^{-1} [21]. The anti-Stokes and pump laser beams are eliminated from the recollimated laser beam with dichroic mirrors and silicon semiconductor plates, or with optical glass filters, arranged at Brewster's angle and paired in order to compensate for beam walking as the laser frequency is tuned. The first Stokes laser light is allowed to pass through a vacuum viewport and interact with the negative ion beam in the UHV chamber. After having passed through a second viewport, the light is finally detected by a pulse-energy meter. Average pulse energies of 3.3–3.6 mJ are obtained in the UHV chamber. Since the photons of the weak ($\leq$0.5 mJ per pulse) second Stokes component are not sufficiently energetic to detach the negative ions of ruthenium, even from an excited state, no effort was made to filter that component from the beam.

A threshold energy is extracted by fitting a Wigner threshold law [22] to the collected data. For a photon energy ε and threshold energy ε_0, the Wigner threshold law states that the cross section for detachment vanishes for $\varepsilon \leq \varepsilon_0$, and is proportional to $(\varepsilon-\varepsilon_0)^{\ell+1/2}$ for $\varepsilon > \varepsilon_0$, where ℓ is the angular momentum of the detached electron. Therefore, since the electron is detached into a p-wave continuum in the case of Ru^-, we expect the cross section to have a $\frac{1}{2}$ power-law dependence on photon energy near the threshold.

IV. THEORETICAL RESULTS

RCI calculations begin by making single and pair excitations from the outermost s electrons; these pair excitations

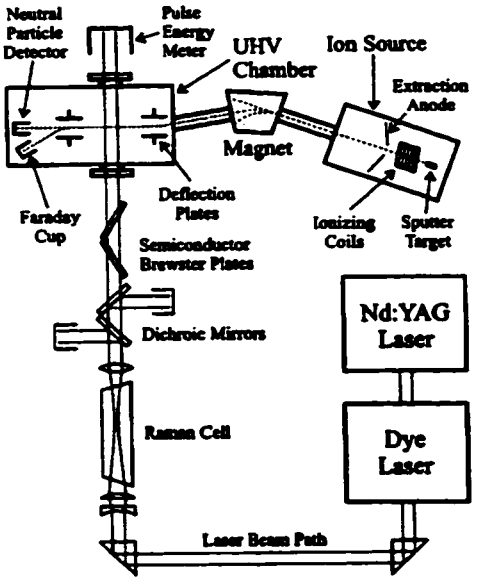

FIG. 1. Schematic illustrating the experimental apparatus (see accompanying text for details).

are present only in the negative ion. Energy contributions, determined by use of second-order perturbation theory [16], are shown in Table I for the $2J=9$ state of Ru^-. The most important of these valence correlations are $s^2 \rightarrow p^2$, $s \rightarrow s$, and $s^2 \rightarrow s^2$. We carefully monitor these contributions as we excite (open) from the core, and when we observe significant changes, introduce triple and quadruple excitations, which tend to partially compensate for these losses. Valence excitations seem (see Table I) to be adequately described by $l=0,4$ and by one radial function per l, except for the p symmetry, which uses two. The first p "virtual" is generated from a MCDF $5s^2+5p^2$ calculation.

The next step is to include the pair excitations $ds \rightarrow$ and single excitations from the d shell. These are major contributors to the Ru EA (the DF contributions are negative in fact), with the $ds \rightarrow sd+p^2+pf$ being the largest. As Table I shows, here it is necessary to include symmetries up to $l=5$. Introduction of these excitations decreases the valence contributions, particularly $s^2 \rightarrow p^2$, by as much as 100 meV. This number is obtained by comparing to a calculation where only excitations from $5s^2$ are allowed (not shown). This is partly because we have treated d^7s^2 and d^7p^2 unequally; we have included $ds \rightarrow$ in the former, but not dp excitations in the latter. When these are introduced (and they are triple excitations with respect to d^7s^2; the specific triples included are listed in Table I by symmetry type), about 1/3 of the energy lost is restored. Coefficients of these triples can be as large as 0.01 in magnitude. Both ds and dp excitations generated manifolds that are so complicated (number of parents, determinants) that the REDUCE methodology [13,14] is used to introduce them.

A nearly complete restoration, as compared to a calculation where only excitations from $5s^2$ are allowed (not shown), of the $5s^2 \rightarrow p^2$ valence correlation energy is achieved with the inclusion of the quadruple excitations $4d^25s^2 \rightarrow p^2f^2+p^4+p^3f+p^2sd$ using the newly modified REDUCE program [13]. Of these, the first is most important. The restoration can be most clearly seen by comparing the two Ru^- columns in Table I (without and with these quadruples). These differ by 98 meV, so the net effect on the binding energy for $2J=9$ is to increase it by 98 meV.

We note that no d^2 excitations are included here. We exclude them, because we believe their large contributions to the total energy make almost no contribution to the Ru EA. This seems confirmed by our DF + $\epsilon(5d^2)$ calculations on Os-Os^- [15]. Furthermore, if they were introduced they would have to be treated in a very balanced way (equivalent basis sets) for atom and ion, and they would have a significant impact on the valence correlations, necessitating the introduction of further (partially) compensating triple and quadruple excitations.

The next computation step is to include ps excitations. From Table I, it is seen these contribute 61 meV to the EA of Ru. Opening this shell also impacts the valence excitations, which is partially compensated for by the inclusion of pp' excitations from d^7p^2. In the process of opening this subshell, it was noted that there was a decrease in the important $ds \rightarrow pf$ contributions (there is a strong $d^2 \rightarrow pf$ interaction between the two, as expected [23]). It is important to note, however, that this change (total energy) had almost zero impact on the EA.

We also included the effect of $4p \rightarrow p+f$ excitations, by doing separate calculations (DF+$4p \rightarrow p+f$) so as to avoid the need for compensating triple excitations. The net effect is to lower the $2J=9$ binding energy by 19.1 meV.

For Ru $2J=10$, we also opened the $4s$ subshell. Since the contribution to the total energy is so small (6.4 meV), it has not been included in any of the Ru EAs. To simplify calculations for the $2J=7,5,3$ Ru^- states, we argue as in Sn^- [12] that there is much correlation in common with the $2J=9$ state. There is a "first-order" theoretical basis for this [24], which applies if (among other conditions) the radial functions for the states do not vary much, and at least one of the two subshells being excited is initially closed. Greater cancellation also ensues because all ion states are associated (mainly) with the same $d^7\ ^4F$ configuration. In this case, we specifically have not opened the p subshell for the $2J=7,5,3$ states, locating them instead with respect to the $2J=9$ state (using a wave function with the p subshell closed).

The binding energies for all states are reported in Table II. Those for $2J=9$ may be extracted from Table I using the formula BE = DF + CA−CI−Breit, where CA (CI) is the correlation energy for the atom (ion). It can be seen that the ion is unbound at the DF level and the Breit contribution is small. Because the binding energies are quite large, we looked at the first excited negative ion state for all J's, but none of these appear bound (all had d^7s^2 configurations). We also did a MCDF ($5s^2+5p^2$) calculation for $2J=1$, and found the energy to be 1.301 eV above the MCDF energy of the Ru^- $2J=3$ state, suggesting that $2J=1$ is not bound.

Table II also includes results for magnetic dipole (A) and electric quadrupole/quadrupole moment (B/Q) constants. Nuclear constants are taken from Fuller and Cohen [25] and Raghavan [26]. For Ru I, very accurate experimental results are available [27] for A and B/Q. Our results are in good agreement with these, though the accuracy could be im-

TABLE II. Binding energies (BE), hyperfine structure constants (A,B), and magnetic dipole decay rates (A).

State	BE (eV)			HFS[b] A (MHz)			HFS[b] B/Q (MHz/b)			$M1$ (s^{-1})[c]
	DF	corr	Total[a]	DF	RCI	Expt.	DF	RCI	Expt.	A[d]
$Ru^- 4d^7 5s^2$										
$2J=9$	−0.3167	1.3866	1.076 1.05(15)[f] 1.04638(25)[g]	−90	−113		338	302		*N/A*[e]
$2J=7$	−0.4936	1.3833	0.905 0.8653(10)[g]	−97	−97		243	220		0.213
$2J=5$	−0.6080	1.3832	0.795	−117	−111		180	162		0.0229
$2J=3$	−0.6802	1.3819	0.725	−192	−165		168	151		0.00741
Ru $4d^7 5s$										
$2J=10$	*N/A*[e]	*N/A*[e]	N/A[e]	1043	1052	948[h]	529	448	459[h]	*N/A*[e]

[a]DF + corr. + magnetic Breit.

[b]For Ru/Ru^-, $\mu=-0.69$, $I=5/2$, $Q=0.457$ barns; μ and I from Fuller and Cohen [25], and Q from Raghavan [26].

[c]In accordance with magnetic dipole selection rules ($dJ=0,\pm1$), decay from the J level occurs only to the $J+1$ level.

[d]RCI values; DF values differ ~1%.

[e]*N/A* = not applicable to this state.

[f]Semiempirical (extrapolated) value from Feigerle *et al.* [3].

[g]Experimental result from this work.

[h]Experimental values [27] for HFS are given to more significant figures.

proved by including core excitations such as $4s\rightarrow s+d$ and $4p\rightarrow p+f$, as we do in more thorough HFS studies [16]. Finally, Table II contains RCI magnetic dipole decay rates for the ion states; these differ little (1%) from the DF values.

V. EXPERIMENTAL RESULTS

The energy level structure of Ru^- is illustrated in Fig. 2. A portion of the data collected from a series of coarse scans, covering photon energies of 7275–9930 cm^{-1}, is shown in Fig. 3. The higher-energy threshold seen here is identified with the $^4F_{9/2}\rightarrow{}^5F_5$ detachment channel, since this channel is expected to be the strongest. Using a "cool" cathode configuration, in order to suppress the background from lower

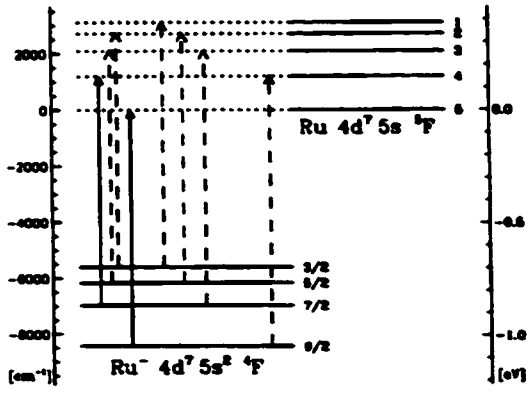

FIG. 2. Energy level diagram of Ru^- and the Ru ground state. The arrows, indicating the allowed detachment thresholds, are spaced proportionally to the threshold energies and ordered by increasing energy from left to right. The solid arrows indicate the thresholds observed in the present study; the other thresholds are dashed.

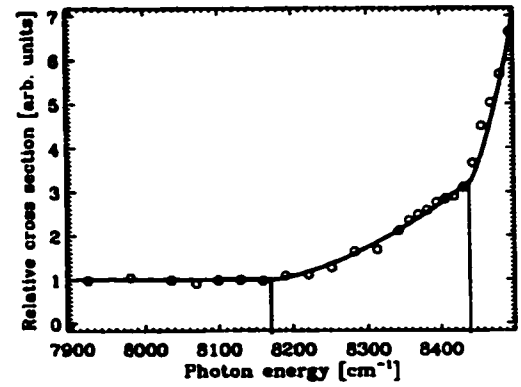

FIG. 3. A portion of the region covered by the series of coarse scans discussed in the text. The higher-energy threshold seen here is the $^4F_{9/2}\rightarrow{}^5F_5$ detachment threshold of Ru^- (see Fig. 4) and the lower-energy threshold corresponds to the $^4F_{7/2}\rightarrow{}^5F_4$ detachment threshold (see Fig. 5). The solid curve was calculated assuming the measured threshold positions (indicated by vertical lines), determined from high-resolution scans. Each data point represents the sum of the signal from 1000 laser pulses. Note that this data was collected with a "hot" cathode, so while the relative cross-section scale in this figure does match that of Fig. 5, it does not match that of Fig. 4.

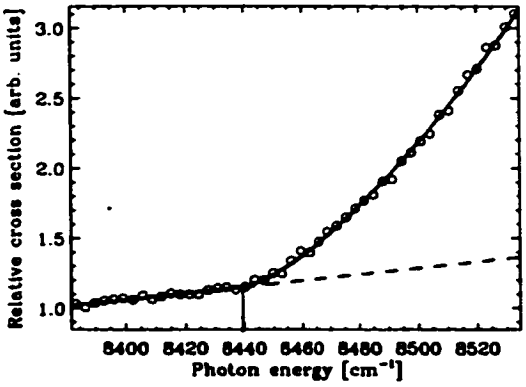

FIG. 4. The $^4F_{9/2} \rightarrow {}^5F_5$ detachment threshold of Ru^-. The solid curve represents the fitted Wigner p wave, including a sloped background, with the best-fit threshold position indicated by the vertical line. The below-threshold signal (extrapolated with the broken line) is largely due to detachment from the excited states of Ru^- (see Fig. 3). Each data point represents the signal collected from 2000 laser pulses. The data for this plot were collected with a "cool" source in order to minimize the background signal due to excited-state population.

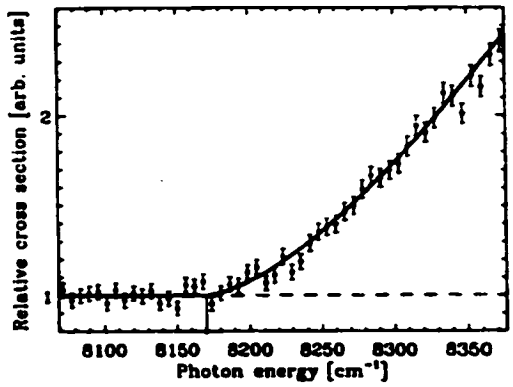

FIG. 5. The $^4F_{7/2} \rightarrow {}^5F_4$ detachment threshold of Ru^-. The solid curve is the Wigner p-wave fit, with the vertical line indicating the best-fit threshold position. The background signal observed here (extrapolated with the dashed line) remains constant over a large range (see text for details). Individual data points represent the signal obtained from 2000 laser pulses. Error bars are one standard deviation, estimated on the basis of counting statistics. To increase the threshold strength, a "hot" ion source was used here.

thresholds (see discussion below), an ≈ 150 cm^{-1} range is selected and repeatedly scanned at a much higher resolution. Figure 4 presents the result of these scans. As can be seen by the fitted solid curve, the expected $\frac{3}{2}$ power-law behavior agrees well with the data, and yields a best-fit threshold energy of 8439.6(20) cm^{-1} (all quoted uncertainties are to one standard deviation and include the systematic errors associated with this apparatus of <0.1 cm^{-1} [21]). Therefore the binding energy of the $^4F_{9/2}$ level, and hence the EA of Ru, is 8439.6(20) cm^{-1} [1.046 38(25) eV, using 8065.5410(24) cm^{-1} eV^{-1} [28]].

Table III lists relative threshold strengths for a "cool" (650 K) and a "hot" (1300 K) ion source, assuming a thermal distribution and L-S coupling [5]. As can be seen from the table, only two other thresholds have a sufficiently high fractional intensity to likely be observed: the $^4F_{7/2} \rightarrow {}^5F_4$ and $^4F_{9/2} \rightarrow {}^5F_4$ detachment thresholds. The latter threshold would be difficult to observe because of the large background signal that would be present from the other seven lower-energy detachment channels. Furthermore, no additional information would be obtained about the negative ion, since the $^4F_{9/2}$ level can be accurately positioned from the observed $^4F_{9/2} \rightarrow {}^5F_5$ threshold (Fig. 4). Therefore, running the ion source "hot," a selected region of ≈ 300 cm^{-1} around the lower energy threshold of Fig. 3, is repeatedly scanned at a high resolution. The result of this set of scans is presented in Fig. 5, where the solid curve represents the best-fit Wigner law with a threshold value of 8170(8) cm^{-1}. Since the signal below this threshold appears to remain constant over the entire range of photon energies of 7275–8150 cm^{-1}, it is improbable that this signal is a result of detachment from a higher-lying excited state of Ru^-, but rather is likely due to a small amount of mass-coincident or nearly mass-coincident impurity molecules such as hydrides. Considering the predicted relative threshold strengths and the ranges scanned, we must assign this second threshold to detachment from the negative ion $^4F_{7/2}$ level to the neutral atom $^5F_4$ level (the leftmost arrow appearing in Fig. 2). By subtracting the $^5F_5$-$^5F_4$ neutral atom splitting of 1190.64 cm^{-1} [29] from the measured threshold energy, we obtain a binding energy for the $^4F_{7/2}$ level of 6979(8) cm^{-1} [0.8653(10) eV]. As a further check, a scan of the $^4F_{9/2} \rightarrow {}^5F_5$ threshold is repeated immediately following the high-resolution $^4F_{7/2} \rightarrow {}^5F_4$ scans. Comparing the amplitudes of the Wigner fits to these two data sets yields an experimental relative strength for the $^4F_{7/2} \rightarrow {}^5F_4$ detachment, with a "hot" ion source, of 12(1) percent, in reasonable agreement with the expected threshold intensity given in Table III.

TABLE III. Calculated intensities of Ru^- thresholds.

Threshold[a]	Relative intensity[b] $T=650$ K	$T=1300$ K	$T=\infty$ [c]
$^4F_{7/2} \rightarrow {}^5F_4$	2.7	13.6	68.2
$^4F_{5/2} \rightarrow {}^5F_3$	0.3	3.3	40.9
$^4F_{3/2} \rightarrow {}^5F_2$	<0.1	0.8	18.2
$^4F_{9/2} \rightarrow {}^5F_5$	100.0	100.0	100.0
$^4F_{3/2} \rightarrow {}^5F_1$	0.1	1.2	27.3
$^4F_{5/2} \rightarrow {}^5F_2$	0.2	2.2	27.3
$^4F_{7/2} \rightarrow {}^5F_3$	0.9	4.5	22.7
$^4F_{9/2} \rightarrow {}^5F_4$	13.6	13.6	13.6

[a]Thresholds are ordered from low to high energies.

[b]Relative intensities are given in percent of the strongest detachment channel.

[c]In the $T=\infty$ case, the population is distributed according to L-S coupling statistics only, and therefore yields the largest relative intensities that can be obtained from a "thermal" ion source.

VI. CONCLUSION AND SUMMARY

In summary, the binding energies of the ^4F $2J=9$ and $2J=7$ levels of Ru^- were successfully measured with infra-

red LPT experiments. The binding energies of the $2J=5$ and $2J=3$ levels were not measured, primarily because of the very low relative intensities of the associated detachment thresholds. It may be possible to increase the detachment signals from these levels by using an alternate "nonthermal" ion production mechanism (such as charge exchange in a metal vapor cell) to increase excited state populations. In addition, a channel-sensitive LPT approach, similar to that used by Dellwo *et al.* on Li^- [30], might allow measurements of the higher-energy thresholds that are difficult to observe due to a large background signal from the lower-lying detachment channels.

The theoretical results for the $2J=9$ and $2J=7$ binding energies are in excellent agreement with experiment. We have identified (and calculated) the important role that a few quadruple excitations have on the Ru EA. The treatment has been sufficiently automated to permit their inclusion in a variety of problems. As might be expected, due to the similarity of correlation effects, the $2J=9\rightarrow 2J=7$ splitting is determined more accurately (~ 10 meV uncertainty) than the absolute value of the $2J=9$ binding energy (~ 30 meV uncertainty).

ACKNOWLEDGMENTS

Support from the National Science Foundation under Grant 96-05213 for the theoretical part of this work is gratefully acknowledged. We are also thankful to the National Research Council of Canada (NSERC) for providing the funding for the experimental work.

[1] T. Andersen, H. H. Andersen, P. Balling, P. Kristensen, and V. V. Petrunin, J. Phys. B **30**, 3317 (1997).
[2] H. Hotop and W. C. Lineberger, J. Phys. Chem. Ref. Data **14**, 731 (1985).
[3] C. S. Feigerle, R. R. Corderman, S. V. Bobashev, and W. C. Lineberger, J. Chem. Phys. **74**, 1580 (1981).
[4] R. C. Bilodeau, M. Scheer, and H. K. Haugen, J. Phys. B **31**, 3885 (1998).
[5] M. Scheer, C. A. Brodie, R. C. Bilodeau, and H. K. Haugen, Phys. Rev. A **58**, 2051 (1998).
[6] See, e.g., W. P. Wijesundera, Phys. Rev. A **55**, 1785 (1997).
[7] E. N. Avgoustoglou and D. R. Beck, Phys. Rev. A **55**, 4143 (1997).
[8] See, e.g., E. Eliav, Y. Ishikawa, P. Pyykko, and U. Kaldor, Phys. Rev. A **56**, 4532 (1997).
[9] See, e.g., V. A. Dzuba and G. F. Gribakin, Phys. Rev. A **55**, 2443 (1997).
[10] J. P. Desclaux, Comput. Phys. Commun. **9**, 31 (1975).
[11] D. R. Beck, program RCI (unpublished).
[12] S. M. O'Malley and D. R. Beck, Phys. Rev. A **57**, 1743 (1998).
[13] D. R. Beck, program REDUCE (unpublished).
[14] D. R. Beck and D. Datta, Phys. Rev. A **48**, 182 (1993).
[15] P. L. Norquist and D. R. Beck (unpublished).
[16] S. M. O'Malley and D. R. Beck, Phys. Rev. A **54**, 3894 (1996).
[17] I. Lindgren and A. Rosen, Case Stud. At. Phys. **4**, 93 (1974).
[18] I. P. Grant, J. Phys. B **7**, 1458 (1974).
[19] D. R. Beck and Z. Cai, Phys. Rev. A **41**, 301 (1990).
[20] H. F. King *et al.*, J. Chem. Phys. **47**, 1936 (1967).
[21] M. Scheer, R. C. Bilodeau, C. A. Brodie, and H. K. Haugen, Phys. Rev. A **58**, 2844 (1998).
[22] E. P. Wigner, Phys. Rev. **73**, 1002 (1948).
[23] D. R. Beck and C. A. Nicolaides, Phys. Rev. A **26**, 857 (1982).
[24] D. Datta and D. R. Beck, Phys. Rev. A **47**, 5198 (1993).
[25] G. H. Fuller and V. W. Cohen, At. Data Nucl. Data Tables **5**, 433 (1969).
[26] P. Raghavan, At. Data Nucl. Data Tables **42**, 189 (1989).
[27] S. Buttgenbach, *Hyperfine Structure in 4d- and 5d- Shell Atoms* (Springer-Verlag, New York, 1982).
[28] E. R. Cohen and B. N. Taylor, Rev. Mod. Phys. **59**, 1121 (1987).
[29] C. E. Moore, *Atomic Energy Levels* (U.S. GPO, Washington, D.C., 1971), NSRDS-NBS 35.
[30] J. Dellwo, Y. Liu, D. J. Pegg, and G. D. Alton, Phys. Rev. A **45**, 1544 (1992).

4.2 s-wave Detaching Species

4.2.1 Paper 4 — Electron affinity of Bi using high resolution photodetachment threshold spectroscopy

The Wigner law for s-wave detachment has an infinite slope at threshold (see Figure 2.3). This fact allows very high accuracy measurements to be performed. The favourable combination of a small energy range with a high signal-to-noise ratio and low background signal in these experiments on Bi^- has allowed for the most accurately determined threshold energy among the measurements conducted at McMaster. As such, it offers a benchmark for the accuracy that can be achieved with LPTS experiments and indicates the concerns which must be addressed in order to push these accuracies even further. These concerns include certain systematic errors such as the Doppler and ponderomotive shifts which have been discussed in detail in Section 3.3, but also the effects of hyperfine structure and stray fields which can change the shape of the threshold law.

All of the high resolution s-wave thresholds observed with the McMaster apparatus have exhibited small oscillations in the detachment cross sections which span a range of one or two cm^{-1} (in addition to this paper, see comments in Section 7.1 and discussions in [1] and Paper 10 listed in the Preface). These oscillations result from the presence of a small static electric field, which appears to be relatively uniform over the interaction region with a magnitude of about 10 V/cm. The effects of this small field are well modelled by theory and are believed to produce no significant error in the determined threshold energy. The effects of the electric field and a description of the model used are detailed in this article.

Bi^- has a large nuclear magnetic moment and spin, which produce significant hyperfine splitting in the neutral and ionic states. As a result, instead of a single

ground state threshold, 14 closely spaced hyperfine thresholds are present. Unfortunately, these thresholds are broadened by the finite laser bandwidth and electric field effects, and the structure cannot be resolved. Instead a smearing of the threshold is observed. The threshold model used in this section therefore includes the theoretically determined hyperfine structure. The hyperfine averaged threshold position is determined from the fit and is corrected to obtain the EA defining threshold energy — i.e. the energy of the lowest hyperfine state of the negative ion with respect to the lowest hyperfine state of the neutral atom.

I was responsible for the completion of all aspects of the work presented in this article, including the experimental realization, data analysis, and writing of the manuscript. The work was done under the supervision of H. K. Haugen, who supplied valuable suggestions and input, especially in editing the manuscript.

Electron affinity of Bi using infrared laser photodetachment threshold spectroscopy

René C. Bilodeau and Harold K. Haugen*

Department of Physics and Astronomy, McMaster University, Hamilton, Ontario, L8S 4M1, Canada

(*Physical Review A*, Volume 64, 024501; ©2001 The American Physical Society)

(Received 4 March 2001; published 17 July 2001)

Abstract

We report the results of high-resolution infrared laser photodetachment threshold experiments on the negative ion of bismuth. Hyperfine structure of the neutral and negative ion ground states are included in the threshold model. The electron affinity of ^{209}Bi is determined to be 7600.66(10) cm^{-1} [942.362(13) meV].

32.10.Hq, 32.80.Gc, 32.10.Fn

Studies of atomic negative ions have led to continued improvements in the binding energies of negative ions in general and the electron affinities (EAs) of atoms in particular, as illustrated by the recent review on the subject [1,2]. The most accurately determined species are among the main body of the periodic table (groups 13 – 17). This situation can be largely attributed to the fact that the negative ions of these elements are formed by the attachment of a p-orbital electron, and thus photodetach into an *s*-wave continuum -- a very favorable condition for laser photodetachment threshold (LPT) spectroscopy measurements [1,3]. Only a handful of elements in these groups remain poorly known, principally because they are either very weakly bound or radioactive, and thus present unfavorable conditions for experimentation. A notable exception is bismuth. The most recent, and accurate, determination of the EA of Bi, 7640(80) cm^{-1}, now dates two decades to the studies on Bi^- by Feigerle *et al.* [4], using laser photodetachment electron spectrometry. The present article updates this value with high-resolution LPT spectroscopy on $^{209}Bi^-$, improving the EA of Bi by nearly three orders of magnitude.

Details of the experimental apparatus and technique can be found elsewhere [3,5]. An 8 keV beam of negative ions is extracted from a cesium sputter source, using a target cathode constructed by compacting high purity bismuth granules into a copper sleeve. The beam is mass analyzed by 30° deflection in a 0.5 T magnetic field. The resulting 6 nA ion beam of Bi^- is then directed with a pair of electrostatic deflection plates into an ultrahigh vacuum (UHV) chamber (with pressures of $\sim 10^{-8}$ mbar) where it interacts with an infrared laser light beam. The infrared beam is generated by Raman shifting the 850 nm output of a pulsed (10 Hz, 8 ns) tunable dye laser in a high pressure H_2 cell. Measurements of optogalvanic lines yield a Raman shift of 4155.197(20) cm^{-1}, consistent with the expected shift of 4155.187(5) cm^{-1} [6] for a H_2 pressure of 22(1) bar (all uncertainties are quoted to one standard deviation, unless otherwise noted). The residual dye laser light and anti-Stokes components are eliminated with a pair of dichroic mirrors and a pair of Si semiconductor plates, arranged at Brewster's angle. The collimated laser light is then directed through a viewport into the UHV chamber to intersect the ion beam at 90°. The neutral atoms

produced by the photodetachment process are detected with a discrete-dynode electron multiplier, while a second set of electrostatic plates deflects the residual negative ions into a Faraday cup. The pre-amplified signal obtained from the detector is integrated with a gated boxcar averager, and finally recorded with a personal computer for analysis.

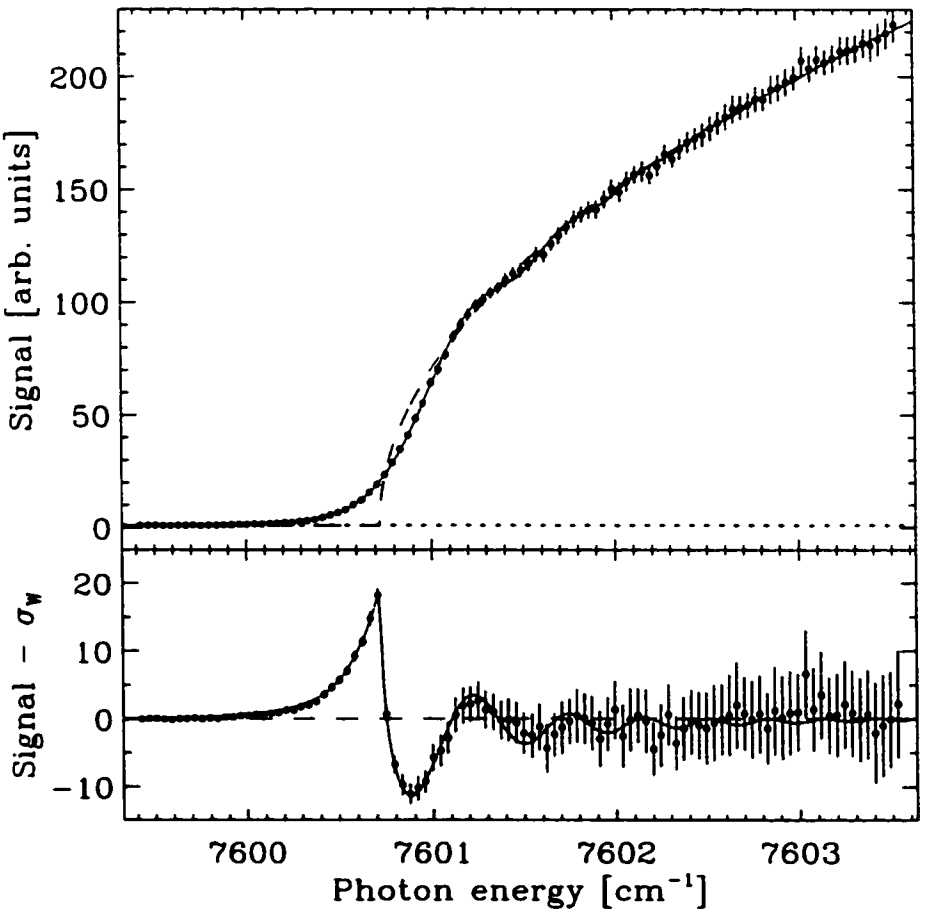

FIG. 1. Photodetachment signal of Bi^- near the $6p^4\ ^3P_2 \rightarrow 6p^3\ ^4S_{3/2}$ threshold. The dashed curve is a Wigner s-wave threshold (Eq. 1). The full curve is the fit to the data using a model that includes broadening effects discussed in the text (Eq. 2). The bottom panel shows the deviation of the observed signal from the Wigner law due to these effects. Error bars are two standard deviations, based on the observed scatter from 1000 laser pulses per data point. The vertical scale has been normalized such that the magnitude of the photodetachment background signal (dotted line) is 1.

The detachment signal observed over a range of photon energies ($h\nu$) covering the EA defining threshold ($6p^4\ ^3P_2 \rightarrow 6p^3\ ^4S_{3/2}$) is shown in Fig. 1. Since the photodetachment process results in the detachment of a p-orbital electron, the photoelectron is ejected as an s-wave (the d-wave component is effectively suppressed by the centrifugal barrier near the threshold). The dashed curve in the figure shows the Wigner threshold law for s-wave detachment:

$$\sigma_w(h\nu; E_o) = \sigma_o + \begin{cases} 0 & (h\nu \leq E_o) \\ a_o\sqrt{h\nu - E_o} & (h\nu > E_o) \end{cases}, \tag{1}$$

where a_o is the threshold amplitude, E_o is the threshold energy, and σ_o is a small (constant) photodetachment background signal, originating from a weakly populated exited state of the ion or a nearly mass coincident impurity ion.

A significant deviation from the Wigner law is clearly observed near the threshold. Similar broadening of the threshold was seen in studies on other s-wave detaching species [3,7,8], and is mainly due to finite laser bandwidth, Doppler broadening, and hyperfine structure of the ion and neutral states. Each hyperfine sublevel F of the ionic $^2P_2$ ground state can detach to a number of hyperfine sublevels F' of the neutral $^4S_{3/2}$ ground state, producing many closely spaced thresholds with energy $E_{FF'} = E_{F'} - E_F$, where $E_{F'}$ and E_F are the energies of the neutral and ionic hyperfine sublevels respectively. Given the average energy E_J of a fine structure level J, the energy of a hyperfine sublevel can be obtained from:

$$E_F = E_J + \frac{AC}{2} + B\,\frac{3C(C+1) - 4IJ(I+1)(J+1)}{8IJ(2I-1)(2J-1)},$$

with $C = F(F+1) - J(J+1) - I(I+1)$. Finally, the relative strengths $S_{FF'}$ of hyperfine thresholds $F \rightarrow F'$ can be calculated using:

$$S_{FF'} = \bar{S} \sum_{j=\frac{1}{2},\frac{3}{2}} (2F+1)(2F'+1) \begin{Bmatrix} I & J & F \\ j & F' & J' \end{Bmatrix}^2,$$

where $\bar{S}$ is defined such that $\sum_{F,F'} S_{FF'} = 1$.

TABLE I. Relative energy and strength of hyperfine thresholds.

F (of ion)	F' (of neutral)	$\Delta E_{FF'}$[a] [cm^{-1}]	Strength ($S_{FF'} \times 100\%$)
2.5	3	0.080	7.9
2.5	4	0.027	4.1
3.5	3	0.088	6.4
3.5	4	0.035	5.9
3.5	5	−0.037	3.7
4.5	3	0.102	3.2
4.5	4	0.049	6.9
4.5	5	−0.023	8.2
4.5	6	−0.119	1.8
5.5	4	0.071	5.7
5.5	5	−0.001	10.3
5.5	6	−0.097	8.0
6.5	5	0.033	5.3
6.5[b]	6	−0.063	22.8

[a]Energy of threshold relative to the average threshold energy, i.e. $\Delta E_{FF'} = E_{FF'} - E_o$.

[b]EA defining threshold.

Unfortunately, due to the other broadening effects and the very small energy shifts produced by the hyperfine structure, it is not possible to obtain an experimental estimate of the hyperfine constants A and B from the observed signal. Table I lists the expected threshold positions and strengths of the 14 allowed detachment thresholds for the ^{209}Bi isotope ($I = 9/2$), based on the known hyperfine constants for the neutral ground state, $A = -446.942(1)$ MHz and $B = -304.654(2)$ MHz [9], and the recently calculated hyperfine constants for the negative ion ground state obtained by Beck [10], $A = -121$ MHz and $B = -415$ MHz. (Note: ^{209}Bi is the only naturally occurring isotope of bismuth.) The total

signal, including the contribution from all the hyperfine components, is then given by:

$$R(h\nu) = \int_{-\infty}^{+\infty} \mathcal{L}(\varepsilon, h\nu) \sum_{F,F'} \sigma(\varepsilon; E_{FF'})\, S_{FF'}\, d\varepsilon.$$

$\mathcal{L}(\varepsilon, h\nu)$ is the lineshape (including the laser bandwidth and Doppler broadening) with a line center at $h\nu$, and $\sigma(\varepsilon; E_{FF'})$ is given by the Wigner law (Eq. 1) or by some more general formula (see below). For more general forms of $\sigma(\varepsilon; E_{FF'})$, a more computationally efficient formula can be obtained with the change of variable, $\varepsilon' = \varepsilon - \Delta E_{FF'}$. We can then write, with the background detachment signal (σ_0) explicitly included,

$$R(h\nu) = \sigma_0 + \int_{-\infty}^{+\infty} \sigma(\varepsilon'; E_0)\, \mathcal{S}(\varepsilon', h\nu)\, d\varepsilon'. \tag{2}$$

Here, $\mathcal{S}(\varepsilon', h\nu)$ is an *effective* lineshape, which includes the effect of hyperfine structure. In particular, assuming a Lorentzian dominated laser lineshape with a full width at half maximum $\Gamma = 0.08$ cm^{-1} we have:

$$\mathcal{S}(\varepsilon', h\nu) = \frac{2\Gamma}{\pi} \sum_{F,F'} \frac{S_{FF'}}{4(\varepsilon' + \Delta E_{FF'} - h\nu)^2 + \Gamma^2}.$$

The function $\mathcal{S}(\varepsilon', h\nu)$ is therefore completely determined from the values of $S_{FF'}$ and $\Delta E_{FF'} = E_{FF'} - E_0$ found in Table I.

Finally, although the interaction region is shielded against electric fields, a small stray electric field is known to remain [3] (likely originating from the electrostatic deflection plates). The effect of a static electric field on the photodetachment cross section has been investigated extensively both experimentally [11] and theoretically [12], and can be modeled to a high accuracy with:

$$\sigma(\varepsilon'; E_0) = a_0'\, \varepsilon' \int_{-\gamma}^{\infty} \mathrm{Ai}^2(\gamma')\, \mathrm{d}\gamma',$$

where $\mathrm{Ai}(\gamma')$ is the Airy function and $\gamma = (2/\mathcal{F}^2)^{1/3}(\varepsilon' - E_0)$ (in atomic units), with $\mathcal{F}$ the magnitude of the electric field. In the present case, the electric field has the effect of increasing the below-threshold signal (through tunneling) and producing a small modulation in the detachment signal above threshold (see bottom panel of Fig. 1). It should be noted

that although the inclusion of an electric field and laser bandwidth improves the quality of the fit, essentially the same threshold energy is obtained.

Since σ_o can be obtained from the level of the below threshold signal, only three parameters remain to be fit: the threshold amplitude a'_o, the electric field magnitude $\mathcal{F}$, and the hyperfine averaged threshold energy E_o. The solid curve in Fig. 1 is the best-fit result of Eq. 2, and yields an electric field of $\mathcal{F}$ = 11 V/cm, consistent with the previously observed value [3]. The most significant sources of error in the determination of the threshold position are from the the laser calibration and possible Doppler shift. (The uncertainties associated with the LPT technique using the McMaster apparatus are discussed in detail elsewhere [3]). The laser is calibrated against optogalvanically active transitions in an argon filled hollow cathode discharge lamp (Hamamatsu). Lines lying near the region scanned are observed immediately following the measurement with a resulting uncertainty of 0.05 cm^{-1}, including the uncertainty in the Stokes conversion value (0.02 cm^{-1}) discussed above. A small, approximately linear, wavelength drift ($\approx$0.01 cm^{-1} per hour) was also observed over the course of the experiment, presumably due to thermal changes in the laser system. We estimate that this effect can be corrected to within an error of 0.015 cm^{-1}. The ion-laser beam crossing angle has been previously calibrated with an uncertainty of 0.1° by careful measurements of the accurately known $O^-(^2P_{3/2} \rightarrow {}^3P_2)$ detachment threshold [1,3]. This alignment can be easily maintained to within 1° between experiments. Given an ion velocity of 90 km/s and photon energy of 7601 cm^{-1}, this can introduce an error due to the Doppler effect of 0.04 cm^{-1}. Finally, it is known that measured thresholds can experience an energy shift in the presence of high intensity, low frequency light fields, due to the ponderomotive potential [13]. However, with peak intensities obtained in the experiment of only $\sim 5 \times 10^6$ W cm^{-2}, a shift of <0.01 cm^{-1} is expected. Including all these possible systematic errors and the statistical uncertainty of the fit (0.02 cm^{-1}), we obtain the final value for the hyperfine averaged threshold of E_o = 7600.72(10) cm^{-1}.

In summary, due to the high resolution of the experiment and large hyperfine splitting of Bi, an analysis including the effects of the hyperfine structure of the neutral and ionic

ground states was required in order to describe the observed spectrum. The EA is defined as the separation between the lowest neutral and lowest negative ion hyperfine states. For ^{209}Bi, this is the $6p^4\ ^3P_2$ ($F = 6.5$) $\longrightarrow$ $6p^3\ ^4S_{3/2}$ ($F = 6$) threshold, which is 0.063 cm^{-1} less than E_o (see Table I). The EA of ^{209}Bi is therefore found to be 7600.66(10) cm^{-1} [942.362(13) meV, using 1 eV = 8065.54477(32) cm^{-1} [14]].

We thank Donald R. Beck for providing theoretical input on the hyperfine constants and Michael Scheer for assisting with the initial experimental work and data analysis. In addition, we gratefully acknowledge the financial support of the Natural Science and Engineering Research Council of Canada (NSERC).

REFERENCES

* Also with the Department of Engineering Physics, the Brockhouse Institute for Materials Research, and the Center for Electrophotonic Materials and Devices, McMaster University.

[1] T. Andersen, H. K. Haugen, and H. Hotop, J. Phys. Chem. Ref. Data **28**, 1511 (1999).

[2] Note: The review article of Ref. [1] lists the EA of Bi obtained from a preliminary analysis of the data presented here. The most recent previous determination of the EA of Bi is 7640(80) cm^{-1}, obtained by Feigerle *et al.* [4].

[3] M. Scheer, R. C. Bilodeau, C. A. Brodie, and H. K. Haugen, Phys. Rev. A **58**, 2844 (1998).

[4] C. S. Feigerle, R. R. Corderman, and W. C. Lineberger, J. Chem. Phys. **74**, 1513 (1981).

[5] M. Scheer, C. A. Brodie, R. C. Bilodeau, and H. K. Haugen, Phys. Rev. A **58**, 2562 (1998).

[6] W. K. Bischel and M. J. Dyer, Phys. Rev. A **33**, 3113 (1986); E. C. Looi, J. C. Stryland, and H. L. Welsh, Can. J. Phys. **56**, 1102 (1978), and references therein.

[7] M. Scheer, H. K. Haugen, and D. R. Beck, Phys. Rev. Lett. **79**, 4104 (1997).

[8] M. Scheer, R. C. Bilodeau, and H. K. Haugen, J. Phys. B **31**, L11 (1998).

[9] R. J. Hull and G. O. Brink, Phys. Rev. A **1**, 685 (1970).

[10] D. R. Beck (private communication).

[11] N. D. Gibson, B. J. Davis, and D. J. Larson, Phys. Rev. A **47**, 1946 (1993).

[12] N. L. Manakov, M. V. Frolov, A. F. Starace, and I. I. Fabrikant, J. Phys. B **33**, R141 (2000).

[13] M. D. Davidson, J. Wals, H. G. Muller, and H. B. van Linden van den Heuvell, Phys.

Rev. Lett. **71**, 2192 (1993), and references therein.

[14] P. J. Mohr and B. N. Taylor, Rev. Mod. Phys. **72**, 351 (2000).

4.2.2 Paper 7 — Negative Ion of Boron: An Experimental Study of the ^3P Ground State

B^- is a light system, having only 6 electrons. As such it has been the target of many theoretical studies. The work presented in this paper was primarily motivated to improve the knowledge of the binding energy of B^- to a level that verifies and challenges these theoretical investigations. This was particularly important since the various theories used different approaches which led to conflicting results. The present results thus allow for a conclusive test of which approach is the most appropriate. Also, the first experimental determination of the fine-structure of B^- was achieved, and indicated that the splittings are considerably larger than the best theoretical prediction. This offers an additional goal for future efforts.

In the context of this thesis, the additional result of the high photon-energy behaviour of the threshold law observed in boron is also of interest. The data obtained in the investigations will be used in Section 4.3, to gain further insight into the correction terms to the Wigner law discussed in Section 2.2.

Although M. Scheer was primarily responsible for the work presented in this paper, I participated heavily in the experimental realization and, to a lesser extent, in the data analysis and editing of the article. H. K. Haugen provided supervision and input in all stages of the work.

VOLUME 80, NUMBER 12 PHYSICAL REVIEW LETTERS 23 MARCH 1998

Negative Ion of Boron: An Experimental Study of the ^3P Ground State

Michael Scheer, René C. Bilodeau, and Harold K. Haugen*
Department of Physics and Astronomy, McMaster University, Hamilton, Ontario L8S 4M1, Canada
(Received 15 October 1997)

An investigation of the $B^-(2p^2\,^3P_J) \rightarrow B(2p\,^2P_{J'})$ photodetachment thresholds using a tunable infrared laser source has yielded a substantially improved value for the electron affinity of boron and the first experimental data on the fine structure of the ionic ground state. The $J = 0-1$ and $J = 1-2$ splittings are found to be 3.23(15) cm^{-1} and 5.18(15) cm^{-1}, respectively, and the electron affinity is determined to be 2256.12(20) cm^{-1} [(279.723(25) meV]. The present result for the electron affinity is the first to challenge the extensive and controversial theoretical studies of this system. [S0031-9007(98)05630-0]

PACS numbers: 32.80.Gc, 32.10.Fn, 32.10.Hq

Present day high-performance computers enable sophisticated *ab initio* calculations of increasingly complex systems with unprecedented precision. Within the realm of atomic physics, negative ions are currently a subject of intensive studies (for recent reviews see Ref. [1]). In general, the fundamental interest in negative ions is motivated by a number of features which are qualitatively different from neutral or positively charged systems; short range interactions lead to a finite number of bound states, and strong electron correlations give rise to correlation energies which are often larger than or comparable to the binding energies in these systems. New experimental techniques now allow the determination of binding energies, fine structure, and excited states in a number of negative ion systems with very high accuracy [2]. The interplay of high-resolution experiments on negative ions and state-of-the-art theoretical calculations provides an important platform for advances in atomic physics. Finally, in terms of applications, negative ions play a role in a variety of atomic and plasma phenomena, as well as in some advanced experimental techniques (e.g., accelerator mass spectrometry).

The negative ions of the light elements, hydrogen through fluorine, have been studied extensively. The electron affinities (EA) of H, C, O, and F were measured via tunable laser threshold photodetachment leaving the neutral atom in its ground state [3–6], whereas the binding energies of Li^- [7,8] and the metastable He^- [9] and Be^- [10] ions have been determined through laser photodetachment involving an excited state of the atom and state-selective detection schemes. Accuracies of experimental EA's for these seven elements range from 0.3 meV (C^-) to 0.001 meV (O^-). In strong contrast, the EA of boron still relies on an early laser photodetached electron spectrum recorded by Feigerle *et al.* [11] which resulted in a value of 277(10) meV (after a subsequent recalibration [5]). Various approaches to the *ab initio* calculation of electron affinities of the light elements have been attempted in recent years [12,13], but even these small systems remain challenging as electron correlations play a dominant role. This is particularly true for boron which forms the most weakly bound stable ion among the light elements. Of the numerous theoretical studies of the EA of boron [12–16], three recent works were aiming at accuracies better than 10 meV. Noro *et al.* [13] obtained an EA of 278 meV as the result of a large-basis-set multireference singly and doubly excited configuration-interaction calculation. Large-scale finite element multiconfiguration Hartree-Fock (MCHF) calculations, which do not suffer from basis set limitations, have been performed by two groups, Sundholm and Olsen [14], and Froese Fischer *et al.* [15]. They report EA's of 268.6(17) and 273.2(2) meV, respectively, as the result of an initial valence correlation MCHF calculation that neglects core polarization effects. Sundholm and Olsen estimate core-valence correlations to lower the EA to 267.8(20) meV, whereas Froese Fischer *et al.* predict the EA to increase to 279.5(20) meV through the inclusion of core-valence and core-core correlations (the latter via core rearrangement). However, the experimental EA of 277(10) meV [11] agrees with all of the above values within uncertainties; hence the fundamental question as to the effect and strength of core-valence and core-core correlations in B^- remains open and controversial. The work reported in this Letter is the first experimental investigation aimed at resolving this important issue, and furthermore provides the first experimental values for the fine structure splittings of the $B^-(2p^2\,^3P_J)$ ground state.

An energy level diagram of B^- in the vicinity of the ground and first excited states of boron is shown in Fig. 1. The $B^-(2p^2\,^3P_J)$ ground state is expected to have fine structure levels with splittings estimated from isoelectronic extrapolations of 4(1) cm^{-1} for $J = 0-1$ and 9(1) cm^{-1} for $J = 0-2$ [17]. The ^1D and ^1S terms of $B^-(2p^2)$ are likely unbound; a recent communication on resonance structures in collisionally detached electron spectra of B^- tentatively identified the ^1D term with a resonance located 104(8) meV above the ground state of boron [18]. The latter is a $2p\,^2P_J$ state with a fine structure $J = 1/2-3/2$ splitting of 15.254 cm^{-1}

 0031-9007/98/80(12)/2562(4)$15.00

VOLUME 80, NUMBER 12 PHYSICAL REVIEW LETTERS 23 MARCH 1998

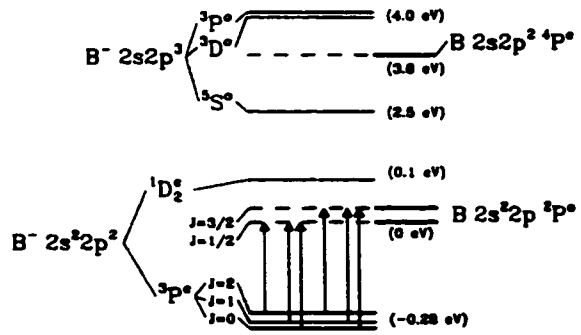

FIG. 1. Schematic energy level diagram of B^- and B. Arrows indicate photodetachment thresholds in order of increasing photon energy. For clarity of presentation, level spacings are not shown to scale. Parity labels on term symbols as shown here are omitted in the text.

[19]. The core excited $2s2p^2$ configuration gives rise to the first excited state of boron, a ^4P_J term which is located 3579(2) meV above the ^2P_J atomic ground state as derived on the basis of isoelectronic extrapolation [20]; as yet no intercombination lines between the doublet and quartet systems have been observed. The EA of the first excited state, i.e., the binding energy of the metastable $2s2p^3\,^5S_2$ negative ion level, was the subject of a recent theoretical study and predicted to be 1072(2) meV [21]. One experimental [22] and two theoretical [23,24] studies of the B^- photodetachment cross section in the vicinity of the ^4P threshold find the ^3P and ^3D terms of the $2s2p^3$ configuration quasibound and responsible for a resonance structure in that energy region. An accurate determination of the ^4P threshold would still be possible if state-selective detection (as in Li^- [7]) and tunable light around 320 nm were employed, and would, in fact, seem to be more convenient than the experimentally challenging infrared photodetachment around the ^2P threshold. Unfortunately, the uncertainty in the ^4P energy would prevent a determination of the EA of boron to a high accuracy. Therefore, our experimental approach involves tunable infrared laser spectroscopy in the 3.8 to 4.5 μm region.

The experimental setup is described in detail elsewhere [25]. Nanosecond laser pulses in the 920–950 nm range were produced with a dye laser, pumped by the second harmonic of a 10 Hz Q-switched Nd:YAG laser. Raman scattering in a high pressure hydrogen cell was employed to convert the dye laser output into tunable infrared radiation via second Stokes generation, with a measured Raman shift of 4155.20(2) cm^{-1}. The infrared pulse energies were $\approx$120 μJ, and the bandwidth was $\approx$0.1 cm^{-1}. Calibrations of the dye laser setup were routinely performed using an optogalvanic cell filled with argon. Second Stokes photon energies were also calibrated directly against well known transitions in N_2O using an absorption cell. A Cs sputter ion source with a cathode prepared from ^{10}B powder provided a 17 keV B^- beam. The ion beam and infrared laser beam were crossed at 90° within an ultrahigh vacuum chamber. At this stage the $^{10}B^-$ current was $\approx$60 nA. Neutral atoms resulting from photodetachment were detected with a discrete dynode electron multiplier.

Numerous infrared laser scans of the ^2P threshold region have been conducted. Figure 2 shows the sum of several scans over the region of 2240–2280 cm^{-1}. Approximately 5000 laser shots were utilized per wave number. Five nested thresholds are evident in Fig. 2, corresponding to the following transitions (from low to high energy): $^3P_2 \rightarrow {}^2P_{1/2}$, $^3P_1 \rightarrow {}^2P_{1/2}$, $^3P_0 \rightarrow {}^2P_{1/2}$, $^3P_2 \rightarrow {}^2P_{3/2}$, and $^3P_1 \rightarrow {}^2P_{3/2}$. It was possible to fit Wigner s-wave thresholds very accurately to the data, and the resulting threshold energies are summarized in Table I. The quoted uncertainties on the values are largely associated with the fits to the nested thresholds but also allow for systematic errors in the calibration and potential Doppler shifts. The sixth and last threshold ($^3P_0 \rightarrow {}^2P_{3/2}$) could not be resolved due to a weak transition strength and the noise in the other detachment signals. Thus, the fit was extrapolated beyond the sixth threshold using its calculated transition strength [26]. The $^3P_0 \rightarrow {}^2P_{1/2}$ threshold provides the EA of B and yields 2256.12(20) cm^{-1} or 279.723(25) meV (with 8.065 541 cm^{-1}/meV [27]). The well-known fine structure splitting of the atomic ground state can be obtained from the difference of the threshold values for the $^3P_2 \rightarrow {}^2P_{1/2,3/2}$ as well as $^3P_1 \rightarrow {}^2P_{1/2,3/2}$ transitions. This leads to values of 15.19(15) and 15.24(20) cm^{-1}, respectively, which are in excellent agreement with the accepted value of 15.254 cm^{-1} [19]. The fine structure splittings of the ion are obtained from the first three thresholds ($^3P_J \rightarrow {}^2P_{1/2}$): 3.23(15) cm^{-1} and 5.18(15) cm^{-1}, respectively, for $J = 0-1$ and $J = 1-2$ [and 8.41(20) cm^{-1} for $J = 0-2$]. A second determination of the $J = 1-2$ splitting of 5.23(20) cm^{-1} is provided by the next two thresholds ($^3P_{2,1} \rightarrow {}^2P_{3/2}$). The respective magnitudes of our threshold signals are in good agreement with theory [26], assuming a statistical population of the ionic levels. The calculated values for the relative strengths of the transitions are shown in Table I, together with the experimental values. The relative photodetachment cross section further above threshold was investigated by scanning the laser over the full tuning range of the dye used (LDS 925). The result of this scan, after correction for variations in the infrared pulse energy, is shown in the inset of Fig. 2. A single Wigner s wave has been fitted to the data (dashed line) as well as an s wave including the leading correction term to the Wigner law (solid line), as derived by Farley [28] on the basis of the zero-core-contribution (ZCC) model of photodetachment [29]. The latter curve fits the data well; hence, the ZCC model seems to be applicable here. In contrast, a limitation of the ZCC model was found in the case of Al^- photodetachment [30,31].

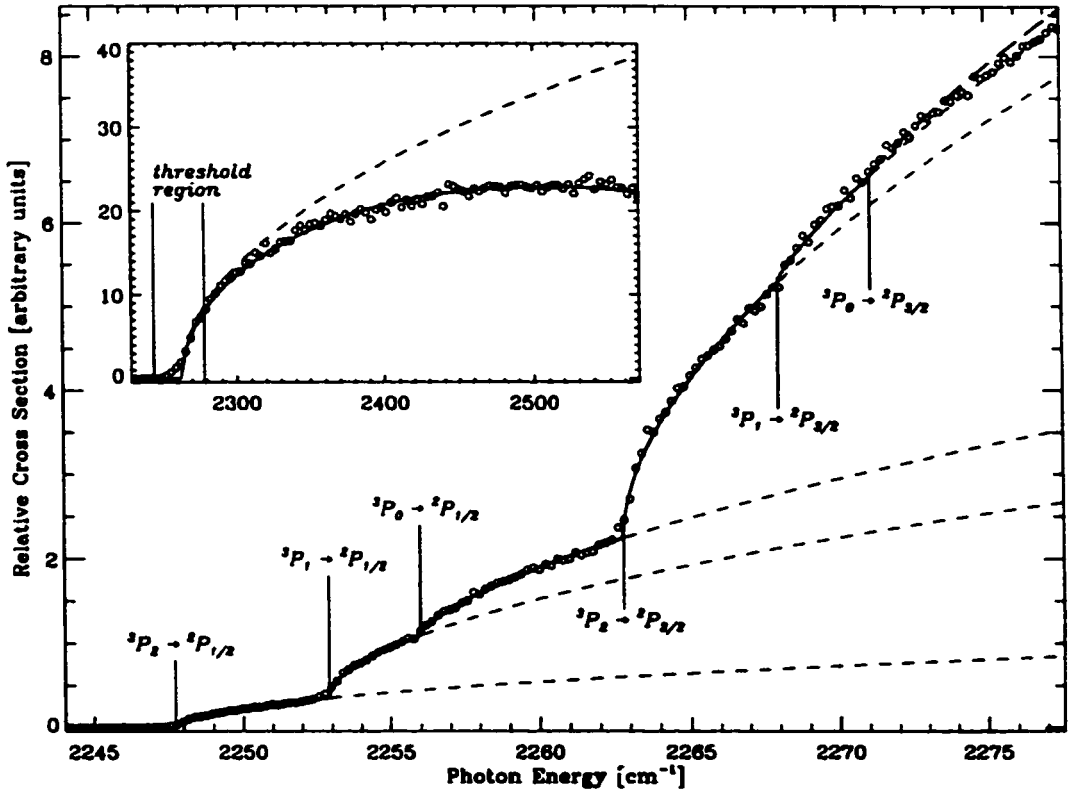

FIG. 2. Photodetachment yield versus laser wavelength. The overall result of a Wigner s-wave fit is indicated by the solid line (and extrapolated with long dashes). Individual thresholds are extrapolated with dashed lines. Inset: Relative photodetachment cross section up to 320 cm^{-1}(15%) above threshold. The dashed line represents a fitted Wigner s wave and the solid line an s wave with leading correction. These two lines define the upper and lower limits of s-wave thresholds within the ZCC model.

The present result for the electron affinity of boron [279.723(25) meV] is in agreement with the earlier measurement of Feigerle *et al.* [11,17] of 277(10) meV, in excellent agreement with the very recent theoretical result of Froese Fischer *et al.* [15] who obtained 279.5(20) meV, but in definite disagreement with the theoretical result of 267.8(20) meV obtained by Sundholm and Olsen [14]. Both theoretical works employ iterations of systematic MCHF calculations with orbital sets of increasing size. Thus, for a given model they are able to obtain the EA as the series limit with an uncertainty due to the necessary extrapolation. But even with an inactive $1s^2$ shell (i.e., valence correlation only) a complete active space calculation cannot be sustained to the limit, and some restrictions to the number of active orbitals need to be applied. This problem was handled differently by Sundholm and Olsen, and Froese Fischer *et al.* which seems to be responsible for their different results at this level, 268.6(17) and 273.2(2) meV, respectively. The choice of model restrictions becomes even more important if core polarizations are included through excitations of one of the $1s$ electrons. This was demonstrated by Froese Fischer *et al.* who treated core polarizations with two slightly different models, resulting in EA's of 273.1 and 279.5 meV, respectively (after a relativistic correction of −1.1 meV). Froese Fischer *et al.* consider the second core polarization model which increased the EA by 6.3 meV the more accurate one as it included core-valence correlation to a higher degree and even some core-core correlation via core rearrangement. Nevertheless, they estimated the uncertainty on their final EA value to be 2 meV, mainly due to the

TABLE I. Results of the s-wave fits to the data.

Transition	Threshold Energy [cm^{-1}]	Relative strength Measured	Calculated
$^3P_2 \rightarrow {}^2P_{1/2}$	2247.71(15)	4.0(4)	5
$^3P_1 \rightarrow {}^2P_{1/2}$	2252.89(15)	8.6(6)	9
$^3P_0 \rightarrow {}^2P_{1/2}$	2256.12(20)	4.2(4)	4
$^3P_2 \rightarrow {}^2P_{3/2}$	2262.90(15)	27(3)	25
$^3P_1 \rightarrow {}^2P_{3/2}$	2268.13(25)	8(2)	9
$^3P_0 \rightarrow {}^2P_{3/2}$	...	...	2

uncertainty associated with the choice of a particular model. Sundholm and Olsen used yet another core polarization model which lowered the EA by 0.8 meV. It should be noted that the calculated EA's above represent weighted averages over the levels of each term and have to be reduced by 0.56 meV to give the EA of $^3P_0$ relative to $^2P_{1/2}$ (which would be the conventional defi-nition for the EA of B). The final EA of Froese Fischer *et al.* would then be 279(2) meV, a value that is only 0.7 meV lower than our experimental result. Earlier values for the fine structure splittings of B^-, 4(1) and 9(1) cm^{-1} for $J = 0-1$ and $J = 0-2$, respectively, which were based on isoelectronic extrapolations [17], are valid within quoted uncertainties if compared with our experimental values [3.23(15) and 8.41(20) cm^{-1}, respectively]. Unfortunately, Froese Fischer *et al.* perform a full Breit-Pauli calculation of the fine structure only in the context of their valence calculation. This calculation was later refined [32] yielding $B^-(^3P_J)$ splittings of 2.92 and 7.79 cm^{-1} for $J = 0-1$ and $J = 0-2$, respectively. These values are too small in comparison with experiment, but they are expected to increase in a Breit-Pauli calculation that includes core-valence correlations [32]. It is hoped that the present results will stimulate renewed theoretical interest in B^-.

In summary, we have obtained the first experimental values for the fine structure of the $B^-(^3P)$ ground state and have determined the electron affinity of boron with a 400-fold increase in accuracy over the previous experimental value. The new EA is in very good agreement with the most recent calculation [15] and thereby confirms the importance of core-valence and core-core correlation for the accurate treatment of this six-electron system.

We gratefully acknowledge the Natural Science and Engineering Research Council of Canada (NSERC) for support of this work.

*Also with the Department of Engineering Physics, the Brockhouse Institute for Materials Research, and the Center for Electrophotonic Materials and Devices.

[1] D.R. Bates, Adv. At. Mol. Opt. Phys. **27**, 1 (1991); T. Andersen, Phys. Scr. **T34**, 23 (1991); S.J. Buckmann and C.W. Clark, Rev. Mod. Phys. **66**, 539 (1994); C. Blondel, Phys. Scr. **T58**, 31 (1995).

[2] P. Kristensen, C.A. Brodie, U.V. Pedersen, V.V. Petrunin, and T. Andersen, Phys. Rev. Lett. **78**, 2329 (1997); J. Thøgersen, M. Scheer, L.D. Steele, H.K. Haugen, and W.P. Wijesundera, Phys. Rev. Lett. **76**, 2870 (1996); V.V. Petrunin, J.D. Voldstad, P. Balling, P. Kristensen, T. Andersen, and H.K. Haugen, Phys. Rev. Lett. **75**, 1911 (1995); P. Kristensen, H. Stapelfeldt, P. Balling, T. Andersen, and H.K. Haugen, Phys. Rev. Lett. **71**, 3435 (1993).

[3] K.R. Lykke, K.K. Murray, and W.C. Lineberger, Phys. Rev. A **43**, 6104 (1991).

[4] D. Feldmann, Chem. Phys. Lett. **47**, 338 (1977).

[5] D.M. Neumark, K.R. Lykke, T. Andersen, and W.C. Lineberger, Phys. Rev. A **32**, 1890 (1985).

[6] C. Blondel, P. Cacciani, C. Delsart, and R. Trainham, Phys. Rev. A **40**, 3698 (1989).

[7] J. Dellwo, Y. Liu, D.J. Pegg, and G.D. Alton, Phys. Rev. A **45**, 1544 (1992).

[8] G. Haeffler, D. Hanstorp, I. Kiyan, A.E. Klingmuller, and U. Ljungblad, Phys. Rev. A **53**, 4127 (1996).

[9] P. Kristensen, U.V. Pedersen, V.V. Petrunin, T. Andersen, and K.T. Chung, Phys. Rev. A **55**, 978 (1997).

[10] P. Kristensen, V.V. Petrunin, H.H. Andersen, and T. Andersen, Phys. Rev. A **52**, R2508 (1995).

[11] C.S. Feigerle, R.R. Corderman, and W.C. Lineberger, J. Chem. Phys. **74**, 1513 (1981).

[12] K. Raghavachari, J. Chem. Phys. **82**, 4142 (1985); J.J. Novoa, F. Mota, and F. Arnau, J. Phys. Chem. **95**, 3096 (1991); R.A. Kendall, T.H. Dunning, Jr., and R.J. Harrison, J. Chem. Phys. **96**, 6796 (1992).

[13] T. Noro, M. Yoshimine, M. Sekiya, and F. Sasaki, Phys. Rev. Lett. **66**, 1157 (1991).

[14] D. Sundholm and J. Olsen, Chem. Phys. Lett. **171**, 53 (1990).

[15] C. Froese Fischer, A. Ynnerman, and G. Gaigalas, Phys. Rev. A **51**, 4611 (1995).

[16] W.P. Wijesundera, Phys. Rev. A **55**, 1785 (1997); E. Eliav, Y. Ishikawa, P. Pyykkö, and U. Kaldor, Phys. Rev. A **56**, 4532 (1997).

[17] H. Hotop and W.C. Lineberger, J. Phys. Chem. Ref. Data **14**, 731 (1985).

[18] D.H. Lee, W.D. Brandon, D. Hanstorp, and D.J. Pegg, Phys. Rev. A **53**, R633 (1996).

[19] G.A. Odintzova and A.R. Striganov, J. Phys. Chem. Ref. Data **8**, 63 (1979).

[20] B. Edlén, H.P. Palenius, K. Bockasten, R. Hallin, and J. Bromander, Sol. Phys. **9**, 432 (1969).

[21] C. Froese Fischer and G. Gaigalas, J. Phys. B **29**, 1169 (1996).

[22] P. Kristensen, H.H. Andersen, P. Balling, L.D. Steele, and T. Andersen, Phys. Rev. A **52**, 2847 (1995).

[23] C.A. Ramsbottom and K.L. Bell, J. Phys. B **28**, 4501 (1995).

[24] G.Y. Kaskenock and V.K. Ivanov, J. Phys. B (to be published).

[25] J. Thøgersen, L.D. Steele, M. Scheer, C.A. Brodie, and H.K. Haugen, J. Phys. B **29**, 1323 (1996); M. Scheer, C.A. Brodie, R.C. Bilodeau, and H.K. Haugen (to be published).

[26] P.C. Engelking and W.C. Lineberger, Phys. Rev. A **19**, 149 (1979).

[27] E.R. Cohen and B.N. Taylor, Rev. Mod. Phys. **59**, 1121 (1987).

[28] J.W. Farley, Phys. Rev. A **40**, 6286 (1989).

[29] R.M. Stehman and S.B. Woo, Phys. Rev. A **20**, 281 (1979).

[30] D. Calabrese, A.M. Covington, J.S. Thompson, R.W. Marawar, and J.W. Farley, Phys. Rev. A **54**, 2797 (1996).

[31] M. Scheer, R.C. Bilodeau, J. Thøgersen, and H.K. Haugen, Phys. Rev. A **57**, R1493 (1998).

[32] C. Froese Fischer (private communication).

4.2.3 Paper 8 — Threshold photodetachment of Al^-: Electron affinity and fine structure

This work is the first fine-structure resolved measurement of Al^-. As with boron, it demonstrates that the extraction of fine-structure splittings can be obtained with high accuracy even though the signals from the *s*-wave thresholds appear superimposed, or "nested". This work also corrects a previous erroneous experimental study on the electron affinity of Al.

As should be expected, the structure of the negative ion of Al bears a striking similarity to that of B^-, with the most significant difference being a substantial change in the energy scale. We shall see in Section 4.3 that this situation offers an excellent opportunity to draw interesting and useful comparisons on the relative importance of the different correction terms to the Wigner law.

While I participated in all aspects of the realization of this work, the primary investigator for this paper was M. Scheer. As the supervisor, H. K. Haugen provided input in all stages of the work. Finally, J. Thøgersen was involved in the early stages of the study.

RAPID COMMUNICATIONS

PHYSICAL REVIEW A VOLUME 57, NUMBER 3 MARCH 1998

Threshold photodetachment of Al^-: Electron affinity and fine structure

Michael Scheer, René C. Bilodeau, Jan Thøgersen,* and Harold K. Haugen†
Department of Physics and Astronomy, McMaster University, Hamilton, Ontario, Canada L8S 4M1
(Received 14 July 1997)

Tunable infrared laser spectroscopy of $Al^-(3p^2\ ^3P_J)$ has yielded an improved value for the electron affinity of aluminum and experimental data on the previously unobserved fine structure of the ionic ground state. The electron affinity is determined to be 3491.0(4) cm^{-1} [432.83(5) meV], and the $J=0$-1 and $J=1$-2 splittings are found to be 22.7(3) and 45.7(2) cm^{-1}, respectively. The result for the electron affinity is in substantial disagreement with a very recent experimental investigation. Our work also indicates that isoelectronic extrapolations for the ionic fine structure were accurate within uncertainties, and is in good agreement with recent calculations of the electron affinity. [S1050-2947(97)50512-9]

PACS number(s): 32.10.Hq, 32.80.Gc, 32.10.Fn

The study of atomic negative ions continues to be an active area of investigation [1] and many improvements in the knowledge of electron affinities and ionic fine structure have been obtained since the 1985 review of Hotop and Lineberger [2]. In part, the interest in atomic negative ions stems from the qualitatively different features resulting from the short range potential, and is due to the theoretical challenges posed by the relativistic and strong electron correlation effects. Nevertheless, negative ions are of practical interest as well, including in the ultrasensitive detection of atoms and isotopes through accelerator mass spectrometry [3]. The negative ion of aluminum has been the subject of substantial experimental and theoretical work. Utilizing laser photodetachment electron spectrometry, Feigerle *et al.* [4] measured the electron affinity (EA) of Al to be 442(10) meV, and found the $Al^-(^1D_2)$ level to lie 332(10) meV above ground-state Al^-, with a binding energy of 110(10) meV. The latter value for the $^1D_2$ level agreed with the result of electric-field dissociation by Oparin *et al.* [5], where a binding energy of ~95 meV was obtained. As a result of subsequent refined calibrations [6], an improved value for the EA of Ref. [4] was suggested to be 441(10) meV [2]. Recently, Calabrese *et al.* [7] measured the electron affinity of Al to be 440.94(+0.66/−0.48) meV by utilizing a tunable F-center laser and a coaxial ion-laser beam apparatus. Although they were unable to investigate the actual threshold region and the associated fine structure, they compensated for lack of data in this region via extrapolating from higher photon energy data. In the past few years, calculations have been reported by Arnau *et al.* [8], who used a configuration-interaction (CI) method with pseudopotentials, Woon and Dunning [9], who employed a CI method with correlation-consistent basis sets, and Wijesundera [10], who utilized a multiconfiguration Dirac-Fock method. They obtained values of 450 meV [8], 437 meV [9], and 433 meV [10], respectively. The present Rapid Communication reports an accurate experimental determination of the electron affinity of aluminum. In addition, the fine-structure splittings of the $Al^-(3p^2\ ^3P_J)$ term have been measured, to our knowledge, for the first time.

An energy-level diagram of Al^- and the ground state of Al is shown in Fig. 1. The $Al^-(3p^2\ ^3P_J)$ ground state is expected to have fine-structure levels with splittings estimated from isoelectronic extrapolations, of 26(3) cm^{-1} for $J=0$-1 and 76(7) cm^{-1} for $J=0$-2 [2]. The ground state of Al is a $3p\ ^2P_J$ state with a fine-structure $J=1/2$-3/2 splitting of 112.061 cm^{-1} [11]. Our experimental approach to the determination of the EA of aluminum involves tunable infrared laser spectroscopy and keV-energy ion-beam technology. Details of the apparatus are described elsewhere [12,13]. Nanosecond-duration laser pulses in the 820–880-nm range were generated using a dye laser, pumped by the second harmonic of a 10-Hz Q-switched Nd:YAG (neodymium-doped yttrium aluminum garnet) laser. The dye laser output was converted into tunable infrared radiation via second Stokes generation using stimulated Raman scattering in a high-pressure hydrogen cell, with a measured Raman shift of 4155.20(2)cm^{-1}. The infrared light had a bandwidth of

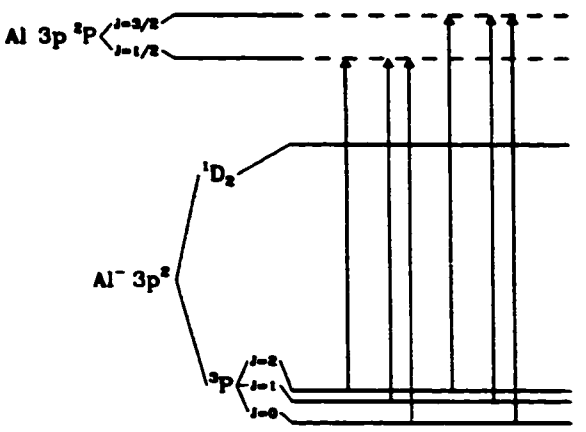

FIG. 1. Schematic energy-level diagram of Al^- and Al. Arrows indicate photodetachment thresholds in order of increasing photon energy. For clarity of presentation, fine-structure splittings are not shown to scale.

*Present address: Department of Chemistry, University of Aarhus, DK-8000 Aarhus C, Denmark.

†Also with the Department of Engineering Physics, the Brockhouse Institute for Materials Research, and the Center for Electrophotonic Materials and Devices.

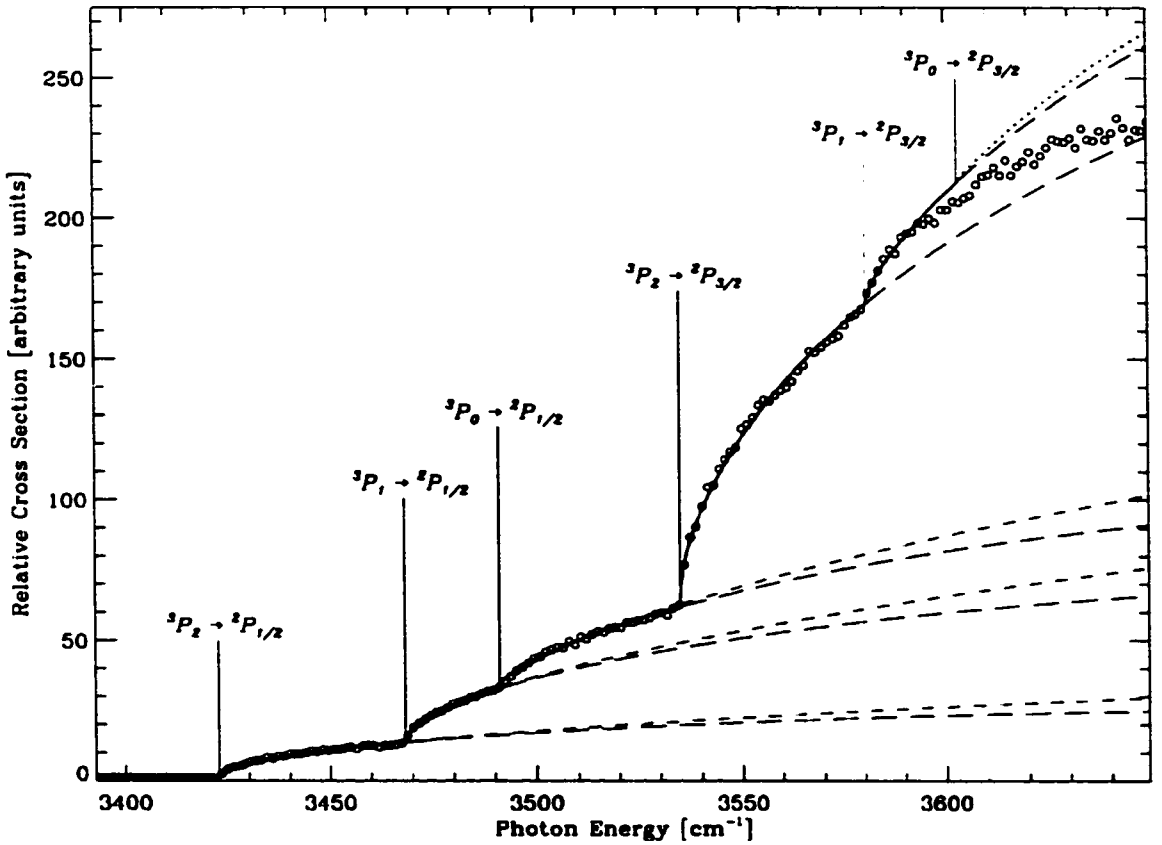

FIG. 2. Photodetachment yield versus laser wavelength. The overall result of a Wigner s-wave fit including the leading correction term is indicated by the solid line (and extrapolated with a dotted line). Individual thresholds are extrapolated with dashed lines: short dashes for a Wigner s wave (first three thresholds only), and long dashes for a Wigner s wave with leading correction. These two lines define the upper and lower limits of s wave thresholds within the ZCC model.

$\sim$0.1 cm^{-1} and pulse energies were $\sim$0.5 mJ at 3 μm. A 16-keV Al^- beam was extracted from a Cs sputter ion source. Ultrapure aluminum cathodes were utilized in order to greatly minimize the potential contamination from prolific Si^- impurity beams, although our mass resolution discriminates quite effectively against mass 28 at mass 27. The beam was then magnetically analyzed and deflected 30° into an ultrahigh-vacuum chamber. There it was further charge-state analyzed in an electric field before being crossed at 90° with a collimated infrared laser beam. The Al^- current at this stage was typically several nA. The charge states created in the interaction region were analyzed by a second set of electric-field deflection plates. The photodetached neutral atoms impinged on a discrete dynode electron multiplier for analog data acquisition via a gated integrator and boxcar averager. Calibrations of the dye laser setup were routinely performed using an optogalvanic cell, but rigorous comparisons of the wavelength of the second Stokes generated light with known ionic energy intervals have also been performed, including in the cases of Te^- [14] and Cs^- [2]. Various tests indicate that the second Stokes wavelength calibration is reliable to at least 0.2 cm^{-1}.

We have conducted numerous infrared laser scans of the threshold region for Al^- photodetachment. The sum of several scans over the region of 3400–3650 cm^{-1} is shown in Fig. 2. The data correspond to approximately 1200 laser shots per wave number. Five nested thresholds are seen in the figure, corresponding to the following transitions (from low to high energy): $^3P_2 \rightarrow {}^2P_{1/2}$, $^3P_1 \rightarrow {}^2P_{1/2}$, $^3P_0 \rightarrow {}^2P_{1/2}$, $^3P_2 \rightarrow {}^2P_{3/2}$, and $^3P_1 \rightarrow {}^2P_{3/2}$. Wigner s-wave thresholds could be fitted very accurately to the data and the resulting threshold energies are summarized in Table I. The same threshold energies but a slightly closer fit to the data above

TABLE I. Results of the s-wave fits to the data.

Transition	Threshold Energy (cm^{-1})	Relative strength Measured	Calculated
$^3P_2 \rightarrow {}^2P_{1/2}$	3422.6(2)	5.0(3)	5
$^3P_1 \rightarrow {}^2P_{1/2}$	3468.3(2)	8.5(7)	9
$^3P_0 \rightarrow {}^2P_{1/2}$	3491.0(4)	4.8(9)	4
$^3P_2 \rightarrow {}^2P_{3/2}$	3534.8(2)	29(6)	25
$^3P_1 \rightarrow {}^2P_{3/2}$	3579.8(8)	8(2)	9
$^3P_0 \rightarrow {}^2P_{3/2}$			2

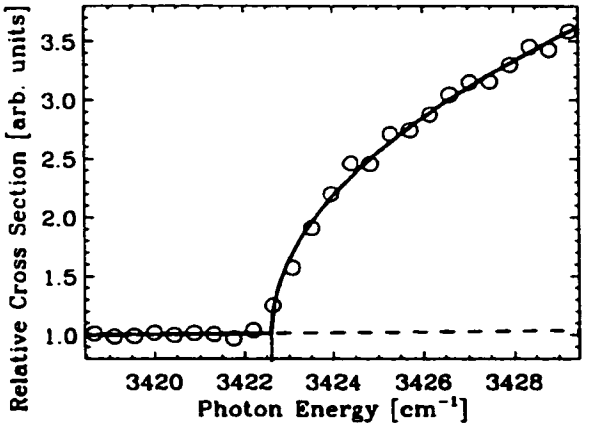

FIG. 3. High-resolution scan of the $^3P_2 \rightarrow {}^2P_{1/2}$ threshold region. The solid line represents a fitted s wave.

threshold were obtained by including in the fitting routine the leading correction term to the Wigner law, as derived by Farley [15] on the basis of the zero-core-contribution (ZCC) model of photodetachment [16]. The result of this fit is indicated by the solid line in Fig. 2. The sixth and last threshold ($^3P_0 \rightarrow {}^2P_{3/2}$) could not be resolved due to a weak transition strength combined with the fact that it appears on top of the other detachment signals. The fit to the data was therefore extrapolated beyond the sixth threshold (dotted line in Fig. 2) using its calculated transition strength [17] (see below). The increasing deviation between the fit and the data in this region seems to indicate a limitation of the ZCC model, which was also observed and discussed by Calabrese *et al.* [7] (it should be noted, however, that some equations in Ref. [7] contain typographical errors). The first three thresholds were also scanned at a very slow rate of 8000 laser shots per wave number in order to improve the accuracy of the fitted threshold values. As an example, the region of the first threshold is shown in Fig. 3, which also demonstrates the small but measureable signal resulting from photodetachment of the weakly populated $Al^-(^1D_2)$ level. The EA of Al is found from the $^3P_0 \rightarrow {}^2P_{1/2}$ threshold, and is determined to be 3491.0(4)cm^{-1} or 432.83(5) meV (using 8.065 541 0 cm^{-1}/meV [11]). The well-known fine-structure splitting of the Al ground state can be extracted from the difference of the thresholds for the $^3P_2 \rightarrow {}^2P_{1/2,3/2}$ transitions as well as $^3P_1 \rightarrow {}^2P_{1/2,3/2}$. This yields experimental values of 112.2(3) and 111.5(8) cm^{-1}, respectively, which are in excellent agreement with the tabulated value of 112.061 cm^{-1} [11]. The first three thresholds ($^3P_J \rightarrow {}^2P_{1/2}$) provide values of the fine-structure splittings of the ion: 22.7(3) cm^{-1} and 45.7(2) cm^{-1}, respectively, for $J=0$-1 and $J=1$-2 [and 68.4(3) cm^{-1} for $J=0$-2]. The next two thresholds ($^3P_{2,1} \rightarrow {}^2P_{3/2}$) enable a second determination of the $J=1$-2 splitting of 45.0(8) cm^{-1}. The quoted uncertainties of the values are largely associated with the fits to the nested thresholds. The respective magnitudes of our threshold signals are in good agreement with theory [17], assuming a statistical population of the ionic levels. The calculated values for the relative strengths of the transitions are shown in Table I, together with the experimental values. The errors in the experimental values account for the fact that the two different s-wave fits give slightly different values for the relative strengths of the thresholds.

Our experimental result [432.83(5) meV] for the electron affinity of Al is in agreement with the earlier measurement of Feigerle *et al.* [4,2] of 441(10) meV, but in definite disagreement with the very recent result of Calabrese *et al.* [7], who obtained 440.94(+0.66/−0.48) meV. The photodetachment data of Ref. [7] have a signal-to-noise ratio of ≈10 while ours is ≈100. This difference in statistics should be reflected in the respective uncertainties of the final EA values, but the two results still differ by about 16 standard deviations, based on the lower error margin quoted in Ref. [7]. There are major differences between the experiments, which we will therefore outline briefly. Calabrese *et al.* conducted their photodetachment study with a cw F-center laser, with a stated resolution of ≈0.13 cm^{-1}, in a coaxial (3-keV) ion-laser beam configuration. Our laser resolution is very similar to theirs, and our average laser power very comparable. Our typical ion currents are two orders of magnitude higher than those of Ref. [7], but our interaction region is also two orders of magnitude shorter. More importantly, the setup of Ref. [7] was very prone to intracavity and extracavity water absorption lines, such that their laser power was reduced to near zero in several wavelength regions. We are much less susceptible to this problem since our infrared light is generated just before the interaction region, and the remaining infrared beam path is effectively purged with dry nitrogen gas. As Calabrese *et al.*, we still normalize the data to the laser power transmitted through the ultrahigh-vacuum region. The most striking difference, however, between the experiments is that Calabrese *et al.* were not able to make measurements at or below the threshold region due to an upper limit of 2820 nm on the wavelength scan for the KCl:Li color center laser crystal. Thus they were unable to truly exploit the narrow linewidth of the cw laser, and in contrast to our measurements, could not explore the multiple thresholds due to fine-structure splittings (the lower end of their scan range is 3585 cm^{-1}). Fitting a single s wave to their data Calabrese *et al.* obtain an approximate electron affinity of 3580.5(2.0) cm^{-1}, which coincides with our value for the $^3P_1 \rightarrow {}^2P_{3/2}$ threshold. Due to its small relative strength of 17%, it seems unlikely, however, that this threshold was observed alone, without substantial contributions from the first four thresholds (compare Fig. 2). Therefore, Calabrese *et al.* extrapolate their data to threshold via higher-order fits and weighted averages over the transitions between all possible levels of the ion and atom, using the appropriate theoretical frameworks [15–17]. We have tested their procedures by applying them to our data in the region above 3585 cm^{-1}. This yielded an electron affinity of 3480(15) cm^{-1}, which agrees with the value for the $^3P_0 \rightarrow {}^2P_{1/2}$ threshold within error margins. Hence, the extrapolation procedures seem valid. All in all, it appears that the low-energy data (first six points) of Ref. [7] for some reason rise too steeply with increasing photon energy if compared with our data for this energy region. The respective slopes differ by approximately a factor of 3. We conclude that some systematic error has probably arisen in the work of Calabrese *et al.*, in addition to the statistical errors incurred by the low signal-to-noise ratio and the necessary extrapolation to threshold.

Although much theoretical effort has been directed to calculations on even lighter species, aluminum is sufficiently light that advanced calculations are being attempted. There have been three recent theoretical works on the electron affinity of aluminum. Arnau *et al.* obtained 450 meV [8], Woon and Dunning [9] a value of 437 meV, and Wijesundera 433 meV [10]. All three numbers, which have uncertainties of the order of 10 meV, are in good agreement with experiment. Our experimental determination of the fine-structure splittings of Al^- indicates that the earlier values based on isoelectronic extrapolations [2], 26(3) cm^{-1} and 76(7) cm^{-1} for $J=0$-1 and $J=0$-2, respectively, were essentially valid within quoted uncertainties. The negative ion of aluminum has also been the subject of recent experimental and theoretical studies [18] in terms of the continuum far above the detachment threshold. As regards future studies of Al^-, a highly accurate value of the binding energy of the $^1D_2$ term might, in principle, be obtained via a multiphoton detachment scheme. However, the expected low transition probability of the $^3P \rightarrow {}^1D$ transition ($\sim 10^{-4}$ s^{-1}) [19] would seem to make a 1 + 1 photon detachment scheme via an electric-dipole-forbidden bound-bound resonance rather unlikely [20]. Alternatively, one could use charge-exchange production techniques to maximize the population in the excited level, and employ resonant ionization spectroscopy [21] with detachment to an excited state of the aluminum atom. In contrast, single-photon detachment from $Al^-(^1D_2)$ would be technically very demanding from a nonlinear optical standpoint, requiring tunable midinfrared radiation.

In summary, we have measured the electron affinity of aluminum with an accuracy of 0.05 meV, and have resolved the fine structure of the ion. The measurement is in good agreement with recent calculations [8–10] but calls seriously into question the very recent experimental result of Calabrese *et al.* [7]. Several considerations would suggest that the present EA value be adopted. Perspectives for future work have also been briefly discussed.

We gratefully acknowledge the Natural Science and Engineering Research Council of Canada (NSERC) for support of this work. We also thank T. Andersen for his helpful comments on the manuscript.

[1] D. R. Bates, Adv. At., Mol., Opt. Phys. **27**, 1 (1991); T. Andersen, Phys. Scr. **T34**, 23 (1991); S. J. Buckmann, C. W. Clark, Rev. Mod. Phys. **66**, 539 (1994); C. Blondel, Phys. Scr. **T58**, 31 (1995).

[2] H. Hotop and W. C. Lineberger, J. Phys. Chem. Ref. Data **14**, 731 (1985).

[3] A. E. Litherland, Annu. Rev. Nucl. Part. Sci. **30**, 437 (1980); W. Kutschera and M. Paul, *ibid.* **40**, 411 (1990).

[4] C. S. Feigerle, R. R. Corderman, and W. C. Lineberger, J. Chem. Phys. **74**, 1513 (1981).

[5] V. A. Oparin, R. N. Il'in, I. T. Serenkov, and E. S. Solov'ev, Zh. Eksp. Teor. Fiz. **66**, 2008 (1974) [Sov. Phys. JETP **39**, 989 (1974)].

[6] D. M. Neumark, K. R. Lykke, T. Andersen, and W. C. Lineberger, Phys. Rev. A **32**, 1890 (1985).

[7] D. Calabrese, A. M. Covington, J. S. Thompson, R. W. Marawar, and J. W. Farley, Phys. Rev. A **54**, 2797 (1996).

[8] F. Arnau, F. Mota, and J. J. Novoa, Chem. Phys. **166**, 77 (1992).

[9] D. E. Woon and T. H. Dunning, Jr., J. Chem. Phys. **99**, 3730 (1993).

[10] W. P. Wijesundera, Phys. Rev. A **55**, 1785 (1997).

[11] J. R. Fuhr, W. C. Martin, A. Musgrove, J. Sugar, and W. L. Wiese, NIST Atomic Spectroscopic Data Base, http://physics.nist.gov.

[12] J. Thøgersen, L. D. Steele, M. Scheer, C. A. Brodie, and H. K. Haugen, J. Phys. B **29**, 1323 (1996).

[13] M. Scheer, C. A. Brodie, R. C. Bilodeau, and H. K. Haugen (unpublished).

[14] J. Thøgersen *et al.*, Phys. Rev. A **53**, 3023 (1996).

[15] J. W. Farley, Phys. Rev. A **40**, 6286 (1989).

[16] R. M. Stehman and S. B. Woo, Phys. Rev. A **20**, 281 (1979).

[17] P. C. Engelking and W. C. Lineberger, Phys. Rev. A **19**, 149 (1979).

[18] B. J. Davies, C. W. Ingram, D. J. Larson, C.-N. Liu, and A. F. Starace, Phys. Rev. A **56**, 378 (1997).

[19] C. Mendoza and C. J. Zeippen, Mon. Not. R. Astron. Soc. **199**, 1025 (1982).

[20] J. Thøgersen, M. Scheer, L. D. Steele, H. K. Haugen, and W. P. Wijesundera, Phys. Rev. Lett. **76**, 2870 (1996).

[21] V. V. Petrunin *et al.*, Phys. Rev. Lett. **75**, 1911 (1995).

4.3 Further Comments on Threshold Laws

A number of studies have observed deviations from the Wigner threshold law in a range of elements (for reviews see [2,3]). The pioneering experiments conducted by Lineberger and coworkers in the early 1970's on Se^- [4], Pt^- and Au^- [5], are of particular interest (see also the work on S^- [6]). For these spectra, it was concluded that a k^2 dependent correction term was required, in addition to O'Malley's polarisability term, to explain the observed deviations. It was also observed that this "extra" correction reduced the observed signal in all cases. This is in accordance to what is expected from the ZCC model, which was developed nearly two decades later. However, even recent works (e.g. [7-10]) have opted to use either only Farley's or only O'Malley's correction.

Section 4.2.2 indicated that an apparently very accurate description of the B^- spectrum could be obtained if Farley's leading correction was included. On the other hand, this was not the case in the very similar spectrum obtained with Al^-. The same conclusion was made in a previous photodetachment study on Al^- by Calabrese *et al* [9], of which Farley is a co-author. However, following the discussion of the correction terms in Chapter 2 and the above paragraph, it should be clear that the Farley correction alone may not be sufficient to describe some spectra. We return now to the B^- and Al^- spectra with the goal of better understanding the effects of the correction terms to the Wigner law. The understanding gained from this analysis will then aid in addressing the concerns expressed for the spectra of Ir^- and Pt^- in Section 4.1.2.

4.3.1 The Threshold Law in B^-

We begin with the B^- spectrum. For the purpose of this section, the threshold region can largely be ignored, and we will concentrate on the spectra covering the high photon energies. The range scanned covers energies up to about 320 cm^{-1} above threshold (i.e. about 14% above threshold). We noted in Chapter 2, especially Section 2.2.3, that the Farley correction becomes significant (at the 10% level) only 2.5% above threshold; we should therefore expect it to be very significant in the present study. Since the polarisability of the B ground state is very small (only 20.43 a.u. [11]), the polarisation term of O'Malley should be much less significant. Finally, the quadrupole moment for the ground state of boron is much smaller than the polarisablity term; in fact $B^{qm} \equiv 0$ for the $J = \frac{1}{2}$ state. We shall therefore ignore this contribution.

Referring back to Equation 2.5, generalized to include the effect of the 6 thresholds in B^-, we write:

$$\sigma_d = A \sum_{i=1}^{6} a_i \, k_i^{2\ell+1} \left[1 - B^{dp} \, k_i^2 \, \ln a_o k_i - (C^{sr} + C^{lt}) \, k_i^2\right], \qquad (4.1)$$

where A is an overall amplitude, which must be fit. The relative strength of the i^{th} threshold (a_i) was obtained in Section 4.2.2, and $\hbar^2 k_i^2 = 2m_e(h\nu - \varepsilon_i)$, with ε_i being the energy of the i^{th} threshold, also obtained in Section 4.2.2. It has been implicitly assumed here that the three correction coefficients (C^{lt}, B^{dp}, and C^{sr}) are the same for all the thresholds. While C^{sr} is a free parameter, the other two correction coefficients are in principle exactly determined under the respective theories, $C^{lt} = C_1^{lt}$ (Equation 2.9b, with $r_o \approx 2a_o$) and $B^{dp} = \frac{4}{3}\alpha$ (Equation 2.6). In order to develop an appreciation for the relative importance of the three terms, three fitting methods are used:

1. α (and hence B^{dp}) is allowed to vary assuming $C^{lt} = 0$ and $C^{sr} = 0$;

Table 4.9: Coefficients for the correction terms determined from fits to the B^- detachment spectrum. For each fit set, the value in bold indicates the parameter that was allowed to vary, while the other parameters were held fixed to the value indicated. Quoted uncertainties include possible systematic errors.

	Including entire scan range			Including only $h\nu < 2398.13$ cm^{-1}		
Fit	α	C^{lt}/C_1^{lt}	C^{sr}/C_1^{lt}	α	C^{lt}/C_1^{lt}	C^{sr}/C_1^{lt}
1	**42.4(13)**	0	0	**41(6)**	0	0
2	**0.0(15)**	1	0	**4(6)**	1	0
3	24.34	1	**−0.48(4)**	24.34	1	**−0.43(15)**
3[a]	24.34	1	**−0.21(6)**	24.34	1	**−0.3(2)**

[a]Fit 3 but corrected for the full ZCC model; errors are approximate (see text).

2. α is allowed to vary assuming $C^{lt} = C_1^{lt}$ and $C^{sr} = 0$;

3. C^{sr} is allowed to vary assuming $C^{lt} = C_1^{lt}$ and $\alpha = 24.34$ a.u.

Furthermore, to verify that the range included in the fit is not significant, the fits were performed over two ranges: the entire range scanned and only half of the range scanned. As can be seen from Table 4.9, the values returned are the same within the expected uncertainties for both fit ranges. The quoted uncertainties take into account systematic errors estimated by including the possibility of weak saturation of the signal, and by varying the positions and relative strengths of the thresholds, in accordance to the uncertainty in those previously determined values.

The very small value of α obtained from fit method 2 indicates why the Farley correction alone appeared to give a good description of the data. However this is largely coincidental, as a proper description of the photodetachment process must ultimately also include the effects of the atomic polarisability, i.e. results of O'Malley's theory.

Up to now, we have ignored the higher order correction terms. Although Farley gave an explicit expression only for the coefficient of the k^2-order term (i.e. $C_{\ell_o}^{lt}$),

he also produced plots of the full ZCC correction, which includes the correction to all orders. In particular, Figure 1b of his work [13] indicates that the ZCC model predicts a correction to the Wigner law that is about 73(2)% and 86(4)% that obtained by the leading term alone, for s-wave detachment 14% and 6% above threshold respectively. This would indicate that the next higher order correction term under the ZCC theory (which has an opposite sign) is not entirely insignificant in the present case. On the other hand, an inclusion of the full ZCC theory in the fit would have (for fit method 3) the main effect of increasing the fitted value of C^{sr}. To a first approximation, values of $C^{sr} \approx -0.21 \times C_1^{lt}$ and $-0.29 \times C_1^{lt}$ respectively for the full-range and restricted-range fits, might be expected instead.

4.3.2 The Threshold Law in Al^-

The much larger electron affinity and polarisability of Al offers a complementary situation to that of B. Although approximately the same *absolute* photon energy range was scanned as in B, the *relative* range above the (first) threshold is approximately half as large, and Farley's correction is therefore considerably smaller. On the other hand, the polarisability of Al is nearly twice as large (α = 45.9 a.u. [12]), meaning that the O'Malley correction is now the dominant for this detachment spectrum. Unfortunately, the large fine-structure splitting of the ion and neutral atom complicates the analysis, because it is no longer reasonable to fit the correction terms independently of the relative strengths, as the latter can affect the former considerably. The total number of parameters to be fit is then increased from 2 to 7. In order to reduce the number of fitting parameters, fitting ranges including only the first threshold or only the first three thresholds were performed. Otherwise proceeding in the same fashion as for B, the results of Table 4.10 are obtained (r_o = 3.44 a.u. for Al [9]). Note that larger uncertainties in the results for Al^- arise mostly because the relative

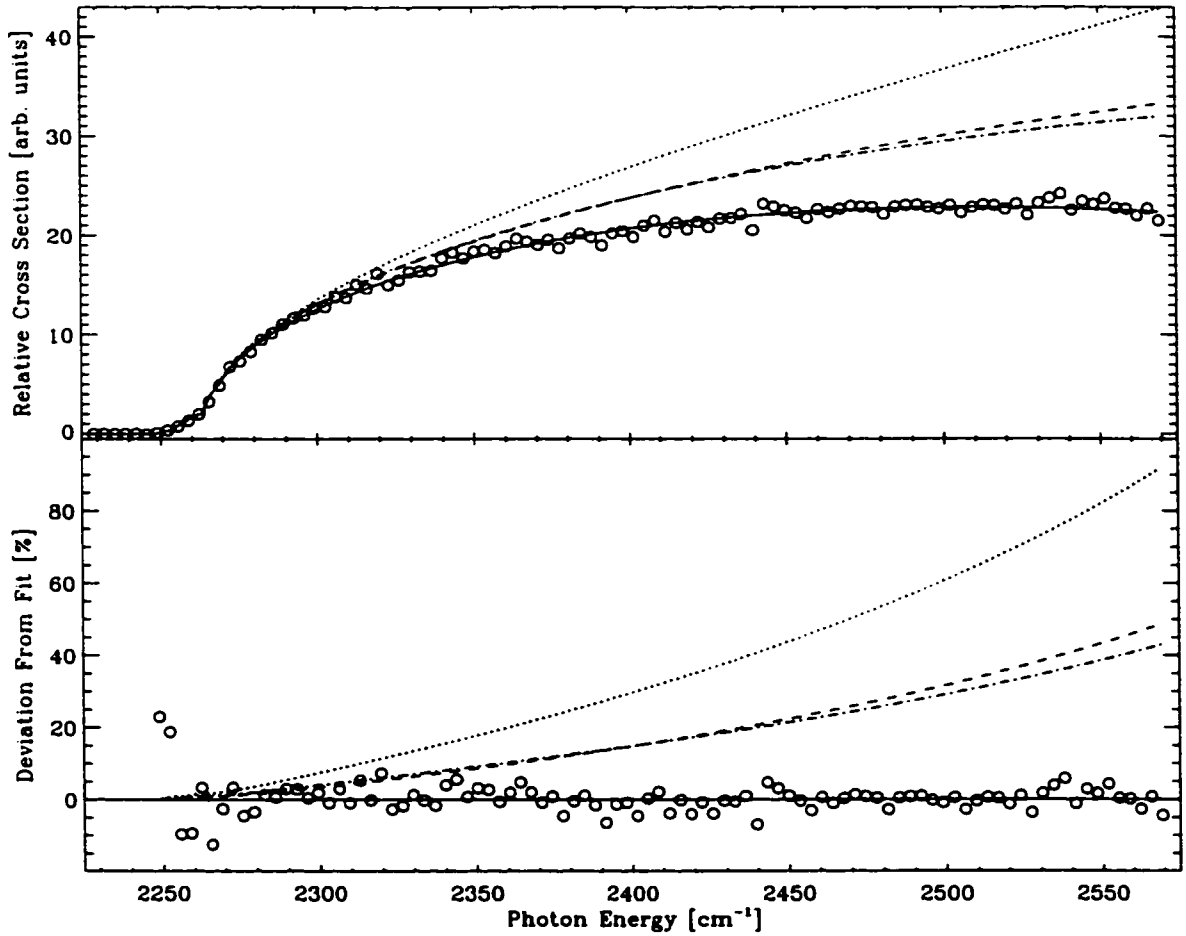

Figure 4.21: Comparison of threshold law correction terms for boron. The full curve (——) is the result obtained with fit method 3; however the other fit methods produce essentially indistinguishable curves. The dotted (·····), dashed (– – –), and chain (· – · – ·) curves are produced assuming the results of the full curve, but with including respectively only the Wigner law with no correction terms, the Wigner law with the polarisability correction (B_0^{dp} with $\alpha = 24.34$) only, and the Wigner law with the k^2 correction (i.e. the $C_1^{lt} + C^{sr}$ term) only. The background signal has been subtracted here.

strengths of the thresholds are much more significant, due to the large fine-structure splitting, but also because a smaller data set is used.

On the basis of these results it is easy to understand why the Farley correction alone did not describe the Al^- spectrum as well as it did for B^-, namely that the

Table 4.10: Coefficients for the correction terms determined from fits to the Al^- detachment spectrum. For each fit set, the value in bold indicates the parameter that was allowed to vary, while the other parameters were held fixed to the value indicated. Quoted uncertainties include possible systematic errors.

	Fit with $h\nu < 3530$ cm^{-1}			Fit with $h\nu < 3465$ cm^{-1}		
Fit	α	C^{lt}/C_1^{lt}	C^{sr}/C_1^{lt}	α	C^{lt}/C_1^{lt}	C^{sr}/C_1^{lt}
1	**63(8)**	0	0	**78(21)**	0	0
2	**40(8)**	1	0	**56(21)**	1	0
3	45.9	1	**−0.3(3)**	45.9	1	**0.4(10)**

polarisation term is much more significant in Al than it is in B. Note that the results obtained from the two ranges again agree within uncertainties, indicating that the model is consistent with observation. Also the value of C^{sr} is consistent with that obtained for boron, being near $-0.2 \times C_1^{lt}$ in both cases; unfortunately, the magnitude of the uncertainties makes it impossible to conclude that they are equal. If the entire range scanned is fit, then a value of $C^{sr} = -0.48(25) \times C_1^{lt}$ is obtained. However, while for the smaller ranges the higher order correction terms under the ZCC model are clearly insignificant ($<6\%$ of C_1^{lt}, even for the highest relative photon energy), this is not the case if the full range is used. Although a simple correction for the full ZCC model, as was done with B, is not valid here since the relative energy above threshold is significantly different for each of the thresholds, it is reasonable to expect that including the full ZCC correction would increase the value of C^{sr} by between 0 and $0.15 \times C_1^{lt}$. Regardless, the value is in agreement with the results of the other fit ranges.

Fitting the entire data range scanned, with the inclusion of the threshold correction terms, also allows a better determination of the relative threshold strengths. Table 4.11 lists the results obtained from this fit. For convenience, the results of Section 4.2.3 and the expected strengths are also included. In addition to decreasing

Table 4.11: Relative strengths of the fine-structure thresholds observed in the Al^- detachment spectrum, expressed as percent of the total strength. Uncertainties include estimates of possible systematic errors.

	Strengths determined from:		Expected Strengths[a]		
Threshold	Equation 4.1	Section 4.2.3	LS only	1300 K	900 K
$^3P_2 \rightarrow {}^2P_{1/2}$	6.9(6)	9.0(6)	9.3	9.0	8.9
$^3P_1 \rightarrow {}^2P_{1/2}$	12.9(11)	15.4(13)	16.7	17.1	17.3
$^3P_0 \rightarrow {}^2P_{1/2}$	9.7(7)	8.7(16)	7.4	7.8	8.0
$^3P_2 \rightarrow {}^2P_{3/2}$	52.2(5)	52.4(11)	46.3	45.1	44.6
$^3P_1 \rightarrow {}^2P_{3/2}$	18(4)	14(4)	16.7	17.1	17.3
$^3P_0 \rightarrow {}^2P_{3/2}$	< 1.2	≈ 0	3.7	3.9	4.0

[a]Calculated on the basis of LS coupling and thermal populations, assuming the given temperature.

the uncertainties in the fitted threshold strengths, the inclusion of the correction terms also changes the measured relative threshold strengths by a small, but non-negligible, amount. Especially notable is the observation of the weakest threshold, which was not possible without the threshold corrections (see Section 4.2.3). Notice also that the departure from LS coupling in Al appears to be considerably larger than in B, as might be expected. Considering the far superior fit to the data when the correction terms are included, as can be seen in Figure 4.22, the new values should be more reliable.

4.3.3 Summary and Conclusions

The inclusion of the correction terms clearly improves the agreement of the threshold law to the data. It was possible to fit the photodetachment spectra of B and Al over a range that greatly exceeds what is normally considered the threshold region. However, for both Al and B, it was necessary to include the correction terms from both Farley's and O'Malley's theory which was not done in the original papers[1] (Section 4.2.2

[1]In fact, to my knowledge, no previous work has taken this approach.

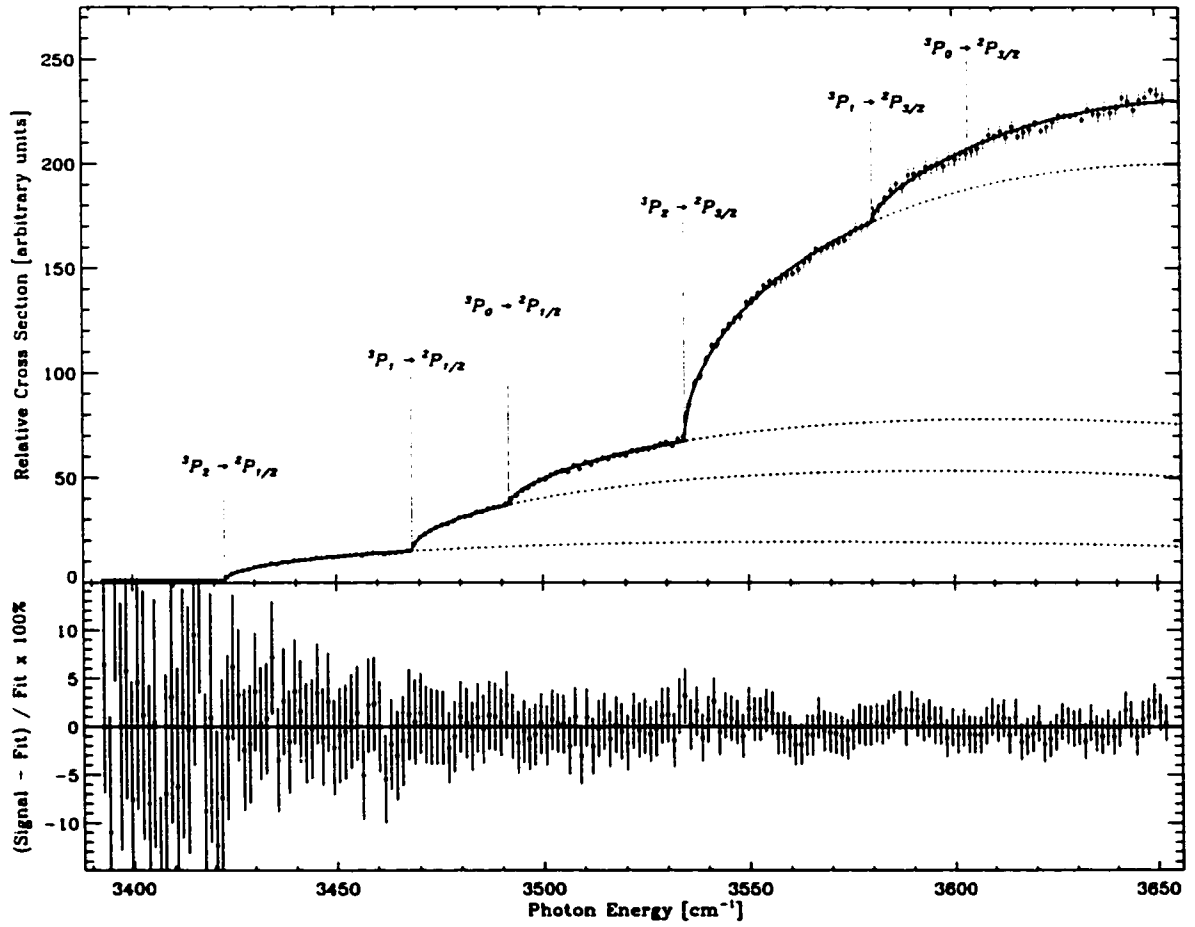

Figure 4.22: Comparison of threshold law correction terms for aluminum. Error bars are two standard deviations, based on the observed scatter in the signal from pulse to pulse. Presented data is not corrected for saturation. The signal has been normalized such that the background signal is 1.

and Section 4.2.3). It was also possible to obtain improved relative strengths of the Al^- detachment thresholds. The small but significant changes to these new relative strengths, compared to those originally reported, demonstrate that these correction terms cannot be ignored in some situations. These represent the key updates obtained in Section 4.3.1 and Section 4.3.2 to the original papers.

It also appears that the next higher order correction term becomes significant even at modest energies above threshold ($\gtrsim$5% above threshold). A more refined

analysis may benefit from using the complete ZCC approximation, which includes the correction to all orders. Albeit involved, expressions for the full ZCC model are available and including them in a fit should not pose excessive difficulty.[2] Perhaps a larger concern is the lack of an estimate for the magnitude of C^{sr}. The present work suggest that this value is small but not negligible, perhaps about 20% of (and with an opposite sign of) C_1^{lt} for B and Al. Therefore although much progress has been made in this area, further theoretical and experimental investigations of these threshold correction terms are of definite interest.

The situation in Pt^- and Ir^- is still an outstanding problem. In both of these cases the ZCC terms, including Farley's leading correction term, should be very small. If C^{sr} does not change dramatically for p-wave detachment, then B^{dp} should be the dominant correction. Unfortunately, as discussed in Section 4.1.2, the value of α would have to be $\sim$10 times larger in order to explain the deviation. If we assume that the tabulated values for α are correct, and given that the correction terms predicted by Farley and O'Malley are in good agreement with the observations in B and Al, it seems reasonable to expect that the correction terms should be relatively good in Pt^- and Ir^-. In this light, it may be appropriate to revise the assumptions made when analysing the Pt^- and Ir^- spectra. In particular, it was assumed that the effect of the quadrupole moment is negligible in these systems.

There have been very few studies aimed at determining the magnitude of quadrupole moments (theoretical studies include [14–17] and experimental studies include [18–21]). For all the states reported in these works, values for Q_{av} of $<$10 a.u. are expected, and therefore it is usually well justified to ignore B^{qm}. However, all of these states involve light systems with rather small L and J, while the ground state

[2]See [13]. Unfortunately a simple dimensional analysis suffices to show that a number of typographic errors, which have not yet been addressed, are present in the expressions.

of Ir and Pt are $^3F_4$ and $^2D_{5/2}$ respectively, and could have considerably larger Q_{av}. Since the quadrupole correction term depends quadratically on Q_{av} even a modest increase may be significant. Also in p-wave detaching species, the importance of B^{dp} is considerably diminished ($|B_1^{dp}/B_0^{dp}| = \frac{1}{5}$), thereby possibly increasing the relative importance of B^{qm}. Unfortunately, no expression for $B_{\ell=1}^{qm}$ is available, and a better understanding of the quadrupole correction is therefore needed. As an estimate, if we assume that $B_1^{qm} \approx B_0^{qm}$, and that C^{sr} is not appreciably different, then a value of $Q_{av} \approx 40$ would be sufficient to explain the observations.

Historically, the threshold law correction terms have attracted attention largely as a means to improve the fits of the measured threshold region, and hence the determination of threshold energy. Although this is important for the study of ionic structure, the discussions in the preceding paragraphs suggest another important application. If the correction terms were well understood, the accuracy achieved with the fits in B^- and Al^- indicate that it would be possible to extract the value of α to within 5% for B and ≈17% for Al. Even modern measurements rarely exceed this level of accuracy (see for example [12,22-27]). One should also remember that the measurements performed here did not originally target this purpose and a more carefully designed experiment could easily reduce these uncertainties to below 1%, at least for B. This could therefore present a valuable alternative for polarisability measurements. Perhaps of particular interest is that, in combination with state-selective techniques (e.g. resonant ionization spectroscopy [28]), photodetachment thresholds could be easily used to study the polarisabilities of excited states of the neutral atoms, for which very few experimental measurements exist [23], presumably because such experiments are difficult. Finally, in cases where the quadrupole term dominates, photodetachment studies could provide an excellent method to determine the quadrupole moment of the neutral state. A new technique for positive ions [29] has recently led

to a few experiments that obtained quadrupole moments for a number of atomic and molecular positive ions [30–32]. However, with the exception of a few rare measurements conducted in the early 1970's [18–21], most of which target excited states of the noble gases, no experimental measurements of quadrupole moments for neutral atoms are available [17].

Finally, it should be stressed that although B and Al served to illustrate the importance of these correction terms, the fine structure of the neutral and negative ion make them relatively difficult systems for such studies, especially for Al. Better systems for studying the polarisability term would be ones with a high threshold energy (in order to reduce the effect of Farley's term) and reasonable polarisability. Iodine is perhaps the best candidate in this respect for s-wave thresholds. I^- has no fine structure and, although the polarisability of the neutral is small, the EA is so large that the polarisability term should be clearly dominant. Chlorine and bromine may also be good candidates. Gold is promising for p-wave detachment for similar reasons, but the alkali elements may make especially good targets, since they have very large polarisabilities and no neutral or ionic ground-state fine structure. For investigations of the ZCC terms (including Farley's correction), an element with a low electron affinity and low polarisability is desirable, such as Cr and Mo, which have the added advantage that both the neutral and ionic ground states have no fine structure. There are no obvious "ideal" candidates for s-wave detaching species, but the heavier elements in the boron group (especially In) would be of definite interest.

4.4 References

[1] M. Scheer, *Single- and Multiphoton Infrared Laser Spectroscopy of Atomic Negative Ions*, Ph.D. thesis, McMaster University (1998).

[2] R. D. Mead, Keith R. Lykke, and W. C. Lineberger, in *Photodetachment Threshold Laws*, Invited papers of the XIII International Conference on the Physics of Electronic and Atomic Collisions, Berlin, 1983, edited by J. Eichler, I. V. Hertel, and N. Stolterfoht, (Elsevier Science, New York, 1984).

[3] A. R. P. Rau, Comments At. Mod. Phys. **14**, 285 (1984).

[4] H. Hotop, T. A. Patterson, and W. C. Lineberger, Phys. Rev. A **8**, 762 (1973).

[5] H. Hotop and W. C. Lineberger, J. Chem. Phys. **58**, 2379 (1973).

[6] W. C. Lineberger and B. W. Woodward, Phys. Rev. Lett. **25**, 414 (1970).

[7] R. J. Champeau, A. Crubellier, D. Marescaux, D. Pavolini, and J. Pinard, J. Phys. B **31**, 249 (1998).

[8] P. Kristensen, U. V. Pedersen, V. V. Petrunin, and T. Andersen, Phys. Rev. A **55**, 978 (1997); Erratum: Phys. Rev. A **56**, 1674 (1997).

[9] D. Calabrese, A. M. Covington, J. S. Thompson, R. W. Marawar, and J. W. Farley, Phys. Rev. A **54**, 2797 (1996).

[10] J. Dellwo, Y. Liu, D. J. Pegg, and G. D. Alton, Phys. Rev. A **45**, 1544 (1992).

[11] A. K. Das and A. J. Thakkar, J. Phys. B **31**, 2215 (1998).

[12] P. Milani, I. Moullet, and W. A. de Heer, Phys. Rev. A **42**, 5150 (1990).

[13] J. W. Farley, Phys. Rev. A **40**, 6386 (1989).

[14] K. Schroder, V. Staemmler, M. D. Smith, D. R. Flower, and R. Jaquet, J. Phys. B **24**, 2487 (1991).

[15] R. Jaquet, V. Staemmler, M. D. Smith, and D. R. Flower, J. Phys. B **25**, 285 (1992).

[16] K. Andersson and A. J. Saglej, Phys. Rev. A **46**, 2356 (1992).

[17] D. Sundholm and J. Olsen, Phys. Rev. A **47**, 2672 (1993).

[18] J. R. P. Angel, P. G. H. Sanders, and G. K. Woodgate, J. Chem. Phys. **46**, 1552 (1967).

[19] T. A. Miller and S. R. Freund, Phys. Rev. A **4**, 81 (1971).

[20] T. A. Miller and S. R. Freund, Phys. Rev. A **5**, 588 (1972).

[21] P. G. H. Sandars and A. J. Stewart, in *Atomic Physics 3,* Proceeding of the Third International Conference on Atomic Physics, 1992, edited by S. J. Smith and G. K. Walters (Plenum, New York, 1973), p. 429.

[22] L. Windholz and M. Musso, Phys. Rev. A **39**, 2472 (1989).

[23] Y. Zhang, M. Ciocca, L.-W. He, C. E. Burkhardt, and J. J. Leventhal, Phys. Rev. A **50**, 1101 (1994).

[24] D. Goebel and U. Hohm, Phys. Rev. A **52**, 3691 (1995).

[25] D. Goebel, U. Hohm, and G. Maroulis, Phys. Rev. A **54**, 1973 (1996).

[26] M. K. Kadar-Kallen and K. D. Bonin, Phys. Rev. Lett. **72**, 828 (1994).

[27] C. R. Ekstrom, J. Schmiedmayer, M. S. Chapman, T. D. Hammond, and D. E. Pritchard, Phys. Rev. A **51**, 3883 (1995).

[28] The RIS technique is reviewed in: T. Andersen, H. K. Haugen, and H. Hotop, J. Phys. Chem. Ref. Data **28**, 1511 (1999).

[29] S. L. Palfrey and R. S. Lundeen, Phys. Rev. Lett. **53**, 1141 (1984).

[30] W. G. Sturrus, E. A. Hessels, P. W. Arcuni, and S. R. Lundeen, Phys. Rev. A **44**, 3032 (1991).

[31] P. L. Jacobson, R. D. Labelle, W. G. Sturrus, R. F. Ward, Jr., and S. R. Lundeen, Phys. Rev. A **54**, 314 (1996).

[32] R. F. Ward, Jr., W. G. Sturrus, and S. R. Lundeen, Phys. Rev. A **53**, 113 (1996).

Chapter 5

E1 Transitions and Continuum Structure in Atomic Negative Ions

The short-range potential which binds negative ions cannot support many bound states. Typically only one state, plus possible fine structure, is bound. Only in very few cases are two configurations expected to be bound in the same system[1] (e.g. Pd^-, Pt^-, and La^-), and only in a small subset of these are the configurations of opposite parity. It is then not surprising that, prior to the present work, no negative ions were known to posses bound states of opposite parity.

Studies on Cs^-, Os^-, and W^- are presented in this chapter. The main results on Os^- and Cs^- have been previously published in Physical Review Letters, which are reproduced in Section 5.1.1 and Section 5.1.2. These papers describe the search for, and eventual discovery of, bound-bound electric dipole (E1) transitions in atomic negative ions. Those results will then be viewed in a larger context in Section 5.2 and Section 5.3, where a modified threshold law for near-threshold resonances is developed

[1]To my knowledge, except for Pd^-, which has two bound states belonging to different configurations of even parity (see Paper 11), and the present work on Os^-, no experimental evidence of bound states belonging to different configurations exists [1].

and applied to the spectra of Os^- and W^-. Finally, the results are summarized and shown to be in general agreement with a simple semi-classical model for shape resonances in Section 5.4.

5.1 Opposite Parity States in Atomic Negative Ions

5.1.1 Paper 9 — Experimental Evidence that the $6s6p\ ^3P_J$ States of Cs^- are Shape Resonances

The negative ion of Cs has been the subject of many theoretical studies. Partly it has attracted interest due to its relatively simple structure, although it is a heavy system, but also because it is one of the very few systems which have been predicted to have bound states of opposite parity. A number of theoretical studies suggested that the $6s6p\ ^3P$ excited states in Cs^- were bound, although some recent studies indicated that they may be slightly unbound. However, no experimental studies were available to confirm or refute these findings. An infrared photodetachment study of Cs^- with the McMaster setup was therefore of interest.

Since the publication of the present Letter, two theoretical studies by Bahrim and Thumm have revisited the negative ion of Cs^-. In the first work [2], the elastic scattering of electrons on Cs is studied. The ionic $^3P^o_{0,1,2}$ states were observed as resonances with positions at 1.69, 5.53, and 12.74 meV [13.6, 44.6, and 102.7 cm^{-1}] respectively, which compares well with the experimental determination of 8.0(3) meV [64.5(24) cm^{-1}] for the $^3P^o_1$ state (see below). (Note that since the McMaster experiment was a single-photon detachment experiment from the $6s^2\ ^1S^e_0$ state, only the $6s6p\ ^3P^o_1$ state could be observed due to the E1 selection rule: $\Delta J = 0, \pm 1$, and not $J = J' = 0$.) The second paper by Bahrim and Thumm [3] calculates the Cs^- photodetachment cross section in an effort to reproduce the spectrum presented

in the Letter below. Except for a small correction in the resonance position, these theoretical results are in impressive agreement with the observed spectrum.

This Letter presents the results of laser spectroscopy experiments conducted at McMaster (which constitutes the bulk of the article), and lifetime experiments conducted on the ASTRID storage-ring at Aarhus University in Denmark. The storage-ring experiments provide additional support for the conclusions drawn from the LPT experiments, but represent only a small portion of the paper. Although M. Scheer was primarily responsible for the McMaster work presented in the Letter, I participated heavily in the experimental realization as well as the data analysis and editing of the article. J. Thøgersen was involved in some of the early experiments at McMaster. Finally, H. K. Haugen, C. A. Brodie, H. H. Andersen, P. Kristensen, and T. Andersen were involved in the storage-ring work. H. K. Haugen also supervised all stages of the McMaster work.

VOLUME 80, NUMBER 4 PHYSICAL REVIEW LETTERS 26 JANUARY 1998

Experimental Evidence that the $6s6p\ ^3P_J$ States of Cs^- Are Shape Resonances

M. Scheer, J. Thøgersen,* R. C. Bilodeau, C. A. Brodie, and H. K. Haugen†
Department of Physics and Astronomy, McMaster University, Hamilton, Ontario, L8S 4M1, Canada

H. H. Andersen, P. Kristensen, and T. Andersen
Institute of Physics and Astronomy, University of Aarhus, DK-8000 Aarhus C, Denmark
(Received 23 June 1997)

An experimental study of the previously unobserved and controversial $Cs^-(6s6p\ ^3P_J^o)$ states has been conducted using a combination of infrared laser and storage ring experiments. This first application of photodetachment spectroscopy to the study of low-lying resonances in atomic negative ions has resulted in the observation of a narrow resonance structure, lying only 8.0(3) meV above the first detachment threshold of Cs^-. The storage ring experiments suggest that all fine structure levels of the $6s6p$ configuration are unbound, thereby eliminating possibly the only serious candidate for a stable atomic negative ion with opposite parity bound states. [S0031-9007(97)05108-9]

PACS numbers: 32.80.Gc, 32.80.Dz

Atomic negative ions are a topic of considerable current interest [1], in part motivated by a number of practical implications. Negative ions play an important role in a variety of atomic and plasma phenomena, and in a more specialized context, they provide the basis of ultrasensitive atom and isotope detection through accelerator mass spectrometry (AMS) [2]. In a general context, the interest in negative ions stems from the fact that they are qualitatively different in their structure from neutral atoms and positive ions. To a large extent these differences are a result of the short range interactions between the extra electron and the atomic core; in a mean field treatment the electron is bound in the dipole potential that it induces in the atom. Negative ions therefore offer the unique opportunity to study short range potentials on an atomic scale, which are of fundamental importance to other fields such as nuclear physics. In contrast to a Coulomb potential, a short range potential cannot support an infinite number of bound states; in fact, most negative ions have only one. On the other hand, all negative ions possess many unstable excited states which are embedded as resonances in the energy continuum associated with an atom and a free electron. The extensive theoretical and experimental work on atomic negative ion resonances was recently reviewed by Buckman and Clark [3]. Resonances involving the atom in its ground state occur when the extra electron is trapped in a potential well resulting from the overlap of the attractive short range potential of the polarized atom and the repulsive centrifugal potential. Traditionally, these low-lying shape resonances have been investigated via electron-atom scattering or ion-atom collisions, but the study of very low-lying resonances has proven to be rather challenging with these techniques. Despite considerable efforts on various atomic ions the recently observed $Li^-(2s2p\ ^3P)$ resonance at 50(6) meV [4] is the lowest-lying feature previously reported. The present work therefore employs photodetachment spectroscopy which is new to the study of low-lying atomic shape resonances.

The cesium negative ion, which is the important example of a H^--like two-electron system with a polarizable core and strong relativistic effects, has been the subject of considerable investigation in the past, both experimental and theoretical. A diagram of the energy level structure of Cs^- and Cs, up to $Cs(6p)$, is given in Fig. 1. Two decades ago, laser-based experiments [5] of the Cs^- continuum just below the $Cs(6p)$ threshold

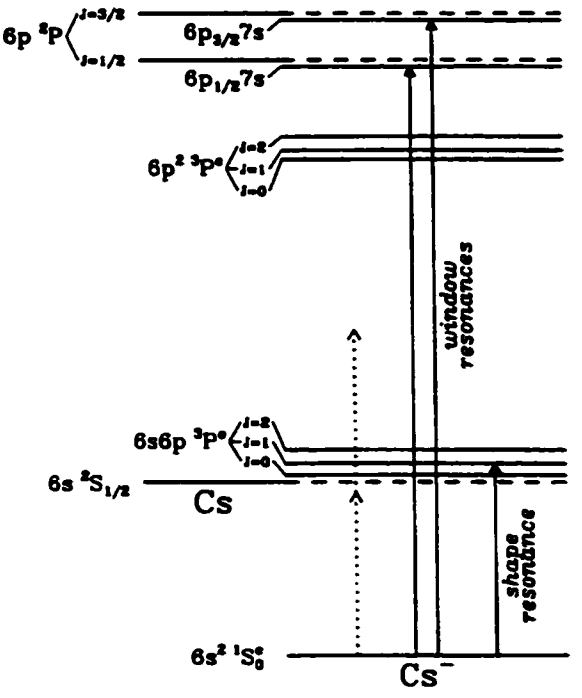

FIG. 1. Schematic energy level diagram of Cs^- and Cs. For clarity of presentation level splittings are not to scale.

 0031-9007/98/80(4)/684(4)$15.00

VOLUME 80, NUMBER 4 PHYSICAL REVIEW LETTERS 26 JANUARY 1998

revealed a narrow window resonance. Recently, Greene [6] conducted an extensive theoretical study of Cs^-, in part reproducing the window feature. Also, multiphoton studies have incorporated the narrow window resonances in Cs^- and Rb^- [7]. The cesium negative ion has been much discussed in numerous theoretical studies as potentially the only known candidate for a stable atomic negative ion that possesses an *excited bound configuration of opposite parity to the ground state*. Initially, several calculations on $Cs^-(6s6p\ ^3P_J^o)$ indicated that the $^3P_J^o$ state might be slightly bound, by a maximum of a few tens of meV [6,8–10], although Fabrikant [8], and Krause and Berry [9] expressed that this might not hold true if their calculations were refined. More recently, a relativistic scattering calculation based on the Dirac R-matrix method by Thumm and Norcross predicted the $J = 0, 1, 2$ levels to be narrow shape resonances just above the Cs(6s) threshold [11]. This result contradicted earlier scattering calculations [12] which employed a semirelativistic Breit-Pauli R-matrix formalism, and which did not show any low energy resonance structure. This discrepancy was partially resolved in a subsequent theoretical study by Bartschat [13], in favor of the conclusions by Thumm and Norcross. This study compared the two different methods directly, but the earlier Breit-Pauli formalism was modified, in particular through the inclusion of a dielectronic core polarization term. The work reported in the present Letter is the first experimental investigation aimed at resolving this long-standing issue.

The experimental approach involved tunable infrared laser spectroscopy at McMaster University, and heavy ion storage ring experiments at Aarhus University using the ASTRID [14] storage ring. The experimental setup at McMaster is described in detail elsewhere [15,16]. A tunable laser source consisting of a Nd:YAG pumped dye laser and nonlinear optical conversion equipment provided nanosecond infrared pulses with energies of ≈0.5 mJ at 3 μm. In an ultrahigh vacuum chamber the infrared laser beam was crossed at 90° with a 10 keV Cs^- beam, which was extracted from a Cs sputter ion source. Photodetached neutral atoms were detected by a discrete dynode electron multiplier.

A series of careful experiments was conducted with tunable infrared laser light, either in a 1 + 1 (two-photon) detachment scheme, in search of a possibly bound $6s6p\ ^3P_1^o$ level, or aimed at observation of a resonant feature above threshold in the one-photon detachment spectrum. A resonant enhancement of the two-photon detachment yield due to a spin-forbidden $^1S_0^e \rightarrow {}^3P_1^o$ electric dipole transition would be expected in the 1 + 1 photon detachment regime. The laser-based experiment is only sensitive to the $J = 1$ level of $6s6p\ ^3P_J^o$. Greene [6] predicted binding energies of 32, 25 and 11 meV for the $J = 0, 1, 2$ levels, respectively, while Fabrikant [8], Krause and Berry [9], and Froese Fischer and Chen [10] determined the average binding energy for the $^3P_J^o$ term to be 27, 12, and 1 to 11 meV, respectively. In addition, Greene predicted an Einstein A coefficient for the $6s6p\ ^3P_1^o$ level of 77 s^{-1}, but other theoretical estimates indicate that the A coefficient would be substantially larger [17]. Since we have previously demonstrated [18] that we can readily observe signals for resonantly enhanced 1 + 1 transitions via magnetic dipole transitions with A coefficients of $\sim 1\ s^{-1}$, then a large signal, in the case of a bound excited level, would be expected in the present case.

We have performed a series of experiments in the near-threshold region of Cs^- without observing any indication of a bound $6s6p\ ^3P_1$ level. The experiments were carried out under a wide range of experimental conditions, utilizing a tightly focused laser beam or an unfocused beam in order to allow for a range of oscillator strengths and detachment cross sections. The expected experimental signals were modeled on a computer program. Both analog and digital data collection methods were utilized. In all, the first 100 meV below threshold were probed.

Subsequently, we conducted one-photon infrared laser detachment spectroscopy above the Cs(6s) threshold. We obtained good signals for the Wigner p-wave threshold and also explored the relative single photon detachment cross section to an energy of 75 meV above the photodetachment threshold. The results are shown in Fig. 2. A feature which represents an enhancement of ≈25% over the direct, p-wave photodetachment yield is seen centered at a photon energy of 479.6(3) meV, 8.0(3) meV above threshold, with a width of 5.0(5) meV (full width at half maximum) according to a Lorentzian fit. We attribute this relatively weak resonant feature to the $Cs^-(6s6p\ ^3P_1^o)$ level embedded in the continuum. A blowup of the resonant feature, with the photodetachment "background" subtracted, is shown in Fig. 3. Numerous checks were done in an attempt to verify the validity of this feature. In order to remove the effects of atmospheric absorption of the

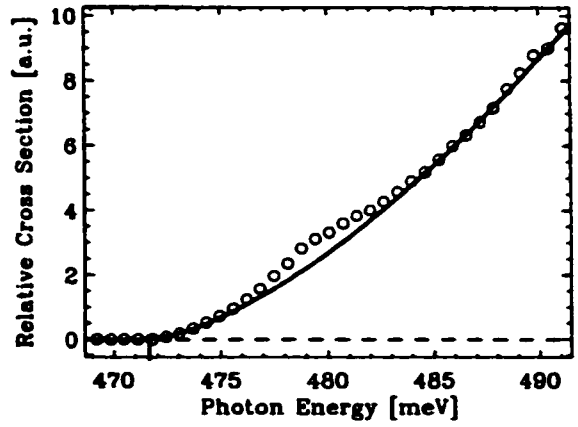

FIG. 2. Photodetachment yield versus laser wavelength. The solid line represents a fitted Wigner p-wave threshold.

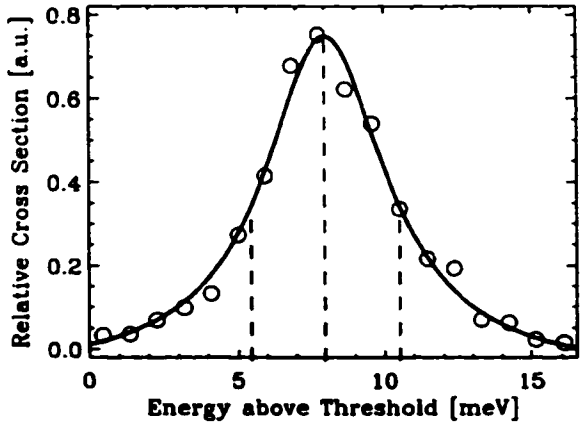

FIG. 3. Blowup of the one-photon detachment scan showing the resonant feature with the p-wave "background" subtracted. The result of a Lorentzian fit is indicated by the solid line.

infrared light the laser path was purged with dry nitrogen and the data normalized to the laser power in the interaction region. We do not believe that this results in any artifact in the final data for the following reasons: the absorption features are small and much narrower than the observed feature, they do not coincide with the proposed resonance, and variations in purge quality in different experiments have led to the same result. It is also possible that a molecular impurity ion, with a mass close to that of Cs^-, could lead to a false resonance, but the relative size of the feature was constant in measurements separated by a few months. Moreover, this is the only feature which we observe in the entire spectral region, including a 100 meV region below threshold where a (unstructured) very weak background was obtained. We consider it very unlikely that a single impurity-ion-based feature would manifest itself solely at this photon energy.

In addition, our infrared photodetachment data enable an accurate determination of the electron affinity (EA) of Cs. We obtain a final value of 471.64(6) meV. A somewhat more accurate value, 471.630(25) meV, which was determined by Lineberger and co-workers via photodetachment to Cs($6p$) using visible cw laser light, was only tabulated in the Hotop and Lineberger review [19] from 1985. Our tunable infrared laser work provides a second and entirely complementary measure of the EA of Cs with high accuracy.

The absence of a $1 + 1$ resonant signal in our laser based studies, combined with the observation of a resonant feature in the single-photon detachment yield, which we attribute to the $6s6p\ ^3P_1^o$ level, is in excellent agreement with the theoretical work of Thumm and Norcross [11] and Bartschat [13]. These advanced theoretical works predict the resonant structure in the case of electron scattering on Cs, and seem to have achieved a high level of accuracy. Thumm and Norcross calculated the $J = 0, 1, 2$ levels to lie 1.78, 5.56, and 12.76 meV above threshold with widths of 0.42, 2.42, and 9.32 meV, respectively (Bartschat obtained very similar results), compared to our values for the $J = 1$ photodetachment resonance, 8 and 5 meV for position and width, respectively. Our increased width would appear to be qualitatively consistent with the increased energy above the Cs($6s$) threshold. The excellent agreement of theory [11,13] and the present experiment on the $J = 1$ resonance energy is even more convincing when presented with respect to the energy of the Cs^- ground state: 477.2 meV versus 479.6 meV, respectively. We do not yet have theoretical input on the expected magnitude of the feature due to an unbound $^3P_1^o$ level in the optical case, since the existing theoretical results apply to electron scattering. Crude extrapolations from the isoelectronic neutral Ba atom might suggest an order of magnitude of a few percent enhancement in the photodetachment yield.

Although we cannot probe $J = 0, 2$ in the laser-based experiments, the theoretical predictions on fine structure splittings would suggest that $J = 0$ is also unbound, based on our position for $J = 1$. Greene [6], Thumm and Norcross [11], and Bartschat [13] predict the $J = 0 - 1$ splitting to be 7, 3.78, and 3.33 meV (Breit-Pauli approach), respectively. In order to make an entirely separate check on the possibility of bound excited levels in Cs^- (especially $J = 0$), we conducted a series of storage ring experiments at the ASTRID facility in Aarhus. The Cs^- ions were produced in either of two different ways, which enhanced the probability of effectively populating a weakly bound Cs^- level. In one run, the ions were extracted directly from a cesium sputter (negative) ion source. Subsequently, in a separate run, Cs^+ ions were extracted from a positive ion source at a kinetic energy of 100 keV, and were charge exchanged in a K metal vapor cell to produce Cs^- ions, which were then injected into the storage ring. The Cs^- beam currents were a few nA. Neutral atoms stemming from either collisional or blackbody-radiation-induced detachment were detected at one corner of the storage ring. The measured 1.1 s lifetime of the Cs^- ground state was consistent with the expected collisional detachment rate. Blackbody-radiation-induced photodetachment on a short ms time scale would provide a sensitive measure of a weakly bound level, up to a binding $\approx$150 meV. A description of the blackbody-radiation effects on weakly bound negative ions can be found in Ref. [20]. We observed no signal associated with a weakly bound level, despite a sensitivity of $\approx 5{:}10^4$ or better [20]. The storage ring experiment has limitations, but offers a very useful double check. The most notable limitation in the present context is that the experiment is insensitive for binding energies less than $\approx$3 meV. Our calculations, based on Ref. [21] indicate that the Lorentz force generated during passage of the 90° bending magnets would destroy more weakly bound ions before they could be observed [14,20]. Hence our final conclusion that $J = 0$ is likely unbound

depends on the validity of the earlier fine structure calculations [11,13]. In contrast to the magnetic field stripping effect, our simulations predict no serious limitation due to an excessive blackbody detachment rate for very weak bindings since the Planck radiation flux drops off rapidly at long photon wavelengths—corresponding to an ionic binding of a few meV.

In summary, we have reported the first experimental evidence that the $J = 1$ level of the $Cs^-(6s6p\ ^3P^o_J)$ state is a shape resonance, rather than a bound state of opposite parity to the $Cs^-(6s^2\ ^1S^e_0)$ ground state. We have further obtained substantial evidence that the $J = 0$ and $J = 2$ levels are also unbound, although the conclusion for $J = 0$ hinges on earlier calculations of the $^3P^o_J$ fine structure. To this extent, Cs^- can be eliminated as possibly the only known good candidate for a stable atomic negative ion with a second bound state of opposite parity to the ground state [22], thereby resolving a long-standing controversy. With regards to future experimental work, the successful application of photodetachment spectroscopy to the study of low-lying shape resonances in the present work strongly suggests similar investigations in other atomic negative ion systems. For Cs^-, Thumm and Norcross [11] and Bartschat [13,23] have also predicted the existence of a $6p^2\ ^3P^e_J$ state embedded in the continuum, below $Cs(6p)$. A multiphoton experiment aimed at the first optical observation of these levels might proceed using Raman coupling via the window resonance, ideally using picosecond-duration optical pulses. We finally note that the cesium negative ion is forming the basis of a relatively new tracer in AMS [24], and that knowledge of its excited states is of practical importance.

We gratefully acknowledge the Natural Science and Engineering Research Council of Canada (NSERC) for support of the experimental work at McMaster University, and the National Research Council (SNF) and the Aarhus Center for Advanced Physics (ACAP) for support of the work in Aarhus. We especially wish to thank C. H. Greene, L. R. Kilius, A. E. Litherland, S. H. Vosko, and W. P. Wijesundera, who have been part of an (NSERC-based) initiative aimed at the study of Ba^- and Cs^-, for numerous helpful discussions. The contributions of Linas Kilius and Sy Vosko were greatly appreciated and they will be sorely missed. U. Thumm has also provided very helpful theoretical input during the course of this project.

*Present address: Department of Chemistry, University of Aarhus, DK-8000 Aarhus C, Denmark

†Also with the Department of Engineering, the Brockhouse Institute for Materials Research, and the Center for Electrophotonic Materials and Devices.

[1] D. R. Bates, Adv. At. Mol. Opt. Phys. 27, 1 (1991); T. Andersen, Phys. Scr. T34, 23 (1991); S. J. Buckmann and C. W. Clark, Rev. Mod. Phys. 66, 539 (1994); C. Blondel, Phys. Scr. T58, 31 (1995).

[2] A. E. Litherland, Annu. Rev. Nucl. Part. Sci. 30, 437 (1980); W. Kutschera and M. Paul, Annu. Rev. Nucl. Part. Sci. 40, 411 (1990).

[3] S. J. Buckman and C. W. Clark, Rev. Mod. Phys. 66, 539 (1994).

[4] D. H. Lee, W. D. Brandon, D. Hanstorp, and D. J. Pegg, Phys. Rev. A 53, R633 (1996).

[5] T. A. Patterson, H. Hotop, A. Kasdan, D. W. Norcross, and W. C. Lineberger, Phy. Rev. Lett. 32, 189 (1974); J. Slater, F. H. Read, S. E. Novick, and W. C. Lineberger, Phys. Rev. A 17, 201 (1978).

[6] C. H. Greene, Phys. Rev. A 42, 1405 (1990).

[7] H. Stapelfeldt and H. K. Haugen, Phys. Rev. Lett. 69, 2638 (1992); H. Stapelfeldt, P. Kristensen, U. Ljungblad, T. Andersen, and H. K. Haugen, Phys. Rev. A 50,1618 (1994).

[8] I. I. Fabrikant, Opt. Spectrosc. 53, 131 (1982) [Opt. Spektrosk. 53, 223 (1982)].

[9] J. L. Krause and R. S. Berry, Comments At. Mol. Phys. 18, 91 (1986).

[10] C. Froese Fischer and D. Chen, J. Mol. Struct. 199, 61 (1989).

[11] U. Thumm and D. W. Norcross, Phys. Rev. Lett. 67, 3495 (1991); Phys. Rev. A 45, 6349 (1992); 47, 305 (1993).

[12] N. S. Scott, K. Bartschat, P. G. Burke, O. Nagy, and W. B. Eissner, J. Phys. B 17, 3755 (1984); P. G. Burke and J. F. B. Mitchell, J. Phys. B 6, L161 (1973).

[13] K. Bartschat, J. Phys. B 26, 3595 (1993).

[14] L. H. Andersen *et al.*, Phys. Lett. A 162, 336 (1992).

[15] J. Thøgersen, L. D. Steele, M. Scheer, C. A. Brodie, and H. K. Haugen, J. Phys. B 29, 1323 (1996).

[16] M. Scheer, C. A. Brodie, R. C. Bilodeau, and H. K. Haugen (to be published).

[17] W. P. Wijesundera and A. E. Litherland (private communication).

[18] J. Thøgersen, M. Scheer, L. D. Steele, H. K. Haugen, and W. P. Wijesundera, Phys. Rev. Lett. 76, 2870 (1996).

[19] H. Hotop and W. C. Lineberger, J. Phys. Chem. Ref. Data 14, 731 (1985).

[20] H. K. Haugen *et al.*, Phys. Rev. A 46, R1 (1992).

[21] M.-J. Nadeau and A. E. Litherland, Nucl. Instrum. Methods Phys. Res., Sect. B 52, 387 (1990); V. A. Oparin, R. N. Il'in, I. T. Serenkov, and E. S. Solov'ev, Sov. Phys. JETP 39, 989 (1974) [Zh. Eksp. Teor. Fiz. 66, 2008 (1974)].

[22] Theoretical studies of the negative ions of some lanthanides and actinides seem to indicate the possibility of opposite parity bound states in these complex systems; S. H. Vosko, J. B. Lagowski, I. L. Mayer, and J. A. Chevary, Phys. Rev. A 43, 6389 (1991); D. Datta and D. R. Beck, Phys. Rev. A 50, 1107 (1994); K. Dinov, D. R. Beck, and D. Datta, Phys. Rev. A 50, 1144 (1994).

[23] K. Bartschat, A. R. Johnston, and P. D. Burrow, J. Phys. B 27, L231 (1994).

[24] T. Lee, T.-L. Ku, H. L. Lu, and J.-C. Chen, Geochim. Cosmochim Acta 57, 3493 (1993).

5.1.2 Paper 5 — Experimental Studies of Os^-: Observation of a Bound-Bound Electric Dipole Transition in an Atomic Negative Ion

Prior the the present work, Os^- remained as one of the few negative ions which had not been studied experimentally or theoretically. An experimental investigation of Os^- is then important on this basis alone. The first theoretical work on the bound ^4F states of Os^- was conducted by D. Beck and co-workers in parallel to the McMaster work, but published in a separate article.

Perhaps more significantly, however, this paper presents the first observation of a bound-bound E1 transition in an atomic negative ion. Since E1 transitions are between states of opposite parity, this means that Os^- is the only known atomic negative ion with bound states of opposite parity. A second state is also observed in Os^-, although slightly unbound, and is best described as a shape resonance. Similarly to Cs^- these states appear to be due to the attachment of a p-orbital electron to the neutral ground state. As will be discussed in subsequent sections of this chapter, it appears that such states resulting from p-orbital attachment to low-lying neutral states may be a relatively common situation in these heavy systems.

I was the principal investigator for this work. I conducted all of the experimentation and analysis, and wrote the manuscript. H. K. Haugen supervised the project, and in particular provided valuable input in editing the manuscript and numerous discussions on expected sizes of signals and possible pitfalls associated with the measurement. In addition, I would like to draw attention to the last paragraph of the paper which acknowledges a number of individuals who provided valuable comments and suggestions.

VOLUME 85, NUMBER 3 PHYSICAL REVIEW LETTERS 17 JULY 2000

Experimental Studies of Os^-: Observation of a Bound-Bound Electric Dipole Transition in an Atomic Negative Ion

René C. Bilodeau and Harold K. Haugen*

Department of Physics and Astronomy, McMaster University, Hamilton, Ontario, Canada L8S 4M1

(Received 21 December 1999)

The first experimental studies of Os^- reveal the presence of two very strong resonances. One state is a narrow shape resonance lying only 3.52(12) meV above the ground state detachment threshold, while the other is bound by 11.48(12) meV. Convincing evidence that these states have odd parity is presented, making Os^- the only known atomic negative ion with bound states of opposite parity. Additionally, the binding energies for the Os^- ground state ($^4F^e_{9/2}$) and first excited state ($^4F^e_{7/2}$) are measured to be 1.077 80(12) eV and 0.553(3) eV, respectively.

PACS numbers: 32.80.Gc, 32.10.Hq, 32.70.Cs, 32.80.Dz

A number of atomic negative ion states remain poorly known or even completely unknown, despite considerable ongoing theoretical and experimental efforts [1–3]. For example, until now no experimental studies had been conducted on the negative ion of osmium. In fact, until very recent calculations [4], the knowledge of Os^- was limited to the semiempirical extrapolated estimate of 1.1(2) eV for the electron affinity (EA) of Os [3]. In addition to important applications [1,3], negative ions are of considerable interest on a fundamental level. Unlike neutral atoms and positive ions, which are bound by the Coulomb potential, negative ions are bound by a short range potential, more akin to a nuclear potential but on an atomic scale. Consequently, very few states (often only one term) are bound in the negative ion potential, in sharp contrast to the infinite number of bound states in other atomic systems. To date, bound-bound transitions observed in negative ions are always between levels from the same configuration and are thus electric dipole ($E1$) forbidden, making experimental studies very challenging [5]. Over the past few decades considerable effort has been invested into finding an atomic negative ion with opposite parity bound states [3,6]. Although a number of theoretical studies indicated that Cs^- was a strong candidate for opposite parity bound states, recent detailed experimental studies eliminated this possibility [7] and left very few good potential systems [6].

This Letter reports the findings of the first experimental studies of Os^-. Infrared laser photodetachment indicates the presence of an unexpected pair of odd parity states in Os^-. One state is slightly unbound by only 3.52(12) meV, making it the lowest lying continuum feature ever observed in an atomic negative ion [7]. The other state is bound by 11.48(12) meV and is thus the most weakly bound state in an atomic negative ion observed to date [3]. More importantly, since the only other bound configuration of Os^- has even parity, Os^- is the only known negative ion with opposite parity bound states. This discovery offers a close to a long-standing question in atomic physics.

The experimental apparatus is described in detail elsewhere [8]. A Nd:YAG pumped dye laser, operating at a 10 Hz repetition rate with an ≈8 ns temporal width, is Raman shifted in a high pressure H_2 cell to produce the tunable infrared light required in the experiments. The collimated laser light is sent through a CaF_2 viewport into an ultrahigh vacuum chamber where it crosses at 90° with an 8 keV, 150 nA beam of Os^-, extracted from a Cs sputter source utilizing a high purity solid metal Os cathode. Using crossed polarizers, the laser pulse energies could be controllably tuned from under 20 μJ to over 3 mJ, while preserving the spatial and temporal characteristics of the laser pulse.

A schematic energy level diagram of Os^- and Os is presented in Fig. 1, based on the present experiments and very recent calculations by Norquist and Beck [4]. The relative cross section for detachment obtained from a scan covering 850 cm^{-1} near the EA defining $5d^76s^2\,{}^4F^e_{9/2} \rightarrow 5d^66s^2\,{}^5D^e_4$ detachment threshold is shown in Fig. 2. Two very strong peaks are evident from this scan: a "narrow peak" located near 8600 cm^{-1} and a "wide peak" located near 8700 cm^{-1}. Figure 3a shows the data from a high resolution scan covering a range around the narrow peak. The shape is consistent with a Lorentzian profile having a line center at 8600.42(15) cm^{-1} [1.066 316(19) eV] (using 1 eV = 8065.544 77(32) cm^{-1} [9]) and a full width at half maximum (FWHM) of 0.166(3) cm^{-1}, approximately the bandwidth of the laser. A similar high resolution scan around the wide peak (Fig. 3b) shows that this peak also has a Lorentzian shape, but is slightly asymmetric.

The Wigner law has been shown to accurately describe the threshold detachment behavior of a large number of negative ions [3,8,10,11]. The removal of a d electron results in an outgoing p-wave electron giving rise to a cross section following a 3/2 power law (the f wave is not expected to contribute near threshold). However, the law poorly describes the threshold behavior in the present Os^- case, as seen by the dashed curve in Fig. 2. This is due to the presence of the large shape resonance just above the threshold. A similar shape resonance was seen in (metastable) He^- due to the presence of the excited He^- $1s2p2p'\,{}^4P^e$ state lying less than 11 meV above the

 0031-9007/00/85(3)/534(4)$15.00

VOLUME 85, NUMBER 3 PHYSICAL REVIEW LETTERS 17 JULY 2000

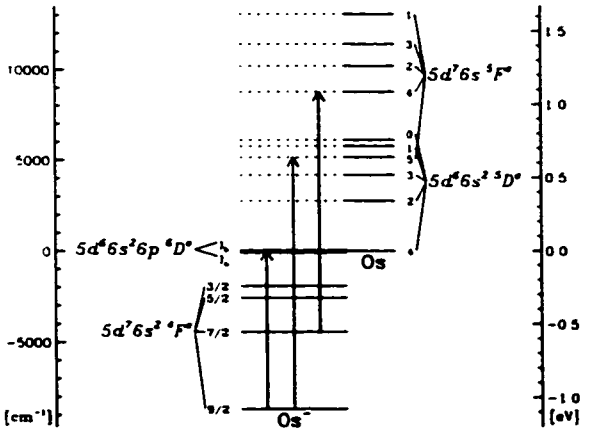

FIG. 1. Energy level diagram for Os^-. Arrows indicate the three measured thresholds. A tentative designation for the new ionic states is included.

$1s2s2p\,^4P^o \rightarrow 1s2p\,^3P^o$ threshold [12]. In that experiment, the Wigner law was also found to be inadequate, even very near to the detachment threshold. However, for photon energies ε greater than the threshold energy ε_0, the following equation was found to have excellent agreement with the observations [12,13]:

$$\sigma = a_0 + c(\varepsilon - \varepsilon_0)^{3/2}/[(\varepsilon - \varepsilon_r)^2 + (\Gamma/2)^2], \quad (1)$$

where c is a constant, ε_r is the resonance position, and Γ is the FWHM parameter of the resonance. Below threshold ($\varepsilon < \varepsilon_0$) σ equals the background a_0.

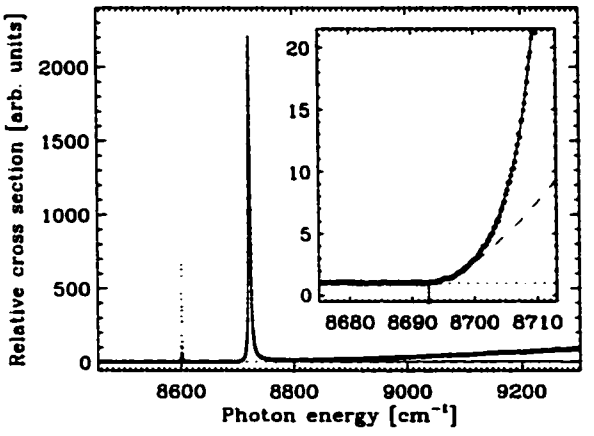

FIG. 2. Photodetachment of Os^-. Inset: High resolution scan around the ground state threshold, fitted to Eq. (1) (solid curve) and the Wigner law (long-dashed curve). The scale is normalized to the background signal (short dashes), due to small amounts of excited Os^- $^4F^e$ ions in the beam. The data have been corrected for variations in pulse energies (between 0.4 and 0.7 mJ per pulse) over this range.

The resonance parameters $\varepsilon_r = 8721.4(3)\ cm^{-1}$ [1.081 32(4) eV] and $\Gamma = 3.66(3)\ cm^{-1}$ are obtained from the fit of Eq. (1) to the data of Fig. 3b. To obtain an accurate value for the threshold position, Eq. (1) is fit to the high resolution scan shown in the inset in Fig. 2, with the two resonance parameters held fixed to the determined values. The threshold position is determined to be 8693(1) cm^{-1} [1.077 80(12) eV], consistent with 1.048 eV, calculated by Norquist and Beck [4]. Although this model agrees very well with the data near the threshold, it is clear from Fig. 2 that the function deviates from the data at photon energies ≈8750 cm^{-1} and higher. In particular, Eq. (1) predicts that the cross section should approach zero with increasing photon energy, while the data increase toward higher photon energies. A deviation from Eq. (1) at higher photon energies is not unexpected, as this function is expected to hold only near the threshold [12]. However, three possible explanations, in addition to the possible breakdown of Eq. (1), can be considered: (i) the presence of yet another resonance at even higher photon energies, (ii) the opening of a new detachment channel from one of the excited states of Os^-, or (iii) signal from the detachment of impurity ions possibly present in the ion beam. The saturation arguments discussed below suggest that the signal observed over the entire range of Fig. 2 originates from the same population, indicating that possibilities (ii) and (iii) are very unlikely. Also, although the resolution of the mass analyzing magnet (better than ≈4%) is not sufficient to eliminate near-mass coincident molecular ion impurities (e.g., OsH^-), the relative size of the features did not vary in measurements carried out over a few months. Moreover, the very narrow and isolated features observed here are not characteristic of signals obtained from molecular ions. Finally, since the structures appear precisely in the expected threshold

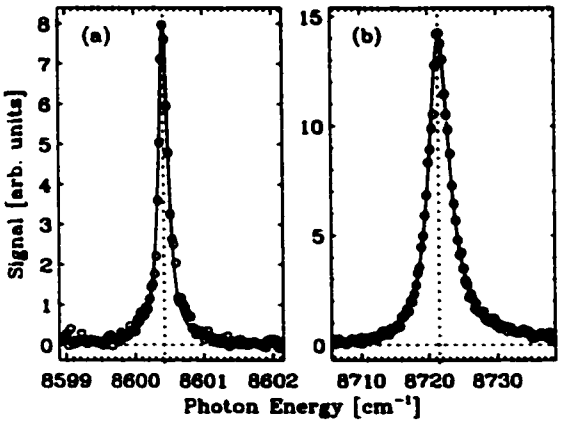

FIG. 3. High resolution scans of (a) the bound-bound resonant transition (narrow peak) and (b) the shape resonance (wide peak), obtained at relatively low pulse energies (≈0.4 mJ per pulse) to avoid saturation broadening.

VOLUME 85, NUMBER 3 PHYSICAL REVIEW LETTERS 17 JULY 2000

region and Os^- is such a prolific ion from a sputter source, we consider it very unlikely that impurity ions could account for the observed signals.

To confirm the position of the Os^- ground state, a 400 cm^{-1} scan around the $5d^76s^2\,{}^4F^e_{9/2} \rightarrow 5d^76s\,{}^5F^e_5$ threshold was conducted, locating this threshold at 13 800(80) cm^{-1}. This determines the binding for Os^- ${}^4F^e_{9/2}$ to be 8660(80) cm^{-1}, in agreement with the above value. Finally, the ${}^4F^e_{7/2} \rightarrow {}^5F^e_4$ threshold was observed at 13 205(24) cm^{-1}; thus the binding of Os^- ${}^4F^e_{7/2}$ is 4462(24) cm^{-1} [0.553(3) eV]. (The larger uncertainties obtained are a consequence of the large backgrounds observed when detaching to excited neutral states.) The measurement of the ${}^4F^e_{9/2}$ level sets the ${}^4F^e_{9/2} - {}^4F^e_{7/2}$ fine structure splitting to 4231(25) cm^{-1} [0.525(3) eV], which agrees within 15 meV to the theoretical splitting of 0.540 eV [4].

Given the very large range of signal strengths and relatively large cross sections observed, due consideration of signal saturation is warranted. Although saturation of the detector and electronics can be easily avoided by careful selection of sensitivity ranges, saturation by depletion of the ion population in the interaction region is also possible. We therefore observed the saturation behavior of the detachment signal at three different photon energies: (a) at the maximum of the narrow peak, (b) at the maximum of the wide peak, and (c) at high photon energies (9300 cm^{-1}). At each photon energy, the intensity of the laser light was varied. Assuming uniform illumination and ion density in the interaction region, the signal N obtained from a single photon detachment process with cross section σ_b, follows the relation [14]

$$N = N_0(1 - e^{-\sigma_b P}), \qquad (2)$$

where N_0 is a constant equal to the maximum signal that would be detected if all the ions were detached, and depends on the ion density, the ion-laser overlap, the efficiency of the detector, and the amplification of the detection electronics. If we assume the ions are stationary over the duration of the laser pulse $\tau \approx 8$ ns, then $P = \int \Phi\, dt = E_p/Sh\nu$ is the number of photons per unit area, where Φ is the photon flux, E_p is the laser pulse energy, and S is the area of the laser beam cross section. Figure 4 is a plot of the signal measured over a large range of pulse energies at the three wavelengths. The solid curve (b) is the best fit result of Eq. (2) to the data points obtained at the maximum of the wide peak (b). The excellent agreement between the data and this model confirms that the detachment process is indeed due to absorption of a single photon into an excited Os^- state with subsequent autodetachment. In contrast, this function does not describe the data obtained at the maximum of the narrow peak (a) for pulse energies $\lesssim 1$ mJ (long-short broken curve in Fig. 4). In fact, at low pulse energies, the shape of the curve approaches that of a quadratic function, indicating the absorption of two photons. With

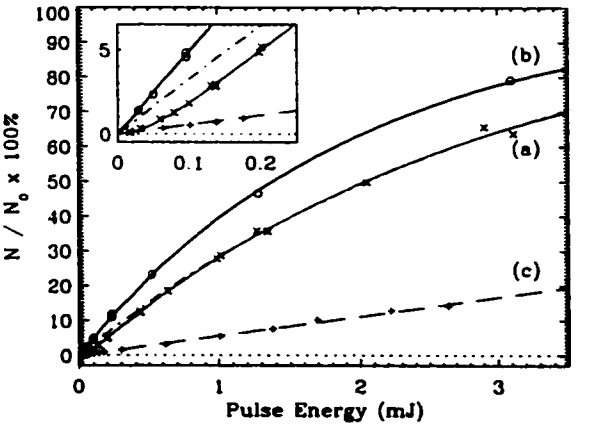

FIG. 4. Percent of population detached versus pulse energy, observed at (a) the maximum of the narrow peak, (b) the maximum of the wide peak, and (c) high photon energies. [For clarity of presentation, the signal for (c) has been multiplied by a factor of 5.] The fitted curves are described in the text. Inset: Expanded view of the low pulse-energy data.

the current experimental parameters, a standard rate-equation approach [15] can be used to determine the signal dependence on pulse energy for a resonant two-photon process. Given σ_a and σ_d, the cross sections for the resonant and detachment steps, respectively, we obtain

$$N = N_0\left(1 - \frac{\sigma_{(+)}e^{-\sigma_{(-)}P} - \sigma_{(-)}e^{-\sigma_{(+)}P}}{\sigma_{(+)} - \sigma_{(-)}}\right), \qquad (3)$$

where $\sigma_{(\pm)} = \frac{1}{2}(2\sigma_a + \sigma_d) \pm \frac{1}{2}\sqrt{4\sigma_a^2 + \sigma_d^2}$. As can be seen from the solid curve (a) in Fig. 4, this model describes the data very well. The value of the maximum signal amplitude N_0 obtained is the same (within the uncertainty of 10%) as that obtained from the wide peak, which confirms that the signal is derived from the same initial state of Os^-, i.e., the ground state. The high photon energy signal (c) is also consistent with an unsaturated signal originating from the Os^- ground state.

For an accurate determination of the cross sections σ_a, σ_b, and σ_d, a more detailed model and more precise determination of the laser pulse and ion beam characteristics would be necessary. However, the approximations made are sufficiently accurate to obtain order of magnitude estimates for these quantities. For $S \approx 0.4$ cm^2, we obtain [16] $\sigma_a \sim 6 \times 10^{-16}$ cm^2, $\sigma_d \sim 5 \times 10^{-17}$ cm^2, and $\sigma_b \sim 4 \times 10^{-17}$ cm^2. The Einstein A coefficient for a resonant transition is related to the resonant cross section σ by $A \approx 4\pi^2\sigma\Gamma/\lambda^2$, where λ is the resonant wavelength [15]. With $\Gamma = 0.17$ and 3.7 cm^{-1}, we have $A \sim 10^4$ s^{-1} for both resonances. We can also obtain an estimate of A for the bound-bound transition (narrow peak) by comparing the signal level obtained in this experiment with that obtained from other resonant transitions (of known strengths) observed with this apparatus [5]. If we assume

that the detaching step has the same cross section in all cases, we deduce $A \sim 10^5\ s^{-1}$ for the bound-bound transition. All known magnetic dipole transitions have A coefficients at least 100 times smaller than these [5,17] (when properly scaled for wavelength [15]), thus ruling out a same-parity transition. In fact, although the transition strength appears to be somewhat weak for a fully allowed $E1$ transition, strengths of $\sim 10^4$ or $\sim 10^5\ s^{-1}$ fall squarely within the expected range of values for a spin forbidden $E1$ transition at these wavelengths, in heavy elements such as Os [17]. This is therefore convincing evidence that the excited states have opposite parity to the ground state of Os^-. Finally, since the narrow resonance appears at lower energies than the ground state of Os, we conclude that it is bound. The requirement that these states have odd parity suggests that they may have a $5d^6 6s^2 6p$ or $5d^7 6s 6p$ configuration. Preliminary calculations by Beck [18] for the binding of a p electron to neutral Os show that $5d^6 6s^2 6p$ lies about 4000 cm^{-1} below $5d^7 6s 6p$, indicating that the excited states may be due to the attachment of a p electron to the ground state of Os. Given the approximate A coefficients obtained, and since conservation of angular momentum requires that $J = 7/2$, $9/2$, or $11/2$ for both levels, we can deduce that the only two likely terms from this configuration are ^6D and ^6F. The calculations by Beck confirm that the $5d^6 6s^2 6p$ state is mostly ^6D (≈75%) and ^6F (≈15%) in character, with the remainder being largely ^4F in character. We therefore suggest $5d^6 6s^2 6p\ ^6D^o$ as a likely designation for the new levels.

In conclusion, we have discovered two excited ionic states of odd parity in the negative ion of osmium. This makes Os^- the only known atomic negative ion with bound states of opposite parity. Also, our preliminary investigations of W^- indicate similar continuum resonances in that system. These discoveries strongly suggest that a wealth of interesting structure remains to be discovered in the transition metal negative ions.

We gratefully acknowledge the Natural Science and Engineering Research Council of Canada (NSERC) for support of this work. We thank M. Scheer for numerous insightful comments, T. Andersen, R.L. Brooks, and V. V. Petrunin for helpful discussions, and D. R. Beck for providing his preliminary results.

Note added.—The increase in the detachment signal at higher photon energies (Fig. 2) is explained by a breakdown of Eq. (1) and can be accurately described by a more detailed model. These results will be published in a separate article.

*Also with the Department of Engineering Physics, McMaster University, Ontario, Canada.

[1] S. J. Buckmann and C. W. Clark, Rev. Mod. Phys. **66**, 539 (1994); C. Blondel, Phys. Scr. **T58**, 31 (1995), and references therein.

[2] V. K. Ivanov, J. Phys. B **32**, R67 (1999).

[3] H. Hotop and W. C. Lineberger, J. Phys. Chem. Ref. Data **14**, 731 (1985); T. Andersen, H. K. Haugen, and H. Hotop, J. Phys. Chem. Ref. Data **28**, 1511 (1999).

[4] P. L. Norquist and D. R. Beck, Phys. Rev. A **61**, 014501 (2000).

[5] M. Scheer, H. K. Haugen, and D. R. Beck, Phys. Rev. Lett. **79**, 4104 (1997); M. Scheer, R. C. Bilodeau, C. A. Brodie, and H. K. Haugen, Phys. Rev. A **58**, 2844 (1998); M. Scheer, R. C. Bilodeau, and H. K. Haugen, J. Phys. B **31**, L11 (1998).

[6] Theoretical studies suggest that there may be opposite parity bound states in some lanthanides and actinides: S. H. Vosko, J. B. Lagowski, I. L. Mayer, and J. A. Chevary, Phys. Rev. A **43**, 6389 (1991); D. Datta and D. R. Beck, Phys. Rev. A **50**, 1107 (1994); K. Dinov, D. R. Beck, and D. Datta, Phys. Rev. A **50**, 1144 (1994). However, the claims have not been confirmed [A. M. Covington, D. Calabrese, J. D. Thompson, and T. J. Kvale, J. Phys. B **31**, L855 (1998)].

[7] M. Scheer, J. Thøgersen, R. C. Bilodeau, C. A. Brodie, H. K. Haugen, H. H. Andersen, P. Kristensen, and T. Andersen, Phys. Rev. Lett. **80**, 684 (1998), and references therein.

[8] M. Scheer, C. A. Brodie, R. C. Bilodeau, and H. K. Haugen, Phys. Rev. A **58**, 2051 (1998).

[9] P. J. Mohr and B. N. Taylor, J. Phys. Chem. Ref. Data (to be published).

[10] M. Scheer, R. C. Bilodeau, C. A. Brodie, and H. K. Haugen, Phys. Rev. A **58**, 2844 (1998); R. C. Bilodeau, M. Scheer, and H. K. Haugen, J. Phys. B **31**, 3885 (1998); P. L. Norquist, D. R. Beck, R. C. Bilodeau, M. Scheer, R. A. Srawley, and H. K. Haugen, Phys. Rev. A **59**, 1896 (1999).

[11] R. C. Bilodeau, M. Scheer, H. K. Haugen, and R. L. Brooks, Phys. Rev. A **61**, 012505 (2000).

[12] J. R. Peterson, Y. K. Bae, and D. L. Huestis, Phys. Rev. Lett. **55**, 692 (1985); C. W. Walter, J. A. Seifert, and J. R. Peterson, Phys. Rev. A **50**, 2257 (1994); C. A. Ramsbottom and K. L. Bell, J. Phys. B **32**, 1315 (1999).

[13] V. A. Esaulov, Ann. Phys. (Paris) **11**, 493 (1986).

[14] H. Hotop and W. C. Lineberger, J. Chem. Phys. **58**, 2379 (1973); P. Balling, C. Brink, T. Andersen, and H. K. Haugen, J. Phys. B **25**, L565 (1992).

[15] See, for example, R. Loudon, *The Quantum Theory of Light* (Oxford, New York, 1983), 2nd ed.

[16] Note that two pairs of roots for σ_a and σ_d are possible for any given pair of parameters $\sigma_{(+)}$ and $\sigma_{(-)}$. The second pair of solutions, $\sigma_a \sim 2 \times 10^{-17}\ cm^2$ and $\sigma_d \sim 2 \times 10^{-15}\ cm^2$, is rejected because $2 \times 10^{-15}\ cm^2$ is 2 or 3 orders of magnitude larger than expected for a detachment cross section in an atomic negative ion (barring strong continuum resonance enhancements) [2,13,14].

[17] A. A. Radzig and B. M. Smirnov, *Reference Data on Atoms, Molecules, and Ions* (Springer-Verlag, New York, 1985); J. R. Fuhr, G. A. Martin, and W. L. Wiese, J. Phys. Chem. Ref. Data **17**, 1 (1988).

[18] D. R. Beck (private communication).

5.2 Further Analysis of Near-threshold Photodetachment in Os^-

This section describes further analysis of the photodetachment spectrum of Os^-. While the focus of Section 5.1.2 was on determining the character of the newly observed opposite-parity states in Os^-, and the structure of the ion in general, here we will focus on modifying established continuum resonance models so as to better describe the physics of the detachment process in this ion. The main goal is to develop a model that describes the $5d^76s^2\ {}^4F^e_{9/2} \rightarrow 5d^66s^2\ {}^5D^e_4 + \epsilon p$ detachment threshold which is highly modified by the presence of a low lying state presumed to be the $5d^66s^26p\ {}^6D^o_{j_b}$ state (here after called "state j_b"). Improvements in the fit to the data are substantial, and some insight into the detachment process is gained. We shall begin with a brief background of models used to describe continuum structure in negative ions, and will apply some modifications to accommodate the present situation.

5.2.1 Background on Continuum Resonances in Negative Ions

Many continuum resonances have been studied in negative ions (for reviews see [4, 5]). Ideally, continuum resonances are placed into one of two traditional categories: *Feshbach* resonances and *shape* (or *potential*) resonances. If the attachment of an electron to an excited neutral atomic state (the *parent state*) results in an ionic state with lower energy than the parent state, the resulting negative ion state cannot autodetach into the parent state. In such a case, in addition to the removal of the excess electron, the detachment process requires that the core electrons simultaneously rearrange to conform to that of a lower-lying neutral state. The state is thus relatively stable against autodetachment. A Feshbach resonance originates from the coupling

between this excited negative ion state and the decay channel. To put it differently, a Feshbach resonance results from the interference of two (or more) channels: the *open channel*, which is the usual detachment channel in absence of the resonant state, and the *closed channel*, resulting from excitation to the metastable excited ionic state followed by autodetachment. In general the interference of these two channels results in a complicated variation, or *line shape*, of the photodetachment cross section in the vicinity of the autodetaching state. If the autodetaching state is well separated from all other structure (including thresholds) then these line shapes can be very accurately described by the *Fano profile* [6], which will be discussed below.

In contrast to a Feshbach resonance, a shape resonance results when an attractive short range potential[2] is modified by the centrifugal potential so as to produce an effective potential that has a *centrifugal barrier*, as depicted in Figure 5.8. In some cases it is possible for a quasi-bound state to exist within the resulting potential barrier. Therefore, even if the excited ionic state lies above its neutral parent state, the detaching electron may become trapped behind the barrier produced by the centrifugal potential, provided that $\ell \geq 1$. Very few near-threshold shape resonances have been measured in atomic negative ions. Aside from the resonances in Cs^- and Os^-, the most relevant for the present discussion is the shape resonance observed in (metastable) He^- by Peterson *et al.* [7,8].

In general, the detachment process cannot be described by a simple one-electron model, and interactions between the outermost electrons can play an important role in the potential that traps the excess electron in the shape-resonance

[2]A short range potential in this context is one which falls off more quickly than the centrifugal potential: $\hbar^2\ell(\ell+1)/2\mu r^2$, where ℓ is the angular momentum of the escaping electron (as usual) and μ is the reduced mass of the electron-nucleus system ($\mu \approx m_e$). The centrifugal potential arises, for a single electron system, from the reduction of the Hamiltonian for the full three-dimensional problem into the equivalent one-dimentional problem. Simply put, it is the angular kinetic energy of the electron for any particular orbital radius, while holding the angular momentum constant. Classically, $V_c = L^2/2I$, where $I = \mu r^2$ is the moment of inertia and L is the angular momentum.

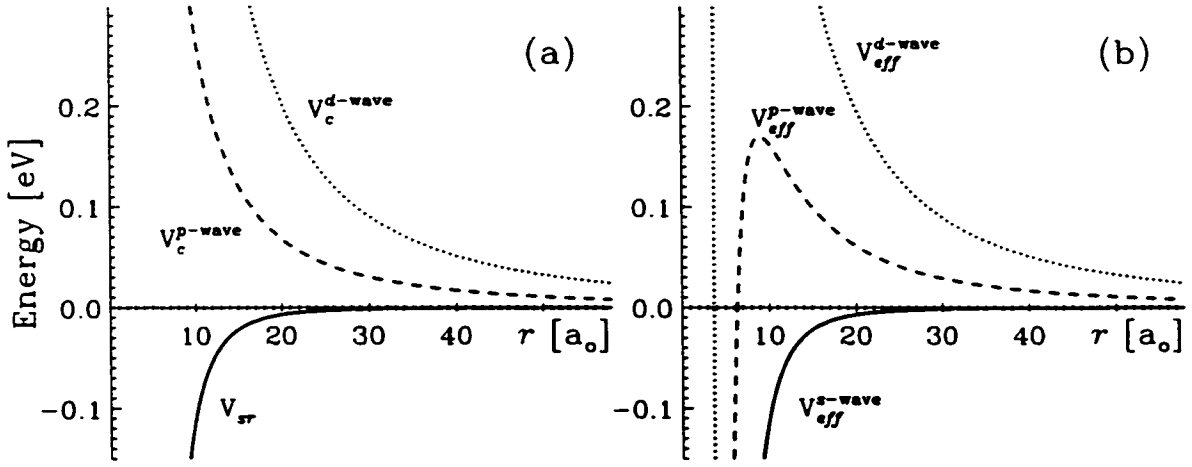

Figure 5.8: A centrifugal barrier is formed from the combination of a short-range potential and the centrifugal potential. (a) Potentials of interest are the model short-range binding potential $V_{sr} = -\alpha/2r^4$ (in a.u.; $\alpha = 80$ in figure) and the centrifugal potential for a p- and d-wave, $V_c = \ell(\ell+1)/2r^2$ (in a.u.). (b) $V_c \equiv 0$ for s-waves and there is no possibility of forming a barrier. However, for larger angular momentum the effective potential $V_{eff} = V_{sr} + V_c$ develops a barrier, through which the electron must tunnel. This barrier is responsible for the shape of the detachment threshold (see Chapter 2) and may support a quasi-bound state — a shape resonance.

scenario. Likewise, the centrifugal potential can also play an important role in a Feshbach resonance. As a result, it is sometimes difficult to exactly categorize the nature of the resonance.[3] The resonances discussed in this Chapter are the result of the attachment of a p-orbital electron to the parent state of the neutral, and therefore would give rise to shape resonances within the single-electron approximation. However, given that the negative ions of interest here (Cs^-, Os^-, and W^-) are all very heavy systems with one or two partly filled shells, it is rather unlikely that the resonances arise from a simple one-electron process. Therefore, although we shall continue to use this traditional language, we do so with the understanding that it is not immediately obvious which picture best describes their true nature.

[3]Buckmann and Clark [4] warn of the difficulty of ascribing a "shape" or "Feshbach" character for negative ion resonances (see also [9]). One example where such a characterization is misleading is Si^- (see for example [10,11]).

Modifying the Fano Profile

Typically, a Fano profile can be used to accurately describe a Feshbach resonance [6]:

$$\sigma_{Fano} = \sigma_1 F(h\nu), \tag{5.1}$$

where σ_1 corresponds to the oscillator strength expected for a transition into the continuum of the open channel if no resonance was present, and $F(h\nu)$ is the Beutler-Fano function:

$$F(h\nu) = \frac{(q+e)^2}{1+e^2}, \tag{5.2}$$

where, $e = 2(h\nu - \varepsilon_r)/\Gamma$ is the *reduced energy*, with ε_r and Γ the resonance energy and width (FWHM) respectively, and q is the *shape parameter* which depends on the ratio of the dipole transition matrix element of the "dressed" excited state (closed channel) to the dipole matrix element for the transition directly into the continuum (open channel). In particular, we can write:

$$\sigma_1 = \frac{2\mu}{\hbar^2} d_1^2 h\nu, \tag{5.3a}$$

$$q = \frac{d_2}{d_1 \pi \gamma}, \tag{5.3b}$$

$$\Gamma = 2\pi|\gamma|^2, \tag{5.3c}$$

$$\varepsilon_r = E_r + \Delta E_r. \tag{5.3d}$$

Here, $d_1^2 \propto (h\nu - \varepsilon_t)^{\ell+1/2}$, with ℓ the angular momentum of the detached electron and ε_t the threshold energy; d_2 is dependent on the specifics of the (coupled) excited ionic state wave function, and does not vary significantly for energies near to E_r, the energy of the excited ionic state in the absence of channel coupling; $\Delta E_r = \langle \phi_0 | V_{21} G V_{12} | \phi_0 \rangle$ depends on the specifics of the radial wave function of the (bound) excited ionic state $|\phi_0\rangle$ in the absence of channel coupling, the Green's function G for the channel coupling problem, and the coupling potential matrix elements $V_{12} = V_{21}$; and finally,

$\gamma = \langle \phi_{reg} | V_{12} | \phi_0 \rangle$, where $|\phi_{reg}\rangle$ is the regular solution of the open channel radial wave function.[4]

Although all the parameters, σ_1, ε_r, and Γ are strictly speaking energy dependent,[5] if the resonance is observed far from the detachment threshold (as is usually the case) then the energy dependence is overwhelmingly dominated by the Beutler-Fano function (Equation 5.2) and the very weakly energy-dependent q, A, and Γ can be taken as constant parameters. However, for the resonance studied here, the excited ionic state lies so close to the decay channel opening (< 30 cm^{-1}) that the energy dependence of these parameters may be significant.

The energy dependence of Γ and q can be taken into account through [12]:

$$\Gamma = \frac{(h\nu - \varepsilon_t)^{3/2}\gamma_1}{1 + (h\nu - \varepsilon_t)\gamma_2}, \tag{5.4a}$$

$$q = 2q_o/\Gamma, \tag{5.4b}$$

where γ_1, γ_2, and q_o are constants, and ε_t is the threshold energy. It was found that the additional energy dependence of Γ and q does not change the fits by any observable amount for the present cases. We will therefore proceed with the assumption that Γ and q are constant. However, the energy dependence of σ_1 is found to have a significant impact on the fits and cannot be ignored. We therefore set $\sigma_1 = A_1 W(h\nu)$, where A_1 is a constant and,

$$W(h\nu) = (h\nu - \varepsilon_t)^{3/2} \tag{5.5}$$

is the Wigner threshold law for detachment into a p-wave continuum, with a threshold

[4]This includes modifications to the outgoing wave functions due to the short-range potential, in which the electron is initially bound, as well as due to the centrifugal potential.

[5]It may be disturbing to think of the resonance position and width as energy dependent. There should after all be only one position and width of a state. However, ε_r and Γ are really only parameters which, under the Fano formulation, approximate what we understand as the "true" position and width of the resonance.

energy ε_t. With this notation, Equation 5.1 becomes:

$$\sigma_{f_1} = A_1 W(h\nu) F(h\nu). \tag{5.6}$$

Near-threshold Shape Resonance Model in He^-

A shape resonance resulting from the $1s2p2p'\ ^4P^e$ state has been observed just above the $1s2s2p\ ^4P^o \rightarrow 1s2p\ ^3P^o$ threshold in He^- by Peterson *et al.* [7,8]. In that study, the Wigner law was found to be inadequate even very near to the detachment threshold. Based on scattering theory, and assuming photon energies near the threshold *and* near the resonance ($\varepsilon_t \approx h\nu \approx \varepsilon_r$), Peterson *et al.* developed a model for the shape resonance in He^-, and later also applied it to the Ca^- spectrum [13]. The model function, which is essentially the product of the Wigner p-wave law and the Breit-Wigner resonance formula, was found to have excellent agreement with the observed He^- spectrum [7,8,14,15]. The model also appears to describe the resonance in Os^- very well (see Section 5.1.2), but only for a limited range near the threshold. Defining a Lorentzian profile as,

$$L(h\nu) = \frac{1}{(h\nu - \varepsilon_r)^2 + (\Gamma/2)^2}, \tag{5.7}$$

their result becomes simply:

$$\sigma_{f_2} = A_1 W(h\nu) L(h\nu). \tag{5.8}$$

The reader should note that sufficiently close to the threshold, $\sigma_{f_2} \sim \sigma_{f_1} \sim A_1 W(h\nu)$, and we recover the Wigner law as required. Furthermore, the energy dependence of q (e.g. Equation 5.4b) is such that q is expected to increase as $h\nu$ approaches ε_t (i.e. near the threshold). In fact, near the threshold $q \gg e$ and so $L(h\nu)$ approximates $F(h\nu)$, in which case Equation 5.6 reduces to Equation 5.8. In this sense Equation 5.8 is simply a specific case of Equation 5.6. One significant

difference between these two formulations is the energy dependence at large photon energies ($h\nu \to \infty$): $\sigma_{f_2} \to 0$ while $\sigma_{f_1} \to A_1 W(h\nu)$. Although the validity of both models is questionable in this region, it seems reasonable to expect the Wigner law to be valid at photon energies sufficiently far from the resonance,[6] ignoring the effects of the correction terms which have not been included in the models.

5.2.2 Near-threshold resonance in Os^-

The models described above have been fit to the experimental data covering the Os^- resonance and threshold region discussed in Section 5.1.2. The data and fits are shown in Figure 5.9. Unfortunately, neither Equation 5.6 nor Equation 5.8 fits the data at photon energies greater than ≈ 8750 cm^{-1}. It is found that an additional p-wave Wigner law is required to obtain a satisfactory fit to the data over the entire range. That is to say, Equation 5.6 and Equation 5.8 become respectively:

$$\sigma_{f_3} = W(\varepsilon)\,(A_1 F(\varepsilon) + A_2) \tag{5.9}$$

and

$$\sigma_{f_4} = W(\varepsilon)\,(A_1 L(\varepsilon) + A_2)\,. \tag{5.10}$$

It is evident from Figure 5.9 that both of these functions fit the data very well, although Equation 5.9 appears to describe the region near 8800 cm^{-1} slightly better.

The best fit parameters returned for Equation 5.9 and Equation 5.10 are presented in Table 5.1. Of particular interest is the significant difference between the values for the threshold position, while the values for the resonance position are essentially identical. Notice that the value returned by Equation 5.9 for the threshold

[6]This is also the case in near-threshold Coulomb-barrier resonances in negative ions (see for example, Paper 13 listed in the Preface). A Coulomb barrier is formed in exactly the same way as a centrifugal barrier, with a Coulomb repulsion potential taking the place of, or acting in addition to, the centrifugal potential.

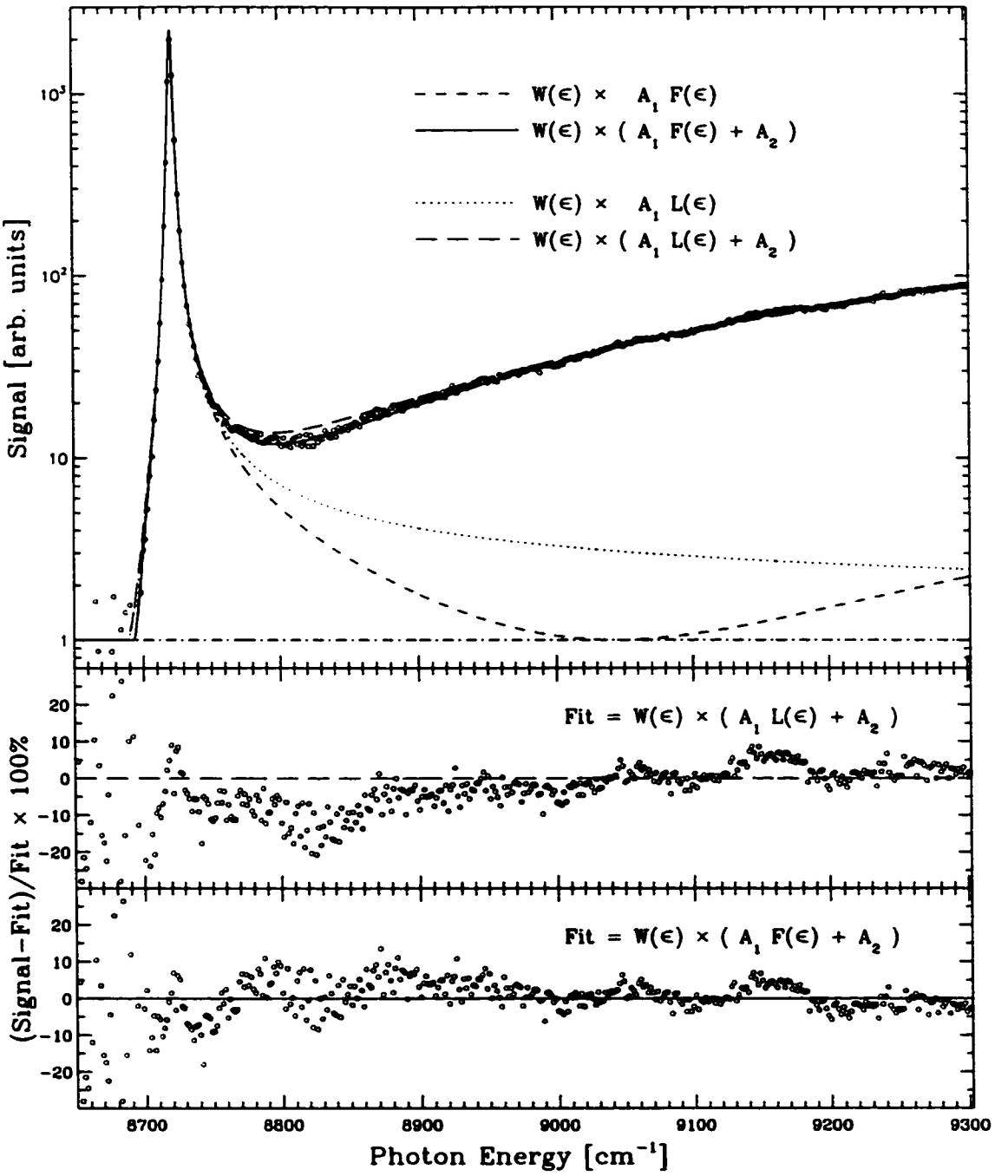

Figure 5.9: Top panel: Circles are the observed photodetachment signal for Os^-. The curves are labelled in the legend, see text for details. Long-short dashed line indicates the background signal (normalized to 1). Middle and bottom panels: Percent deviation of the signal from σ_{f_4} and σ_{f_3} respectively.

Table 5.1: Values of parameters obtained from best-fit curves of σ_{f_4} and σ_{f_3} to the Os^- detachment threshold.

Parameter	Values obtained from fit using[a]	
	Equation 5.9	Equation 5.10
ε_0 [cm^{-1}]	8693.1(2)	8688.3(3)
ε_r [cm^{-1}]	8721.64(1)	8721.65(1)
Γ [cm^{-1}]	3.42(2)	3.32(2)
q [unitless]	−188(4)	N/A
A_1 [arb. units]	0.00041(4)[b]	32.1(4)[b]
A_2 [arb. units]	0.00593(2)	0.00559(2)

[a]Uncertainties are statistical only (1 standard deviation).

[b]Since $F(\varepsilon)$ and $L(\varepsilon)$ have different normalization, the values for A_1 are not directly comparable.

position is consistent with that reported in Section 5.1.2: $\varepsilon_0 = 8693(1)$ cm^{-1}. In that paper, the threshold value and resonance parameters were obtained by using two much higher resolution scans, one covering a region only very close to the threshold and the other covering a narrow region around the resonance. Since those data cover only a small energy range very near to the threshold, the extensions to the detachment model developed here are insignificant, and we would therefore expect those results to be correct. The general better agreement of Equation 5.9 is an indication that the model based on the modification of a Fano profile is the most appropriate to describe the spectrum. This conclusion is reinforced by the small, but significant, improvement in the fit as can be seen by the plots of the residuals in Figure 5.9.

The origin of the "extra" p-wave, with amplitude A_2, can be simply understood by recognizing that the resonant transition is spin forbidden. The L-S term composition for the $5d^6 6s^2 6p$ configuration (state j_b) has been determined theoretically [17] to be largely ^6D in character, and $< 10\%$ ^4F. This metastable state will therefore decay mainly in the $5d^6 6s^2\ ^5D^e + \varepsilon p$ sextet continuum, with a small portion

exiting in $5d^6 6s^2\ ^5D^e + \varepsilon p$ quartet continuum. In the absence of state j_b, however, the detachment process would proceed exclusively via an electric dipole transition into the quartet continuum. There are therefore two important final continuum states that must be considered for the atom + electron system, which give rise to the two terms in the fitting functions. The cross section into each of these two final states is modified to a different extent by the presence of state j_b. The large resonance structure that dominates the spectrum at energies near the detachment threshold is the result of detachment into the sextet continuum, while the detachment cross section at higher energies is dominated by detachment into the quartet continuum. Since the latter experiences much less modification from the excited state, it is approximated well by a Wigner p-wave threshold law (second term in Equations 5.9 and 5.10). Finally, notice that asymptotically, the two terms of Equation 5.9 have the same shape. It is therefore possible to obtain a ratio of the asymptotic channel strengths from this fit of $A_1/A_2 = 6.9(6)\%$. This indicates that the (spin-allowed) electric-dipole transition into the continuum carries the bulk of the cross section at energies sufficiently far from the resonant state, as one would expect.

In summary, the significant qualitative difference between the spectrum observed in the photodetachment of Os^- and that observed in He^- [7,8] is the rise in cross section immediately following the resonance feature. This rise appears to be due to the fact that a spin-forbidden transition is being driven in the case of Os^-, and therefore two final states of the atom + detached electron system are important.[7] A very similar situation was observed for the $6s6p\ ^3P^o_1$ state which lies 8 meV above the $6s^2\ ^1S^e_0 \rightarrow 6s\ ^2S^e_{1/2} + \varepsilon p$ threshold in the photodetachment spectrum of Cs^- (see Sec-

[7]In the case of He, where state mixing should be minimal, no "background" p-wave is expected. Of course the signal would be expected to eventually rise again at higher photon energies with Equation 5.6. For Ca^- [13], the range scanned is not sufficient to determine which model might yield better agreement.

tion 5.1.1). That case also involves a spin-forbidden electric dipole transition to the excited negative ion state. For Cs^- the continuum resonance is sufficiently far from the threshold, and the relative cross section to the singlet continuum is sufficiently strong, that the spectrum was well characterized simply by a p-wave background + a Lorentzian. Of course, Equations 5.9 and 5.10 would also produce excellent fits. Therefore the Cs^- spectrum can also be divided into signal originating from a singlet continuum and from a triplet continuum, the latter of which is strongly modified by the presence of the $^3P_1^o$ resonance. Therefore the Cs^- case reinforces the validity of the fitting model developed here, namely the introduction of an additional, non-mixing, p-wave "background".

5.3 Continuum Structure in the Photodetachment of W^-

An energy level diagram showing the ground state of W^- and the lower states of W is presented in Figure 5.10. The electron affinity of tungsten has been previously measured to be 6581(64) cm^{-1} [0.816(8) eV] using LPES [16]. Only the ground state of W^- is expected to be bound, and no previous experimental or theoretical investigations of excited states of this ion have been conducted. The ground state threshold ($5d^5 6s^2\ ^6S_{5/2} \rightarrow 5d^4 6s^2\ ^5D_0$) involves the detachment of a d-orbital electron into a p-wave continuum, and therefore very low cross sections are expected.

Figure 5.11 presents the results of 10 scans which cover a combined range of over 3000 cm^{-1}, beginning near the energy where the ground state detachment threshold is expected. Each individual scan covers a range of 200 to 600 cm^{-1}, with a 50 to 150 cm^{-1} overlap between the scans. The data have been corrected for variations in laser pulse energy and ion current as well as for signal saturation, which will be

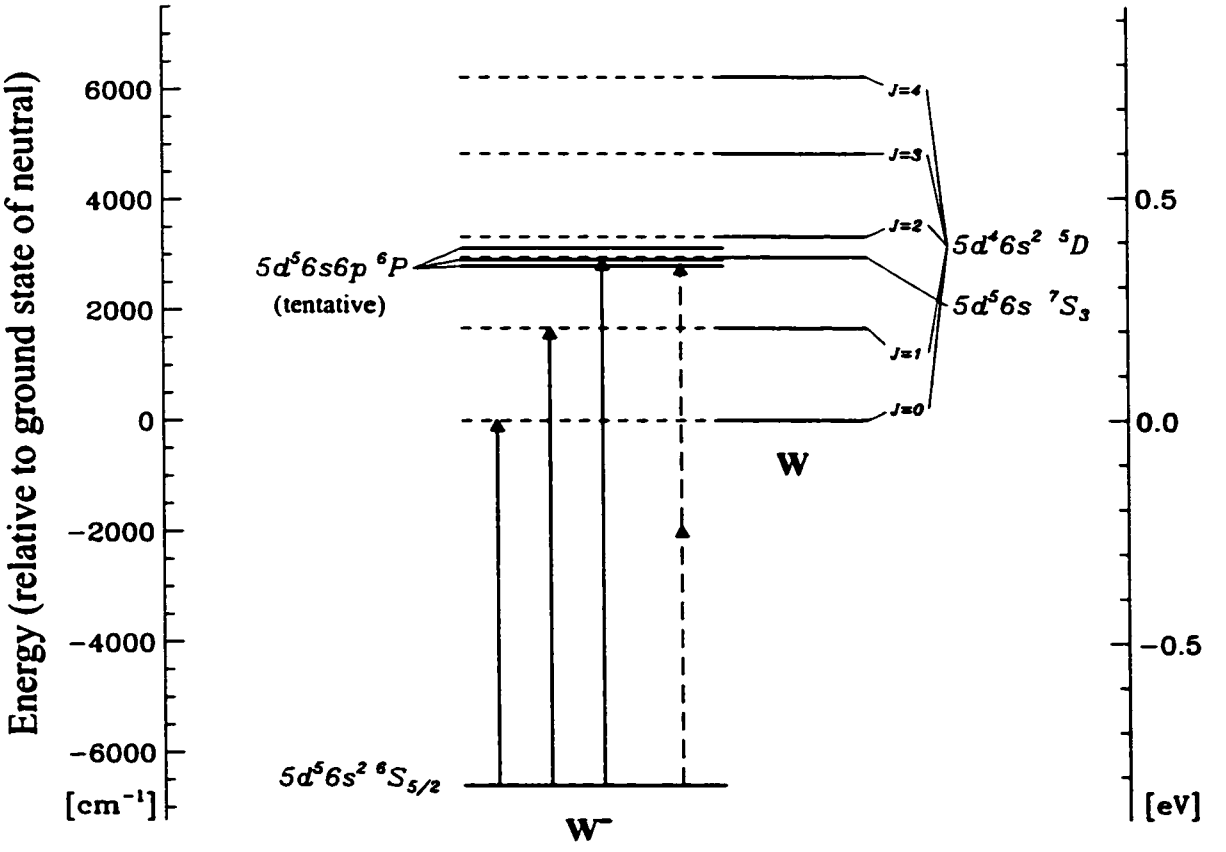

Figure 5.10: Energy level diagram for W^- and low lying states of neutral W. The solid arrows indicate the first three photodetachment thresholds, which lie within the energy range studied in this work. The dashed line shows an attempted two-photon photon detachment experiment.

discussed in more detail in Section 5.3.2.

A total of nearly 40 hours of actual data collection was performed over the period of three days to accumulate the data. Over such a long period of time, variations in the ion current and overlap between the ion beam and laser beam are unavoidable. Although the ion current was monitored, maintaining stable overlap between the ion beam and the laser beam over this period of time is challenging. The situation is further complicated by the fact that a variety of laser dyes was used (a total of 7 different dyes and dye mixtures). Since each dye may have a slightly different index

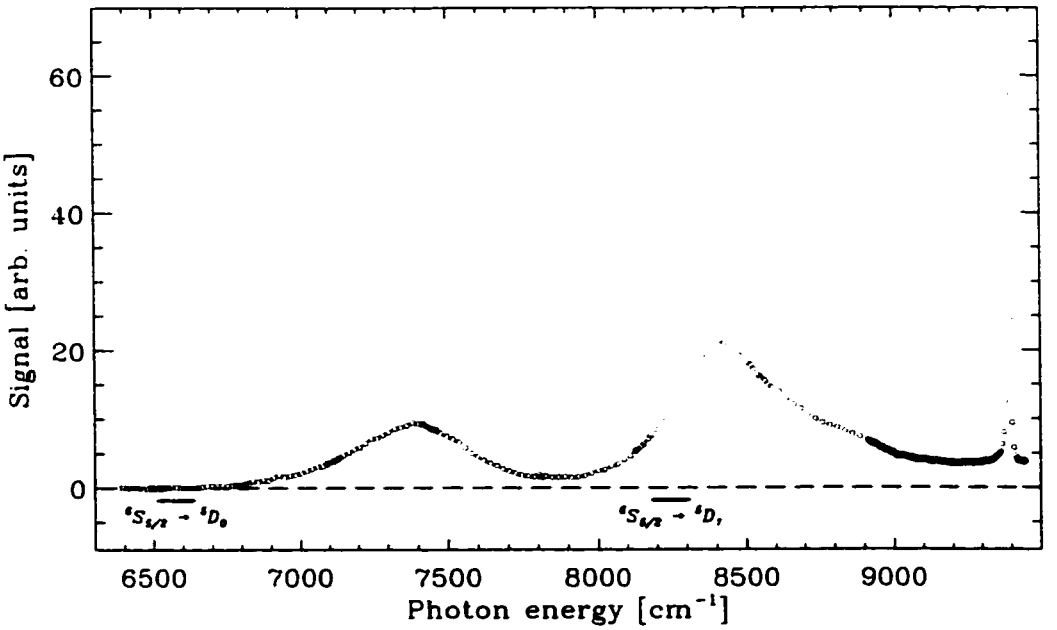

Figure 5.11: Photodetachment of W^- covering approximately 4600 cm^{-1}. Regions in which a detachment channel opening is expected has been indicated by a horizontal bar with a length corresponding to one standard deviation uncertainty, based on EA measurement by Feigerle *et al.* [16] and the known fine-strucure splittings of the neutral states of W.

of refraction, there may have been slight changes in the laser beam path and spatial profile. Also, small amounts of ASE present in the dye laser beam may vary slightly over this very large scan range (see Section 3.3.4). All of these effects can have a small effect on the observed signal. Given the significant complications of collecting data over such a large range of photon energies and over such a long time period, the relative scale of the signal could have easily varied by 30% over the course of the scans. Finally, since the scans were not repeated, it is not easy to identify artifacts in the signal produced by small ion-current fluctuations. Nonetheless, there are large structures visible in the acquired spectrum which cannot be explained as such artifacts.

While it is not possible to conclude with certainty that the observed structure

is not due to a near-mass coincident impurity ion, the fact the signal appears to decrease to zero where the ground state threshold is expected supports the assumption that the spectrum is primarily due to W^- photodetachment (see also comments in Appendix B and Section 3.2.1). Structures of this kind are common in transition metals (see for example [18–20]) and are often associated with shape resonances. This is a likely interpretation[8] of the two broad features centred at approximately 7400 and 8400 cm^{-1} (hereafter referred to as features 1 and 2 respectively). The ionic $5d^46s^26p$ configuration would be the most likely candidate for these features. It is unclear whether the small shoulder at the high photon energy side of the second feature is real or an artifact. A more careful investigation than these preliminary scans is required to extract more quantitative information. On the other hand, the third feature observed near 9400 cm^{-1}, is far too narrow to be a shape resonance located at such a high energy relative to the detachment thresholds, and is likely due to a Feshbach resonance. This feature is more clearly seen in Figure 5.12, labelled as peak A and is discussed in detail in the following section.

5.3.1 Photodetachment Near the $5d^56s^2\ ^6S_{5/2} \rightarrow 5d^56s\ ^7S_3$ Threshold in W^-

Figure 5.12 is the sum of three scans each covering the full range presented, and should therefore be more reliable than the data of Figure 5.11. Furthermore, this spectrum was found to be consistent throughout the lifetime of the sputter cathode. If some of the structure was due to impurity ions it is very likely that variations in the spectrum would be observed, as the ion current derived from a molecular impurity typically

[8] In fact, the first structure lies very close to the peak of the centrifugal barrier. Such correspondence between the barrier height and shape resonances have been previously observed, see [4]. However, another possible description for the structure is simply the interplay of the various partial waves and threshold breakdown due to wave function overlap, which is the spirit of the ZCC calculations of [19].

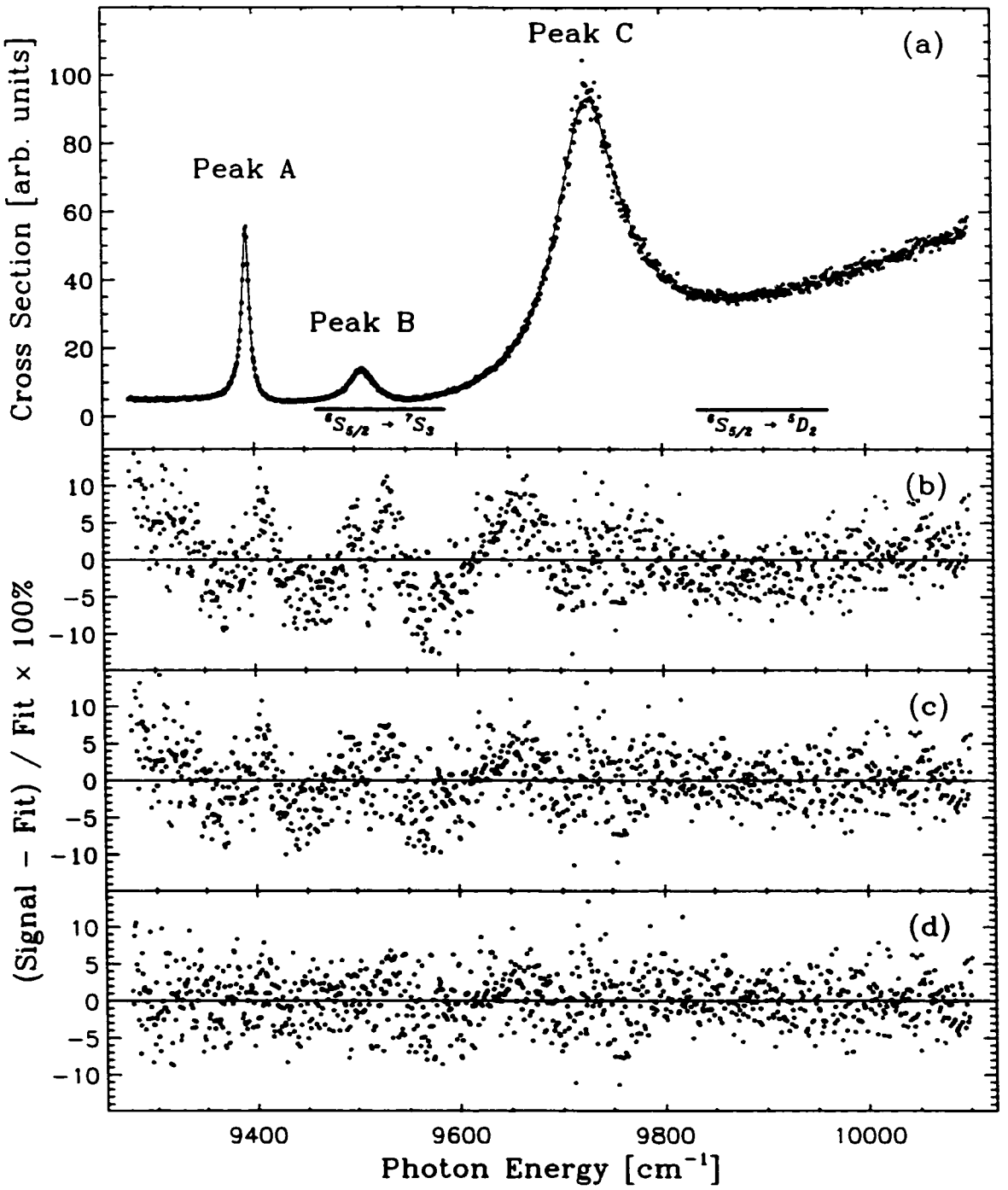

Figure 5.12: Relative cross section for photodetachment of W^- near the $5d^56s^2\ {}^6S_{5/2} \rightarrow 5d^56s\ {}^7S_3$ detachment threshold. Horizontal bars indicate energy ranges in which a threshold is expected. Panels labelled (b), (c), and (d) show percent deviations of the data from three different fitting methods, see text for details.

varies significantly (relative to the W^- current) during the lifetime of the cathode. On the other hand, due to the unexpectedly large photodetachment cross sections observed, significant signal saturation is present in this data. This saturation can be accurately modelled with Equation 3.1. This will be discussed further in Section 5.3.2. The data of Figures 5.11 and 5.12 have been corrected for the effect of saturation and observed variations in pulse energy.

Three resonances appear in the range scanned in Figure 5.12. Based on the isoelectronic Re and on the fact that the resonances are relatively narrow, and therefore cannot be due to daughter states of the W $5d^46s^2$ ground state configuration, the simplest assignment for these resonances would be the $5d^56s6p$ configuration. This assignment is also consistent with the observation that peak C is nearly a factor of 10 wider than peak A (see below). Since peak C is situated well above the $5d^56s\ ^7S_3$ parent state, it's lifetime should be reduced considerably. Peak C is therefore best described as a shape resonance, while A and B are likely Feshbach resonances, although it is unclear whether peak B is just below or just above the ^7S threshold. With this interpretation in mind the data of Figure 5.12 can be analysed further.

Due to the relatively small separation of the resonances, it was found that all the structures must be fit simultaneously.[9] In particular, two Fano profiles (Equation 5.1) were used, one for peak A and one for peak B. Each of these Fano profiles contain 4 fitting parameters: the resonance energy ϵ_r, FWHM Γ, amplitude, and asymmetry parameter q. In order to model peak C and the threshold Equation 5.10 or Equation 5.9 were added to this, which we shall refer to as fit Method 1 and 2 respectively. Finally, notice that the $^5D_2$ threshold is also expected to lie in this region. However it should be very weak (about an order of magnitude weaker than

[9]This is not to imply that we are treating them as interacting resonances. The resonances are separated well enough so that interference between the resonances should be minimal. A description of interference of resonances can be found in [6], especially section 3.2.2.

Table 5.2: Values of parameters obtained from best-fit curves near the ^7S detachment threshold in W^-. The fitting methods are described in the text.

Parameter	Values obtained from fit using:[a]		
	Method 1	Method 2	Method 3
ε_t	9512(10)	9535(10)	9520(12)
ε_{r_A}	9393.40(20)	9393.18(20)	9392.95(20)
Γ_A	9.3(3)	8.8(3)	8.9(3)
q_A	−15(4)	−16(4)	−21(5)
ε_{r_B}	9509.3(8)	9508.7(8)	9509.0(8)
Γ_B	27.3(15)	27.4(15)	30.6(20)
q_B	<-5	<-10	<-10
ε_{r_C}	9723.7(10)	9725.2(10)	9725.5(10)
Γ_C	73(5)	76(5)	76(5)
q_C	N/A	−25(6)	−28(6)

[a]All values are in cm^{-1}, except for q values which are dimensionless. Uncertainties do not include laser calibration error.

the ^7S threshold) and for the sake of keeping the number of fitting parameters to a minimum, this detachment channel has been ignored. Therefore, including a constant background, a total of 14 (Method 1) or 15 (Method 2) fitting parameters are required to be simultaneously fit. Although this seems like a large number of parameters, the energy region over which each parameter has an effect is highly restricted. Nonetheless, many local minima exist and care must be taken to sample the entire parameter space to ensure convergence to the best set of parameters.

Table 5.2 gives the best-fit results obtained. (For brevity the amplitudes and background parameters have been omitted from the table.) In addition, results obtained from a third fitting method (Method 3) are included. Method 3 is the same as Method 2, but includes a sloped linear background. A small negative slope is returned as expected, considering the decreasing signal observed at lower photon energies (see Figure 5.11). The residuals for Methods 1, 2, and 3 are plotted in panels

(b), (c), and (d) respectively of Figure 5.12 (the solid curve of panel (a) is Method 3). There appears to be an improvement in the fit when the generalized Fano profile is used (Method 2 versus Method 1). The addition of a linear slope (Method 3) also appears to improve the fit; a similar improvement is observed if a linear slope is included for Method 1. The values returned are consistent regardless of the fitting method, with the exception of the threshold energy which is lower if Equation 5.10 is used. This is not surprising since the threshold was also found to be lower by a similar amount for Os^- in Section 5.2. With the known excitation energy of the ^7S state, 2951.29 cm^{-1}, a threshold energy of 9533(64) cm^{-1} can be deduced. Unfortunately, this is not accurate enough to distinguish between the two fit methods.

For completeness another model was considered: an *unmodified* p-wave threshold was used with peak C fit to a Fano profile. This corresponds to the interpretation where peak C is a Feshbach resonance, which could not be explained with the configuration assignment above. An excellent fit, comparable to Method 2 (or 3 if a sloped background is included), is also obtained with this model and yields parameter values equivalent to Method 2, with two notable exceptions: a value of 10 to 20 cm^{-1} larger is returned for the threshold energy, and a positive value for the q parameter of peak C is required. However, since we can only realistically excite an s- or d-orbital electron to a p-orbital in a dipole transition,[10] it does not appear to be possible to assign a state that would be long-lived with respect to both the $5d^56s$ and $5d^46s^2$ configurations. Therefore, this approach does not appear to be physically valid.

As a final note, we recall that a number of refinements could be made to improve the models used here. For example, the $^6S_{5/2} \rightarrow {}^5D_2$ threshold has been ignored and no threshold law correction terms have been included. Both of these

[10]Excitation of a d-orbital electron into an f-orbital is of course possible, but would require much higher photon energies.

corrections are small and of the same order. It is unlikely that the addition of these refinements will affect the fits to any significant degree.

5.3.2 Saturation Curves, Photodetachment Cross Sections, and Transition Strengths

As discussed in Appendix C and illustrated in Section 5.1.2 for the case of Os^-, detachment cross sections can be estimated by observing the saturation of the detachment signal. In particular, from Equation 3.1 (also Equation C.4) we have that the observed signal N is given by:

$$N = N_o(1 - e^{-\sigma P}), \tag{5.11}$$

where, σ is the detachment cross section, and P is the number of photons per unit area from the laser beam. N_o corresponds to the signal observed when all ions are detached and is proportional to the number of ions in the interaction region.

Figure 5.13 presents the data acquired at the maximum of peak C and at a high photon energy. Unfortunately, high damage-threshold polarisers for this wavelength region were not readily available and so the variation of pulse-energies was instead accomplished by changing the pumping power applied to the dye laser. To ensure that the spatial and temporal characteristics of the laser pulses did not vary appreciably, it was possible to obtain data for only a relatively small range of pulse-energies. Nonetheless, this range is sufficient for the present purposes.

The values of N_o returned for both sets are consistent within the uncertainty of the fits (8%), which supports that the signal is derived from the same initial state. The cross section returned from the fit to the signal obtained at peak C is $\sim 3 \times 10^{-17}$ cm^2, similar to that found for the shape resonance in Os. On the other hand, the cross section returned for the fit to the higher photon-energy data ($\approx$600 cm^{-1} above the

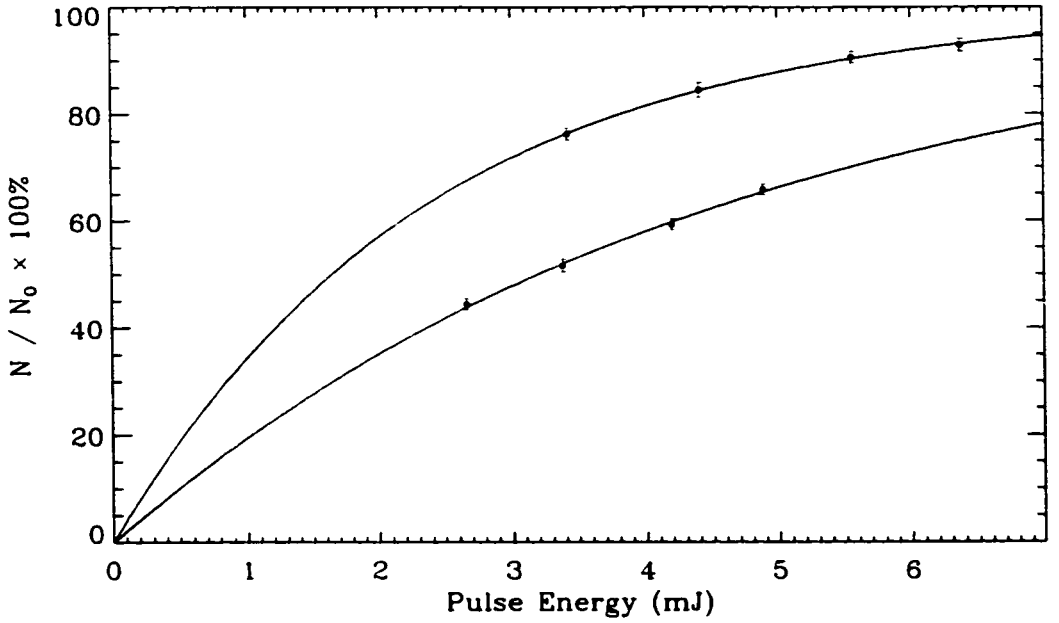

Figure 5.13: Measured signal versus pulse energy for the detachment of W^- at two photon energies: 9725.7 cm^{-1} (upper curve) and 10128.3 cm^{-1} (lower curve). Error bars are three standard deviations based on the observed scatter in the signal obtained from 1000 pulses per data point.

$5d^56s^2\ {}^6S_{5/2} \rightarrow 5d^56s\ {}^7S_3$ threshold) is found to be $\sim 1.7 \times 10^{-17}$ cm^2, which is approximately 20 times larger than that found at the same energy above threshold in Os^-. This is precisely as expected, since in Os^- a *d*-orbital electron was removed while an *s*-obital electron is removed in detaching to the $5d^56s\ {}^7S_3$ state of W. From these cross sections, and using $A \approx 4\pi^2\Gamma/\lambda^2$, we can obtain an order of magnitude estimate of $\sim 3 \times 10^5$ s^{-1} for the Einstein A coefficient of the transition corresponding to peak C. This is considerably larger than for the shape resonance in Os^-, and lies on the border of what is expected for a spin-forbidden and a fully allowed E1 transition at these wavelengths.

We now have enough information to rule out some term assignments. If we assume that the $5d^56s\ {}^7S_3$ W state is the parent state, then only the ${}^8P$ or ${}^6P$ terms are possible. In Re, these also happen to be the lowest-lying terms belonging to

the $5d^56s6p$ configuration. If all three resonances are to be explained by the same term, the octet character can be eliminated since only the $^8P_{5/2,7/2}$ states would be accessible on the basis of the $\Delta J = 0, \pm 1$ selection rule: for a $J = 5/2$ initial state (see Figure 5.10), the excited W^- states must have $J = 3/2$, $5/2$, or $7/2$. On the other hand, the $5d^56s6p$ $^6P_{3/2,5/2,7/2}$ states would be fully allowed E1 transitions, and larger cross sections for peak A and B might be expected. Since the excited W^- states likely have a large amount of term mixing, this may still be reasonable. Of course a number of other terms are possible for the $5d^56s6p$ configuration, stemming from different parent terms. Again using the Re isoelectronic sequence as a guide, we find other possibilities include another ^6P term, stemming from the $5d^56s6p$ ^5S parent state, and $^{4,6}D$ terms, stemming from the $5d^56s6p$ ^5P parent state.[11] The reader should further note that all of these states have small fine-structure splittings, on the order of what is observed for the resonances in W^-. In light of all of these possibilities, a theoretical investigation of p-electron attachment in W would be very helpful.

5.4 Final Remarks and Comparison of Shape Resonances

Section 5.1 presented experimental studies of two negative ion systems directed at exploring the possibility of bound-bound electric dipole transitions in atomic negative ions; that is, whether the negative ion binding potential was capable of supporting bound states of opposite parity. Although Cs^- was expected to be a good candidate for such a system, the state was found to be slightly unbound. However, an opposite parity bound state was found to exist in Os^-, finally bring a close to this long standing

[11] A number of other terms from this configurations are present in Re, but have been ruled out on the basis of the ΔJ selection rule. In addition, many other terms are possible, only the observed terms in the Re isoelectronic sequence have been considered.

question.

In both Os^- and Cs^-, the states of interest were formed by p-electron attachment to the ground state of the neutral. The evidence put forth in Section 5.3 indicates that the resonances observed in W^- also result from p-attachment to low-lying states of W. The current work is the first to systematically target these heavy sixth-row elements, and the interesting, and unexpected, structure found in these experiments is an indication that the transition metal negative ions may be good target systems for future work on near-threshold resonant transitions.

Table 5.3 summarises the results of the shape resonances studied in this chapter (the Feshbach resonances observed in W^- and bound-bound transition observed in Os^- are not included). For comparison, the similar near-threshold shape resonances observed in He^- [7,8] and Ca^- [13] by Petersen and co-workers are also included. In addition, estimates of the expected widths of the shape resonances are included. These estimated widths have been calculate on basis of a simple semi-classical model, which is described presently.

In Section 5.2.1 a shape resonance was described as a result of the photoelectron becoming trapped behind a centrifugal barrier (see in particular, Figure 5.8). It is instructive to develop a simple semi-classical model that describes this process.[12] The effective potential acting on the photoelectron has the form $V_{eff} = V_c + V_{sr}$. Expressed in atomic units,[13] the centrifugal potential is simply $V_c = \ell(\ell+1)/2r^2$ and the short-range binding potential is $V_{sr} = -\alpha/2r^4$. We then have (in a.u.):

$$V_{eff} = \frac{\ell(\ell+1)}{2r^2} - \frac{\alpha}{2r^4}. \tag{5.12}$$

Our objective is to estimate the width of a quasi-bound resonance at an energy

[12]The concerns raised in Section 5.2.1 with regards to the large state-mixing in these resonances notwithstanding.

[13]The atomic unit of energy is the Hartree which is about 27 eV, see Appendix A.

Table 5.3: Summary of observed near-threshold shape resonances discussed in this chapter. The resonances observed in He [7,8] and Ca [13] are included for comparison. Predicted widths are based on the semi-classical model discussed in the text.

Parent Atom		Observed		Predicted	
State	α [a_o^3]	$\varepsilon_r - \varepsilon_t$ [meV]	Γ_{exp} [meV]	Γ_{pred} [meV]	$\Gamma_{pred}/\Gamma_{exp}$
He $1s2p\ ^3P$	46.708[a]	10.80(7)	7.16(7)	6.5	0.9
Ca $4s4p\ ^1P_1$	-200[b]	16.3	34.6	74	2.1
Cs $6s\ ^2S_{1/2}$	399.9(19)[c]	8.0(3)	5.0(5)	21	4.1
W $5d^56s\ ^7S_5$	~ 70[b]	25(3)	9.4(6)	32	3.4
W $5d^46s^2\ ^5D_0$	70[d]	100	55	240	4.4
Os $5d^66s^2\ ^5D_4$	50[d]	3.52(12)	0.438(15)	1.3	3.0

[a]The polarisability of this state has been calculated to an accuracy of 9 digits [21].
[b]The polarisabilities of these excited states are not known. The ground state is used as an order of magnitude estimate here [22].
[c]From reference [23].
[d]Uncertainties of 50% are estimated for these values [22].

ε_r, lying below the peak of the barrier, $V_{max} = \ell^2(\ell+1)^2/8\alpha$. In the semi-classical picture, the electron oscillates between $r = 0$ and the classical turning point $r = r_1$. For each collision with the barrier, there is a chance that the electron will tunnel through the barrier, with a probability P. After the first collision, the probability that the electron remains trapped behind the barrier is then $R_1 = 1 - P$. After n such collisions the probability is reduced to $R_n = (1-P)^n$. The lifetime of a state can be defined as the time when $R_n = e^{-1}$ (i.e. a decay probability of about 64%), which corresponds to $n = -1/\ln(1-P)$ collisions. For an electron with velocity v, the collisions occur with a period of $\tau_{hit} = 2r_1/v$, and the lifetime of the state will then be $\tau = n\,\tau_{hit} = 2n\,r_1/v$. Since the width of the state is $\Gamma \approx \hbar/\tau$ we can predict the width of the resonance with,

$$\Gamma_{pred} \approx -\frac{\hbar v \ln(1-P)}{2r_1}. \tag{5.13}$$

The two parameters, P and v must be estimated. The tunnelling probability

Table 5.4: Summary assumed and calculated parameters used to estimate the resonance width (Equation 5.13).

Parent State	ε_r [meV]	v [km/s]	r_1 [a_o] [a]	r_2 [a_o] [b]	P [%]
He $1s2p\ ^3P$	1232.95(7)	655	4.86	44.9	0.770
Ca $4s4p\ ^1P_1$	2967.3	1016	10.24	39.5	11.5
Cs $6s\ ^2S_{1/2}$	479.64(30)	409	14.61	56.4	11.1
W $5d^56s\ ^7S_5$	1205.83(15)	648	6.02	32.4	4.61
W $5d^46s^2\ ^5D_0$	920	566	6.42	15.1	35.9
Os $5d^66s^2\ ^5D_4$	1081.32(4)	614	5.01	87.7	0.172

[a]Classical turning point of the trapped electron.
[b]Exit point of electron from the potential barrier.

P can be readily estimated with the WKB approximation [24]:

$$\ln P = -2\int_{r_1}^{r_2} \sqrt{\frac{2m_e}{\hbar^2}(V_{eff} - E)}\,\mathrm{d}r, \tag{5.14}$$

where $E = \varepsilon_r - \varepsilon_t$, i.e. the energy of resonance in excess of the threshold energy, and the integration limits r_1 and r_2 are the points where $V_{eff} = E$. On the other hand, v poses a greater difficulty. The short-range potential used here is not valid at small r, since the model does not hold when the electron is close to the radius of the atomic core (a few a_o). We will therefore use the known ground state energy as an estimate of the depth of the well. The kinetic energy of the electron trapped behind the barrier is then equal to the excitation energy ε_r, or equivalently, the energy of the photon that was absorbed to excite the resonance. The parameters needed for the calculation of Equation 5.13 are summarised in Table 5.4.

Considering the uncertainties associated with the above estimates, the predicted values of the resonance widths are in good agreement with the measurements. This gives additional support for the classification of these resonances as p-orbital attachment to the neutral parent state. Since a longer lifetime results in a smaller width, it is tempting to ascribe the systematically larger $\Gamma_{pred}/\Gamma_{exp}$ ratios for the

heavy systems to stabilization of these resonances due to their highly mixed states. However, with the exception of Cs and He, the accuracy of the polarisabilities for the states in Table 5.3 are not sufficient to draw this conclusion. Finally, we have ignored the effect of a quadrupole moment here, which may be significant in some of the systems. On the other hand, the fact that the result for Feature 1 in the W^- spectrum is very similar to the results of the other resonances is a further indication that this feature is likely due to p-attachment to the W $5d^4 6s^2\ ^5D_0$ ground state.

5.5 References

[1] T. Andersen, H. K. Haugen, and H. Hotop, J. Phys. Chem. Ref. Data **28**, 1511 (1999).

[2] C. Bahrim and U. Thumm, Phys. Rev. A **61**, 022722 (2000).

[3] C. Bahrim and U. Thumm, Phys. Rev. A (submitted).

[4] S. J. Buckmann, C. W. Clark, Rev. Mod. Phys. **66**, 539 (1994).

[5] V. K. Ivanov, J. Phys. B **32**, R67 (1999).

[6] H. Friedrich, *Theoretical Atomic Physics* (Springer-Verlag, New York, 1991); see especially Sections 1.3, 1.4, and 3.2.

[7] J. R. Peterson, Y. K. Bae, and D. L. Huestis, Phys. Rev. Lett. **55**, 692 (1985).

[8] C. W. Walter, J. A. Seifert, and J. R. Peterson, Phys. Rev. A **50**, 2257 (1994).

[9] C. Blondel, Phys. Scr. **T58**, 31 (1995).

[10] G. F. Gribakin, A. A. Gribkina, B. V. Gul'tev, and V. K. Ivanov, J. Phys. B **25**, 1757 (1992).

[11] P. Balling, P. Kristensen, H. Staplefeldt, T. Andersen, and H. K. Haugen, J. Phys. B **26**, 3531 (1993).

[12] See Table 2 on page 441 of: T. Wu and T. Ohmura, *Quantum Theory of Scattering* (Prentice-Hall, 1962).

[13] C. W. Walter and J. R. Peterson, Phys. Rev. Lett. **68**, 2281 (1992).

[14] C. A. Ramsbottom and K. L. Bell, J. Phys. B **32**, 1315 (1999).

[15] V. A. Esaulov, Ann. Phys. Fr. **11**, 493 (1986).

[16] C. S. Feigerle, R. R. Corderman, S. V. Bobashev, and W. C. Lineberger, J. Chem. Phys. **74**, 1580 (1981).

[17] R. D. Beck and S. O'Malley, private communication.

[18] V. K. Ivanov, L. P. Krukovskaya, and G. Yu Kashenock, J. Phys. B **29**, L313 (1996).

[19] R. M. Stehman, W. B. Clodius, S. Grot, S. B. Woo, and E. M. Helmy, Phys. Rev. A **31**, 297 (1985), and references therein.

[20] K. F. Scheibner and A. U. Hazi, Phys. Rev. A **38**, 539 (1988).

[21] Z.-C. Yan, Phys. Rev. A **62**, 052502 (2000).

[22] T. M. Miller and B. Bederson, in *Advances in Atomic and Molecular Physics* Volume 13, Edited by D. R. Bates and B. Bederson (Academic Press, New York, 1977).

[23] A. Derevianko, W. R. Johnson, M. S. Safronova, and J. F. Babb, Phys. Rev. Lett. **82**, 3589(1999).

[24] The WKB approximation is described in a number of texts on quantum mechanics. See for example: R. L. Liboff, *Introductory Quantum Mechanics*, 2nd Edition (Addison-Wesley, New York, 1993); especially Section 7.10.

Chapter 6

Multiphoton Detachment Thresholds

6.1 Paper 6 — Control of Near-threshold Detachment Cross Sections via Laser Polarization

Very few multiphoton threshold experiments have ever been conducted. This article determines the two-photon threshold in Au^- to a very high level of detail. Of particular importance is that the effects of the polarization of the laser light field are investigated and an impressive variation of the detachment cross section and threshold shape is achieved. Such variations are expected on the basis of the Wigner threshold law, but have not previously been observed. Of practical interest is that the control over the near-threshold photodetachment cross section demonstrated here could be a valuable tool for the investigation of negative ions when structure is present near a detachment threshold — a category in which many atomic negative ions fall.

I took primary responsibility for all aspects of this work and took sole responsibility for the setup and execution of most of the experiments. M. Scheer provided valuable assistance and input, especially during the early stages of the project. As

usual, H. K. Haugen supervised all aspects of the study and supplied valuable input at all stages.

Control of Near-threshold Detachment Cross Sections via Laser Polarization State

René C. Bilodeau, Michael Scheer*, and Harold K. Haugen†

Department of Physics and Astronomy, McMaster University, Hamilton, Ontario, L8S 4M1, Canada

(Accepted for publication in *Physical Review Letters*: July 18, 2001)

Abstract

The behavior of near-threshold cross sections for dissociation of a target into a pair of particles, as described by Wigner's threshold law, can depend sensitively on the angular momentum of the particles. In this Letter we investigate the near-threshold nonresonant two-photon detachment process in the negative ion of gold. The expected *s*-wave threshold behavior is observed with linearly polarized light and compared with recent theory. Complete closure of the *s*-wave channel is realized by using circular polarization, allowing the first observation of a *d*-wave threshold. Practical applications are discussed, including extensions which could prove valuable for investigations of negative ions with near-threshold structure, particularly in the transition metals.

32.80.Gc, 32.80.Wr

In 1948, Wigner developed general expressions describing the threshold behaviors of the cross section for dissociation of a target into a pair of particles [1]. If one or both particles produced are not charged, then usually [2] the interaction between the particles is shorter-range than the centrifugal potential, $\ell(\ell+1)/r^2$, and the cross section (σ) depends only on the relative linear (k) and angular (ℓ) momentum of the particles: $\sigma \propto k^{2\ell+1}$. This Wigner threshold law has been verified in countless experiments, and is commonly used in laser photodetachment threshold (LPT) spectroscopy for high precision measurements of atomic negative ion binding energies (ε_o) [3]. In particular, for negative ion photodetachment $\sigma \propto \varepsilon^{\ell+1/2}$, where $\varepsilon = h\nu - \varepsilon_o \propto k^2$ is the energy and ℓ is the angular momentum of the photoelectron.

If the excess electron of a negative ion is bound in an orbital with angular momentum ℓ_o, a single-photon detachment process ejects the photoelectron into at most two angular momentum channels: $\ell = |\ell_o \pm 1|$. Furthermore, at sufficiently low photoelectron energies, the centrifugal barrier suppresses the higher angular momentum channel and the photoelectron exits in the lower partial wave. As might be expected, the Wigner law applies equally well if two or more photons are used to detach the negative ion. Both p-wave (in Cl^- [4] and Si^- [5]) and s-wave (in H^- [6]) thresholds have been observed experimentally in two-photon detachment. It is interesting to note that only s- and p-wave detachment thresholds have been observed in either single- or multiphoton detachment. For single photon detachment, higher partial waves ($\ell \geq 2$) can dominate near the threshold only if the excess electron of the negative ion has $\ell_o \geq 3$, e.g. detachment from an f- or g-orbital. There are therefore very few suitable species, and experimental considerations (small binding energies, low cross sections, poor currents, and radioactivity) make these ions unattractive. In contrast to single-photon detachment, the polarization of the light field can play an important role in multiphoton detachment. Indeed, measurements of the angular distributions of the ejected electron in multiphoton detachment can yield new features if observed with elliptically polarized light, and has become an area of recent interest [7]. In general, for an n-photon detachment process, partial waves with $\ell = |\ell_o - n|, |\ell_o - n + 2|, \ldots, |\ell_o + n|$ are possible. If linearly

polarized light is used, the lowest partial wave will again dominate near the threshold [8]. However, the use of circular polarization imposes $\ell = |\ell_o \pm n|$, and can therefore give rise to a dramatic change in the photodetachment threshold behavior. A small polarization dependance the Cl^- detachment cross section has been observed in a two-color experiment [9], but essentially only for two photon-energies far above the two-photon threshold. The primary goal of the experiments presented in this Letter is to demonstrate the change in the threshold law with laser light polarization. We shall also discuss selected novel applications and extensions of this technique.

The tunable infrared laser light required for the experiment is produced by a 10 Hz Nd:YAG pumped dye laser, Raman shifted in a high pressure H_2 cell. In order to control the polarization, the laser light is directed through a rotatable, achromatic quarter-wave plate. The laser light then passes into a 15 cm focal length best-form lens and through a viewport into an ultra high vacuum chamber to focus onto an 8 keV, 500 nA beam of Au^-, extracted from a Cs sputter source. The laser and ion beams are orientated to intersect at 90°. Further details of the apparatus can be found elsewhere [5,10].

The high intensities and long wavelengths ($\lambda \approx 1$ μm) required for these experiments give rise to significant energy shifts, predominantly due to the ponderomotive shift [11]. The ponderomotive shift originates from the fact that a free electron undergoes an oscillatory motion in the high intensity light field [12]. As a result, the energy of the free electron state in a light field is increased by an amount equal to the ponderomotive potential $\Delta = e^2 E^2/4m_e\omega^2 = I \lambda^2 U_{pon}$, where E, I, and $\omega = 2\pi\nu$ are respectively the electric field amplitude, intensity, and frequency of the light field, and $U_{pon} = 7.53 \times 10^{-10}$ cm^{-1} μm^{-2} (W/cm^2)$^{-1}$. Initial experiments aimed at verifying U_{pon} yielded shifts much smaller than expected and resulted in a good deal of controversy on the subject (see [13], and references therein). These observations were explained in part by the phenomenon termed "leakage detachment" in very low frequency light fields [14], and by unfavorable experimental conditions [13,15]. Later, a careful experiment by Davidson *et al.* [13] demonstrated that the ponderomotive shift was consistent with the expected value.

It is important to further consider the effect of threshold shifts for our experimental conditions, as this improves the fit to the data. In a uniform light field the threshold is shifted to higher energies by the ponderomotive potential and the Wigner law for n-photon detachment becomes $\sigma_n = a_n (n h\nu - \varepsilon_o - \Delta)^{\ell+1/2}$, with a_n a constant [16]. In practice the intensity of the light varies both in position and time, causing the threshold to smear out over a photon energy region $\approx \Delta/n$. The local n-photon detachment rate is: $\mathrm{d}R_n = \sigma_n \Phi^n(x,y,z,t)\,\rho(x,y,z)\,\mathrm{d}x\,\mathrm{d}y\,\mathrm{d}z$, with $\Phi = I/h\nu$ the photon flux and ρ the ion beam density. We assume that the laser pulse is propagating along the z-axis, and has a Gaussian profile in the beam cross section (the x-y plane) with a full width at half maximum (FWHM) Γ_x and Γ_y, and a Lorentzian profile in time (t) with a FWHM Γ_t. Since the laser beam is approximately cylindrical in symmetry over the interaction volume with a focus waist much smaller than the width of the ion beam, ρ can be taken as constant in the x-y plane and integration over z only introduces an overall constant. Finally the pulse-to-pulse variations in pulse energy were found to obey the statistics of a normal distribution, and is therefore modelled with a Gaussian having a FWHM $\Gamma_\xi = 16\%$ of the mean pulse energy. Transforming to the (reduced) cylindrical coordinate system, $\tilde{r}\cos\theta = x/\Gamma_x$, $\tilde{r}\sin\theta = y/\Gamma_y$, and $\tilde{t} = t/\Gamma_t$, and integrating over z and θ, the signal $S_n \propto \int R_n\,\mathrm{d}t$ is given by,

$$\frac{S_n(h\nu)}{I_p^n} = a \int_{-\infty}^{+\infty} \int_0^{\infty} \int_0^{\infty} \tilde{r}\,\tilde{I}^n\,\sigma_n(h\nu; b)\,\mathrm{d}\tilde{r}\,\mathrm{d}\tilde{t}\,\varrho\,\mathrm{d}\xi. \qquad (1)$$

Here, $\varrho(\xi) = \varrho_o \exp\left(-4\ln 2\,\xi^2/\Gamma_\xi^2\right)$ is the probability density of having a pulse with peak intensity $(1+\xi)I_p$, $\tilde{I}(\xi,\tilde{t},\tilde{r}) \equiv I/I_p = (1+\xi)(4\tilde{t}^2+1)^{-1}\exp(-4\ln 2\,\tilde{r}^2)$ is the intensity profile of the pulse, and $\sigma_n(h\nu; b)$ is the cross section for n-photon detachment which may be given by the Wigner law or some more general expression (see below). Finally, the amplitude a and the ponderomotive parameter $b = I_p U_{\mathrm{pon}}$ are fitting parameters (note that $\Delta = \tilde{I}\,\lambda^2 b$). The shape of the threshold is then independent of the spatial and temporal scale of the experiment. However, these geometrical parameters are necessary to extract U_{pon} from the fitted value of b. This can be done by deducing I_p from the measured pulse energy:

$$E_{\rm pul} = \iiint I \, dx \, dy \, dt = \left(\frac{\pi^2}{8 \ln 2}\right) \Gamma_x \, \Gamma_y \, \Gamma_t \, I_p. \qquad (2)$$

Using parameters typical for the geometry of the present experiments, $E_{\rm pul} \approx 8$ mJ, $\Gamma_x = \Gamma_y \approx 25$ μm and $\Gamma_t \approx 8$ ns, we obtain $I_p \approx 9 \times 10^{10}$ W/cm^2.

In practice, the pulse energies vary as the laser is tuned in wavelength. Therefore, I_p depends weakly on $h\nu$. In addition, there is a small $(n+1)$-photon excess photon detachment (EPD) background, which depends on I_p^{n+1}. Noting that $I_p(h\nu) \propto E_{\rm pul}(h\nu)$ by Eq. 2 and specialising to $n = 2$, we correct the data for pulse energy variations and EPD using: $S_c(h\nu) = \left[S(h\nu) - A_3 \, E_{\rm pul}^3(h\nu)\right] / E_{\rm pul}^2(h\nu)$, where $S(h\nu)$ is the observed signal and A_3 is a constant such that $A_3 \, E_{\rm pul}^3(h\nu)$ is the estimated three-photon detachment signal, assuming the cross section remains constant and equal to the below threshold value ($\approx$3% of the signal obtained at 9380 cm^{-1}). We found that the below-threshold signal (at 9212 cm^{-1}) depended on pulse energy according to $E_{\rm pul}^{2.9(3)}$, consistent with three-photon detachment (all uncertainties are quoted to one standard deviation, unless otherwise noted). We then have that $S_c(h\nu) \propto S_2 / I_p^2$, given by Eq. 1. The variations of I_p with wavelength also introduces a more subtle error in the measurements. As the laser pulse energy changes so does the ponderomotive shift, which produces an effective uncertainty in the energy position of the data points. The horizontal error bars in the figures reflect the full relative shift expected from these variations.

Figure 1 presents the data, from measurements of the threshold region using linearly polarized light. The fit of Eq. 1 to the data yields $b = 49(3)$ cm$^{-1}\mu$m^{-2}, assuming the known binding energy of Au^-, $\varepsilon_o = 18620.2(2)$ cm^{-1} [3,17]. The small systematic deviations of the model from the data are likely due to additional smearing of the threshold from some details not included in the model, such as the hyperbolic shape of the focus waist, the ion density distribution, a possibly imperfect (i.e. non-Gaussian) laser focus profile, and a more complicated temporal profile. The otherwise excellent general agreement of the model with the data indicates that this technique could be used to obtain high precision measurements of the ponderomotive shift, assuming good characterization of the laser pulse parameters.

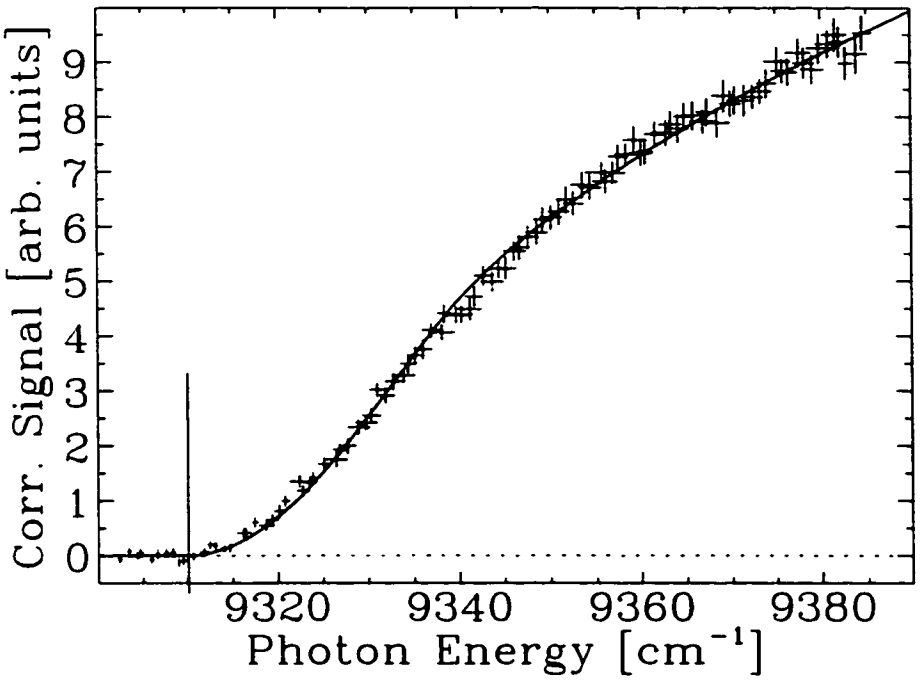

FIG. 1. Detachment signal near the two-photon threshold in Au^-. The data is corrected for variations in pulse energies (≈5% over this region) and three-photon EPD background. Vertical error bars represent 80% confidence limits based on observed statistical scatter; horizontal error bars are discussed in the text. The fitted curve is based on a shifted Wigner threshold law for *s*-wave detachment. A vertical line indicates the position of the nominal two-photon threshold ($h\nu = \varepsilon_o/2$).

We now consider the polarization dependence of the two-photon detachment cross section. Figure 2 presents the data obtained with linearly and circularly polarized light. The remarkable difference in the curves can be entirely explained by the change in the centrifugal potential encountered by the ejected electron. As discussed earlier, for two-photon detachment with linearly polarized light, the photoelectron is ejected with angular momentum $\ell = \ell_o$ or $|\ell_o \pm 2|$. In the case of Au^-, $\ell_o = 0$ and therefore $\ell = 0$ or 2. Near the threshold, the centrifugal potential for *d*-wave detachment effectively suppresses that channel, and a Wigner *s*-wave law is observed. The solid curve is obtained from Eq. 1 using

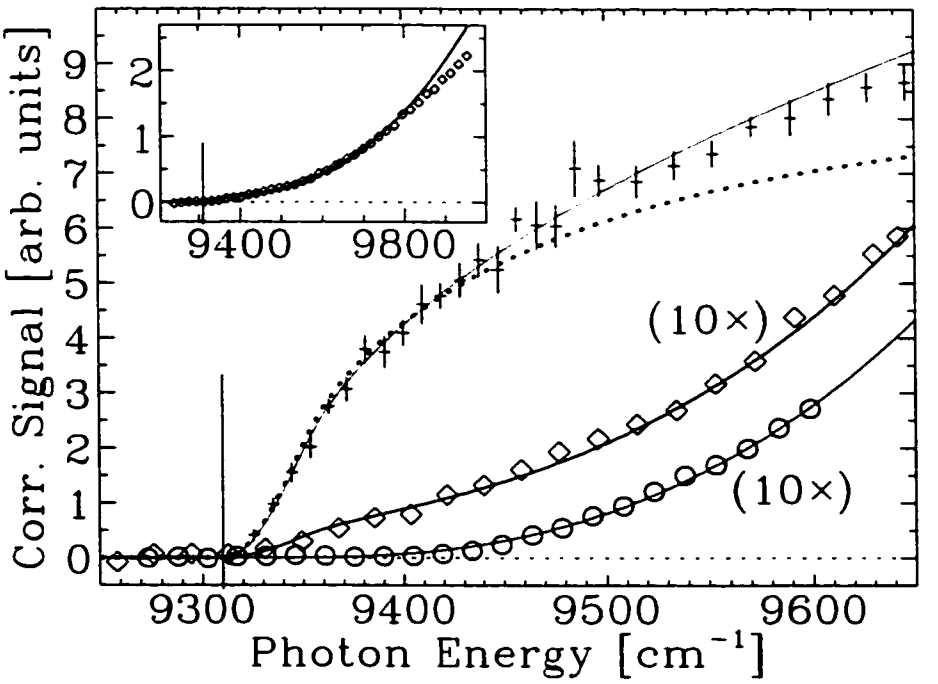

FIG. 2. Corrected signal obtained using linearly (+), elliptically (◇), and circularly (○) polarized light. The scale for the ◇ and ○ data sets has been magnified by a factor of 10. We estimate a 30% uncertainty in the scale of the linear relative to the circular and elliptical data sets. The height of the + symbols indicate 80% confidence limits; errors for the ◇ and ○ data are smaller than their height. Errors in photon energy are smaller than the width of the symbols. The full curves are based on the Wigner law, while the dotted curve is based on theory by Gribakin and Kuchiev, scaled to agree with the near-threshold data. The nominal two-photon threshold is marked by a vertical line.

$\sigma_2 = a_2\left(2h\nu - \varepsilon_o - \tilde{I}\lambda^2 b\right)^{1/2}$, with the amplitude as the only free parameter. The curve fits the data near the threshold well, but begins to diverge at higher photon energies and was observed to lie ≈30% above the data at photon energies ≈6% above threshold. The breakdown of the Wigner law is expected, and has been studied in a number of single-photon detachment experiments [7,17,18] and theoretical treatments [19]. To our knowledge there

has been no experimental work aimed at studying the range of validity of the Wigner law in multiphoton detachment. Recently Gribakin and Kuchiev [20,21] have obtained general expressions for multiphoton detachment cross sections. The dotted curve in the Fig. 2 shows the two-photon detachment signal using Eq. 1 with σ_2 given by their theory, modified to include the effect of threshold smearing. Although the theory appears to predict a somewhat premature breakdown of the Wigner threshold law, the expected accuracy of the theory for two-photon detachment is consistent with the observed deviation [21].

Using circularly polarized light, photons with only one spin orientation are available and the photoelectron can be ejected into the $\ell = |\ell_o \pm 2| = 2$ partial wave only, i.e. as a d-wave. The data denoted with open circles (○) in Fig. 2 were obtained using a quarter-wave plate adjusted for circularly polarized light. The excellent fit to the Wigner d-wave law [Eq. 1 with $\sigma_2 = a_2'(2h\nu - \varepsilon_o - \tilde{I}\lambda^2 b)^{5/2}$] indicates that little or no s-wave component is present over a large energy region. We estimate that the s-wave detachment cross section has been suppressed to $\lesssim$0.5% of that observed for linear polarization. To verify this signal was indeed from a two-photon process, we measured the dependence of the signal on pulse energy at 9635.4 cm^{-1}, and found that $S \propto E_{\rm pul}^{2.3(2)}$; an exponent slightly larger than 2 may be due to the small EPD background.

Figure 2 also shows data (diamonds ◇) obtained with a small adjustment of the quarter-wave plate ($\approx$1°), corresponding to slightly elliptically polarized light. The near-threshold data are systematically above the d-wave curve due to the introduction of a small amount of s-wave detachment. To obtain the solid curve following these data, we added 2% of the linear polarization signal to the d-wave model. As can be seen in the inset, this model is in good agreement up to photon energies $\approx$9750 cm^{-1}, i.e. $\approx$5% above the threshold. The eventual departure from the Wigner law far above threshold is expected and is also seen in single-photon s- and p-wave detachment [7,17–19], as noted above.

In conclusion, we have shown that it is possible to dramatically change the energy dependence of the near-threshold cross section in two-photon detachment. These measurements have led to the first observation of a Wigner d-wave law in a negative ion. Higher partial

waves could be studied with higher order processes; for example, a three-photon process could be made to yield an f-wave.

The technique demonstrated here can be directly applied or naturally extended to study a range of interesting structure in negative ions. Two-photon detachment offers a convenient control over the magnitude of the threshold signal and, in some cases, a way to effectively "switch on" (or off) structure lying near the threshold. The two-photon threshold signal could be greatly reduced (by using circularly polarized light) in order to better observe near-threshold structure. For example, the $4d^9 5s^2\ ^2D_{3/2}$ excited state of Pd^- is expected to be bound by 50±350 cm^{-1} [22] placing it in the vicinity of the $4d^{10}5s\ ^2S_{1/2} \rightarrow 4d^{10}\ ^1S_0$ ground state detachment threshold. An attempt to detect this excited state in a single-photon magnetic dipole resonance experiment was unsuccessful [10], and may be an indication that it is slightly unbound. While the state should be visible as a two-photon electric dipole (E1) resonance, it is unlikely that such a feature would be observable on top a two-photon s-wave. The use of circularly polarized light would greatly reduce the threshold signal while simultaneously increasing the signal from the resonance, thus significantly improving the detection sensitivity. Another important example is provided by Os^-, where unwanted structure could be eliminated with two-photon detachment. A very strong E1 resonance lying only 3.5 meV above the ground state detachment threshold results in a situation that is unfavorable for an accurate determination of the electron affinity of Os [23]. Since this resonant transition would be strongly forbidden under two-photon detachment, a "clean" s-wave threshold could be observed. An accurate determination of the threshold value would then be possible, assuming a good characterization of threshold shifts. W^- [23], Cs^- [24], and He^- [25] have similar near-threshold E1 structure, and may also benefit from such an approach.

As a final note, in some experiments accurate knowledge of the magnitude of the threshold shift [11] may be required. Previous investigations of the ponderomotive shift in negative ions have been conducted in the presence of two laser fields: a high intensity, low frequency field (infrared or microwave) to produce the shift, and a high frequency field to detach the

ions. Because good overlap of the light fields is crucial, the use of two fields can complicate experiments, and likely gave rise to some of the discrepancies observed in early studies [13]. As we have demonstrated here, using a single light field makes the process easier to model and eliminates these focus matching problems, thus offering a simple and effective method to accurately measure the magnitude of the shift which could be exploited in future work.

We thank the Natural Science and Engineering Research Council of Canada (NSERC) for support of this work. RCB would like to thank the Ontario Ministry of Education and Training for a graduate fellowship (OGSST).

REFERENCES

* Currently with High Performance Optical Components Solutions, Nortel Networks, Ottawa.

† Also with the Department of Engineering Physics, the Brockhouse Institute for Materials Research, and the Center for Electrophotonic Materials and Devices, McMaster University.

[1] E.P. Wigner, Phys. Rev. **73**, 1002 (1948).

[2] For an exception see: J.R. Smith, J.B. Kim, and W.C. Lineberger, Phys. Rev. A **55**, 2036 (1997).

[3] T. Andersen, H.K. Haugen, and H. Hotop, J. Phys. Chem. Ref. Data **28**, 1511 (1999).

[4] R. Trainham, G.D. Fletcher, and D.J. Larson, J. Phys. B **20**, L777 (1987).

[5] M. Scheer, R.C. Bilodeau, C.A. Brodie, and H.K. Haugen, Phys. Rev. A **58**, 2844 (1998).

[6] C.Y. Tang *et al.*, Phys. Rev. Lett. **66**, 3124 (1991).

[7] F. Dulieu, C. Blondel, and C. Delsart, J. Phys. B **28**, 3845 (1995); *ibid.*, 3861.

[8] Although the lowest partial wave always dominates near the threshold, higher partial waves can dominate far above threshold, e.g. see: L. Præstegaard, T. Andersen, and P. Balling, Phys. Rev. A **59**, R3154 (1999).

[9] W.G. Sturrus, L.P. Ratliff, and D.J. Larson, J. Phys. B **25**, L359 (1992).

[10] M. Scheer, C.A. Brodie, R.C. Bilodeau, and H.K. Haugen, Phys. Rev. A **58**, 2051 (1998).

[11] Discrete bound states can also be shifted by the laser field, which is the conventional *ac* Stark effect. This also contributes to the shifting of the detachment threshold, but to a much smaller extent than the ponderomotive shifting of the continuum states.

[12] For a general discussion, see e.g.: P. Agostini and G. Petite, Contemp. Phys. **29**, 57

(1988). Note that numerical factor in Equation (17) of this article is incorrect. The value of the coefficient should be 9.3×10^{-10}.

[13] M.D. Davidson, J. Wals, H.G. Muller, and H.B. van Linden van den Heuvell, Phys. Rev. Lett. **71**, 2192 (1993).

[14] L.A. Bloomfield, Phys. Rev. Lett. **63**, 1578 (1989).

[15] A.R.P. Rau, Phys. Rev. A **54**, 717 (1996).

[16] This combination of the Wigner law and the ponderomotive potential has been used in a number of previous works, see e.g. [8,13]. Note also that the laser intensities used here are at least two orders of magnitude lower than the onset for non-perturbative effects; see J.H. Eberly, J. Phys. B **23**, L619 (1990).

[17] H. Hotop and W.C. Lineberger, J. Chem. Phys. **58**, 2379 (1973).

[18] M. Scheer, R.C. Bilodeau, and H.K. Haugen, Phys. Rev. Lett. **80**, 2562 (1998); R.C. Bilodeau, M. Scheer, H.K. Haugen, and R.L. Brooks, Phys. Rev. A **61**, 012505 (1999), and references therein.

[19] T.F. O'Malley, Phys. Rev. **137**, A1668 (1965); J.W. Farley, Phys. Rev. A **40**, 6286 (1989).

[20] G.F. Gribakin and M.Yu. Kuchiev, J. Phys. B **30**, L657 (1997); Corrigendum: *ibid.* **31**, 3087 (1998).

[21] G.F. Gribakin and M.Yu. Kuchiev, Phys. Rev. A **55**, 3760 (1997).

[22] C.S. Feigerle, R.R. Corderman, S.V. Bobashev, and W.C. Lineberger, J. Chem. Phys. **74**, 1580 (1981).

[23] R.C. Bilodeau and H.K. Haugen, Phys. Rev. Lett. **85**, 534 (2000).

[24] M. Scheer, J. Thøgersen, R.C. Bilodeau, C.A. Brodie, H.K. Haugen, H.H. Andersen, P.

Kristensen, and T. Andersen, Phys. Rev. Lett. **80**, 684 (1998).

[25] J.R. Peterson, Y.K. Bae, and D.L. Huestis, Phys. Rev. Lett. **55**, 692 (1985).

Chapter 7

Summary and Perspectives

This thesis has described laser photodetachment spectroscopic studies of a number of atomic negative ion systems using a tunable infrared laser source. In total, experiments on 14 elements were discussed in detail. The work is most conveniently split into two categories. In the first category are the experimental investigations of atomic negative ion structure. These investigations include both studies on the ground and excited bound states of a number of negative ions, and studies of the nearly-bound states in Cs^-, Os^-, and W^-. Secondly, a study of the threshold laws was presented. This includes the two-photon threshold experiments conducted in Au^-, as well as the single-photon threshold law correction terms investigated in Al^-, B^-, Ir^-, and Pt^-. A summary of the results and perspectives are discussed below.

7.1 Negative Ion Structure

An important aspect of the work consisted of high precision measurements of bound and unbound states of atomic negative ions. These measurements consist of a number of threshold detachment studies as well as bound-bound and continuum resonance

Table 7.1: Summary of measured ground and excited state binding energies for the negative ions of the main group elements, arranged by group. Binding energies are given in meV relative to the ground state of the neutral atom.

Ion	Level[a]	This Work		Previous Works		
		Binding Energy	Method[b]	Binding Energy	Method[b]	Ref.
B^-	$^3P_0$	279.723(25)	LPTS	277(10)	LPES	[1,2]
	$^3P_1$	279.323(20)	LPTS			
	$^3P_2$	278.681(20)	LPTS			
Al^-	$^3P_0$	432.83(5)	LPTS	$440.94(^{+66}_{-48})$	LPTS	[3]
	$^3P_1$	430.01(3)	LPTS			
	$^3P_2$	424.35(3)	LPTS			
C^-	$^4S_{3/2}$	1262.118(20)	LPTS	1262.9(3)	LPTS	[4]
Si^-	$^4S_{3/2}$	1389.521(20)	LPTS	1389.49(6)	LPTS	[5]
	$^2D_{3/2}$	527.234(25)	LPTS	523(5)[c]	LPES	[6]
	$^2D_{5/2}$	525.489(20)	LPTS			
Ge^-	$^4S_{3/2}$	1232.712(15)	LPTS	1232.73(5)	LPTS	[5]
	$^2D_{3/2}$	401.44(10)	LPTS	400(200)[c]	SE	[7]
	$^2D_{5/2}$	377.57(6)	LPTS			
Sn^-	$^4S_{3/2}$	1112.066(15)	LPTS	1112.09(6)	LPTS	[5]
	$^2D_{3/2}$	397.617(15)	RMD[d]	400(200)[c]	SE	[7]
	$^2D_{5/2}$	304.635(15)	RMD[d]			
Bi^-	$^3P_2$	942.362(13)	LPTS	946(10)	LPES	[1]
Te^-	$^2P_{3/2}$	1970.872(22)	[e]	1970.875(7)	LPTS	[8]
	$^2P_{1/2}$	1350.289(14)	RMD[d]	1349.9(6)	LPES	[7]

[a]Configurations are that of the ground state.

[b]Methods are: SE = semi-empirical extrapolations
LPES = laser photodetachment electron spectrometry
LPTS = laser photodetachment threshold spectroscopy
RMD = resonant multiphoton detachment
CRE = single-photon continuum resonance enhancement

[c]Term averaged value.

[d]Also observed using LPTS.

[e]Combined LPTS and RMD result, see Section 3.3.5.

Table 7.2: Summary of measured ground and excited state binding energies for the negative ions of cesium and the transition metals, arranged by group. Binding energies are given in meV relative to the ground state of the neutral atom.

Ion	Level[a]	This Work		Previous Works		
		Binding	Method[b]	Binding	Method[b]	Ref.
Cs^-	$^1S_0$	471.64(6)	LPTS	471.630(25)	LPTS	[7][c]
	$6s6p\ ^3P_1$	−8.0(3)	CRE			
Cr^-	$^6S_{5/2}$	675.84(12)	LPTS	666(12)	LPES	[9]
Mo^-	$^6S_{5/2}$	747.2(2)	LPTS	748(2)	LPES	[10]
W^-	$^6S_{5/2}$	815(3)	LPTS	816(8)	LPES	[9]
Ru^-	$^4F_{9/2}$	1046.38(25)	LPTS	1100(200)	SE	[9]
	$^4F_{7/2}$	865.3(10)	LPTS			
Os^-	$^4F_{9/2}$	1077.80(12)	LPTS	1100(200)	SE	[7]
	$^4F_{7/2}$	553(3)	LPTS			
	$\sim^d$	11.48(12)	RMD			
	$\sim^d$	−3.52(12)	CRE			
Co^-	$^3F_4$	663.3(6)	LPTS	662(3)	LPES	[11]
	$^3F_3$	554.8(20)	LPTS	549(10)	LPES	[12]
Rh^-	$^3F_4$	1142.89(20)	LPTS	1138(8)	LPES	[9]
Ir^-	$^3F_4$	1564.36(15)	LPTS	1563.8(5)	LPTS	[13]
Ni^-	$^2D_{5/2}$	1157.16(12)	LPTS	1157(10)	LPES	[12]
	$^2D_{3/2}$	973.0(4)	LPTS	975(12)	LPES	[12]
Pd^-	$^2S_{1/2}$	562.14(12)	LPTS	558(8)	LPES	[9]
	$4d^95s^2\ ^2D_{5/2}$	422.4(5)	LPTS	422(8)	LPES	[9]
Pt^-	$^2D_{5/2}$	2125.10(5)	LPTS	2125.2(8)	LPTS	[5]
				2123.2(11)	LPTS	[14]
				2128(2)	LPTS	[15]
Cu^-	$^1S_0$	1235.78(4)[e]	LPTS	1235(5)	LPES	[16]
Ag^-	$^1S_0$	1304.47(2)	LPTS	1302(7)	LPES	[17]

[a]The ground state configuration is assumed unless otherwise specified.
[b]Methods are defined in footnote [b] of Table 7.1.
[c]This result was reported in the review article, but remains unpublished.
[d]The $5d^66s^26p\ ^6D_{9/2,11/2}$ levels have been tentatively assigned.
[e]Note that a typographic error is present in Table 1 of Section 4.1.1 (Paper 1).

structure. A significant improvement in the knowledge of the binding energies of many negative ion states have resulted from this work, and many states were observed for the first time. For many of these ions, all of the expected bound states have now been observed. This represents a significant step towards a complete knowledge of bound negative ion states. Furthermore, including the measurements presented here, experimental results are now available for the electron affinities of all the elements which are expected to form bound negative ions, with the notable exception of the lanthanides and a few radioactive elements. Nonetheless, the bound excited states of many negative ions still have not been observed, and future experiments targeting these states are of obvious interest.

The negative ion structure measurements presented in this thesis can be naturally divided into results on *s*-wave detaching species (namely the main group elements: groups 13–17) and *p*-wave detaching species (namely the transition metals and Cs). These are summarized in Table 7.1 and Table 7.2 respectively. For completeness, the results obtained in Papers 10, 11, and 12 listed in the Preface are also included. It should be noted that level splittings are typically known to higher accuracy than that of the absolute binding energies listed. The table also includes the best measurements available prior to the McMaster results. With the exceptions of Al^- and Pt^-, excellent agreement is observed in all cases. In fact, it is of interest to note that our measurements lie well within one standard deviation of the errors quoted for all of the 16 previous measurements obtained by Lineberger and co-workers in Colorado using the LPES technique. This is an indication that the error bars on those previous values were likely quite conservative.

The *s*-wave threshold results are in general considerably more accurate than the *p*-wave results. Due to the conspicuous nature of *s*-wave thresholds, the accuracy is frequently limited by systematic errors in the apparatus, for which the main

contributions arise from the laser calibration error and from possible Doppler shifts resulting from misalignment of the laser-ion crossing angle (see Section 3.3). In some cases it may be desirable to improve the accuracy of these measurements even further. For example an improved determination of the O^-, S^-, and Si^- thresholds could provide valuable benchmarks with which to compare other high accuracy measurements and techniques, such as the new electron microscopy technique (see below). An independent high accuracy measurement in O^- would be especially valuable since the two currently available measurements are not in agreement at the one standard deviation level.

Significant improvement of the laser calibration could be obtained by using more sophisticated calibration techniques, such as monitoring the lines of a Fabry-Perot interferometer in addition to optogalvanic lines. The Doppler shift uncertainty can be substantially reduced by making use of a co-axial beam alignment and comparing the co-propagating measurement with the counter-propagating result. Such an arrangement has been used in a number of very high resolution LPTS experiments [18–20]. Although this arrangement would require considerable modifications to the current setup at McMaster, it is possible to achieve similar reductions of the Doppler uncertainty by folding the laser beam so as to cross the ion beam twice in a near-perpendicular arrangement, as was done in recent LPTS experiments on F^- and Br^- [21]. With modifications such as these, it should be possible to achieve close to an order of magnitude reduction in the laser frequency uncertainty.

All of the high resolution *s*-wave thresholds observed with the McMaster apparatus have exhibited small oscillations in the detachment cross sections which span a range of one or two cm^{-1} (see discussions in Section 4.2.1 as well as [22] and Paper 10). These oscillations resulted from the presence of a small static electric field, which appears to be relatively uniform over the interaction region. While shielding

from stray electric fields is provided by grounded plates near the interaction region, the observed oscillations are evidence of incomplete shielding of one set of the electrostatic deflection plates, likely the set of upstream plates (see Section 3.1.1). The observed field in all the cases was rather small (10–15 V/cm) and well modelled by theory. As a result, the effects of the field introduced no difficulties in obtaining measurements at the $\lesssim 0.01$ cm^{-1} statistical accuracy. However, if higher resolution measurements were desired, a more complete shielding of the interaction region would be required. In particular, the presence of the tunnelling region below the detachment threshold imposes a lower limit on the useful range over which data can be used in the fit. A further suppression of the electric fields would therefore allow an even narrower range to be scanned, thus allowing better statistics and an improved determination of the threshold energy. The similar smearing caused by the laser bandwidth could be improved by injection-seeding a pulsed laser system with a continuous-wave laser having a narrow bandwidth. If a near transform-limited bandwidth could be achieved, then even the nested hyperfine structure of Bi^- might be observed (see Section 4.2.1).

Recently Blondel *et al.* [23–26] have applied a new technique to the study of atomic negative ions, called photodetachment microscopy. In the presence of an external (uniform) electric field, the photoelectron can travel along two classical trajectories to reach any given point on the detector. By observing the interference of these two trajectories, this clever method obtains impressively precise measurements of electron affinities. Since the photoelectron energy must be very small (~ 50 μeV), the technique is effectively limited to species where the cross section is high even very near to the detachment threshold, namely to *s*-wave detaching species. By the same token, since a large number of detachment events are required, it is not yet clear how easily the technique could be used to study excited ionic states in general, where thermal populations can be very low. Regardless, in a very recent study [26], the elec-

tron affinity of Si^- was measured to be 1389.5220(24) meV, an order of magnitude improvement over the McMaster measurement. This technique therefore presents a powerful new tool for high precision measurements in atomic negative ions.

In most of the *p*-wave detaching species, the statistical errors from the fit dominate the quoted error bars. This is due to the zero-slope onset of *p*-wave thresholds, which makes them very sensitive to the slope and fluctuations of the background signal. Improvements are therefore largely limited by the signal-to-background ratio. As was discussed in Section 4.1.2, careful signal gating and cathode sputtering have already led to large improvements in the signal-to-background ratio, compared to early experiments. Further improvements may be obtained by using alternate ion production methods which, for some systems, could produce larger ion currents and non-thermal population distributions. For elements which produce poor ion currents, the collisional background can sometimes be a limiting factor. This collisional background could be significantly reduced with an improved pumping system — a factor of 10 reduction in vacuum pressures should be readily achievable. In some cases the photodetachment signal from excited ionic states is a significant source of background. This is especially a concern in *p*-wave detaching species (e.g. especially Ru^-, Section 4.1.3), but also in *s*-wave detachment where nested thresholds are observed (e.g. B^- and Al^-, Section 4.2). This background could be removed by using an intense preparation pulse, which has photon energies insufficient to detach the ionic state of interest, but sufficient to detach all other more weakly bound states. A preparation of this sort should also remove all the photodetachment background produced by contaminants in the beam. After the ions have been further charge-state analysed to remove the neutral atoms which are produced, a second tunable pulse could then be used to measure the threshold in the usual fashion. An effective isolation of nested thresholds should also be possible in this way. Finally, alternate

measurement techniques could be explored, such as resonant ionization spectroscopy (RIS) (the RIS technique is reviewed in [27]). In RIS the negative ion is first detached to an excited state in the neutral atom. The neutral state is then probed by ionization through a resonant process. Since this is a state-selective process, vastly reduced background signals are typically observed. Moreover, the negative ion can be detached to an excited neutral atomic configuration where an *s*-wave threshold is expected, and can therefore be measured to a higher accuracy.

Recent technological advances could also be exploited. For example, Nd:YAG and excimer lasers running at a 100 Hz repetition are now readily available. If such a laser was used to pump the dye laser, a factor of 10 increase in signal could be achieved, thereby reducing the statistical noise by a factor of three for the same given scan time. Optical parametric oscillators also produce intense infrared radiation and with typically less pulse-energy variations observed within a given tuning range. This could be useful in experiments where a large scan range is required, such as was the case in W^- (see Section 5.3). On a similar note, difference frequency mixing in crystals can produce radiation at wavelengths > 10 μm. Long wavelengths such as these could be valuable for studies on very weakly bound systems such as the rare earths (lanthanides) which remain largely unstudied experimentally despite the fact that these systems have attracted considerable theoretical interest (see references in [27]). Lanthanum is another negative ion which has recently attracted much interest, largely because it may possess opposite parity bound states [28]. A recent LPES experiment by Covington *et al.* [29] on La^- has measured the EA of La [0.47(2) eV] for the first time, and confirmed that at least one excited bound state is present in this system. Unfortunately LPES is not sensitive to the parity of the states, nor can it detect states which are not initially populated by the ion production method used. It would therefore be of great value to study La^- using LPTS and associated techniques.

An improved mass resolution could also be of value (see also Appendix B). In general, for the systems studied here, some previous knowledge was available which could be used to rule out any possibility of misidentification with a contaminant. Also, no significant photodetachment background from impurities were observed for any of the systems. However, if ions with very low sputter currents (e.g. La and In) were studied, the number of weak contaminant ions which could cause problems is increased, and a better mass separation may be required. A 90° deflection could be achieved with a more powerful magnet and should be sufficient to obtain one atomic mass unit resolution for all the stable elements.

RIS and other channel selective techniques may also be useful to obtain higher accuracy measurements for states which have been observed only as nested or excited state thresholds, and where M1 or E2 resonant multiphoton detachment is not possible. Although several nested thresholds have been measured to a high accuracy, in many cases the background signal produced by lower lying thresholds typically leads to a poorer accuracy, especially for p-wave thresholds (e.g. in Ru, Section 4.1.3). The excited state threshold in W^- is a case which begs for the application of a channel-selective technique. If the signal from the detachment leading to the ^7S state could be separated from that leading to the ^5D states, lower-lying structure could be eliminated and the threshold position may then be accurately determined. Furthermore, this would likely produce conclusive evidence of whether peak B in W^- is bound relative to the ^7S state, which is still an outstanding question (see Section 5.3). Finally, further indication of the configuration of these states would be gained.

With regard to configuration assignments, electron angular distribution measurements can be a valuable tool to obtain information on the partial waves of the detachment channels. This can in turn be used to deduce the configurations of the negative ion states in question. Such measurements on Os^- and W^- would be of

particular interest.

7.2 Single- and Multiphoton Detachment Thresholds

A good understanding of the detachment threshold laws is central to the successful application of the LPTS technique. In fact, to date these thresholds laws have been used almost exclusively for such purposes. Investigations of the threshold behaviour are important on this basis alone. In addition, as was discussed in detail in Chapter 4, high resolution measurements of the threshold behaviour may be avenues to explore the physics of the detachment process, and possibly fundamental properties of atomic systems. It was shown that the currently available correction terms to the Wigner law provide good qualitative agreement, and reasonable quantitative agreement, with the observed threshold behaviour. However, even the leading order correction terms are not satisfactorily known (see Section 2.2 and discussion in Section 4.3). From a theoretical standpoint, more work is therefore required in developing models for the detachment process. Further experimental investigations are also clearly needed. As most LPTS measurements do not investigate a sufficiently large region to determine deviations from the Wigner law, an experimental investigation specifically targeting such deviations is required. Of particular interest would be an investigation of a few systems with similar electronic structure. A number of candidates were suggested in Section 4.3.3.

Finally, the work in Au^- demonstrated that the threshold law can be changed by varying the laser polarization state. This control over the near-threshold detachment cross section represents an additional tool in the laser spectroscopy arsenal for studying negative ion structure, particularly for states which lie near a detachment

threshold (see also discussion in Chapter 6). As there is a growing accumulation of evidence that suggests such near-threshold structure is in fact relatively common in negative ions, a tool of this kind may indeed be very useful in future experiments.

7.3 References

[1] C. S. Feigerle, R. R. Corderman, and W .C. Lineberger, J. Chem. Phys. **74**, 1513 (1981).

[2] D. M. Neumark, K. R. Lykke, T. Andersen, and W. C. Lineberger, Phys. Rev. A **32**, 1890 (1985).

[3] D. Calabrese, A. M. Covington, J. S. Thompson, R. W. Marawar, and J. W. Farley, Phys. Rev. A **54**, 2797 (1996).

[4] D. Feldmann, Chem. Phys. Lett. **47**, 338 (1977).

[5] J. Thøgersen, L. D. Steele, M. Scheer, C. A. Brodie, and H. K. Haugen, J. Phys. B **29**, 1323 (1996).

[6] A. Kasdan, E. Herbst, and W. C. Lineberger, J. Chem. Phys. **62**, 541 (1975).

[7] H. Hotop and W. C. Lineberger, J. Phys. Chem. Ref. Data **14**, 731 (1985).

[8] G. Haeffler, A. E. Klinkmüller, J. Rangell, U. Berzinsh, and D. Hanstorp, Z. Phys. D **38**, 211 (1996).

[9] C. S. Feigerle, R. R. Corderman, S. V. Bobashev, and W. C. Lineberger, J. Chem. Phys. **74**, 1580 (1981).

[10] R. F. Gunion, S. J. Dixon-Warren, and W. C. Lineberger, J. Chem. Phys. **104**, 1765 (1996).

[11] D. G. Leopold and W. C. Lineberger, J. Chem. Phys. **85**, 51 (1986).

[12] R. R. Corderman, P. C. Engelking, and W. C. Lineberger, J. Chem. Phys. **70**, 4474 (1979).

[13] B. J. Davies, C. W. Ingram, D. J. Larson, and U. Ljungblad, J. Chem. Phys. **106**, 5783 (1997).

[14] N. D. Gibson, B. J. Davies, and D. J. Larson, J. Chem. Phys. **98**, 5104 (1992).

[15] H. Hotop and W. C. Lineberger, J. Chem. Phys. **58**, 2379 (1973).

[16] D. G. Leopold, J. Ho, and W. C. Lineberger, J. Chem. Phys. **86**, 1715 (1987).

[17] H. Hotop, R. A. Bennett, and W. C. Lineberger, J. Chem. Phys. **58**, 2373 (1973).

[18] D. M. Neumark, K. R. Lykke, T. Andersen, and W. C. Lineberger, Phys. Rev. A **32**, 1890 (1985).

[19] D. Hanstorp and M. Gustafsson, J. Phys. B **25**, 1773 (1992).

[20] K. T. Andersson, J. Sandström, I. Yu. Kiyan, D. Hanstorp, and D. J. Pegg, Phys. Rev. A **62**, 022503 (2000).

[21] C. Blondel, P. Cacciani, C. Delsart, and R. Trainham, Phys. Rev. A **40**, 3698 (1989).

[22] M. Scheer, *Single- and Multiphoton Infrared Laser Spectroscopy of Atomic Negative Ions*, Ph.D. thesis, McMaster University (1998).

[23] C. Blondel, C. Delsart, and F. Dulieu, Phys. Rev. Lett. **77**, 3735 (1996).

[24] C. Valli, C. Blondel, and C. Delsart, Phys. Rev. A **59**, 3809 (1999).

[25] C. Blondel, C. Delsart, F. Dulieu, and C. Valli, Eur. Phys. J. D **77**, 207 (1999).

[26] C. Blondel, C. Delsart, and F. Goldfarb, J. Phys. B **34** (accepted).

[27] T. Andersen, H. K. Haugen, and H. Hotop, J. Phys. Chem. Ref. Data **28**, 1511 (1999).

[28] S. H. Vosko, J. B. Lagowski, and I. L. Mayer, Phys. Rev. A **39**, 446 (1989).

[29] A. M. Covington, D. Calabrese, J. D. Thompson, and T. J. Kvale, J. Phys. B **31**, L855 (1998).

Appendix A

Physical Constants and List of Symbols Used

For convenience a list of symbols that are frequently used in this thesis are given in Table A.1. In addition, Table A.2 lists a few fundamental constants and conversion factors which are often referred to in the text. The reader should be aware that slight variations on the symbols are sometimes used in the published articles reproduced in this thesis.

Table A.1: List of symbols used in this thesis. The symbols are grouped according to similar type.

Symbol	Defining Expression	Description
ν, λ	$c = \lambda\nu$	Lab-frame laser frequency, wavelength
$h\nu$		Lab-frame photon energy
E_p		Pulse energy
I		Laser intensity
ε_o		Electron binding energy
ε_t	$E_{atom} - E_{negative\ ion}$	Detachment threshold energy (often $\varepsilon_t = \varepsilon_o$)
ε	$h\nu - \varepsilon_t$	Photoelectron energy (single-photon detachment)
$\tilde{\varepsilon}$	$(nh\nu - \varepsilon_t)/h\nu$	Photoelectron energy in units of the photon energy
ε_r		Energy of resonance above ground ionic state
Δ	Equation 3.7	The ponderomotive energy
r		Electron-atom separation
ℓ_o		Orbital angular momentum of bound electron
ℓ		Angular momentum of photoelectron
σ_d		Photodetachment cross section
σ_a		Photoexcitation cross section
A_m	Equation 2.3	Threshold law expansion coefficients
B_ℓ^{dp}	Equations 2.5, 2.6	O'Malley's dipole polarisability coefficient
B_ℓ^{qm}	Equations 2.5, 2.7	O'Malley's quadrupole moment coefficient
C^{sr}	Equation 2.5	k^2-term coeff. from the short-range potential
$C_{\ell_o}^{lt}$	Eqns. 2.5, 2.9a,b,c	Farley's leading term coefficient
α	$\alpha_o/4\pi\epsilon_o$	Atomic polarisability in units of [length]^3
Q, Q_{av}	Equation 2.8	Permanent quadrupole moment, average

Table A.2: List fundamental constants and unit conversion factors frequently used in this thesis. All values are taken from [1].

Symbol	Numerical Value	Description
m_e	$9.109\,381\,88(72)\times10^{-31}$ kg	Rest mass of the electron
q_e	$1.602\,176\,462(63)\times10^{-19}$ C	Magnitude of the electron charge
a_o	0.529 177 2083(19) Å	Bohr radius
ϵ_o	$8.854\,187\,817\cdots\times10^{-12}$ (exact)	Permitivity of free space
$\hbar$	$1.054\,571\,596(82)\times10^{-34}$ J s	Reduced Planck's constant ($h/2\pi$)
c	$2.997\,924\,58\times10^{8}$ m/s (exact)	The speed of light in vacuum
eV	$1.602\,176\,462(63)\times10^{-19}$ J 8065.544 77(32) cm^{-1} $3.674\,932\,60(14)\times10^{-2}$ Hartree $2.417\,989\,491(95)\times10^{14}$ Hz $1.160\,4506(20)\times10^{4}$ K	Electron volt [1 eV = (q_e/C) J]
cm^{-1}	$1.239\,841\,857(49)\times10^{-4}$ eV $2.997\,924\,58\times10^{10}$ Hz (exact)	Wave numbers $[k = \lambda^{-1} = \nu/c = E/hc]$
m_u	$1.660\,538\,73(13)\times10^{-27}$ kg $9.31494013(37)\times10^{8}$ eV	Atomic mass unit $[m_u = \frac{1}{12}\times\text{mass}(^{12}\text{C})]$

A.1 References

[1] P. J. Mohr and B. N. Taylor, Rev. Mod. Phys. **72**, 351 (2000); The same article was also published in *ibid.* J. Phys. Chem. Ref. Data **28**, 1713 (1999).

Appendix B

Observed Ion Currents with Selected Cathodes

The negative ion source was briefly discussed in Section 3.1.1. Here we give three examples of cathodes used in the experiments described in this thesis, and list the ion current obtained with these cathodes. The mass spectra observed with copper, osmium, and tungsten cathodes will be discussed. The copper cathode is given as an example since it is used as the base material for most of the cathodes and very small amounts of Cu^- are often observed with all the cathodes. Unexpected structure was observed in the Os^- and W^- experiments, so those cathodes will also be discussed with reference to possible contaminants in the ion beam. The quoted ion currents (i) are those observed in the UHV chamber, i.e. that available for experiments. The mass m of the ions is deduced from the measured magnetic field B (using a Hall probe) and assuming $m \propto B^2$. For ion currents of 1 nA or more, the peak of the current profile can usually be found to $\approx$0.1 atomic mass units (m_u). However, the actual mass resolution (how near two peaks can be and still be resolved) is considerably lower and depends on the FWHM of the peaks, which in turn depends on the ion

beam energy and the magnetic field. A mass resolution considerably better than 5% is usually achieved.

High mass resolution measurements (typically better than 1 m_u) of ion currents obtained with various cathodes can be found in the work by Middleton [1]. The ion currents observed with the McMaster source are typically in good agreement with that work, although much lower currents are observed with the McMaster source.[1]

B.1 Currents Observed with a Copper Cathode

As an example, the mass spectrum obtained with a copper cathode is given in Table B.1, using a total acceleration voltage of 11 kV. Among the ions with a mass ≤ 139 m_u (the maximum achievable with a 11 keV beam and < 5.22 kGauss field), only O^-, OH^-, Cu^-, CuO^-, and Cu_2^- ions produce currents ≥ 1 nA. A few other ions are seen with currents $\ll 1$ nA but except for H^-, C^-, and CH^- they are not included in the table. The observed ratio $i(Cu_2^-)/i(Cu^-) \approx 2\%$ is as expected from [1]. Notice that the observed mass difference between the ^{63}Cu and ^{65}Cu atomic and molecular ions are smaller than expected. This is because the mass peaks are not separated with the mass resolution of about 3.5% obtained at these masses and ion beam energies, and only a shallow valley is observed between the two peaks. As a result, the less abundant ^{65}Cu isotope appears on the decreasing edge of the ^{63}Cu peak, causing the peaks to appear closer together. This also explains why $i(^{65}CuO^-)/i(^{63}CuO^-) \approx i(^{65}Cu^-)/i(^{63}Cu^-) \approx 75\%$ appears to be larger than 45% expected from the natural abundance of these two isotopes.

[1]The smaller observed currents are mainly due to the narrow ion beam aperture between the source and UHV chambers, which is required in order to obtain differential pumping.

Table B.1: Summary of selected ions and ion currents (i) observed with a copper cathode. The ion mass (i) is deduced on the basis of the measured field.

Ion of	H	C	CH	O	OH	^{63}Cu	^{65}Cu	^{63}CuO	^{65}CuO	Cu_2
i [nA]	0.18	0.56	<0.01	135	1.6	510	375	9.0	7.8	20
m [m_u]	1.0	12.1	13.3[a]	15.9	17.1	63.1	64.6	79.1	80.4	127.3

[a]Note: it is difficult to obtain accurate mass readings with very low ion currents.

B.2 Currents Observed with an Osmium Cathode

Both Cu an Al form ionic clusters with masses near that of Os: $m(^{35}Cu_3) = 189$ m_u and $m(Al_7) = 189$ m_u while $m(Os) \approx 190$ m_u. An aluminum cathode was found to produce currents of about 12, 90, and 12 nA for Al^-, Al_2^-, and Al_3^- ions respectively (16 keV beam). These ratios are consistent with what is expected from a sputter source. Although the larger clusters were not observed, they are expected to be less than 10% of the elemental current, i.e. $\lesssim 1$ nA. Furthermore, since the binding energy of Al_7 is very large (2.43(6) eV [2]), no signal should be observed from this ion at the wavelengths used in the Os^- experiments. A blank made of Al was therefore chosen for the Os^- experiment. Os powder was arc-melted in an argon gas atmosphere to form a ball of metalic Os, which was then welded onto the aluminum cathode blank. No evidence of sputtering of the Al blank was observed with this cathode. It is therefore believed that a negligible amount of Al_7 (if any) was present in the beam.

There was apparently some contamination of carbon in the osmium metal, possibly originating from some stage of the cathode manufacturing process (likely the arc-melting process). However, the contaminants appear to have been mostly on the surface of the cathode, since they steadily decreased over the cathode's lifetime (in excess of 100 hours). For example, the C^- current dropped from 12 to 2 nA. The heavy molecular ion observed in the spectrum is likely due to OsC^-. A high

Table B.2: Summary of selected ions and ion currents (i) observed using an osmium cathode, with an 8.3 keV beam energy. The ion mass (m) is deduced on the basis of the measured magnetic field strength. The currents observed early (young) and later (old) in the cathode's life are listed for comparison.

Negative ion of	H	C	CH	O	Os	OsC
i [nA] (young)	12	22	1.4	20	15	25
i [nA] (old)	21	3.4	$\sim$[a]	22	52[b]	13
m [m_u]	1.0	12.0	13.0	16.0	190.2	202.9

[a]Not observed.
[b]The Os^- current peaked at about 200 nA over the lifetime of the cathode.

degree of correlation[2] is observed between the ion current measured for this molecule and that of the C^- and Os^-. On the other hand, the Os^- current slowly increased from about 15 nA to nearly 200 nA after about 6 days of running the source and then very slowly decreased again. These high ion currents and general behaviour are expected for Os. It should be stressed that except for the scale of the observed signal, which correlated well with the observed Os^- ion current, no variation of the spectrum presented in Section 5.1.2 was observed over the many weeks that data was collected on this ion. It is therefore believed that the observed signal was indeed due to Os^- (see also comments in Section 5.1.2). Middleton also observed evidence for weak OsH^- formation. The mass resolution is insufficient to eliminate this ion from the beam, so small amounts of OsH^- may have been present. Table B.2 summarizes the ions and ion currents which were observed using the osmium cathode. The currents observed during the early (young) and later (old) experiments are listed for comparison.

[2]Notice that $i(\mathrm{OsC}) \approx 0.08 \times i(\mathrm{C}) \times i(\mathrm{Os})$ over the lifetime of the cathode.

Table B.3: Summary of selected ions and ion currents (i) observed using a tungsten cathode, with an 9 keV beam energy. The ion mass (m) is deduced on the basis of the measured magnetic field strength.

Negative ion of	H	C	O	W
i [nA]	0.4 to 2.5	0.2 to 1.3	0.8 to 3.8	3 to 20
m [m_u]	1.0	12.0	16.1	183.9

B.3 Currents Observed with a Tungsten Cathode

The tungsten cathode was constructed by soldering a 4 mm long tungsten rod to a copper blank. The rod protrudes far enough from the copper that no sputtering of the copper blank should occur and practically no Cu^- was formed ($\sim$0.02 nA). Since a Cu_3^- current of only about 2% of the Cu^- current is expected, Cu_3^- contamination not a concern. A very clean spectrum was observed, with low O^-, C^-, and H^- formation. A weak WC^- current was also present (Middleton also observed WC^-). Middleton found no evidence of WH^-, and so negligible quantities of WH^- (if any) are expected to be present. There is therefore no reason to expect any significant signal from impurities for the detachment spectra presented in Section 5.3.

The W^- current also started low ($\approx$3 nA), peaked at about 20 nA after two or three days of running the source, and then quickly declined again. This relatively short-lived behaviour of solid tungsten cathodes was also observed by Middleton. A summary of observed ions and typical ion currents is given in Table B.3.

B.4 References

[1] R. Middleton, *A Negative Ion Cookbook* (unpublished).

[2] X. Li, H. Wu, X. Wang, and L. Wang, Phys. Rev. Lett. **81**, 1909 (1998).

Appendix C

Saturation Models

In this Appendix, formulae that model the saturation of single-photon detachment (Section C.1) and resonant two-photon detachment (Section C.2) are derived using a rate-equation approach, under the assumption of a slow negative ion beam and uniform laser intensity and ion density distribution. Some comments on these assumptions will be given in Section C.3.

The single-photon model is introduced in Section 3.2.1 to correct for saturation effects and is used in Chapter 5 to obtain estimates of photodetachment cross sections in Os^- and W^-. The resonant two-photon model is used in Section 5.1.2 to estimate the excitation cross section of the bound-bound transition in Os^-.

C.1 Single Photon Detachment

Figure C.1(a) depicts a single-photon detachment process. Let $\bar{N}_g$ and $\bar{N}$ denote the populations[1] of respectively the ground state and the continuum states of the negative ion. $\bar{N}$ is then the number of neutral atoms produced in the detachment process. We

[1]Note that a bar placed over the variable indicates that the *number* of atoms or ions in some state are being specified. For example $\bar{N}$ is the *number of neutral atoms* produced in the photodetachment process, while $N = N_0'\bar{N}$ is the *measured signal* due to those atoms.

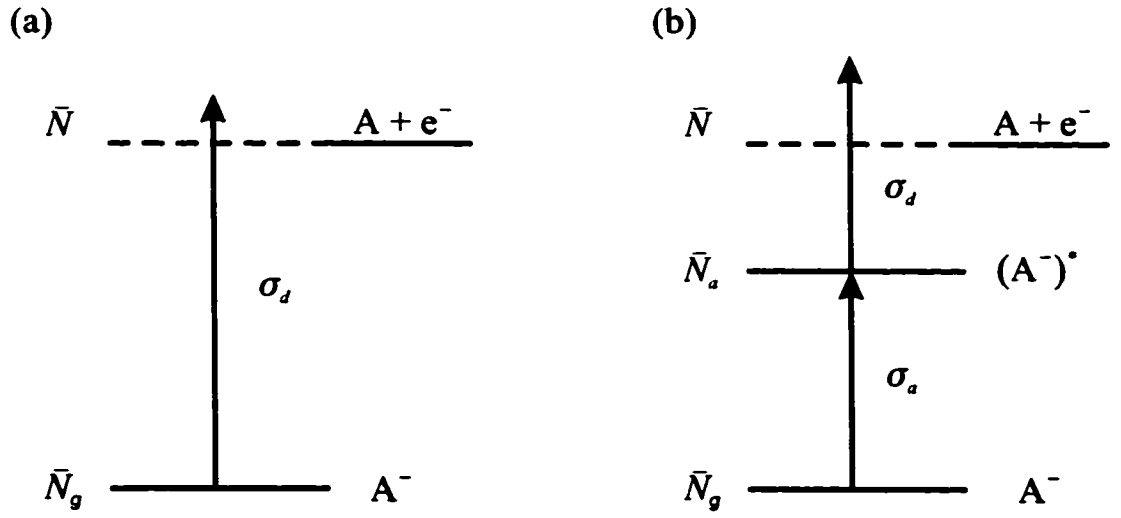

Figure C.1: Diagram for single-photon (a) and resonant two-photon (b) detachment from the negative ion of some atom, A. $\bar{N}_g$, $\bar{N}_a$, and $\bar{N}$ represent respectively the number of ions in the ground (A^-), excited ($(A^-)^*$), and continuum ($A + e^-$) states. The transitions indicated by the arrows are labelled with the corresponding cross sections for excitation (σ_a) and detachment (σ_d).

must have that the total population $\bar{N}_t$ is constant during the detachment process such that,

$$\bar{N}_t = \bar{N}_g + \bar{N} . \tag{C.1}$$

Since the probability of radiative attachment of an electron to a neutral atom is negligibly small, the population $\bar{N}_g$ can only be reduced with time. If Φ is the photon flux and σ_d is the detachment cross section, then the rate at which the ground state is depleted by photodetachment is given by:

$$\dot{\bar{N}}_g = -\sigma_d \Phi \bar{N}_g . \tag{C.2}$$

Using the initial condition $\bar{N}_g(t = 0) = \bar{N}_t$, this can be easily integrated to obtain

$$\bar{N}_g = \bar{N}_t \exp\left(-\sigma_d \int_{pulse} \Phi \, dt \right) , \tag{C.3}$$

where the integral is carried out over the duration of a laser pulse. From Equation C.1, the number of ions detached is simply $\bar{N} = \bar{N}_g - \bar{N}_t$. If each atom produces a signal of N'_o then the total observed signal is given by:

$$N = N'_o \bar{N}_t \left[1 - \exp\left(-\sigma_d \int_{pulse} \Phi \, dt \right) \right], \tag{C.4}$$

which is Equation 3.1 with $N_o = N'_o \bar{N}_t$.

C.2 Two-photon Resonant Detachment

Here we investigate the saturation behaviour for a two photon transition which proceeds via a resonant state, as depicted in Figure C.1(b). The ions first undergo an excitation from the ground state with population $\bar{N}_g$, to an excited ionic state with population $\bar{N}_a$. The negative ions are then detached into the continuum, which has a population denoted by $\bar{N}$, the number of neutral atoms produced in the detachment process. Since the process is resonant, it proceeds sequentially, with two different cross sections, the excitation cross section σ_a and the detachment cross section σ_d. $\bar{N}$ is again the number of neutral atoms produced in the detachment process and the total population is:

$$\bar{N}_t = \bar{N}_g + \bar{N}_a + \bar{N} . \tag{C.5}$$

Loudon [1, section 2.14, pages 78-81] concludes that rate equations are valid when either: (1) the bandwidth of the incident light exceeds the atomic transition linewidth, or (2) the combined collision and Doppler linewidth greatly exceeds the radiative linewidth of the transition. Both of these conditions are met for the resonant transition studied in Os^-. Coherent effects (e.g. Rabi flopping) should then have a negligible effect, and we proceed with a rate-equation approach:

$$\dot{\bar{N}}_g = -\sigma_a \Phi \bar{N}_g + \sigma_a \Phi \bar{N}_a , \tag{C.6a}$$

$$\dot{\bar{N}}_a = \sigma_a \Phi \bar{N}_g - \sigma_a \Phi \bar{N}_a - \sigma_d \Phi \bar{N}_a , \tag{C.6b}$$

$$\dot{\bar{N}} = \sigma_d \Phi \bar{N}_a . \tag{C.6c}$$

The second terms in Equation C.6a and Equation C.6b represent the possibility of stimulated emission from the excited ionic state. The rate of spontaneous emission should be much smaller and is therefore neglected.[2] Equations C.6a, C.6b, and C.6c are a system of coupled first-order differential equations. Fortunately, Equation C.6a and Equation C.6b do not depend on $\bar{N}$ and so they can be solved as a pair. The simplest approach is to first decouple the equations by taking the time derivative of Equation C.6b. After some manipulation, the following differential equation is obtained:

$$\ddot{\bar{N}}_a + (2\sigma_a + \sigma_d)\Phi \dot{\bar{N}}_a + \sigma_a \sigma_d \Phi^2 \bar{N}_a = 0. \tag{C.7}$$

Equation C.7 is a linear second-order homogeneous equation with constant coefficients, and can be solved by use of the characteristic equation method. Assuming the initial conditions $\bar{N}_g = \bar{N}_t$ and $\bar{N}_a = \bar{N} = 0$ at $t = 0$, we obtain:

$$\bar{N}_a = \sigma_a \bar{N}_t \frac{e^{-\sigma_{(-)} P} - e^{-\sigma_{(+)} P}}{\sigma_{(+)} - \sigma_{(-)}}, \tag{C.8}$$

where

$$\sigma_{(\pm)} = \frac{1}{2}(2\sigma_a + \sigma_d) \pm \frac{1}{2}\sqrt{4\sigma_a^2 + \sigma_d^2}$$

and

$$P = \int_{pulse} \Phi \, dt.$$

Finally, integrating Equation C.6c and noting that $\sigma_a \sigma_d = \sigma_{(+)} \sigma_{(-)}$ we obtain:

$$\bar{N} = \bar{N}_t \left(1 - \frac{\sigma_{(+)} e^{-\sigma_{(-)} P} - \sigma_{(-)} e^{-\sigma_{(+)} P}}{\sigma_{(+)} - \sigma_{(-)}} \right), \tag{C.9}$$

[2]For the state studied in Os^-, a radiative lifetime of $\sim 10^{-4}$ s is expected, which is about 10 000 times longer than the duration of the laser pulse.

Equation C.9 is the desired result. Three parameters need to be fit: the amplitude $\bar{N}_t$ and the effective cross sections $\sigma_{(\pm)}$. The excitation and detachment cross sections can be extracted from the fitted parameters by using the identities $\sigma_a \sigma_d = \sigma_{(+)} \sigma_{(-)}$ and $2\sigma_a + \sigma_d = \sigma_{(+)} + \sigma_{(-)}$ to obtain:

$$\sigma_a = \frac{1}{4}\left(\sigma_{(+)} + \sigma_{(-)} \pm \sqrt{\sigma_{(+)}^2 + \sigma_{(-)}^2 - 6\sigma_{(+)}\sigma_{(-)}}\right) , \tag{C.10a}$$

$$\sigma_d = \sigma_{(+)} + \sigma_{(-)} - 2\sigma_a . \tag{C.10b}$$

There are therefore two valid pairs of roots for any given pair of parameters $\sigma_{(\pm)}$. In general these will both be positive and therefore some knowledge of the system is required in order to select the correct roots. For example, for the resonance observed in Os^- (see Section 5.1.2), the second set of roots, $\sigma_a \sim 2 \times 10^{-17}$ cm^2 and $\sigma_d \sim 2 \times 10^{-15}$ cm^2, was rejected on the basis that 2×10^{-15} cm^2 is 2 or 3 orders of magnitude larger than expected for a detachment cross section in an atomic negative ion, assuming no strong continuum resonance enhancements.[3]

C.3 Limitations of the Saturation Models

In general, the assumptions made in the above derivations are reasonably well realized, and the predicted shape of saturation curves given by Equation C.4 and Equation C.9 hold to a high accuracy over a very large range of pulse energies. However, caution is warranted when interpreting the fitted values extracted with these models.

[3]Even strong continuum resonances tend to have considerably lower cross sections than 2×10^{-15} cm^2. For example the strong continuum resonance in Cu^- has a peak cross section of about 7×10^{-17} cm^2 [2,3]. The shape resonance in He^- represents one of the largest (if not *the* largest) cross section observed in an atomic negative ion: about 6×10^{-15} cm^2 at its peak [4]. However, this large peak cross section is made possible only because the resonance is very near to the threshold and is thus very narrow. Therefore, to explain this large detachment cross section for the two-photon transition in Os^-, a second very narrow resonance would be required to appear 8589 cm^{-1} above the ground state threshold, to within about ± 30 cm^{-1} (the typical width of these strong, narrow resonances). This would be an extraordinary coincidence.

Typical ion beam velocities in the McMaster setup are $\sim 10^5$ m/s (92 000 m/s for the Os^- experiment, for example). The ions are therefore displaced by $\sim$1 mm (about 0.7 mm for Os^-) over the duration of the laser pulse. This represents a small displacement for a collimated laser beam, only 10 to 20% of the width of the beam. However, if the light is focussed onto the ion beam, the displacement of the ions has the effect of significantly increasing the number of ions exposed to the laser field and reducing the effective pulse duration seen by a given ion.

A full model of the saturation (see [2,5]) requires that P be integrated over the ion trajectories in time. Also, the entire expression must be integrated over the ion density distribution and laser intensity profile. These refinements introduce geometrical factors which can change the value of the fitted parameters, σ_d and N_o. None the less, Equation C.4 and Equation C.9 are certainly valid for order-of-magnitude estimates when a collimated laser beam is used, which is all we shall be concerned with in this thesis. These refinements are also unimportant for the correction of saturation effects, where the interpretation of the parameters are largely irrelevant, so long as the shape of the curve is in good agreement with measured behaviour.

C.4 References

[1] R. Loudon, *The Quantum Theory of Light,* Second Edition (Oxford, New York, 1983).

[2] P. Balling, C. Brink, T. Andersen, and H. K. Haugen, J. Phys. B **25**, L565 (1992).

[3] K. F. Scheibner and A. U. Hazi, Phys. Rev. A **38**, 539 (1988).

[4] C.W. Walter, J.A. Seifert, and J.R. Peterson, Phys. Rev. A **50**, 2257 (1994).

[5] C. Blondel, R.-J. Champeau, M. Crance, A. Crubellier, C. Delsart, and D. Marinescu, J. Phys. B **22**, 1335 (1989).

Appendix D

Permission to Reproduce Articles

Paper 1 was previously published in the Journal of Physics B, who have granted me the right to reproduce the article. I hereby grant McMaster University and the National Library of Canada the non-exculsive right to reproduce this article as part of the present Thesis.

Papers 2 to 9 were previously published in Physical Review A and Physical Review Letters. According to the copyright agreement for articles published in these journals: "As a coauthor of the material, you retain the right, after publication, to use all or part of the article, without revision or modification including the APS formatted version, in personal compilations or other publications of your owns works, including your personal web home page, and to make copies of all or part of the material for your use for lecture or classroom purposes and in your thesis or dissertation." I hereby grant McMaster University and the National Library of Canada the non-exculsive right to reproduce these articles as part of the present Thesis.

McMaster Univesity
Department of Physics and Astronomy
1280 Main Street West
Hamilton, Ontario, CANADA
L8S 4M1

April 19, 2001

Publisher of Journal of Physics B
IOP Publishing Limited
Dirac House
Temple Back
Bristol
BS1 6BE

Dear Madam/Sir:

I am completing a Ph.D. thesis at McMaster University entitled "Single- and multiphoton studies of atomic negative ions: Electron affinities, threshold laws, and near-threshold structure" I would like your permission to reprint the following journal article in my thesis.

R. C. Bilodeau, M. Scheer, and H. K. Haugen, "Infrared laser photodetachment of transition metal negative ions: Studies on Cr^-, Mo^-, Cu^- and Ag^-," *Journal of Physics B* **31**, 3885-3891 (1998).

Please note that I am a coauthor of this work.

I am also requesting that you grant irrevocable, nonexclusive licence to McMaster University and to the National Library of Canada to reproduce this material as a part of the thesis. Proper acknowledgement of your copyright of the reprinted material (including the authors, title, date and publisher) will be given in the thesis. In addition, as previously requested by your office, the Internet address for the journal's website (www.iop.org/Journals/jb) will also be included.

If these arrangements meet with your approval, please sign where indicated below and return this letter to me in the enclosed envelope. Thank you very much.

Sincerely,

René Claude Bilodeau

PERMISSION GRANTED FOR THE USE REQUESTED ABOVE

IOP Publishing Limited

PERMISSION TO REPRODUCE AS REQUESTED IS GIVEN PROVIDED THAT:

(a) the consent of the author(s) is obtained
(b) the source of the material including author/editor, title, date and publisher is acknowledged. ●

Authorized by: _____

Signature: _____

IOP Publishing Limited
Dirac House
Temple Back
BRISTOL 5/5/01
BS1 6BE Date Rights & Permission

● Please add a reference to the Journal's homepage at www.iop.org/Journals/jb Thank you!

AMERICAN PHYSICAL SOCIETY

June 4, 2001

McMaster University
Department of Physics and Astronomy
1280 Main Street West
Hamilton, Ontario CANADA

RE: **Your request to reprint or mount your Article, or any portion of it, in your thesis or dissertation**

Articles: Bilodeau et al., Physical Review A 61, 012505, 2000, Norquist et al., Physical Review A, 59, 1896, 1999, Bilodeau et al., Physical Review Letters, 85, 534, 2000, Scheer et al., Physical Review Letters, 80 2562, 1998, Scheer et al., Physical Review A, 57, R1493, 1998, Scheer et al., Physical Review Letters, 80, 684, 1998.

Dear Dr. Bilodeau:

As the author of the requested material, you retain the right, after publication, to use all or part of the article, without revision or modification including the APS formatted version, in personal compilations or other publications of your owns works, including your personal web home page, and to make copies of all or part of the material for your use for lecture or classroom purposes and in your thesis or dissertation.

Please cite the original publication in full and the copyright line as follows:

> Authors names, journal title, volume number, year of publication, and page numbers.
> "Copyright (year) by the American Physical Society."

If you wish to mount or post your Article on your personal webpage, please set-up a link to the article's abstract page ("wrapper"), using APS's simple URL formula ("link manager," http//publish.aps.org/linkfaq.html).

> For example, the URL for Physical Review Letters, Vol. 83, p. 4872 would be:
> http://publish.aps.org/abstract/prl/v83/p4872

The Article may not be sold in any format. The definitive version of the Article is the APS online version.

For your reference, a copy of the APS Copyright Form can be found at:
ftp://aps.org/pub/jrnls/copy_trnsfr.pdf

If you have any questions, please feel free to contact us.

Sincerely,

Anita Wiley, APS Customer Service

**The APS formatted version is the full text PostScript (PS) or the PDF version produced by APS or its vendors with no links or navigation.*